# UNIVERSITÉ DE STRASBOURG

*ÉCOLE DOCTORALE DES SCIENCES CHIMIQUES*

**ICPEES, UMR 7515**

**Institut de chimie et procédés pour l'énergie, l'environnement et la santé**

# THÈSE

présentée par :

## Zhenxin XU

soutenue le : **22 Mai 2019**

pour obtenir le grade de : **Docteur de l'université de Strasbourg**

Discipline/ Spécialité : Chimie/Chimie

---

## Development of new macroscopic carbon materials for catalytic applications

### Développement de nouveaux matériaux carbonés macroscopiques pour les applications en catalyse

---

**THÈSE dirigée par :**
  Dr. Cuong PHAM-HUU              Directeur de recherche, Université de Strasbourg, Strasbourg

**RAPPORTEURS :**
  Prof. Philippe SERP              Professeur, Université de Toulouse, Toulouse
  Dr. Axel LOFBERG                Chargé de Recherche, Université de Lille, Lille

---

**AUTRES MEMBRES DU JURY :**
  Prof. Vincent RITLENG            Professeur, Université de Strasbourg, Strasbourg

# Acknowledgements

It is an unforgettable and exciting journey for my Ph.D. study in France, which is full of opportunities and challenges as well. This thesis is performed under the supervision of Dr. Cuong PHAM-HUU at the Institut de Chimie et procédés pour l'Energie, l'Environnement et la Santé (ICPEES, CNRS UMR 7515 and the University of Strasbourg) in Strasbourg. Here I wish to express my sincerely gratitude to all the people who have contributed to this work and to those who have helped me during this rewarding period of time. The China Scholarship Council (CSC) is greatly acknowledged for the finical support during my Ph.D. degree. The CSC not only provides me the possibility to complete the Ph.D. study in France, but also gives me the opportunity to experience the different cultures and lives.

I would like to express my great thanks to my supervisor Dr. Cuong PHAM-HUU, who accepted me as a Ph.D. candidate in his laboratory, for his patient guidance and well-timed encouragement during my research. He is always ready to help me and provide me the precious suggestions on the direction of my research. I am deeply affected by his profound knowledge and optimistic and scientific attitude. He also encourages and supports me to try and explore new ideas and think independently. With his indispensable helps, my research vision is wider and my thinking becomes deeper. He is one of the best advisors I know.

I am indebted to my M.S. advisors Prof. Wei CHU and Prof. Shizhong LUO from the College of Chemical Engineering at Sichuan University in China, who recommended me to come to the lab of Dr. Cuong PHAM-HUU after knowing that I wanted to go abroad to pursue a doctorate. I am also grateful to Dr. Yuefeng LIU from Dalian Institute of Chemical Physics (DICP) at Chinese Academy of Science (CAS) in China, who helps me and provides me crucial suggestions in the research work.

I also want to thank all the members of my jury, Prof. Philippe SERP from the Laboratoire de Chimie de Coordination (LCC, CNRS UPR 8241 and the University of Toulouse) in Toulouse, Dr. Axel LOFBERG from the Unité de Catalyse et Chimie du Solide (UCCS, CNRS UMR 8181 and the University of Lille) in Lille and Prof. Vincent RITLENG

# Table of Content

# Résumé-Abstract

## 1. Introduction

Les matériaux carbonés (MC) désignent la vaste gamme de composés carbonés ayant des propriétés physico-chimiques spécifiques, tels que le charbon actif (CA), les nanotubes/fibres de carbone (NTC/NFC) et le graphène [1, 2]. De nos jours, les MC sont utilisés dans un grand nombre de procédés catalytiques, soit comme support, soit directement comme catalyseurs sans-métaux [3, 4]. Les propriétés physico-chimiques de ces MC, en particulier la porosité et la réactivité de surface, qui est essentiellement liée à la présence de groupements fonctionnels ou le dopage par des hétéroatomes tels que l'azote, le soufre ou le phosphore, peuvent être modifiées à volonté pour répondre aux exigences des procédés catalytiques en aval. Elles ont conduit au développement de nouveaux catalyseurs offrant des performances catalytiques améliorées [5-12]. Les défauts structuraux décorés par des groupements fonctionnels, mais aussi le dopage de la structure carbonée avec des hétéroatomes sont capables de jouer le rôle de sites d'ancrage pour des phases actives dans la préparation des catalyseurs [13-15]; ils pourraient également opérer en tant que sites actifs pour des réactions catalytiques spécifiques en lieu et place des catalyseurs contenant un métal comme phase active [16-20].

Ces CM sont généralement utilisés sous deux formes, en poudre ou avec une mise en forme, en fonction des applications en aval. Pour les réactions en phase liquide, la forme poudre est préférable car elle offre une grande surface de contact, alors que pour la réaction en phase gazeuse, la forme structurée sera la plus utilisée afin de réduire les problèmes de perte de charge. Cependant, durant la dernière décennie les catalyseurs structurés ont suscité un intérêt croissant, même pour les réactions en phase liquide, car ils permettent de récupérer facilement le catalyseur et d'éviter une étape de filtration post-réaction qui est une étape consommatrice en temps et en énergie. Il existe des stratégies communes pour la fabrication des supports carbonés sous forme structurée : (i) la méthode de réticulation des nanomatériaux carbonés préexistants (en poudre), tels que les NTC et/ou le graphène multi-feuillet, en différentes formes macroscopiques polymérisées [21, 22], (ii) la croissance in situ par voie catalytique des structures de nano-carbone sur le substrat hôte macroscopique

[23-25], et (iii) la fabrication d'aérogels de carbone autoportants sans utiliser de matrice hôte [26]. Cependant, la synthèse de ces composites hiérarchiques n'est pas simple car elle nécessite des étapes de réaction opérant à haute température ou complexes à mettre en œuvre; elle génère également des déchets ou des sous-produits qui nécessitent un traitement post-synthèse. Il est alors intéressant de trouver une nouvelle méthode plus simple et ayant un impact environnemental moindre.

Dans le cadre du développement de nouveaux matériaux carbonés structurés pour la catalyse hétérogène, nous avons exploré le potentiel du feutre de carbone/graphite commercial (CF/GF). CF et GF sont utilisés sous formes de structures macroscopiques et sont constitués par des fibres micrométriques formant un réseau hiérarchisé avec une forte accessibilité [27]. Les différentes températures du traitement thermique des précurseurs de carbone entraînent une graphitisation différente du matériau final, résultant ainsi à une surface et une porosité variable pour le CF et le GF. La nature du carbone permet de modifier ses propriétés physico-chimiques, notamment la structure des pores, mais également la chimie de surface, alors que le caractère macroscopique du feutre facilite leur mise en forme, tout cela en fonction des applications en catalyse en aval.

Le but du travail décrit dans cette thèse consiste à explorer le potentiel des monolithes à base de feutre GF et CF soit en tant que catalyseur sans-métaux pour les réactions d'oxydation en phase gazeuse, soit en tant que support de catalyseur, notamment pour le palladium, pour les réactions d'hydrogénation en phase liquide. En raison de leur surface présentant une inertie chimique avec une faible mouillabilité, les traitements chimiques ont été développés pour activer la surface de ces matériaux carbonés. Les matériaux sont ainsi activés par divers procédés chimiques tels que l'oxydation, l'amination, la thiolation, et/ou le dopage direct à haute température à l'azote et au soufre. L'oxydation partielle du sulfure d'hydrogène en soufre élémentaire ainsi que l'hydrogénation sélective du cinnamaldéhyde, en tant que réactions sensibles à l'influence des propriétés du catalyseur sur l'activité et la sélectivité, sont utilisées en tant que réactions modèles. Les supports, avant et après activation, ainsi que les catalyseurs sont caractérisés par diverses techniques de caractérisation, notamment la spectroscopie photoélectronique à rayons X, la spectroscopie Raman, la

désorption programmée en température couplée avec la spectrométrie de masse, les microscopies électroniques à transmission et à balayage, l'adsorption et la désorption d'azote, la spectroscopie d'émission atomique à plasma à couplage inductif, les analyses thermogravimétriques, la réduction programmée en température, et l'infrarouge à transformée de Fourier.

## 2. Résultats et discussions

## 2.1 Feutre de graphite oxydés (OGF) en tant que catalyseur sans-métaux pour l'oxydation partielle du sulfure d'hydrogène

L'activation du GF est réalisée en utilisant le traitement à l'acide nitrique gazeux à haute température (Figure 1) et son influence sur la formation de défauts (décorés avec des groupes fonctionnels oxygénés) sur la surface du matériau carboné a été confirmée par les techniques de caractérisation. Après le traitement acide, une structure carbonée hautement poreuse a été observée sur la surface du graphite dense du feutre de départ, induisant ainsi une augmentation remarquable des surfaces spécifiques et effective du matériau final. L'abondance des groupes oxygénés et des défauts de structure ainsi que la grande surface spécifique ont induit une perte de la stabilité thermique par rapport à celle observée sur le matériau de départ.

*Résumé-Abstract*
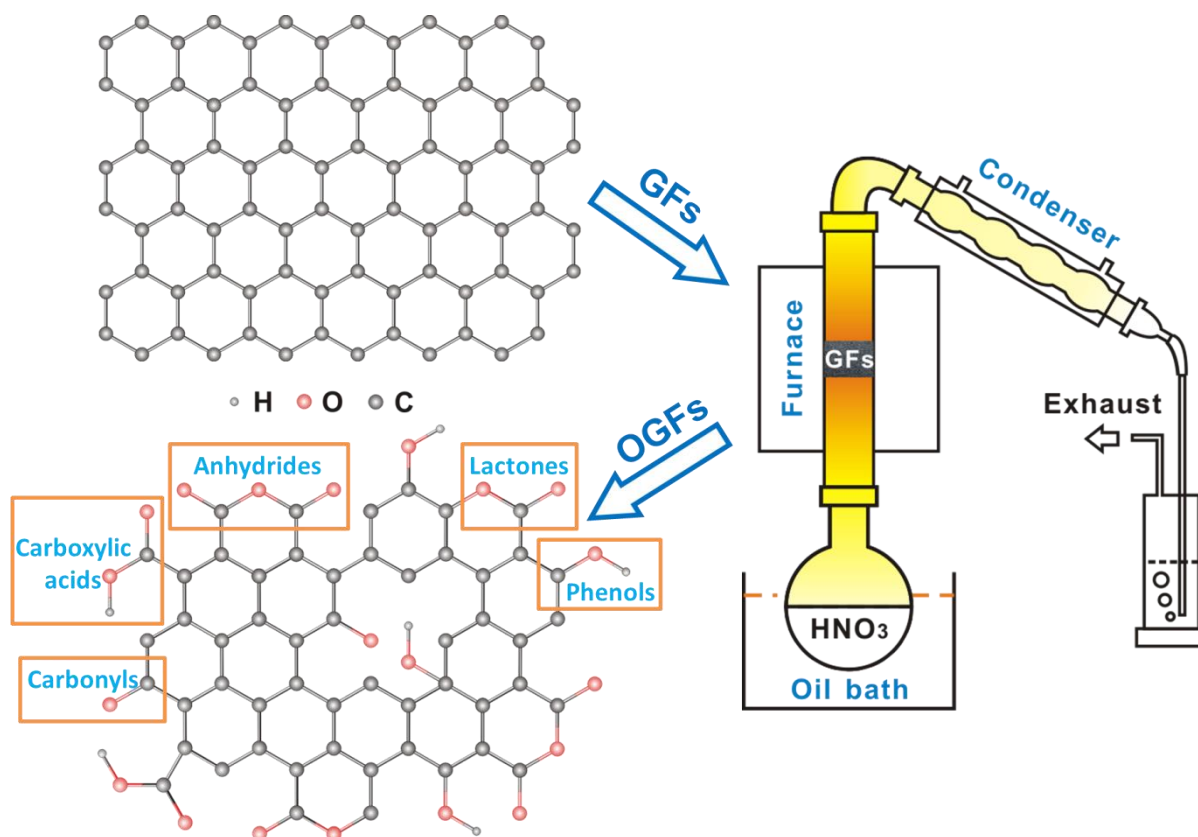


**Figure 1.** Illustration schématique des OGF préparés par le traitement HNO₃ gazeux et des différents groupes fonctionnels oxygénés générés à la surface du graphite après le traitement.

Le GF activé peut être utilisé directement comme catalyseur sans-métaux pour remplacer les catalyseurs traditionnels à base d'oxyde de fer dans l'oxydation sélective de $H_2S$ dans les effluents de déchets industriels. Les résultats ont révélé que les GF contenant les défauts décorés avec des groupements oxygénés présentent une activité de désulfuration relativement élevée et extrêmement stable en fonction du temps par rapport à son homologue non activé. Les performances catalytiques observées peuvent être attribuées à la présence de défauts de structure sur la surface du carbone filamenteux et aux groupements fonctionnels oxygénés qui pourraient jouer le rôle de sites actifs pour l'oxydation sélective de $H_2S$ en soufre élémentaire.
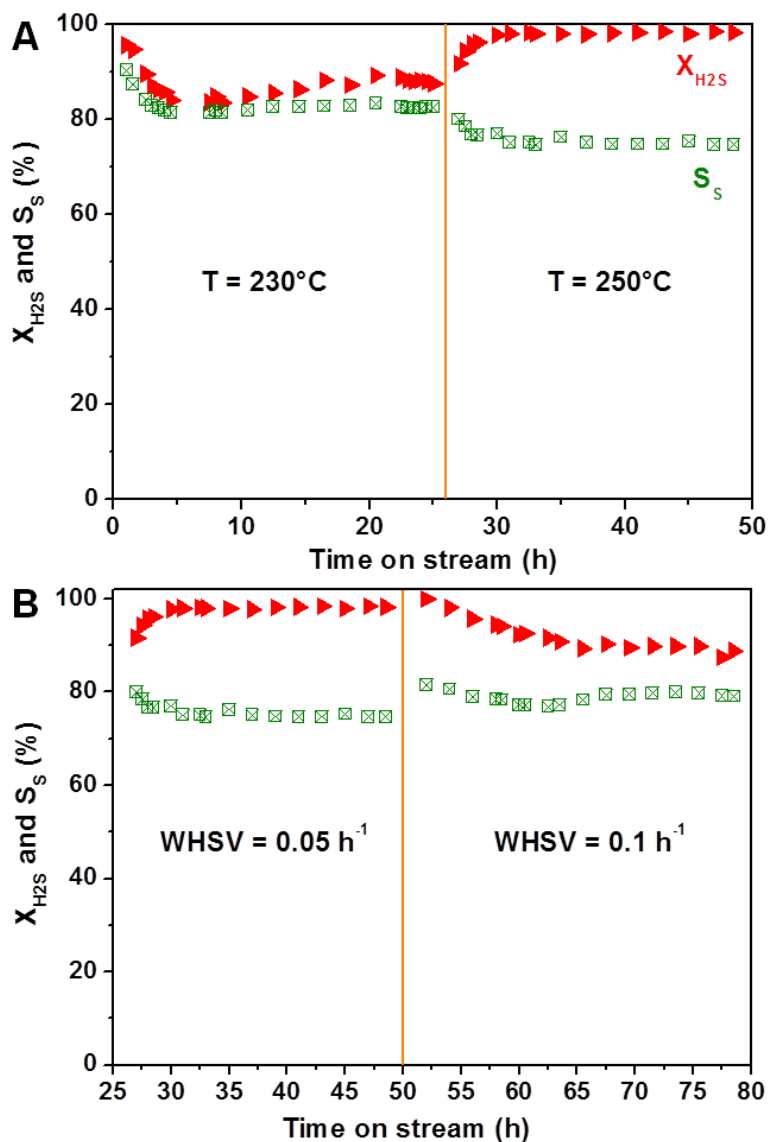
**Figure 2.** Performances catalytiques en désulfuration sur des catalyseurs sans-métaux OGF après traitement sous HNO$_3$ gazeux à 250 $^o$C pendant 16 h. (A) Conditions de réaction: [H$_2$S] = 1 vol. %, [O$_2$] = 2.5 vol. %, [H$_2$O] = 30 vol. %, WHSV= 0.05 h$^{-1}$. (B) Conditions de réaction: [H$_2$S] = 1 vol. %, [O$_2$] = 2.5 vol. %, [H$_2$O] = 30 vol. %, température de réaction = 250 $^o$C.

## 2.2 Feutre de graphite oxydé utilisé comme support de catalyseur au palladium pour l'hydrogénation en phase liquide du cinnamaldéhyde

Dans cette partie, le support carboné activé par les vapeurs d'acide est utilisé en tant que support de catalyseur pour le palladium qui assurera le rôle de phase active pour la

réaction d'hydrogénation. Avant le dépôt du métal actif sur le support GF, celui-ci devrait être modifié par l'introduction de groupements fonctionnels oxygénés qui permettent d'améliorer la mouillabilité du support et la capacité d'ancrage des nanoparticules (NPs) métalliques. L'étude concerne l'influence de l'effet du traitement d'oxydation, par les vapeurs d'acide, du GF sur les performances catalytiques des catalyseurs au Pd supporté sur ce dernier. Tout d'abord, comme le montre la Figure 3, nous avons optimisé le processus de traitement du $HNO_3$ gazeux, en introduisant un flux d'argon pour aider l'oxydant gazeux à traverser le GF de manière efficace et contrôlable.
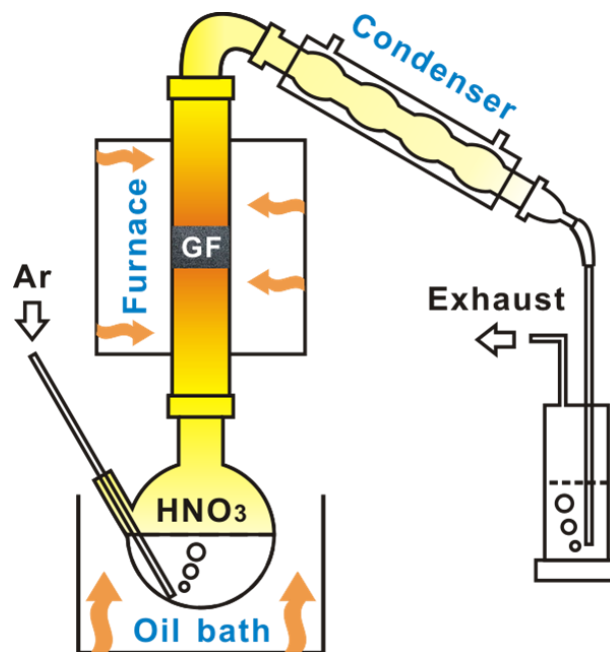


**Figure 3.** Illustration schématique du traitement thermique optimisé $HNO_3$ gazeux.

Les GF fonctionnalisés par l'oxygène (OGF), par l'intermédiaire du traitement à l'acide, ont été préparés en utilisant le traitement avancé au $HNO_3$ gazeux, puis utilisés pour supporter les nanoparticules (NPs) de Pd déposées par imprégnation. Le catalyseur monolithique à base de palladium (Pd/OGF) a ensuite été utilisé comme catalyseur mais aussi comme agitateur catalytique dans l'hydrogénation en phase liquide du cinnamaldéhyde. Le système catalytique ainsi développé présente des performances catalytiques élevées ainsi

qu'une recyclabilité complète (Figure 4). Le catalyseur Pd/CA commercial présente dans les mêmes conditions réactionnelles une perte significative des performances catalytiques en fonction des cycles de test qui peut être attribuée à une perte de catalyseur lors de la filtration et aussi par frittage lent des particules métallique lors de la réaction.

Les interactions entre les groupements oxygénés introduits par le traitement acide et les nanoparticules de Pd déposées génèrent ainsi des transferts électroniques avec la formation d'une espèce $Pd^{\delta+}$ à l'interface métal-support. Tous ces facteurs ont contribué à l'amélioration de la dispersion des particules de Pd et la aussi à l'augmentation de la résistance au frittage lors de la préparation du catalyseur et lors des tests catalytiques.
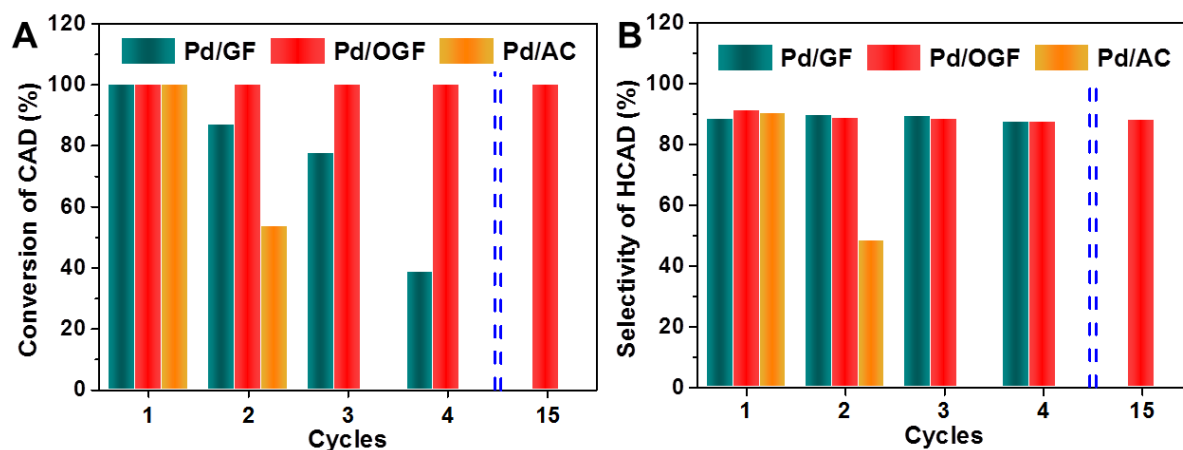


**Figure 4.** (A) Conversion de cinnamaldéhyde (CAD) et (B) sélectivité de l'hydrogénation de la liaison C=C (HCAD) en fonction des tests sur les catalyseurs Pd/OGF, Pd/GF et Pd/AC. Conditions réactionnelles: 80 °C, 50 mL/min $H_2$, 1 atm, 375 rpm et 0.08 mol/L de CAD.

## 2.3 Feutre de carbone modifiés à l'azote en tant que support de catalyseur au Pd pour l'hydrogénation sélective du cinnamaldéhyde

Cette partie de l'étude concerne la synthèse des supports à base de feutre de carbone (CF) décorés par des groupements aminos de surface ou dopés avec de l'azote pour la dispersion des particules de Pd. Les catalyseurs synthétisés seront évalués dans la réaction

d'hydrogénation sélective du cinnamaldéhyde.

L'introduction des groupements fonctionnels contenant de l'azote sur le support de carbone lors de l'étape d'amination réalisée sous condition hydrothermale en présence de l'urée, s'est révélée être liée à la présence de groupements oxygénés en surface à travers les échanges N et O. Les groupements aminos sont ensuite convertis en azote directement dopé dans la charpente graphitique après une graphitisation à haute température. Les groupements oxygénés, les groupements aminos ainsi que les sites dopés à l'azote ont non seulement influencé la polarité de la surface du support, mais ont également altéré l'ancrage des NPs de Pd via l'interaction métal-support, ce qui a entraîné une fluctuation des performances d'hydrogénation (Figure 5). L'effet de la structure électronique des NPs de Pd sur la sélectivité catalytique vis-à-vis de la liaison C=C a été étudié dans ce travail.
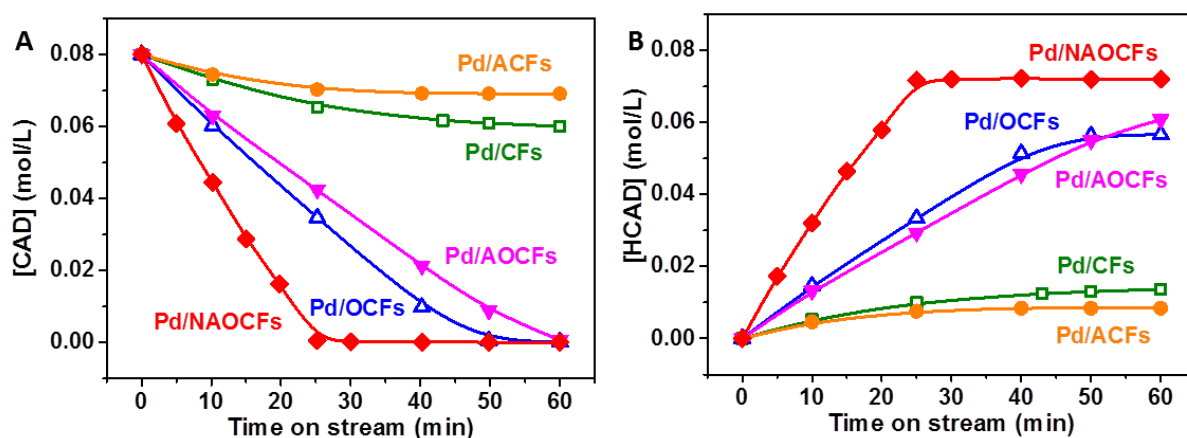


**Figure 5**. (A) Conversion de cinnamaldéhyde et (B) sélectivité d'hydrogénation de la liaison C=C exprimées en termes de concentration de CAD et de HCAD en fonction du temps écoulé sur les Pd/CF, les Pd/ACF (CF aminés sans pré-oxydation), Les catalyseurs OCF (CF oxydés), Pd/AOCF (CF aminés avec pré-oxydation) et Pd/NAOCF (AOCF dopés à l'azote), respectivement. Conditions: 80 $^{o}$C, 25 mL/min H$_2$, 1 atm, 300 rpm et 0.08 mol/L de CAD.

## 2.4 Feutres de carbone modifiés par du soufre en tant que support de catalyseur au Pd pour l'hydrogénation sélective du cinnamaldéhyde

## Résumé-Abstract

Enfin, nous avons étendu ce travail aux CF décorés avec des groupements thiols (TOCF), qui ont été préparés par réaction thermique entre l'H$_2$S et les CF après un traitement à l'acide (OCF). L'effet de la présence de groupements oxygénés sur la formation des groupements de thiol sur la surface du support a été discuté. Les groupements de thiols favorisent l'ancrage des nanoparticules de Pd qui seront utilisées ensuite comme catalyseur modèle dans l'hydrogénation sélective du cinnamaldéhyde. Des études détaillées ont révélé que les groupements de thiol peuvent non seulement servir de sites d'ancrage pour le métal actif à la surface du support, mais également en tant que ligands soufrés de recouvrement à la surface des particules de Pd. Il a été confirmé que les groupements de thiol qui décorent la surface des particules de Pd entravaient l'activité catalytique, générant ainsi l'effet d'empoisonnement illustré sur la Figure 6.
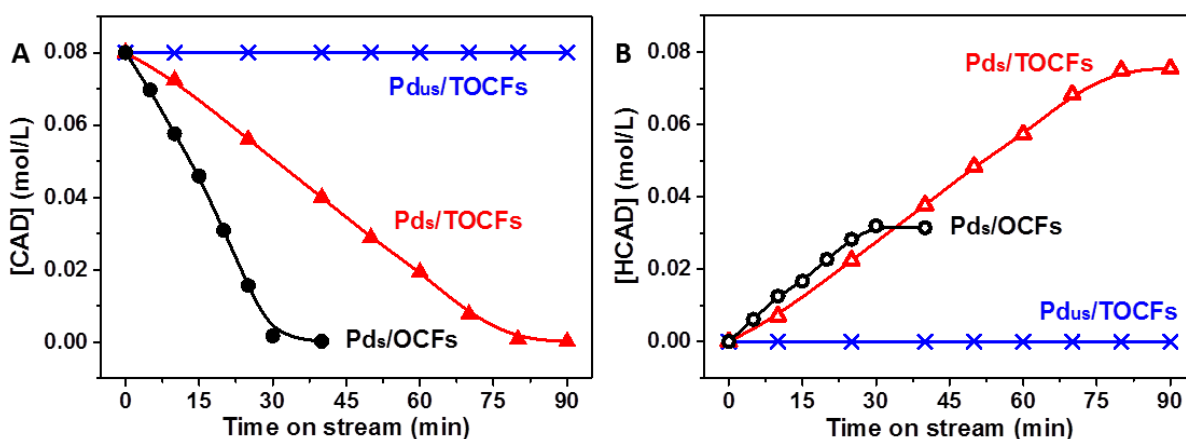
**Figure 6.** (A) Conversion de cinnamaldéhyde et (B) sélectivité d'hydrogénation de la liaison C=C exprimées en termes de concentration de CAD et de HCAD en fonction du temps de traitement sur les Pd$_{us}$/TOCFs (1.5 wt% Pd), Pd$_s$/TOCFs (6.6 wt% Pd) et Pd$_s$/OCFs (5.3 wt% Pd) catalyseurs, respectivement. Conditions: 80 $^o$C, 25 mL/min H$_2$, 1 atm, 300 rpm et 0.08 mol/L de CAD.

Il est à noter que cet empoisonnement superficiel du catalyseur pourrait être évité en ajustant le rapport atomique soufre/palladium. Le thiol-S pourrait influencer la configuration électronique des NPs de Pd par la formation de la liaison Pd-S. Conformément à la discussion

9

ci-dessus sur la sélectivité de l'hydrogénation, la présence des espèces Pd$^{\delta+}$ appauvri en électrons sur une phase métallique active a contribué à améliorer la chemiosélectivité vis-à-vis de l'hydrogénation de la liaison C=C.

## 3. Conclusions et perspectives

En résumé, les résultats décrits dans cette thèse ont montré le potentiel des supports à base de feutre de carbone ou de graphite (CF/GF) avec une forme macroscopique pour une utilisation soit en tant que catalyseur sans-métaux soit en tant que support carboné pour des nanoparticules métalliques pour les réactions en phase gazeuse et liquide. Nous avons réussi à synthétiser des GF et des CF modifiés avec des formes macroscopiques contrôlées, dotés de propriétés physico-chimiques adaptées, grâce à des traitements chimiques appropriés. Les GF oxydés, en tant que catalyseur sans-métaux, présentent une activité élevée dans l'oxydation partielle de H$_2$S en soufre élémentaire. Les supports GF et CF activés, développés par les méthodes d'oxydation, d'amination, de dopages à l'azote et au soufre, ont été utilisés pour ancrer les particules de Pd, qui présentaient une performance catalytique élevée en ce qui concerne l'hydrogénation sélective de cinnamaldéhyde. De plus, la forme macroscopique des catalyseurs ainsi synthétisés permettait une réduction sensible des problèmes de perte de charge pour des procédés en phase gaz et une récupération facile du catalyseur pour des procédés en phase liquide, respectivement. Par conséquent, cette thèse peut fournir certaines stratégies pour concevoir de manière rationnelle un catalyseur ou un support de catalyseur avec des propriétés intéressantes pouvant opérer dans de nombreux procédés catalytiques. L'étude approfondie, qui restera à réaliser, portera sur l'analyse qualitative et quantitative des sites actifs pour établir la relation structure-fonction pour des catalyseurs sans-métaux, ainsi que sur l'effet du support fonctionnalisé sur la dispersion d'autres particules métalliques. Elle portera également sur la compréhension du mécanisme d'interaction entre le métal actif et les sites d'ancrage et enfin sur l'utilisation du chauffage sans contact (par exemple un chauffage par induction électromagnétique) du catalyseur ou support de catalyseur sans-métaux à base de GF/CF pour l'étude de l'influence d'un tel mode de chauffage ciblé sur les performances catalytiques des catalyseurs.

# Références

[1]     D.S. Su, S. Perathoner, G. Centi, Nanocarbons for the development of advanced catalysts, Chemical Reviews, 113 (2013) 5782-5816.

[2]     J.L. Figueiredo, M.F.R. Pereira, M.M.A. Freitas, J.J.M. Orfao, Modification of the surface chemistry of activated carbons, Carbon, 37 (1999) 1379-1389.

[3]     J.L. Figueiredo, Functionalization of porous carbons for catalytic applications, Journal of Materials Chemistry A, 1 (2013) 9351-9364.

[4]     Y. Zhang, J. Zhang, D.S. Su, Substitutional doping of carbon nanotubes with heteroatoms and their chemical applications, ChemSusChem, 7 (2014) 1240-1250.

[5]     J.L. Figueiredo, M.F.R. Pereira, The role of surface chemistry in catalysis with carbons, Catalysis Today, 150 (2010) 2-7.

[6]     J. Zhang, L. Qu, G. Shi, J. Liu, J. Chen, L. Dai, N, P-codoped carbon networks as efficient metal-free bifunctional catalysts for oxygen reduction and hydrogen evolution reactions, Angewandte Chemie International Edition, 55 (2016) 2230-2234.

[7]     L. Dai, Y. Xue, L. Qu, H.J. Choi, J.B. Baek, Metal-free catalysts for oxygen reduction reaction, Chemical Reviews, 115 (2015) 4823-4892.

[8]     D. Geng, Y. Chen, Y. Chen, Y. Li, R. Li, X. Sun, S. Ye, S. Knights, High oxygen-reduction activity and durability of nitrogen-doped graphene, Energy & Environmental Science, 4 (2011) 760.

[9]     M.J. Ledoux, R. Vieira, C. Pham-Huu, N. Keller, New catalytic phenomena on nanostructured (fibers and tubes) catalysts, Journal of Catalysis, 216 (2003) 333-342.

[10]    K. Gong, F. Du, Z. Xia, M. Durstock, L. Dai, Nitrogen-doped carbon nanotube arrays with high electrocatalytic activity for oxygen reduction, Science, 323 (2009) 760-764.

[11]    X. Wang, X. Li, L. Zhang, Y. Yoon, P.K. Weber, H. Wang, J. Guo, H. Dai, N-doping of graphene through electrothermal reactions with ammonia, Science, 324 (2009) 768-771.

[12]    J. Zhang, X. Liu, R. Blume, A. Zhang, R. Schlögl, D.S. Su, Surface-modified carbon nanotubes catalyze oxidative dehydrogenation of n-butane, Science, 322 (2008) 73-77.

[13]    Z. Tian, C. Liu, Q. Li, J. Hou, Y. Li, S. Ai, Nitrogen- and oxygen-functionalized carbon nanotubes supported Pt-based catalyst for the selective hydrogenation of cinnamaldehyde, Applied Catalysis A: General, 506 (2015) 134-142.

[14]    Y. Wang, Z. Rong, Y. Wang, J. Qu, Ruthenium nanoparticles loaded on functionalized graphene for liquid-phase hydrogenation of fine chemicals: Comparison with carbon nanotube, Journal of Catalysis, 333 (2016) 8-16.

[15]    G. Zhang, Z. Li, H. Zheng, T. Fu, Y. Ju, Y. Wang, Influence of the surface oxygenated groups of activated carbon on preparation of a nano Cu/AC catalyst and heterogeneous catalysis in the oxidative carbonylation of methanol, Applied Catalysis B: Environmental, 179 (2015) 95-105.

[16]    G. Tuci, C. Zafferoni, P. D'Ambrosio, S. Caporali, M. Ceppatelli, A. Rossin, T. Tsoufis, M. Innocenti, G. Giambastiani, Tailoring carbon nanotube N-dopants while designing metal-free electrocatalysts for the oxygen reduction reaction in alkaline medium, ACS Catalysis, 3 (2013) 2108-2111.

[17]    C. Tang, H.F. Wang, X. Chen, B.Q. Li, T.Z. Hou, B. Zhang, Q. Zhang, M.M. Titirici, F. Wei, Topological defects in metal-free nanocarbon for oxygen electrocatalysis, Advanced Materials, 28 (2016) 6845-6851.

[18]    C. Duong-Viet, Y. Liu, H. Ba, L. Truong-Phuoc, W. Baaziz, L. Nguyen-Dinh, J.-M. Nhut, C. Pham-Huu, Carbon nanotubes containing oxygenated decorating defects as metal-free catalyst for selective oxidation of $H_2S$, Applied Catalysis B: Environmental, 191 (2016) 29-41.

[19]    K. Zhou, B. Li, Q. Zhang, J.Q. Huang, G.L. Tian, J.C. Jia, M.Q. Zhao, G.H. Luo, D.S. Su, F. Wei, The catalytic pathways of hydrohalogenation over metal-free nitrogen-doped carbon nanotubes, ChemSusChem, 7 (2014) 723-728.

[20]    L. Feng, Y. Yan, Y. Chen, L. Wang, Nitrogen-doped carbon nanotubes as efficient and durable metal-free cathodic catalysts for oxygen reduction in microbial fuel cells, Energy & Environmental Science, 4 (2011) 1892.

[21]    Y. Liu, H. Ba, D.-L. Nguyen, O. Ersen, T. Romero, S. Zafeiratos, D. Begin, I. Janowska, C. Pham-Huu, Synthesis of porous carbon nanotubes foam composites with a high accessible surface area and tunable porosity, Journal of Materials Chemistry A,

1 (2013) 9508.

[22]    H. Ba, Y. Liu, L. Truong-Phuoc, C. Duong-Viet, J.-M. Nhut, D.L. Nguyen, O. Ersen, G. Tuci, G. Giambastiani, C. Pham-Huu, N-doped food-grade-derived 3D mesoporous foams as metal-free systems for catalysis, ACS Catalysis, 6 (2016) 1408-1419.

[23]    J.J. Delgado, D.S. Su, G. Rebmann, N. Keller, A. Gajovic, R. Schlogl, Immobilized carbon nanofibers as industrial catalyst for ODH reactions, Journal of Catalysis, 244 (2006) 126-129.

[24]    C. Mu, K. Huang, T. Cheng, H. Wang, H. Yu, F. Peng, Ni foams decorated with carbon nanotubes as catalytic stirrers for aerobic oxidation of cumene, Chemical Engineering Journal, 306 (2016) 806-815.

[25]    R. Vieira, M.J. Ledoux, C. Pham-Huu, Synthesis and characterisation of carbon nanofibres with macroscopic shaping formed by catalytic decomposition of $C_2H_6/H_2$ over nickel catalyst, Applied Catalysis A: General, 274 (2004) 1-8.

[26]    S. Zhao, H. Yin, L. Du, G. Yin, Z. Tang, S. Liu, Three dimensional N-doped graphene/PtRu nanoparticle hybrids as high performance anode for direct methanol fuel cells, Journal of Materials Chemistry A, 2 (2014) 3719.

[27]    E. Frank, L.M. Steudle, D. Ingildeev, J.M. Spörl, M.R. Buchmeiser, Carbon fibers: Precursor systems, processing, structure, and properties, Angewandte Chemie International Edition, 53 (2014) 5262-5298.

*Résumé Abstract*

# Chapter 1


## Introduction

# Introduction

## 1. Carbon materials for catalytic applications

Carbon material (CM) is a general term used to indicate the broad range of carbonaceous components having tailored physico-chemical properties, such as active carbon (AC), carbon nanotubes/fibers (CNTs/CNFs) and graphene [1, 2]. Nowadays, CMs are facing an increasing number of applications in catalysis, either as supports or directly as metal-free catalysts on their own [3, 4]. These CMs are generally operated in two forms, i.e. powder and structured, depending to the downstream applications. For liquid-phase reaction the powdered form is preferred as it provides high contact surface area while for gas-phase reaction, the structured form is the most used for reducing pressure drop across the catalyst bed. However, structured catalysts have received an increasing interest even for liquid-phase reactions as it allows the easy recovery of the catalyst and to avoid filtration step which is time and energy consuming step. The physico-chemical properties of these CMs, especially the tailored pore structure and surface chemistry, i.e. surface functionalization or doping, can be tailored at will to fulfill the requirements of the downstream catalytic processes and led to the development of new catalysts with improved catalytic performance [5-12].

### 1.1 Carbon material as support

As support, CMs offer large surface area and tunable porosity for the dispersion of active metal phases while their high thermal conductivity allows the avoidance of gradient temperature or hot spot formation within the catalyst bed reducing in such a way by-products. Their high electrical conductivity also allows them to be extensively employed as either support or metal-free catalyst in the field of electrocatalysis. The electrical conductivity of these CMs could also be used for heating up the carbon-based catalysts by a noncontact heating mode, i.e. electromagnetic induction heating [13, 14], which could provide targeted heat into the catalyst as well as extremely fast reaction temperature regulation thanks to the high heating rate, i.e. several hundred degrees per minutes. Compared with the traditional metal oxide carrier, they are more stable in both acidic and basic media, thereby expanding

the range of the reaction medium when using carbon supported catalysts. At present CMs are more widely used to support noble metals, because in addition to the different advantages cites above they also provide an easy method to recover the expensive metals by burning away the carbon support, once the catalyst becomes deactivated [15-20].

Moreover, CMs surface reactivity can be extensively modified by introducing rich functional groups (including oxygen-, nitrogen- and sulfur-containing groups, etc.) or structural defects sites [21, 22], which can play the role of anchoring sites, for the active components or their precursors in the catalyst preparation, and thus enhance the dispersion and stability of active sites during the reaction or directly as metal-free catalyst through the intermediate of oxygenated functional groups decorated defect sites [23, 24]. Luo et al. [25] developed green ozone/$H_2O$ treatment to prepare surface functionalized and defect enriched carbon nanotubes (oCNT). The abundant oxygen functional groups and surface structural defects can efficiently capture Au nanoparticles (NPs) in a colloidal solution. The Au/oCNT, after thermal treatment at 300 $^{o}$C, still remains well dispersed thanks to the existence of strong interaction with the defect sites on the oCNT. The as-prepared catalyst displays a remarkable catalytic performance for the oxidative self-coupling of benzylamine to imine in solvent free conditions.

Besides the functional groups, generally oxygenated functional groups, grafted on the surface of CMs, the heteroatoms (such N and S) dopant can also improve the dispersion and stability of supported metal NPs through the strong metal-support interaction (SMSI). The dopant also introduces change on the basicity or acidity of the CMs surface which could in turn modify the active phase dispersion and/or catalytic reactivity [26-28]. Jiang et al. [29] reported a synthesis of mesoporous carbon nitride (MCN) with high N content (up to 18.5 wt%) which can be efficiently used as support for highly dispersed Pd NPs with well-controlled particle size distribution through the strong interaction between N and Pd. The as-synthesized MCN supported Pd catalyst shows an enhanced activity in selective hydrogenation of aromatic carboxylic acids.

Meanwhile, the carbon support decorated with the functional groups or heteroatom dopants have different interaction strength with the active metal NPs. Shi et al. [30] prepared

the surface-modified carbon nanotubes by oxygenated groups and N heteroatoms for using as support for dispersing Pt nanoparticles. Both oxygenated groups and nitrogen-doped species are at the origin of the high dispersion of Pt NPs on the surface-modified CNTs. On the other hand, the Pt NPs on the N-doped carbon support can be effectively stabilized under thermal and electrochemical conditions through the strong metal-support interaction via N heteroatoms and thus, preventing deactivation through active phase sintering.

The functionalized CMs as catalyst support not only enhance the dispersion and stability of metal NPs by SMSI, but also affect the catalytic activity and selectivity through the electronic metal-support interactions (EMSI). Higgins et al. [31] used a thermal shock/quench anneal process to synthesize sulfur-doped graphene (SG) for being used as support for Pt nanoparticles. The Pt/SG catalyst displays better oxygen reduction reaction (ORR) activity than commercial Pt/C and Pt-graphene, as well as outstanding electrochemical stability. The computational simulations highlight that the interactions between Pt and graphene are enhanced significantly by sulfur doping, which lead to the outstanding electrochemical stability. Importantly, the sulfur dopants modulate the electronic properties of Pt, bringing about a downshift of the platinum d-band center which results in the excellent ORR activity.

In addition, the EMSI effects such as charge transfer between the metal and carbon scaffold can be modified by the controllable functionalization process. Rao et al. [32] demonstrated that the use of simple thermal treatment of CNTs support decorated with oxygenated groups can tune the charge distribution at palladium-carbon interface. This fine turning of electronic structure of the catalytic centers in carbon supported Pd, which generates the electron depletion of the metal active phase and the up-shift of d band center of Pd, can improve the selectivity of C=C bond hydrogenation of cinnamaldehyde.

## 1.2 Carbon-based metal-free catalysts

Carbon materials can be also directly used as catalysts, i.e. metal-free catalysts, in numerous catalytic processes [1, 7, 33-36]. When acting as catalysts on their own, their metal-free nature essentially prevents the catalyst deactivation from the sintering and

aggregation of active metal species as encountered on supported metal catalysts. The acid and alkali resistance of CMs also allows them to be operated in a non-neutral reaction medium where supported metal catalysts cannot be used due to the corrosion of the metal active phase.

**Table 1.** Representative reactions catalyzed by metal-free carbonaceous materials.

| Catalyzed reactions | Probable active sites | References. |
|---|---|---|
| Oxidative dehydrogenation of ethylbenzene | Quinones | [37-40] |
| Oxidative dehydrogenation of propane | Quinones | [41-43] |
| Oxidative dehydrogenation of butane | Quinones | [12, 44] |
| Direct dehydrogenation of ethylbenzene | Quinones | [45-48] |
| Direct dehydrogenation of propane | Quinones | [49] |
| Oxidation of alcohols to aldehydes/ketones | Quinones | [50] |
| NO oxidation | Basic sites | [51, 52] |
| $SO_2$ oxidation | Basic sites | [53] |
| $H_2S$ oxidation | Basic sites | [54-57] |
| $NO_x$ reduction | Basic sites | [58, 59] |
| Alcoholysis of epoxides | Sulfonic acid groups | [60] |
| Esterification | Sulfonic acid groups | [61] |
| Acylation | Sulfonic acid groups | [62] |
| Alkylation | Sulfonic acid groups | [63] |
| Acetalization | Sulfonic acid groups | [64] |
| Oxygen reduction reaction | Electronic structure | [6, 26, 65] |
| Hydrogen evolution reaction | Electronic structure | [66] |
| Oxygen evolution reaction | Electronic structure | [67] |

The structural defects decorated with abundant functional groups as well as heteroatom dopant formed on the surface of functionalized CMs can be the active sites for

specific catalytic reactions [55, 67-70]. The different catalytic processes which involved carbon-based metal-free catalysts are summarized in Table 1. Liu et al. [56] synthesize a macroscopic composite consisting of nitrogen-doped carbon fibers (N@CFs) by electrospinning. The as-prepared N@CF material, after a carbonization step, can be used as metal-free catalyst in the selective catalytic oxidation of $H_2S$ to elemental sulfur, and the desulfurization performance of such metal-free catalyst is two times higher than that of the most active metal-based catalyst ($Fe_2O_3$/SiC).

However, the qualitative and quantitative analysis of the nature of the active sites involved in carbon-based metal-free catalyst still remain an issue to be solved due to the existence of various kinds of functionalized groups and heteroatom dopants compared to supported metal catalyst with well defined structure. In addition, the synthesis of specific functional/doping groups remains difficult due to the complex synthesis process. Due to such reasons a rational design of specific metal-free catalyst for optimization of the catalytic performance remains an issue. Qi et al. [37, 38] identified and quantified the different active sites of metal-free nanocarbon for oxidative dehydrogenation (ODH) of ethylbenzene by chemical titration (Figure 1). It is reported that the active sites for carbon catalysis in ODH reactions are carbonyl groups as the ODH catalytic activity of oxidized CNTs is directly correlated with the surface concentration of ketonic carbonyl groups on CNTs. The correlation of the ODH activity and the ketonic concentration allows one to get access to the intrinsic catalytic performance of such carbon-based metal-free catalyst.
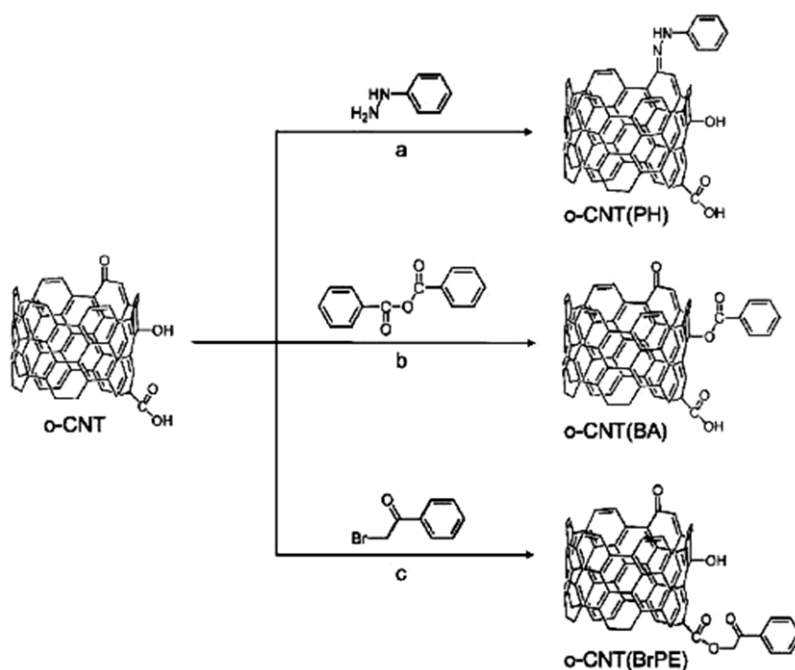
**Figrue 1.** The selective titration methods for (a) ketonic carbonyl, (b) phenol and (c) carboxylic acid groups on CNTs [37].

## 1.3 Comparison of powdery and structured carbon materials

Most of the carbon materials reported in the literature today, such as active carbon, ordered mesoporous carbon, carbon nanotubes/nanofibers and graphene, are mostly in the form of powder. These powdered carbon-based metal supported catalysts are mostly being used in liquid-phase reactions which displaying a maximum contact surface with the reaction medium. However, these powdered CMs are very difficult to handle for the practical catalytic application and also for the catalyst recovery as high performance filtration step is required to deal with such powdered matter recovery [71]. In addition, powdered catalysts cannot be efficiently used in the gas-phase reaction due to the generation of large pressure drop across the catalyst bed leading to erratic fluid distribution and uncontrolled side-reactions along with large energy consumption (Figure 2). In the liquid-phase reaction, it is troublesome for the separation process of the samples with powder form and the liquid product after the completion of reaction. The filtration step encountered is energy and time consuming and catalyst recovery is not complete even with high performant filter devices. Meanwhile the

vigorous mixing with impellers during the process will result in the inevitable mechanical collision of powder in the liquid medium, leading to the abrasion of catalysts with fine formation along with active phase loss inside the reaction medium, which further exacerbates the difficulty of separation as described above. Moreover, the powdery CMs, especially the one with nano- and sub-micron size, could also induce chronic respiratory damage to the operators in the absence of any protection means and will also pose problems for the handling and transportation.
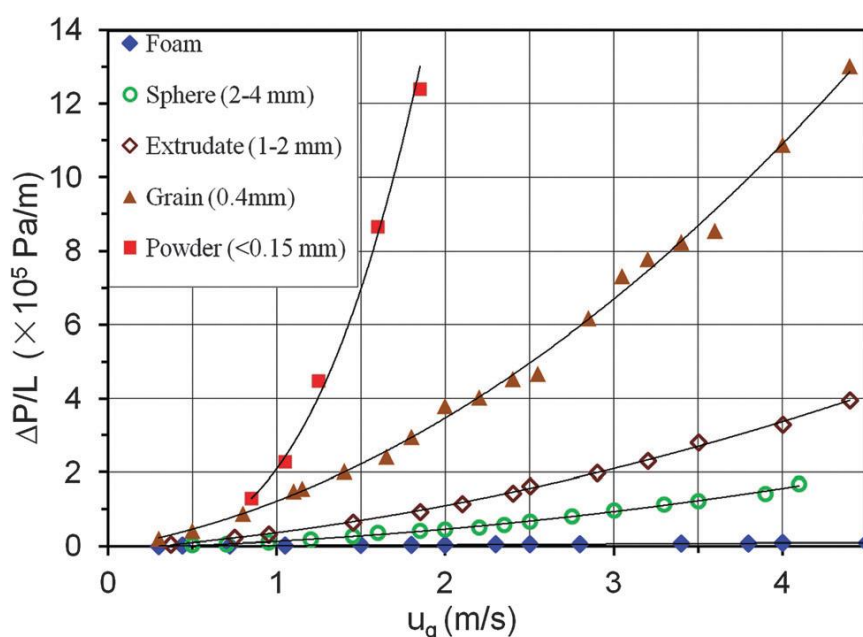


**Figure 2.** Pressure drop measurements as a function of linear gaseous velocities on the various macroscopic catalyst supports with different shapes [46].

The employment of structured carbon materials can address these above mentioned issues linked with the use of nanocarbons-based materials in catalysis. Such structured carbon-based composites display low pressure drop across the catalyst bed for gas-phase operation, easy transport and handling along with facilities for recovery, especially in the case of liquid-phase reactions, and also high accessibility of the metal or metal-free active phase, when used as catalyst support or as direct carbon metal-free catalyst. In addition, these

structured carbon-based catalyst support or metal-free catalyst can be finely tuned, i.e. pore volume and pore size, dimension, exclusive metal-free active phase coating, depending to the downstream applications. Structured catalysts also reduce the sojourn time of the intermediate product and thus significantly improve the selectivity of the process.

There are some common strategies for the fabrication of structured carbon. One method is to cross-link the powdered pre-existing carbon nanomaterials, such as carbon nanotubes (CNTs) and/or few-layer graphene (FLG), into different macroscopic shapes after the carbonization of polymerized binder. Liu et al. [72] developed a low temperature chemical fusion (LTCF) method to synthesize the self-macronized carbon nanotubes foam (CNT-foam) with controlled size and shape. In this process CNT is used as a carbon skeleton to a macroscopic final support. The CNTs was physically mixed with dextrose (carbon source), citric acid (carboxyl group donor reacting with the hydroxyl groups present in dextrose for the pre-polymerization process) and ammonium carbonate (as pore former). The mixture was submitted to different thermal treatment processes to generate a so-called CNTs foam carbon-based structured metal-free catalyst (Figure 3A). The 3D pore structure and the pore size distribution of the final structured material can be finely tuned by modifying the concentration of the ammonium carbonate used as pore former. As shown in Figure 3B and C, these CNT-foams are further successfully used for selective removal of organic compounds in the field of wastewater treatment. The organic compounds were recycled by distillation process and the adsorbent displays a high stability as a function of adsorption/recovery cycles.
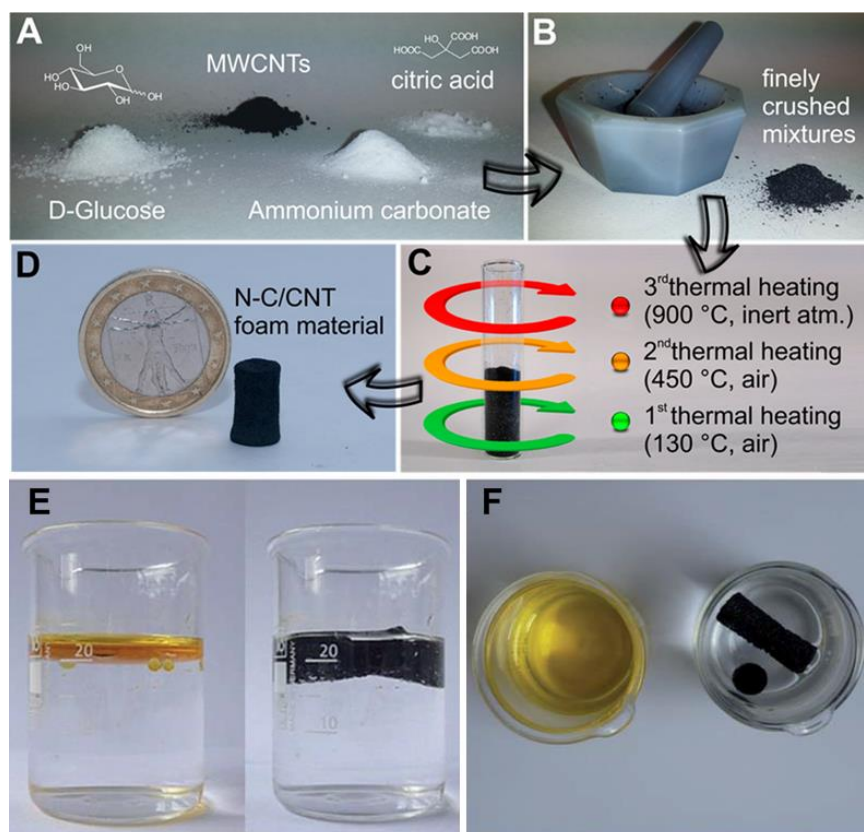
**Figure 3.** (A-D) Illustration of a low temperature chemical fusion (LTCF) method for the synthesis of porous CNT-foam composites [47], and (E and F) photographs showing adsorption of toluene by the CNT-foam. The toluene was colored with ferrocene for sake of clarity [72].

The same synthesis method has been reported by Ba et al. [47] for the synthesis of nitrogen-doped carbon foam which will be used as metal-free catalyst in several catalytic processes. The N-doped carbon phase grown around intertwined carbon nanotubes network and displays a relatively high porosity for the access of the reactant. The easy control of the 3D shape of the final material, by adjusting the amount of ammonium carbonate as pore former, makes it more efficient for being used as metal-free catalyst in gas-phase processes with respect to the classical N-doped CNT powder where high pressure drop and difficulties of transport and handling are the main issues. This 3D metal-free carbon composite displays excellent catalytic performance in both liquid-phase electrochemical oxygen reduction reaction (ORR) and gas-phase direct, steam-free dehydrogenation (DDH) of ethylbenzene to

styrene.

Another way to construct three-dimensional hierarchical architecture composites is based on the in situ growth of nanocarbon, either pure or doped with heteroelements, on the macroscopic substrate material with a regular structure [39].

Shen et al. [73] reported a facile strategy (Figure 4) to fabricate 3D hierarchical architectures consisting of vertically aligned carbon nanofibers (CNFs) arrays anchored to macroscopic graphite felt (GF) supports. The physicochemical properties of CNF@GF monoliths including pore structures, surface areas, porosities and densities could be conveniently tuned by varying the synthesis parameters of the chemical vapor deposition (CVD) method. The resulting CNF@GF monoliths was successfully used as advanced sorbents in the removal of various pollutants including oils, $Pb^{2+}$, organic solvents and Congo red from aqueous solutions.
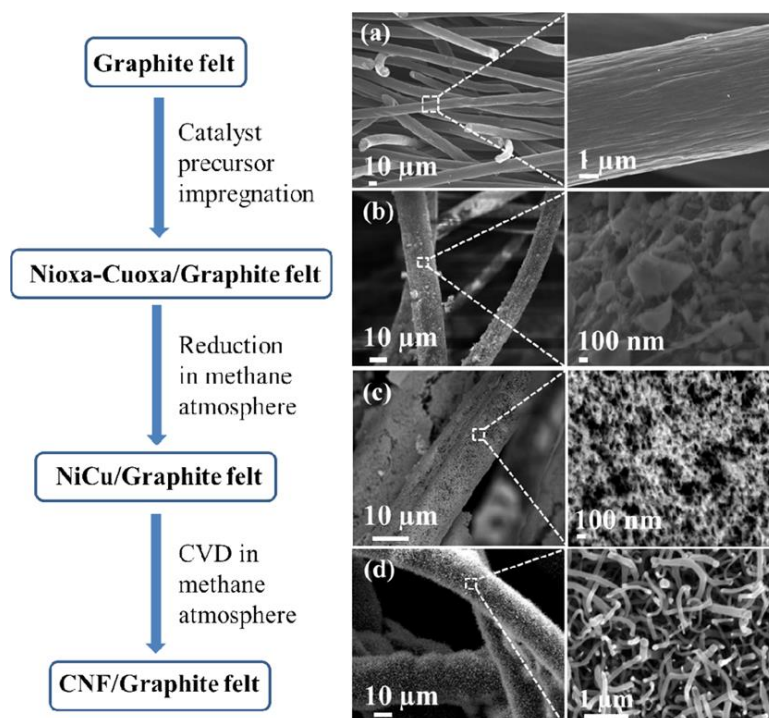


**Figure 4.** Procedures of preparation of 3D hierarchical CNF@GF composite and the corresponding FESEM micrographs of the samples at different stages [73].

Duong-Viet et al. [74] reported the synthesis of hierarchical metal-free catalyst composed of the nitrogen-doped carbon nanotubes decorated silicon carbide (N-CNTs/SiC) macroscopic host structure by the CVD method. The N-CNTs were synthesized using Fe as growth catalyst and $C_2H_6/NH_3/H_2$ as gaseous reactants. The N-CNTs/SiC can be synthesized on different kind of macroscopic host structure, i.e. pellets, foam, which allows it to be efficiently used as metal-free catalyst in fixed-bed configuration in industrial reactors (Figure 5) and to reduce the problems linked with catalyst transportation, handling and pressure drop across the catalyst bed as encountered with nanoscopic carbon-based catalyst. The as-synthesized hierarchical composite displays a high effective surface area along with a short diffusion length associated with the nanoscopic dimension of CNTs in N-CNTs/SiC. The N-CNTs/SiC metal-free catalyst displays a high catalytic performance in the selective oxidation of $H_2S$ into elemental sulfur in a fixed-bed reactor compared to that obtained on a $Fe_2O_3/SiC$ catalyst. .
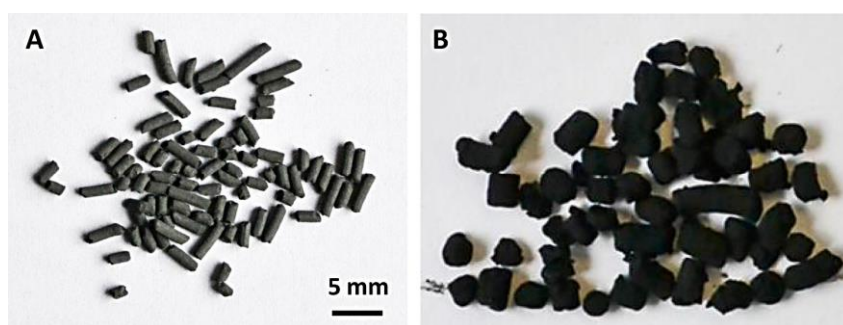


**Figure 5.** Digital photos of the SiC before (A) and after (B) N-CNT loading carried out at 750$^o$C showing the significant increase of the apparent volume of the catalyst due to the formation of a high surface-to-volume N-CNTs [74].

Viera et al. [75] used the macroscopic graphite felt with different sizes and shapes as carbon material host structure for the synthesis of hierarchical carbon-based composites. After the deposition of nickel on the macroscopic support, the carbon nanofibers (CNFs) are successfully synthesized by CVD method using a mixture of $C_2H_6$ and $H_2$. The metal loading ($\leq$ 1wt.%) is chosen to be high enough for the production of a relatively large amount of

CNFs and low enough to avoid the need for further purification.
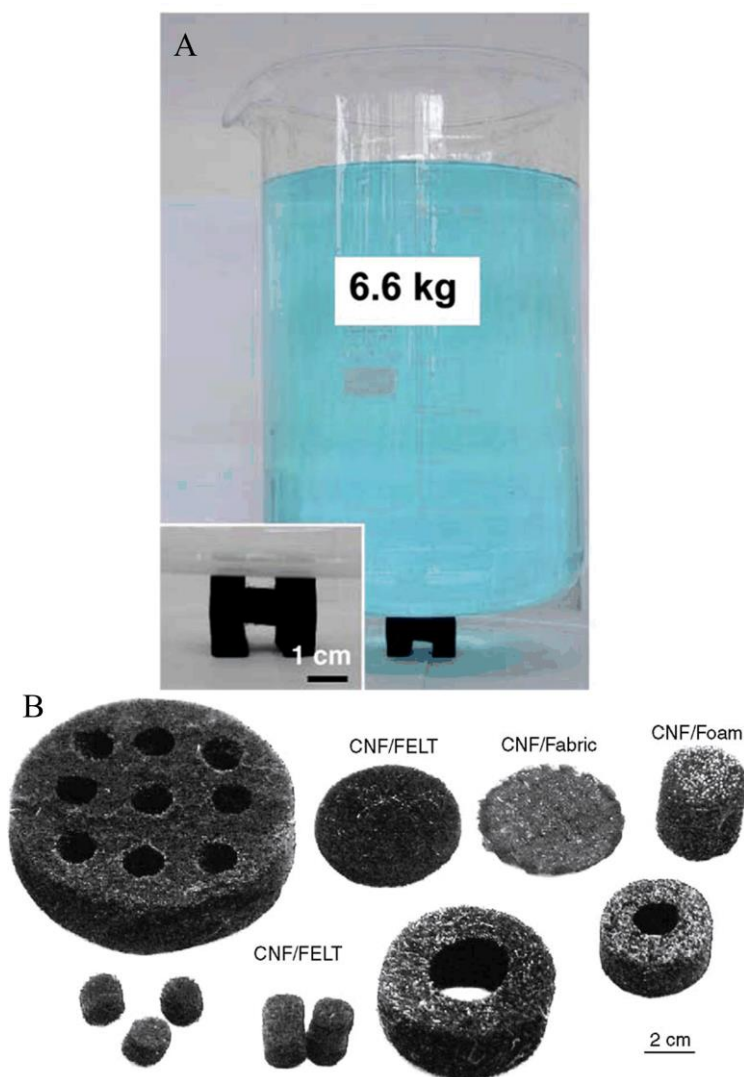


**Figure 6.** (A) Photos showing that a carbon nanofibers composite formed form an ex-graphite felt can withstand a load of about 2,300 times its own weight without breaking [76], and (B) CNFs/GF composite with different macroscopic shapes, sizes and microstructures synthesized by CVD on Ni/GF and $C_2H_6/H_2$ mixture [75].

In addition, it is worthy to note that at the end of the synthesis process, the Ni particles are completely encapsulated by the CNFs or some amorphous carbon layers and thus, are not accessible in the further catalytic uses of the macroscopic composites. The formation of CNFs not only increases the surface area of the composite but also enhances it mechanical resistance

(Figure 6A) when compared to the pristine macroscopic graphite felt [76]. As displayed in Figure 6B, CNFs/GF composite with different macroscopic shapes, sizes and microstructures are obtained, rendering the more reliable applications of these materials in the conventional catalytic processes.

By using the same synthesis method, macroscopic carbon host structure decorated with active species could also be prepared for the potential use as a catalytic stirrer in liquid-phase reactions. Mu et al. [77] prepared a structured CNT-based catalyst composed of the in situ grown CNTs on Ni foam using CVD method. In the synthesis process, firstly, the Ni foam coated with desired amount of porous $Al_2O_3$ barrier layers was prepared by successive immersion-drying-calcination procedure. The porous $Al_2O_3$ layers could facilitate the formation of Ni nanoparticles, which acting as catalyst for the CNT growth in the next CVD process. Furthermore, the oxide layer could also shield the Ni foam from the access to the reactants during the liquid phase reaction. As shown in Figure 7, the resulting structured $CNT/Al_2O_3/Ni$ foams can be used as metal-free catalyst and as mechanical stirrer in a rotating foam stirrer reactor (RFSR) for the aerobic oxidation reaction of cumene to cumene hydroperoxide. The catalytic stirrer performs higher conversion of cumene compared with the commercial CNT in a slurry reactor which could be due to the high mixing of the reactant on the catalyst surface through stirring. The cycling tests, carried out for 5 times, indicated that the catalyst retains its catalytic performance which confirms it relatively high stability.
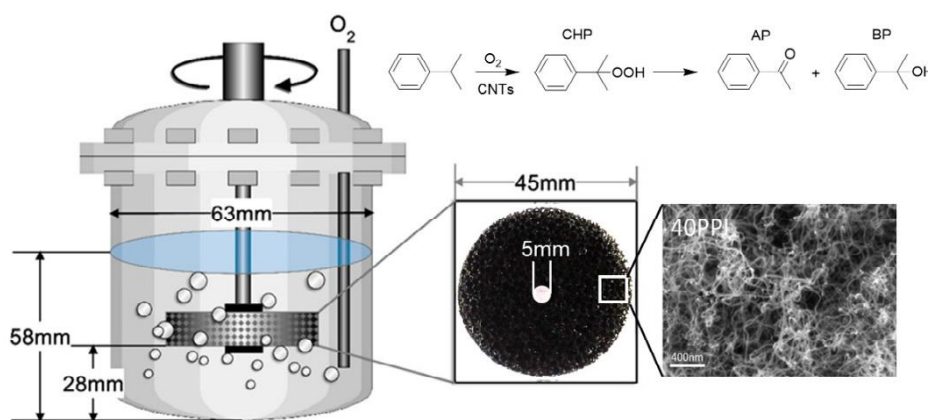


**Figure 7.** Sketch of $CNT/Al_2O_3/Ni$ foams as a catalytic stirrer in rotating foam stirrer reactor for the oxidation reaction of cumene [77].

However, it is worthy to note that during the CVD synthesis, the grown nanocarbon will gradually fill-up the interior space of the monolith support which ultimately led to the breakage of the host matrix structure or to the reduction of the reactant accessibility. Therefore, there is an upper limit on the amount of nanocarbon which can be deposited onto the macroscopic host structure. Meanwhile, the interaction between nanocarbon and support and the interface between them are still not well investigated which could represent a critical factor in the control of the electrical and thermal conductivity of the final composites.

Another strategy is to fabricate free-standing carbon aerogels without using any host matrix. Zhao et al. [78] synthesized a three-dimensional (3D) N-doped graphene aerogel with porous structures for supporting PtRu nanoparticles (N-GA/PtRu). This N-GA/PtRu hybrid displays high catalytic performance when it is used as the anode for direct methanol fuel cells. In the synthesis of N-doped graphene aerogel (N-GA) with 3D architectures, the graphene oxides aqueous solution was mixed with $NH_3 \cdot H_2O$ firstly, after the formation of N-doped graphene by heating the mixture solution at 180 $^{o}$C for 12 h, the dialyzed products with ultrapure water were subjected to freeze-drying at -53 $^{o}$C and -30 Pa for 12 h to generate 3D N-GA.

Yang et al. [79] prepared melamine formaldehyde polymer (PMF) aerogels based on lignin particle-stabilized Pickering oil-in-water high internal phase emulsions. After the pyrolysis at high temperature under nitrogen, the PMF aerogels were converted into the nitrogen-rich carbon (NRC) aerogels with highly porous structure and excellent fire-resistant property (Figure 8). The NRC aerogels exhibit high efficient separation of oils and organic pollutants from wastewater.
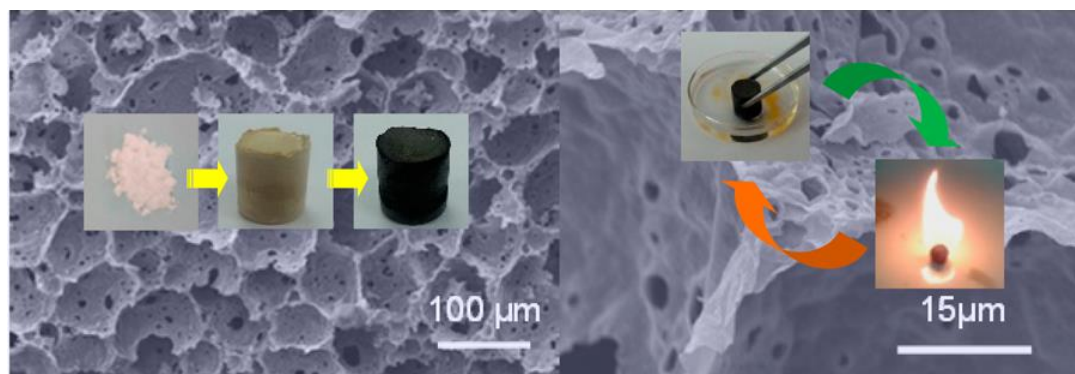
**Figure 8.** Nitrogen-rich and fire-resistant carbon aerogels for the removal of oil contaminants from water [79].

In conclusion, hierarchical nanocarbon decorated macroscopic host structure composites can be produced through different synthesis methods to provide catalyst support or catalyst with controlled macroscopic shapes for industrial applications. These hierarchical composites display relatively high mechanical resistance, high electrical and thermal conductivity and tunable porosity for numerous downstream applications. However, the synthesis of these hierarchical composites is not straightforward, requiring high temperature or complicated chemical steps, and also generates waste or by-products which call for tedious post-synthesis treatment. It is of interest to find new method to produce hierarchical carbon-based catalyst support or catalyst using a much simple synthesis process. Among the different candidates commercial carbon/graphite felt could be regarded as alternative pristine materials which could fulfill the requirements described above and to be used in place of nanocarbon/host matrix composites in several catalytic processes.

## 1.4 Carbon/graphite felt

Commercial carbon/graphite felt (CF/GF) is a hierarchical structure made of carbon microfilamentous fiber (Figure 9). Generally, there are two types of precursors which are most commonly used for CF/GF manufacture, i.e. polyacrylonitrile (PAN) and rayon [80]. Felt materials are prepared by the thermal treatment of carbon precursors to remove organic and volatile compounds leaving behind solid carbon with different porosity and specific surface area. Graphite felt is derived from carbon felt after an additional graphitization at a high

temperature under vacuum or an inert atmosphere. The processing temperature is around 1200-1600 $^{o}$C for CF and 2000-2600 $^{o}$C for GF. The CF and GF display a similar morphology and microstructure as depicted in Figure 9 and 10 and the only difference resides in the lower specific surface area and porosity along with a higher oxidative resistance for the GF compared to the CF which is consecutive to a high temperature annealing.
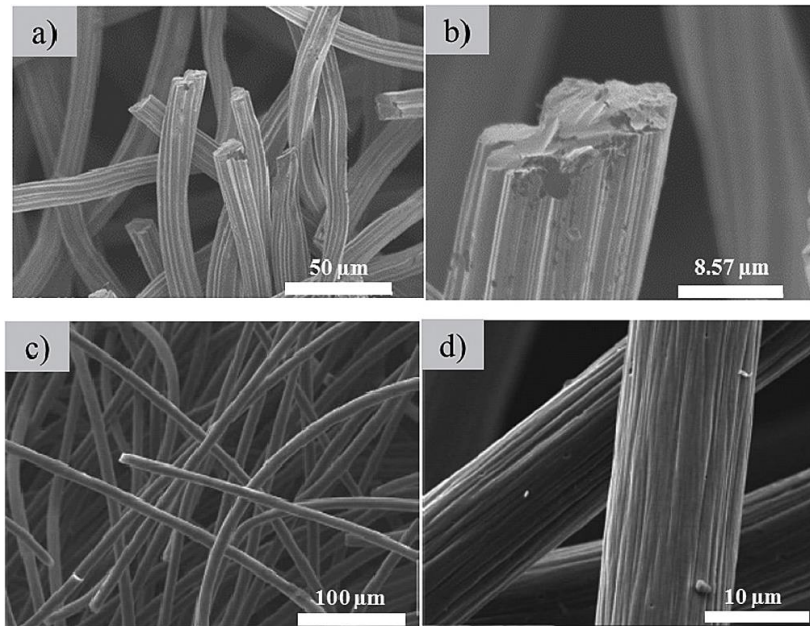


**Figure 9.** SEM images of (a, b) CF (Johnson Matthey Co., Germany, thickness 1.27 cm) and (c, d) GF (GFD 2.5, SGL Group, thickness 2.8 mm) at various magnifications [81-83].
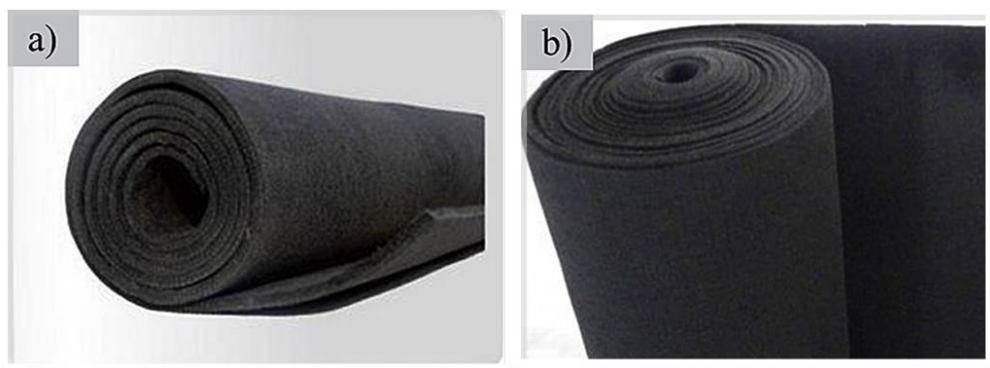


**Figure 10.** Typical shape of commercial (a) CF and (b) GF (Product information from CeraMaterials) [82, 84].

The GF is frequently used as insulator wall for industrial high-temperature furnaces thanks to its high thermal resistance and easy shaping to cope with the application. The high voidage of the material with low thermal propagation also acting as temperature shield, between the inner part of the furnace and it walls, for such application.

Carbon and graphite felts are also commonly used as electrode backings in a variety of redox flow batteries (RFBs) designs including vanadium redox flow batteries (VRFBs) and wastewater treatment by electro-chemical advanced oxidation processes (EAOPs) [82]. The high conductivity, high purity, high effective surface area and porosity able to provide abundant redox reaction sites, relatively low cost, and chemical resistance of felts make them ideal for the demanding design criteria of flow battery developers [85]. However, carbon and graphite felt have some disadvantages which are linked to their inadequate wettability and electrochemical activity in aqueous solutions due to their hydrophobic surface nature (as shown in Figure 11) and poor kinetics for reduction and oxidation reactions. These partly decline the performance of pristine CF/GF when they are applied as electrodes.
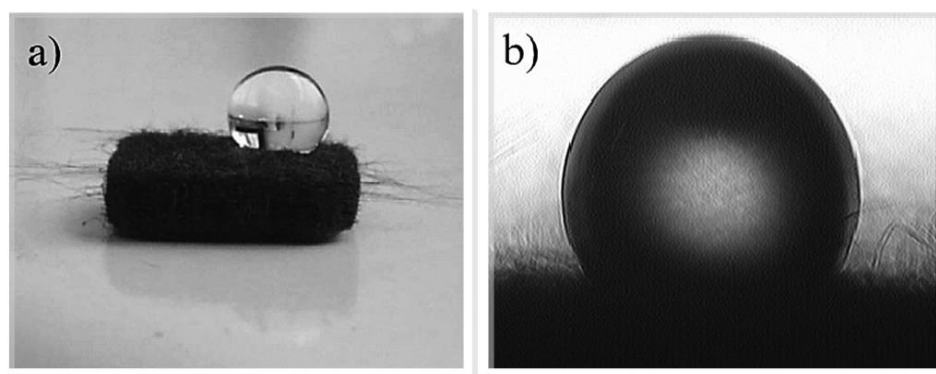


**Figure 11.** Shape of water droplet on (a) GF (SGL GFD2.5, thickness 2.8 mm) and (b) CF (Johnson Matthey Co., Germany, thickness 1.27 cm) confirming the high hydrophobicity character of the materials [81, 82, 86].

Several modification processes operated under various conditions have been employed to make the CF/GF electrodes more active. Zhang et al. [87] reported a simple and effective

method to activate graphite felt by using KOH as chemical etching agent. The KOH etched GF was studied as electrode for vanadium flow battery (VFB). After the etching treatment, the micropores and oxygen-containing functional groups generated on the GF improve the wettability and the electrolyte accessibility, resulting in the better electrochemical activity and VFB performance.

He et al. [88] developed a novel method to modify the graphite felt by combination of etching by HF and oxidation by $H_2O_2$ (Figure 12). After the surface etching from HF and the introduction of oxygen-containing functional groups from oxidation process in the presence of $H_2O_2$, the mass transfer and electrode process can be improved significantly on the surface of GF. The treated GF sample demonstrated enhanced electrochemical performance and improved energy storage for the vanadium flow redox battery.
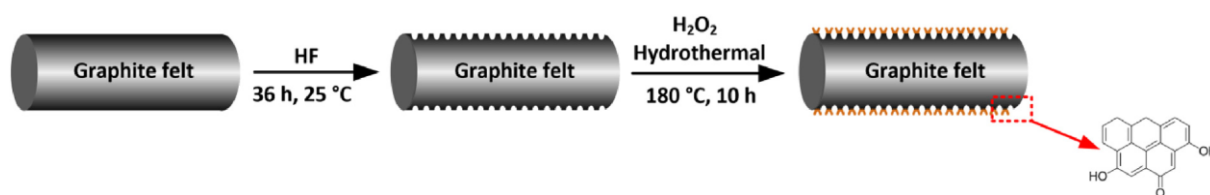


**Figure 12.** Schematic representation of the modification procedure of HF/$H_2O_2$ treatment for graphite felt [88].

Wu et al. [89] used hydrothermal ammoniated treatment to modify the polyacrlonitrile-base graphite felt for vanadium redox flow battery. The GF was treated for different time at 180 $^{o}$C, while the content of nitrogen from nitrogenous groups in the GF reached 5.3% by adjusting treatment time to 15 h in ammonia solution. The increase in the concentration of polar nitrogenous groups on the surface of GF, which facilitated charge transfer between electrode and vanadium ions, might account for the improvement of the electrochemical properties for the treated graphite felt.

Interestingly, although carbon and graphite felt have drown much more attention as electrode used in the electrochemical applications, there are very few reports on their catalytic

applications. It is expected that the advantages of these chemical treated carbon felt materials relevant to high porosity, conductivity, low price and high surface area as well as variety of active sites including functional groups and heteroatoms dopants, not only contribute to the improvement of their electrochemical performance, but could also make them good candidates in the field of catalysis.

## 2. Physico-chemical surface properties of carbon

In catalysis, most reactions occur at the surface of the catalyst where reactants are adsorbed. Therefore, the physico-chemical surface properties of carbon materials (CMs) are essential whether they play the role as the metal-free catalyst or as the catalyst support in catalysis. The physico-chemical surface properties of the carbon-based materials are closely related to the functionalization, porous structure and defects formed on the surface of CMs.

The surface functionalization of carbon materials including the grafting of functional groups on the surface, i.e. mostly oxygenated groups, or heteroatoms doped into the carbon framework, i.e. N, S, P, will introduce not only the anchoring sites for metal nanoparticles on carbon supported metal catalysts but also as active centers for performing catalytic reactions in the metal-free carbon-based catalytic processes [90-96]. The porous structure of CMs also seriously affects their catalytic performance. The high surface area which has been generated through chemical activation process would increase the dispersion of active sites and also to stabilize these later again sintering process during the course of the reaction. It is also worthy to note that the interactions between the carbon surface and the metal active phase is mostly constituted by electrostatic or weak interactions and not through chemical interactions like those usually observed for alumina and other oxide supports. Such interactions are relatively low and thus, prevent the formation of chemical stable phases, during the intermediate thermal treatment to convert the metal precursor into it corresponding active phase, which cannot be further reduced leading to lower catalytic performance. The uniformly ordered mesoporous pore structure would also improve the thermal stability of metal NPs with resistance to sintering and aggregation through the confinement effect of the support [97]. Moreover, the conversion and selectivity of the catalytic reaction could be changed by the

modification of the support pore size, which would affect the adsorption and desorption as well as the diffusion of the reactive molecules which contributes to the reduction of secondary reaction at the origin of selectivity lost [20]. The structural defects would lead to the charge redistribution on the carbon, thereby making the defect sites and their periphery more likely to participate in the reaction by interacting with the reactant molecules. In summary, carbon-based materials are belonging to the class of non-innocent support which actively participates to the stabilization of the supported active phase.

## 2.1 Surface functionalization: functional groups grafting and heteroatoms doping

Although carbon materials, i.e. felt structure, have been demonstrated to have many beneficial characteristics for catalysis, the application of the pristine carbon without any modification still remains constrained due to its shortcoming, such as the inert surface which leads to a poor interaction with the deposited metal active phase [98]. Indeed, in case of using pristine CF/GF support the inert surface of CMs would form the weak interactions with the metal NPs [99], which leads to sintering and/or aggregation of them under reaction conditions, or leaching in the liquid-phase reactions, all of these shortcomings contribute to the shortening of the catalyst lifetime. Besides, the non-activated carbon materials could not be used directly as catalysts due to the lack of active centers for adsorbing the reactants. As a consequence, the surface functionalization of carbon materials, by grafting functional groups on the surface or doping the carbon matrix with heteroatoms is of high interest for the downstream applications. Such processes are mostly developed for nanocarbons materials, i.e. carbon nanofibers/nanotubes and/or graphene and few-layer graphene, while they remain scarcely investigated for hierarchical carbon-based structures such as carbon or graphite felt.

### 2.1.1 Functional groups incorporation and heteroatom dopants

The commonly used functional groups include a series of oxygen-containing functional groups, amino groups and sulfhydryl groups at the edges of the graphene layers and in basal plane defects [5]. Figure 13 depicts the different oxygenated groups which can be incorporated on carbon surface, including the carboxylic acids, anhydrides, lactones, phenols

and carbonyl groups. The familiar nitrogen-containing functional groups are primary amine ($-NH_2$) and secondary amine (-NH-). For the S-doped carbon composites in addition to the sulfhydryl groups (-SH) which is present in large amount, other sulfur-containing functional groups also include oxidized sulfur species ($-SO_x$ and $-SO_3H$).

The heteroatom dopants in carbon network are mostly nitrogen and sulfur heteroatoms, which can be directly incorporated in place of the carbon atom inside the graphite network, have received special interests because they induce a significant modification of the carbon surface properties, i.e. basicity or acidity, and also to generate strong interactions with metal nanoparticles which provide high dispersion and stabilization of the latter during the reaction process. As shown in Figure 13, several nitrogen dopants are present including pyridinic N, pyrrolic N, oxidized nitrogen, and the quaternary/graphitic N which strongly contribute to the modification of the basicity of the resulting carbon surface. The sulfur doping is mainly localized at the edges and defects of graphene in the form of thiophene-like structures (-C-S-C-).
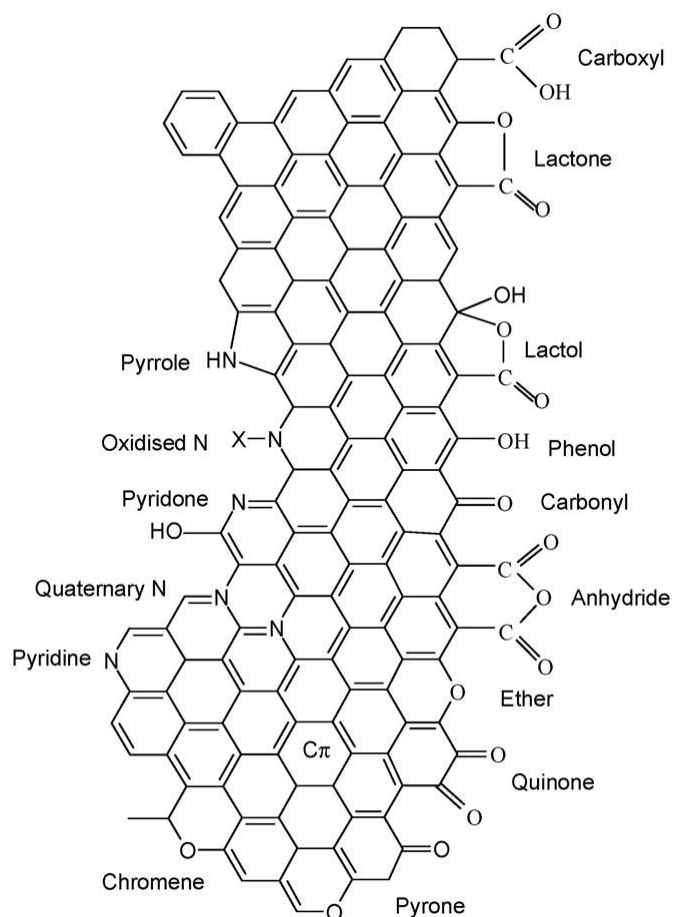
**Figure 13.** Oxygen functionalization and nitrogen doping species in the graphite matrix [5].

**2.1.2 Strategies to modify the surface chemistry of carbon materials**

The oxygen-containing functional groups, amino groups and sulfhydryl groups, could be introduced from a series of post-treating processes based on oxidation, amination or thiolation of the pristine carbon materials, respectively [100-102]. The nitrogen and sulfur doping into graphene structure is mostly achieved through the one-pot synthesis process in the presene of the corresponding heteroatom precursors or the subsequent heat treatment of pristine undoped CMs in the presence of reagents containing N and S atoms [65, 103-105]. In some cases, the pristine carbon can be oxidized first followed by the reaction with N- or S-precursor to achieve multiple doping. The oxygenated functional groups also actively participated in the exchange with the N- or S- dopant.

2.1.2.1 Oxidation

The introduction of the oxygenated functional groups has been extensively studied, because not only they can be spontaneously formed by exposing the carbon materials to the atmosphere containing oxygen compounds, i.e. air, acid or oxidant chemical compounds, but their existence on the surface of CMs are also essential assets for other chemical post-treatment processes, such as the amination and thiolation, in order to perform multiple doping [106-108]. The concentration of these oxygenated functional groups on CMs can be finely tuned by treating the pristine carbon under different oxidizing agents, either in the gas phase (for instance, with oxygen, ozone and nitrogen oxides) or in the liquid phase (for example, using nitric acid and hydrogen peroxide), and under different reaction conditions, i.e. temperature, pressure, or duration [109, 110].

Nitric acid and oxygen (diluted) are the most frequently used oxidants for the incorporation of the oxygenated functional groups on carbon surface through dry and wet methods, respectively [3, 42]. Liquid phase oxidation with nitric acid can be performed by simply immersing the carbon material into the liquid acid under stirring at the desired temperature, and then followed by washing with distilled water, and drying. The extent of CMs oxidation is related to the concentration of the acid, the treatment duration and temperature. Alternatively, the carbon material may be just treated in concentrated $HNO_3$ at boiling point, but this may lead to serious damage of the solid sample with dramatic changes in the textural properties and the graphitic structure. Liquid-phase oxidization of CMs is easy but requires filtration, washing and drying steps [1]. In the gas-phase oxidation using oxygen-related compounds, the carbon sample is heated up at a suitable temperature under a flow of diluted $O_2$ or other oxygenated compounds. The degree of oxidation is directly depended to the duration and temperature of the treatment as well as the oxygen concentration in the gas flow. It is worthy to note that the nature of the oxygen compounds, i.e. diluted oxygen, $O_3$ or $H_2O_2$, could also play an important role in the final functionalization of the CMs. Another advantage of the gas-phase oxidation is that the activation temperature of the carbon sample can be varied on a large range which is not the case for the liquid-phase activation.

Recently, a more effective route has been developed for the oxygen functionalization of CMs in gas phase by means of $HNO_3$ vapors [111]. The setup is shown in Figure 14a. Carbon nanotubes (CNTs) were loaded inside a tubular reactor connected to a round-bottom flask. Concentrated $HNO_3$ (65 vol. %) was added to the round-bottom flask and keep under magnetic stirring. The liquid nitric acid was heated to 125 $^o$C while the CNTs were heated between 125 and 250 ℃ through an electrical furnace. The $HNO_3$ vapor was passed upward through the carbon sample. The condenser was connected with an open-end exhaust line to the air. Because this treatment was fully under gas-phase conditions, the design of this setup effectively prevents the reflux of liquid $HNO_3$ to the CNT sample, which is collected by the condenser, and avoids the wetting of CNTs with liquid acid completely. So this method could reduce the step of filtration and washing as well as drying. Furthermore, this gas-phase oxidation is especially suitable for the functionalization of macroscopically shaped carbon materials.
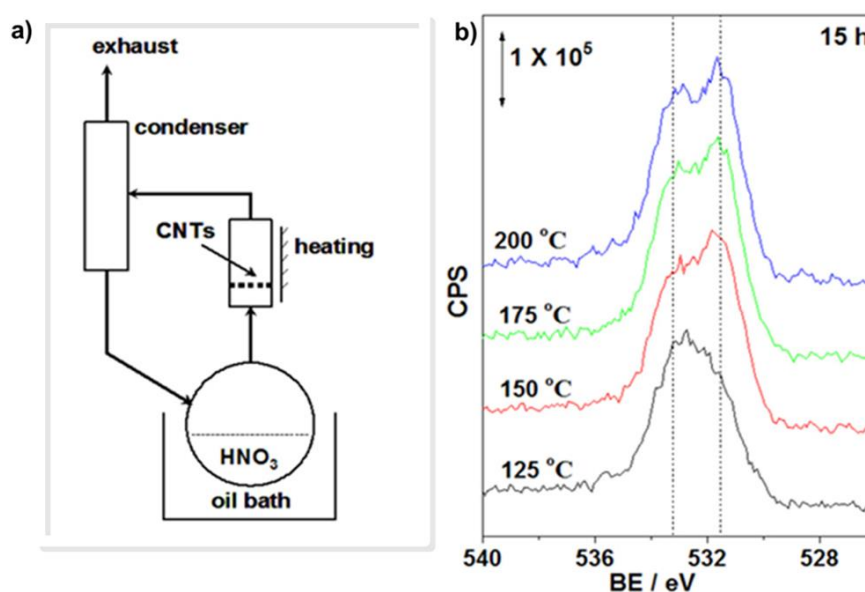


**Figrure 14.** (a) Illustration of the setup used for gas-phase functionalization of CNTs with nitric acid vapor. (b) XPS spectra of CNTs treated by $HNO_3$ vapor at different temperature for 15 h [1, 111].

Different from other gas-phase oxidation treatment, this method allows a selective

oxygen-containing functional groups grafting on the carbon, but strongly depending on the treatment temperature. As shown in Figure 14b, a high concentration of carboxyl groups could be obtained at high treatment temperature for a fixed duration of 15 h. As the decomposition of the carboxylic groups occurs in the lower temperatures range, whereas the phenol, ether and carbonyl groups are more stable and decompose at higher temperatures, the different distribution of the oxygenated groups can be achieved on carbon surface easily by using the appropriate treatment temperature. It is confirmed that as compared to the conventional liquid-phase treatment with liquid nitric acid, this method using the $HNO_3$ vapor not only enhances the total amount but also changes the areal density of different oxygen-containing functional groups on CNTs.

## 2.1.2.2 Amination

The conventional method for the amination of carbon materials includes three steps of the formation and the activation of carboxylic acid groups and the final amination [100]. In this method, the carboxylic acid groups formed on the carbon surface are firstly activated with carbodiimides, or $SOCl_2$ in anhydrous organic solvents, and then react with amine precursors. This process is tedious and not appropriate for large-scale preparation of amine functionalized carbon materials.

Recently, a simple two-step method has been developed for the amination of CMs [112]. In the first step of the process, the abundant oxygen-containing functional groups will be created on the carbon surface after oxidation process as described above, and then the amine groups will be incorporated into the carbon materials matrix by the reduction of oxidized carbon using some reductive nitrogen-containing precursors such as ammonia/water.

Lai et al. [113] reported a one-pot solvothermal process using ethylene glycol as solvent and ammonia water as nitrogen precursor to synthesize $NH_2$-graphene. As shown in Figure 15, the graphene oxide is reduced and functionalized with the primary amine groups. The reaction during the treatment process is featured by the nucleophilic substitution of –COOH and C-O-C groups by the ammonia radicals.
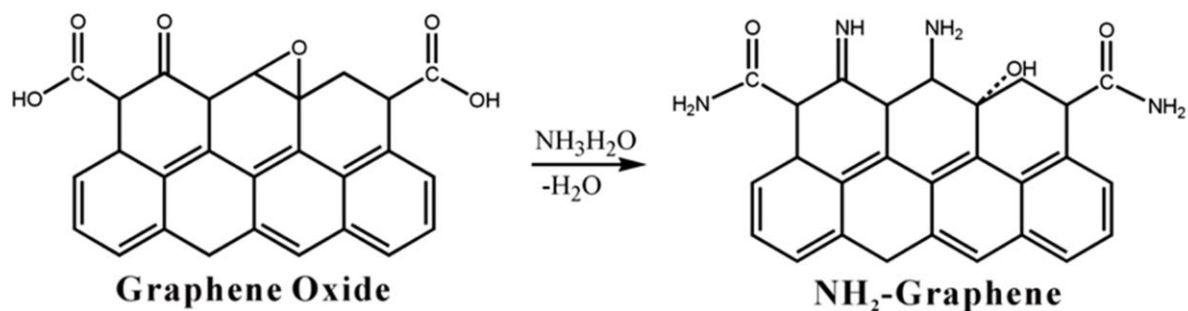
**Figure 15.** Schematic reaction mechanism of one-step conversion from graphene oxide (GO) to amine modified graphene ($NH_2$-G) in the presence of ammonia water [113].

## 2.1.2.3 Thiolation

Carbon materials can be modified by the thiolation involving noncovalent (e.g., $\pi$-$\pi$ interaction) or covalent bonding methods. Yang et al. [91] carried out the functionalization of multi-walled carbon nanotubes (MWCNTs) via $\pi$-$\pi$ interaction with benzyl mercaptan ($C_6H_5$-$CH_2$-SH) for the adhesion of Pt nanoparticles. As shown in Figure 16, the phenyl ring ($C_6H_5$-) only participates in a $\pi$-$\pi$ interaction with the walls of the CNTs, and the thiol group (-SH), which is separated from the phenyl ring by a methylene group (-$CH_2$-) in order to minimize the electron delocalization between the two, is intended to adhere to the Pt nanoparticle by the formation of S-Pt bonds.
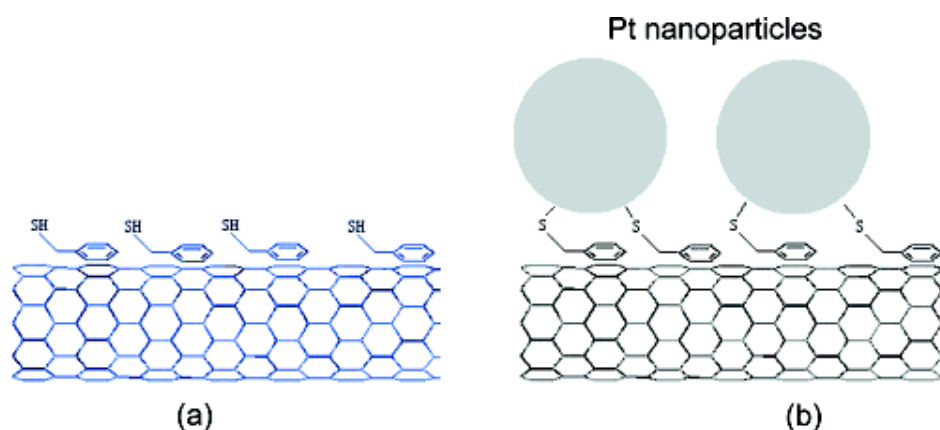


**Figure 16.** Schematics of (a) a CNT functionalized with benzyl mercaptan via $\pi$-$\pi$ bonding and (b) the bonding of Pt nanoparticles to the functionalized CNT via covalent S-Pt bond formation [91].

Generally, the covalent bonding is stronger than the noncovalent bonding. Similar to some amination functionalization methods, in the traditional covalent method, the carboxylic acid groups formed on the carbon surface are firstly chlorinated by $SOCl_2$ in anhydrous organic solvents, and then conjugated with a thiol-containing liker through the amide bond [114]. Hsu et al. [115] established a simple and highly efficient method to directly functionalize the surface of carbon nanotubes with thiol groups. As shown in Figure 17, the thiourea is used as the sulfur precursor, CNTs are firstly treated under the reflux operation with thiourea, hydrobromic acid and glacial acetic acid, after the neutralization with NaOH and the acidification with H₂SO4, the thiolated CNT is formed.
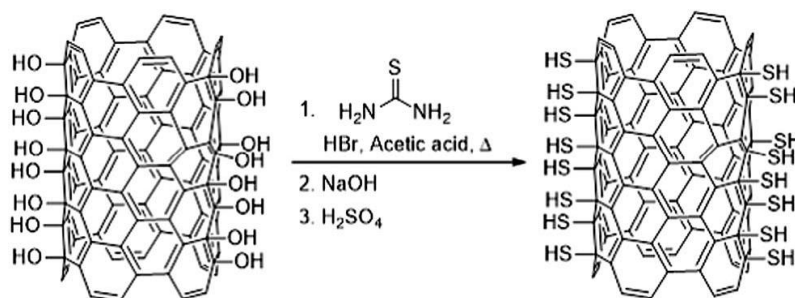


**Figrue 17.** Directly thiolated onto the surface of CNT [115].

To date, the vast majority of the thiolation treatment is a complex and time consuming process with operating in the liquid medium which calls for indispensable tedious filtration and washing, which is not suitable for mass production of thiolated CMs. Thus, the development of a novel, simple and easy for scaling up, thiolation method for carbon materials is of high interest.

2.1.2.4 N-doping

Nitrogen-doped carbon materials can be achieved by two different methods, either the direct synthesis through adding a nitrogen source molecule into the reactant mixture during the production process of the CMs, or the post treatment of the as-synthesized carbon materials with the nitrogen containing molecules [116-123].

Direct synthesis methods include the arc-discharge and laser ablation, which need the high temperature, i.e. > 1000 $^o$C, to evaporate the carbon source (usually graphite) [124]. Nowadays, the chemical vapor deposition (CVD) is a most widely used method for synthesizing the carbon nanotubes/fibers with or without heteroatom dopants [125, 126]. As shown in Figure 18, the CVD method only requires an oven, a tubular reactor, a reactive gas mixture and an appropriate catalyst. During the procedure, the decomposition of the gaseous or volatile compounds containing carbon and/or nitrogen precursor happens on the growth catalyst at the temperature ranged from 550 to 1100 $^o$C, which is much lower than other CNTs synthesis methods. For N-doped CNTs material, the dopant closely depends on the conditions of the CVD process, i.e. the source of nitrogen and carbon and the reaction temperature and the synthesis duration. Various kinds of nitrogen precursor have been used for N-doping synthesis, such as $N_2$ [127], $NH_3$ [128-130], pyridine [131] and melamine [132].
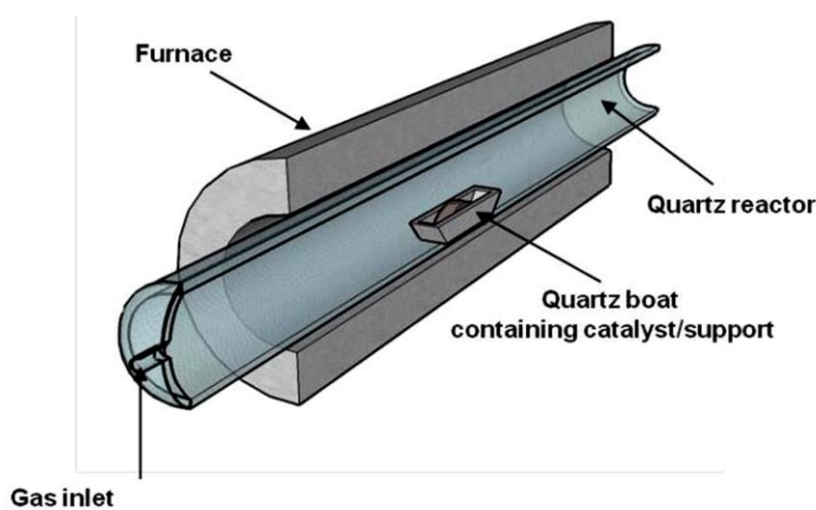


**Figure 18.** Scheme showing the setup for the synthesis of carbon nanotubes and nitrogen-doped carbon nanotubes by CVD method [133].

One of the most popular methods for nitrogen-doping of CMs is the annealing of the pristine CMs in the $NH_3$ atmosphere in a temperature range from 600 to 900 $^o$C [134].

2.1.2.5 S-doping

In spite of the larger radius of sulfur atoms compared to carbon and nitrogen atoms, the introduction of sulfur atoms in the $sp^2$-hybridized carbon network is demonstrated to be possible through experiment results and theoretical studies [104]. Similar to nitrogen doping, the substitutive doping of sulfur atom in the $sp^2$ carbon structures can be achieved by the directly synthesis and post treatment using S precursor. Among the various sulfurizing agents, the following sulfur sources are the most common choices: $H_2S$ (probably the most important one like $NH_3$ in N doping) [135-138], elemental S [139, 140], $CS_2$ [141], dimethyl disulfide [142] and $SO_2$ [143, 144].

## 2.2 Porous structures and structural defects

Normally, the textural properties of carbon materials change after the functionalization process [145]. Especially for the oxidation process, the specific surface area and pore volume as well as pore size of the pristine carbon can be altered as a result of the oxidation process which lead to the widening of existing pores and/or the creation of new ones by the selective gasification reaction of carbon components with oxidizing agents, or by the opening of some of the previously inaccessible pores. The oxidation process could also induce in some case the formation of functionalized defects on the treated material [67]. Such porosity modification and defects formation are accompanied by a change in the specific surface area (SSA) of the final sample. The defects are generally decorated with oxygeneated functional groups. Such defects thus provide anchorage sites for the dispersion of the metal NPs on the support through enhanced interaction compared to the defect-free area. The strong interaction between the deposited metal NPs and the defects could also provide higher sintering resistance to the metal NPs during the course of the reaction.

## 3. Catalytic reactions

### 3.1 Selective oxidation of $H_2S$ into elemental sulfur

Hydrogen sulfide is one of the most toxic and malodorous gases, largely from different kinds of sources, such as coal-based chemistry and power plants, natural-gas processing and utilization, hydrodesulfurization of crude oil, refineries and smelter operation. $H_2S$ can be regarded as a major air pollutant entering the atmosphere, which is harmful to animals and human beings and is at the origin of the acid rain. Moreover, it is highly corrosive to production facilities in whether a gaseous form or in solution. Because of the urgency for the environmental protection $H_2S$ or sulfur-containing effluent gas must be treated prior to it releasing into the atmosphere [146, 147].

Now the most widely used technology consisted by the conversion of $H_2S$ into elemental sulfur using the equilibrated Claus process [148]. In the first step of the conventional Claus process, one-third of the $H_2S$ is converted to $SO_2$, in the presence of an appropriate amount of air, by thermal oxidation at 1000-1200 $^{o}C$ (Equation 1). During this step the direct reaction between $H_2S$ and $SO_2$ leads to the formation of elemental sulfur (Equation 2). However, due to the equilibrium of the reaction at high temperature the conversion of the $H_2S$ is limited to around 60-70%. In order to increase the $H_2S$ conversion, the remained $H_2S$ and $SO_2$ is reacted catalytically at lower temperature, i.e. 200-250 °C, in a series of catalytic converters according to Equation 2. However, because of the thermodynamic equilibrium limitations of the second step (Claus reaction), it is difficult for the complete removal of $H_2S$ from the exhaust gas, and the residual $H_2S$ leaving the Claus plant into the tail gas is ranged between 1 to 3 vol.%. Therefore, it is thus of interest to find a new process to eliminate this harmful compounds completely.

$$H_2S + (3/2)\ O_2 \rightarrow SO_2 + H_2O \tag{1}$$

$$SO_2 + 2H_2S \rightarrow 2H_2O + (3/n)\ S_n \tag{2}$$
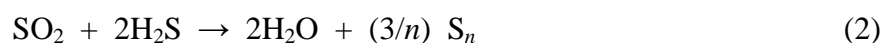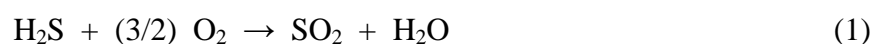
A single step directly catalytic selective oxidation of $H_2S$ to elemental sulfur by oxygen, called Super-Claus process has been developed and operated in several sulfur units during the last decades (Equation 3). One outstanding advantage of the Super-Clause process is the absence of thermodynamic limitations as oxygen is used as oxidant instead of $SO_2$ and thus, the complete conversion of $H_2S$ into elemental sulfur could be achieved under appropriate reaction conditions.

$$H_2S + (1/2)\ O_2 \rightarrow (1/n)\ S_n + H_2O \tag{3}$$
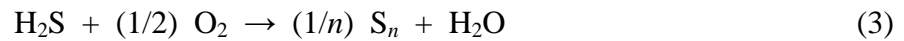
Besides the main Super-Claus reaction, the accompanying side reactions with the further oxidation of the produced sulfur by some excess oxygen to yield $SO_2$ (Equation 4) and the direct complete oxidation of $H_2S$ into $SO_2$ (Equation 5) may decrease the sulfur selectivity during the reaction of the one step selective oxidation of $H_2S$ into elemental sulfur.

$$(1/n)\ S_n + O_2 \rightarrow SO_2 \tag{4}$$

$$H_2S + (3/2)\ O_2 \rightarrow SO_2 + H_2O \tag{5}$$
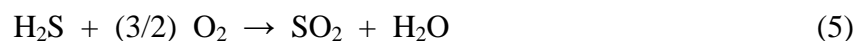
The key feature of this selective oxidation process is to develop a high efficient catalyst which could preventing the reverse-Claus reaction and deep oxidation of the formed elemental sulfur to $SO_2$. The catalytic $H_2S$ oxidation can be conducted above or below the dew-point of sulfur product (180 $^o$C) [149]. Most of the catalytic oxidation processes for the $H_2S$ conversion to elemental sulfur are performed in either discontinuous- or continuous-mode: in the former method (typically operating at T< 180 ℃), sulfur is trapped inside the catalyst and its regeneration is periodically operated by melting down sulfur deposits, in the latter (T> 180 ℃) sulfur is continuously evaporated and condensed at the exit of the reactor. For these processes, the sulfur yield commonly ranges between 90-95% and it can be increased by adding an absorption stage at the outlet of the catalytic reactor. In the

earlier studies, titanium based, chromium based, vanadium based and iron based oxide catalysts were proposed for this selective oxidation process. However, these catalysts display some shortcomings such as the rapid deactivation of titanium-based catalysts in the presence of water vapor, the toxic nature of chromium containing materials, and the requirement of excess oxygen amount for the iron based Super-Claus catalyst, constrain the development of these catalysts. Nowadays, iron-based catalyst remains the most developed industrial catalyst for operating the selective oxidation of $H_2S$.

Recently, it is reported that the some carbon materials, such as basic nitrogen-doped carbon nanotubes or nitrogen-doped mesoporous carbon, can be used as metal-free catalyst in the desulfurization process to prevent the drawbacks of the above-described metal based catalysts [54, 150]. There still however remains a lack of fundamental understanding regarding the exact nature of the various active sites, as well as the development of the novel macroscopic carbon materials, with less drastic synthesis conditions, in the directly catalytic selective oxidation of $H_2S$ to elemental sulfur using the metal-free catalyst.

## 3.2 Selective hydrogenation of cinnamaldehyde

The hydrogenation of α, β-unsaturated aldehydes to α, β-unsaturated alcohols or saturated aldehydes has attracted a large attention due to potential economic benefits and scientific interest [151]. Furthermore, it is a critical step in the synthesis of a large number of fine chemicals, such as pharmaceuticals, perfumes and food additives. In particular, hydrocinnamaldehyde (HCAD) was found recently to be an important intermediate in the synthesis of pharmaceuticals used in the treatment of HIV [152]. Cinnamaldehyde (CAD), as a typical α,β-unsaturated aldehyde, is able to generate various product distributions through different hydrogenation routes (Figure 19) [153], depending on the active metal, promoter and support.
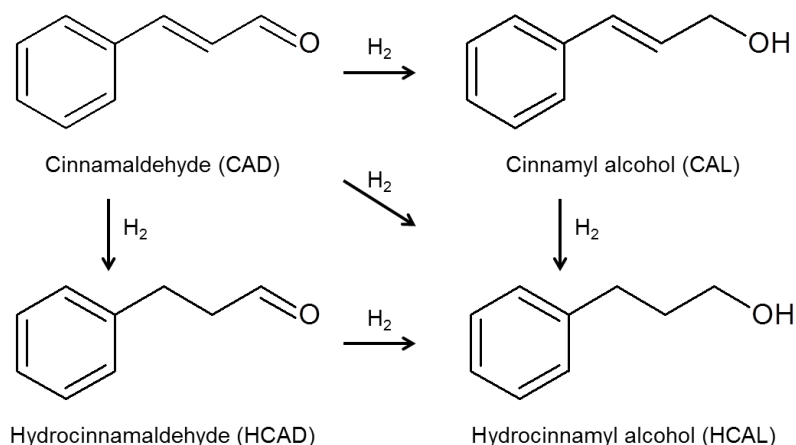
**Figure 19.** Reaction pathways for cinnamaldehyde catalytic hydrogenation process.

### 3.2.1 Effect of active metal nature

The hydrogenation of cinnamaldehyde can be catalyzed by the different noble metals [154], and the sequence for the formation of cinnamyl alcohol (CAL) is Os > Ir > Pt > Ru > Rh > Pd = 0, which is related to the width of the d-band of the metal [155]. The wide d-band of the noble metal can induce the strong four-electron repulsion of the unsaturated aldehyde, which will make it difficult to adsorb the C=C bond. The palladium with the smallest d-band width is easier to carry out the $\eta^4$ conjugate adsorption. Moreover, the hydrogenation of the C=C bond is thermodynamically favorable because the activation energy required for the hydrogenation of C=C bond is lower than that of C=O bond. So the Pd catalysts favor the selectivity to HCAD or hydrocinnamyl alcohol (HCAL), while the Pt and Ru are selective for the C=O bond hydrogenation towards CAL.

### 3.2.2 Effect of metal particle size

The selectivity of CAD hydrogenation is considered to be sensitive with respect to the size of the metal nanoparticles [156], while the effect of particle size on the reaction activity is negligible. The larger metal particles can behave the higher selectivity of CAL [156, 157], which is attributed to the adsorption of CAD on the active metal surface (Figure 20). The adsorption configuration of the CAD molecule on the metal surface was studied by the theoretical calculations: on the large particles with flat metal surface, the repulsion barrier

between the benzene ring in CAD and the metal surface makes it at least 0.3 nm away from the flat metal surface, which makes the C=C bond less accessible to the metal surface than the C=O bond and thus, favors the hydrogenation of C=O bond [158]. But for the small nanoparticles, the repulsion between the metal and the benzene ring will become weak, and the C=C and C=O bonds can be simultaneously adsorbed on the metal surface, thereby reducing the selectivity of CAL. This phenomenon is found not only on the Pt and Ru metals with high selectivity of CAL, but also on the Rh metal, which has a poor selectivity to C=O bond [157].
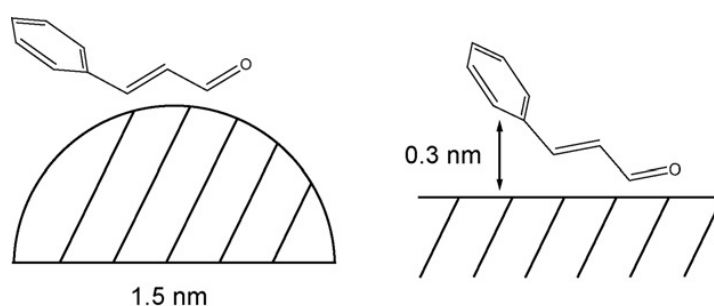


**Figure 20.** Adsorption of cinnamaldehyde on a small metal particle (left) and a large non-curved metal particle (right) [157].

**3.2.3 Effect of carbon surface chemistry on the hydrogenation of cinnamaldehyde**

For the noble metal catalyst using the carbon material as support, the surface chemical properties of carbon support especially the surface functional groups are important factors which can direct the catalytic performance in the hydrogenation of CAD. de Jong et al. [159] studied the influence of oxygen-containing surface groups of carbon nanofibers (CNFs) support on activity and selectivity in the hydrogenation of cinnamaldehyde. They found that the reaction rate of Ru/CNFs catalyst (1-2 nm) increased 22 times after an annealing step in nitrogen atmosphere, which is related to the removel of surface oxygenated groups on CNFs support. But the selectivity to C=O bond is reduced from 48 to 8 % due to the formation of HCAD. For the Pt/CNFs catalyst (1-2 nm) [160], the same heat treatment also increased the

overall catalytic activity by 25 times. The XPS and hydrogen chemisorption characterizations indicate that the presence of oxygen functional groups on the surface of CNFs support induces no clear change on the electronic structure of the metal particles. Furthermore, the kinetic modeling proves that the non-polar carbon support surface resulted from the removal of oxygen-containing functional groups can enhance the adsorption of the CAD molecule [161], thereby increasing the activity of the Pt catalyst (Figure 21).
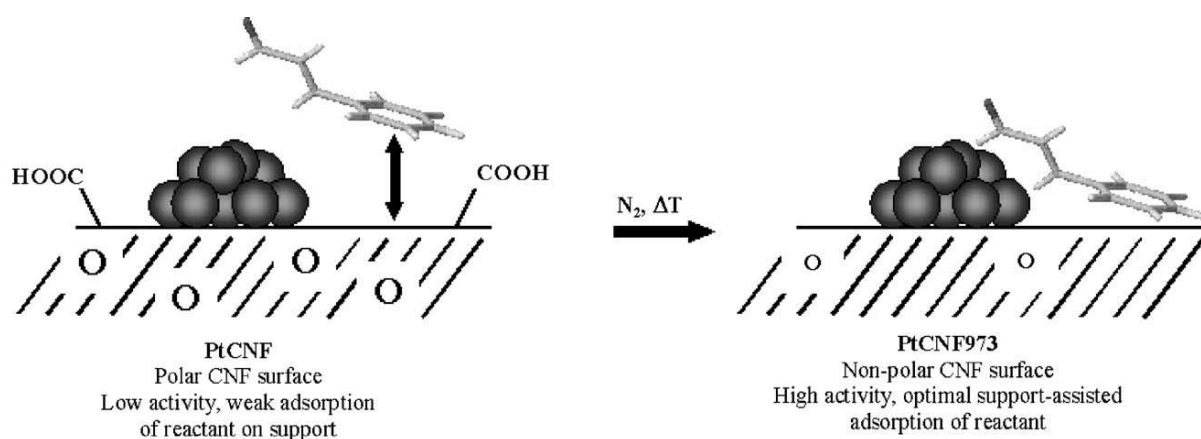


**Figure 21.** Schematic representation of cinnamaldehyde adsorption explaining the enhanced activity for the CNF-supported platinum catalyst after the removal of the majority of the oxygen-containing groups by support-assisted catalysis [161].

de Jong et al. [162] further studied the effects of surface oxygenagted groups combined with the metal particle size on the catalytic performance. For the catalysts with oxygenated groups on the support surface, the larger metal NPs (~3.5 nm) showed higher selectivity to CAL. After the removel of oxygen groups by the heat treatment, the smaller NPs (~2.0 nm) showed higher selectivity to CAL. As the same as the previous studies, the heat treatment increases the activity of these catalysts, but the selectivity to C=O bond upon heat treatment is enhanced rather than decreased. This opposite trend is considered to be caused by the use of different reaction temperatures and pressures. And then they proposed an adsorption/repulsion model of CAD to explain the change of hydrogenation performance (Figure 22). Due to the presence of the oxygenated groups, the surface polar of the carbon

support prevents the adsorption of phenyl group on the support, and then the adsorption of CAD as well as the hydrogenation are only happened on the metal surface. Therefore, as shown in Figure 20, the larger particles show the higher selectivity of CAL. However, the adsorption of CAD will be enhanced on the less polar support surface after the removel of oxygen functional groups by the heat treatment (Figure 21). Meanwhlie the molecules adsorbed in the vicinity and periphery of active metal can be involved in the reaction, and the adsorption of phenyl ring on the support will direct the C=O bond towards the active metal periphery, thereby increasing the reaction activity and the selectivity to CAL. Furthermore, because of their more peripheries the smaller NPs will have higher hydrogenation activity and selectivity to C=O bond than the larger particles.
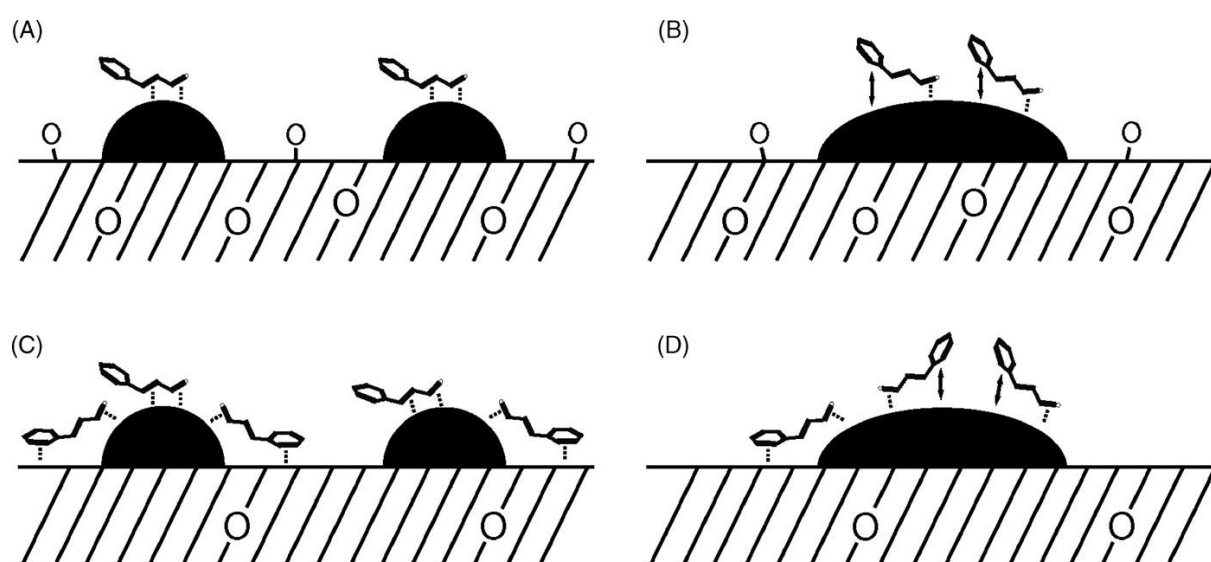


**Figure 22.** Proposed model for the observed particle size effects: (A) small particles on polar surface, (B) large particles on polar surface, (C) small particles on non-polar surface, and (D) large particles on non-polar surface [162].

**3.2.4 Electronic effect on the hydrogenation of cinnamaldehyde**

The electronic property of active metal, which can be tuned by the ways of support and promoter, also plays a key role in the hydrogenation of CAD. Serp et al. [163] studied the

different carbon materials (carbon nanotubes, carbon nanofibers and active carbon) supported monometallic and bimetallic NPs on the hydrogenation of CAD. The carbon nanotubes (CNTs) supported Pt or Ru catalysts exhibited higher selectivity of CAL compared to the carbon nanofibers. Meanwhile the selectivity of the PtRu alloy is higher than that of a single metal. The authors also reported that the CNTs supported PtRu bimetallic catalyst after the heat treatment exhibited the higher selectivity of CAL as well as the enhanced activity. They suggested that the high temperature treatment not only promotes the adsorption of CAD on the surface of carbon support by the removel of oxygen groups, similarly to what reported by de Jong et al. [159-161], but also increases the electrical conductivity of the support, leading to more electron transfer from CNTs to the active metal, which significantly improves the CAL selectivity.

Furthermore, Serp et al. [164] studied the influence of the thermal activation on the CAL selectivity of the CNTs supported Pt or Ir catalysts. They suggested that the opposite trend originally reported by de Jong et al. should be due to the differences in the graphite layers arrangement between CNTs (exclusive exposure of basal planes) and CNFs (exclusive exposure of prismatic planes) rather than the differences of reaction conditions. The delocalized $\pi$ electrons are more fluid in CNTs with parallel oriented graphite layer structure than in the obliquely oriented CNFs, which enhance the electrical conductivity of CNTs and make it easier for the electron transfer from CNTs to the metal. This phenomenon is also found between the carbon supports such as graphite and activated carbon [154], the graphite has more electron transfer to the active metals than the activated carbon, thereby leading to the increased selectivity of CAL.

The theoretical calculations by Delbecq and Sautet [155] show that the electron-rich metal surface can not only bring about the rejection of the $\eta^4$ type conjugate adsorption along with the reduction of the binding energy of C=C bond, but also promote the adsorption of C=O bond by the feedback $\pi$ bond interaction. Therefore, the selectivity of CAL can be increased by tuning the electronic structure of active metal.

Tsang et al. [165] reported a metal size-dependent electronic modification of the binary metal surface for the hydrogenation of cinnamaldehyde (Figure 23). They synthesized

a series of cobalt doped platinum nanocrystals with different sizes. As shown in Figure 23(a), the deposited Co atoms, which mainly occupy the low coordination site in the Pt crystal, will have an electron modification on the adjacent Pt atoms. The positive charge of the doped Co atoms will attract the C=O bond, while the negative charge of the neighboring Pt atoms can destabilize the adsorption of C=C bond. As shown in Figures 23(b) and (c), the electronic influence of Co atoms can cover the entire surface of small Pt crystal which is less than 6 nm. However, this effect will become gradualy declining from 6 nm of crystal size and almost disappeared in the large crystal size such as 22.5 nm. Moreover, the 4.8 nm Pt crystals doped with the approximately same mole of Co atoms can perform the CAL selectivity of more than 99.8 % under a complete conversion of CAD.
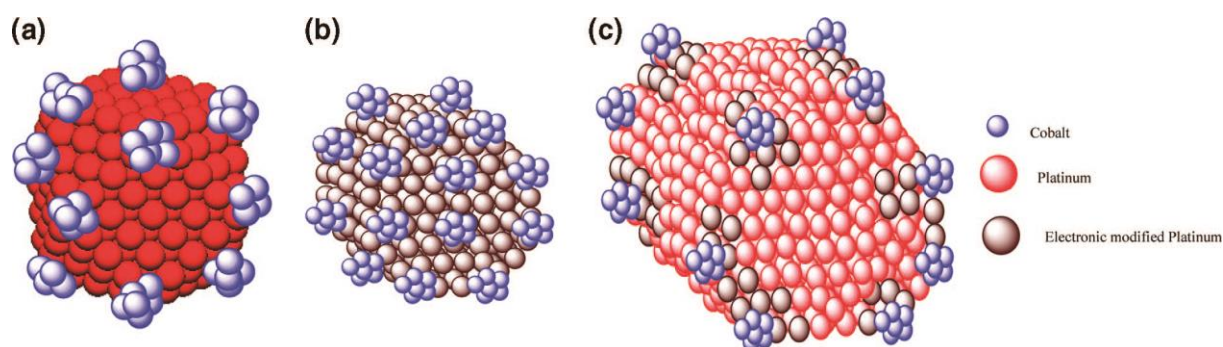


**Figure 23.** Pictorial models accounting for the critical size effect: (a) model showing Co atoms decorating on corner sites of Pt crystal. (b, c) Models accounting the critical size effect: (b) Co atoms decorated on corners electronically influencing the whole small Pt ensemble-left; (c) some normal Pt sites remained without being influenced by decorated Co atoms in a large Pt ensemble [165].

From the results discussed above, it can be seen that the adjustment of catalytic performance in the hydrogenation of cinnamaldehyde needs to be carried out in terms of the metal modulation, such as the metal particle size, the surface chemistry of support and the electronic structure of active metal. Moreover, hydrogenation of cinnamaldehyde is often used as a model reaction to evaluate the structure-activity relationships of the catalyst.

### 3.2.5 Recyclability/recovery of catalysts in the liquid-phase process

The stability and recyclability of catalyst is of high interest for the industrial point of view. In addition, in liquid-phase reaction the loss of the catalytic performance as a function of time not only due to the deactivation of the catalyst through sintering but also to the problem linked with the active phase leaching or catalyst loss during filtration step. In order to avoid such problems, the interaction between the active phase and the support should be finely tuned in order to provide a strong bonding between the two phases, which prevent thus active phase mobility which in turn reduce the problems linked with sintering or leaching. It is expected that the introduction of anchoring sites on the surface of the carbon support, such as defects, functional groups or heteroatom doping, etc., could prevent these problems cited above.

Moreover, the recovery of the conventional powdered catalysts usually used in liquid-phase reaction required cumbersome and energy-intensive filtration process. In addition, the recovery is not complete and catalyst loss represents another drawback of the powdered catalyst recovery process. During the reaction the catalyst particles also faced repeated shocks with the impellers leading to the formation of fine or active phase loss inside the reaction medium. For some supports with a large contribution of micropores the problem of mass transfer inside the catalysts in the liquid phase reaction directly affects the residence time of the reactants, which in turn affects the catalytic performance and recyclability [18]. It is expected that replacing the powdered liquid-phase catalyst by a hierarchical ones, with open porosity and large effective surface area, could be of high interest. The hierarchical catalyst should also display acceptable interaction for maintaining high active phase dispersion and also to prevent excessive catalytic performance degradation through sintering or leaching processes. The hierarchical structured catalyst could also allow one to phase out the traditional use of impellers which are at the origin of catalyst particle breakdown as discussed above.

## 4. Scope and outline of this thesis

In summary, the development of macroscopic carbon materials with controlled porosity and accessibility, easy for recovery, which can be used whether in the gas phase or the liquid phase reaction, whether as a catalyst carrier or as a metal-free catalyst itself, is of great significance. At the same time, exploring the physical structure and surface chemistry of such carbon materials will help to deepen the understanding of the correlation of carbon-based catalytic structure/performance, and it is expected to provide some guidance for the synthesis of new high-efficiency catalysts with enhanced catalytic performance along with improved facility for recovery, especially in the liquid-phase reaction.

This thesis intends to use the multi-model reaction method to design and discuss the utilization of carbon materials, either as metal-free catalyst or as noble metal catalyst support, in order to obtain a more comprehensive understanding of the structure-activity relationship of carbon-based catalysis which could open new era for future catalyst development. Based on the above-mentioned literature bibliography gas-phase selective hydrogen sulfide oxidation to elemental sulfur and liquid-phase cinnamaldehyde hydrogenation to hydrocinnamaldehyde were selected as model reactions, and two kinds of low-cost commercial structured carbon materials, graphite felt and carbon felt, were used to carry out the research work.

Firstly, the graphite felt was activated by gaseous nitric acid oxidation treatment to generate defective carbon-based material (noted OGF) with hierarchical structure. The physical properties of the as-synthesized OGF and optimization process were thus investigated. The OGF carbon-based material containing defects decorated with oxygenated functional groups was further evaluated as metal-free catalyst for the selective oxidation of hydrogen sulfide into elemental sulfur under reaction conditions close to those operated in industry. It is expected that defects and oxygenated functional groups could act as active center for the dissociative adsorption of oxygen and $H_2S$ and to initiate oxidation process. The results obtained in this section will be bench-marked with those obtained on supported oxide, nitrogen-doped carbon catalysts.

Secondly, the oxidized graphite felt (OGF) was used as hierarchical structured support for Pd-based catalyst in the liquid-phase hydrogenation of cinnamaldehyde. In this reaction, the OGF monolith catalyst was employed as a catalytic stirrer which allows one to operate the reaction without mechanical shocks between the impellers and the catalyst and to reduce the problem of fine formation. The macroscopic shape of the catalyst also provides an elegant way for operating the catalyst recovery. The influence of the defect sites on the dispersion and stabilization of the metal active phase was investigated and compared to those obtained on the untreated graphite felt. Finally, the recyclability/recovery of the catalyst was also investigated, and compared with those obtained on the untreated GF and the commercial Pd/activated charcoal catalysts, in order to highlight the exceptional high stability of the OGF based catalyst.

Thirdly, based on the gaseous oxidation treatment, the oxidized carbon felt was further activated by amination and nitrogen-doping, respectively. The materials were used as catalyst supports for palladium. The effect of interaction between the metal and the functionalized carbon supports on the selectivity of the C=C bond hydrogenation of cinnamaldehyde was investigated on the Pd-based catalyst on the different supports: activated carbon felt with oxygenated groups decorated defects, amino groups and nitrogen doping to support palladium.

Finally, the gas-phase thiolation treatment of carbon materials was developed on the basis of the oxygen-containing functional groups grafting. The interaction between sulfydryl groups and palladium was investigated by the thiolated carbon felt as support for Pd-based catalyst for the selective hydrogenation of the C=C bond of the cinnamaldehyde.

The last chapter will be devoted to the general conclusion and to the future prospective of the work realized during this thesis. In this chapter new directions regarding the future development and use of these carbon-based catalysts will be discussed.

# References

[1]     D.S. Su, S. Perathoner, G. Centi, Nanocarbons for the development of advanced catalysts, Chemical Reviews, 113 (2013) 5782-5816.

[2]     J.L. Figueiredo, M.F.R. Pereira, M.M.A. Freitas, J.J.M. Orfao, Modification of the surface chemistry of activated carbons, Carbon, 37 (1999) 1379-1389.

[3]     J.L. Figueiredo, Functionalization of porous carbons for catalytic applications, Journal of Materials Chemistry A, 1 (2013) 9351-9364.

[4]     Y. Zhang, J. Zhang, D.S. Su, Substitutional doping of carbon nanotubes with heteroatoms and their chemical applications, ChemSusChem, 7 (2014) 1240-1250.

[5]     J.L. Figueiredo, M.F.R. Pereira, The role of surface chemistry in catalysis with carbons, Catalysis Today, 150 (2010) 2-7.

[6]     J. Zhang, L. Qu, G. Shi, J. Liu, J. Chen, L. Dai, N, P-codoped carbon networks as efficient metal-free bifunctional catalysts for oxygen reduction and hydrogen evolution reactions, Angewandte Chemie International Edition, 55 (2016) 2230-2234.

[7]     L. Dai, Y. Xue, L. Qu, H.J. Choi, J.B. Baek, Metal-free catalysts for oxygen reduction reaction, Chemical Reviews, 115 (2015) 4823-4892.

[8]     D. Geng, Y. Chen, Y. Chen, Y. Li, R. Li, X. Sun, S. Ye, S. Knights, High oxygen-reduction activity and durability of nitrogen-doped graphene, Energy & Environmental Science, 4 (2011) 760.

[9]     M.J. Ledoux, R. Vieira, C. Pham-Huu, N. Keller, New catalytic phenomena on nanostructured (fibers and tubes) catalysts, Journal of Catalysis, 216 (2003) 333-342.

[10]    K. Gong, F. Du, Z. Xia, M. Durstock, L. Dai, Nitrogen-doped carbon nanotube arrays with high electrocatalytic activity for oxygen reduction, Science, 323 (2009) 760-764.

[11]    X. Wang, X. Li, L. Zhang, Y. Yoon, P.K. Weber, H. Wang, J. Guo, H. Dai, N-doping of graphene through electrothermal reactions with ammonia, Science, 324 (2009) 768-771.

[12]    J. Zhang, X. Liu, R. Blume, A. Zhang, R. Schlögl, D.S. Su, Surface-modified carbon nanotubes catalyze oxidative dehydrogenation of n-butane, Science, 322 (2008) 73-77.

[13]    R. Piner, H. Li, X. Kong, L. Tao, I.N. Kholmanov, H. Ji, W.H. Lee, J.W. Suk, J. Ye, Y. Hao, S. Chen, C.W. Magnuson, A.F. Ismach, D. Akinwande, R.S. Ruoff, Graphene synthesis via magnetic inductive heating of copper substrates, ACS Nano, 7 (2013) 7495-7499.

[14]    S. Ceylan, C. Friese, C. Lammel, K. Mazac, A. Kirschning, Inductive heating for organic synthesis by using functionalized magnetic nanoparticles inside microreactors, Angewandte Chemie International Edition, 47 (2008) 8950-8953.

[15]    J.-P. Tessonnier, L. Pesant, G. Ehret, M.J. Ledoux, C. Pham-Huu, Pd nanoparticles introduced inside multi-walled carbon nanotubes for selective hydrogenation of cinnamaldehyde into hydrocinnamaldehyde, Applied Catalysis A: General, 288 (2005) 203-210.

[16]    R. Nie, M. Miao, W. Du, J. Shi, Y. Liu, Z. Hou, Selective hydrogenation of C=C bond over N-doped reduced graphene oxides supported Pd catalyst, Applied Catalysis B: Environmental, 180 (2016) 607-613.

[17]    R. Yu, R. Liu, J. Deng, M. Ran, N. Wang, W. Chu, Z. He, Z. Du, C. Jiang, W. Sun, Pd nanoparticles immobilized on carbon nanotubes with a polyaniline coaxial coating for the Heck reaction: Coating thickness as the key factor influencing the efficiency and stability of the catalyst, Catalysis Science & Technology, 8 (2018) 1423-1434.

[18]    T. Truong-Huu, K. Chizari, I. Janowska, M.S. Moldovan, O. Ersen, L.D. Nguyen, M.J. Ledoux, C. Pham-Huu, D. Begin, Few-layer graphene supporting palladium nanoparticles with a fully accessible effective surface for liquid-phase hydrogenation reaction, Catalysis Today, 189 (2012) 77-82.

[19]    C. Pham-Huu, N. Keller, M.J. Ledoux, L.J. Charbonniere, R. Ziessel, Carbon nanofiber supported palladium catalyst for liquid-phase reactions. An active and selective catalyst for hydrogenation of C=C bonds, Chemical Communications, (2000) 1871-1872.

[20]    C. Pham-Huu, N. Keller, G. Ehret, L.J. Charbonniere, R. Ziessel, M.J. Ledoux, Carbon nanofiber supported palladium catalyst an active and selective catalyst for hydrogenation of cinnamaldehyde into hydrocinnamaldehyde, Journal of Molecular Catalysis A: Chemical, 170 (2001) 155–163.

[21]   Z. Tian, C. Liu, Q. Li, J. Hou, Y. Li, S. Ai, Nitrogen- and oxygen-functionalized carbon nanotubes supported Pt-based catalyst for the selective hydrogenation of cinnamaldehyde, Applied Catalysis A: General, 506 (2015) 134-142.

[22]   Y. Wang, Z. Rong, Y. Wang, J. Qu, Ruthenium nanoparticles loaded on functionalized graphene for liquid-phase hydrogenation of fine chemicals: Comparison with carbon nanotube, Journal of Catalysis, 333 (2016) 8-16.

[23]   G. Zhang, Z. Li, H. Zheng, T. Fu, Y. Ju, Y. Wang, Influence of the surface oxygenated groups of activated carbon on preparation of a nano Cu/AC catalyst and heterogeneous catalysis in the oxidative carbonylation of methanol, Applied Catalysis B: Environmental, 179 (2015) 95-105.

[24]   Z. Xu, C. Duong-Viet, Y. Liu, W. Baaziz, B. Li, L. Nguyen-Dinh, O. Ersen, C. Pham-Huu, Macroscopic graphite felt containing palladium catalyst for liquid-phase hydrogenation of cinnamaldehyde, Applied Catalysis B: Environmental, 244 (2019) 128–139.

[25]   J. Luo, H. Wei, Y. Liu, D. Zhang, B. Zhang, W. Chu, C. Pham-Huu, D.S. Su, Oxygenated group and structural defect enriched carbon nanotubes for immobilizing gold nanoparticles, Chemical Communications, 53 (2017) 12750-12753.

[26]   G. Tuci, C. Zafferoni, A. Rossin, A. Milella, L. Luconi, M. Innocenti, L. Truong Phuoc, C. Duong-Viet, C. Pham-Huu, G. Giambastiani, Chemically functionalized carbon nanotubes with pyridine groups as easily tunable N-decorated nanomaterials for the oxygen reduction reaction in alkaline medium, Chemistry of Materials, 26 (2014) 3460-3470.

[27]   J. Amadou, K. Chizari, M. Houllé, I. Janowska, O. Ersen, D. Bégin, C. Pham-Huu, N-doped carbon nanotubes for liquid-phase C=C bond hydrogenation, Catalysis Today, 138 (2008) 62-68.

[28]   L. Roldán, Y. Marco, E. García-Bordejé, Origin of the excellent performance of Ru on nitrogen-doped carbon nanofibers for $CO_2$ hydrogenation to $CH_4$, ChemSusChem, 10 (2017) 1139-1144.

[29]   H. Jiang, X. Yu, R. Nie, X. Lu, D. Zhou, Q. Xia, Selective hydrogenation of aromatic carboxylic acids over basic N-doped mesoporous carbon supported palladium

catalysts, Applied Catalysis A: General, 520 (2016) 73-81.

[30]    W. Shi, K.-H. Wu, J. Xu, Q. Zhang, B. Zhang, D.S. Su, Enhanced stability of immobilized platinum nanoparticles through nitrogen heteroatoms on doped carbon supports, Chemistry of Materials, 29 (2017) 8670-8678.

[31]    D. Higgins, M.A. Hoque, M.H. Seo, R. Wang, F. Hassan, J.-Y. Choi, M. Pritzker, A. Yu, J. Zhang, Z. Chen, Development and simulation of sulfur-doped graphene supported platinum with exemplary stability and activity towards oxygen reduction, Advanced Functional Materials, 24 (2014) 4325-4336.

[32]    R.G. Rao, R. Blume, T.W. Hansen, E. Fuentes, K. Dreyer, S. Moldovan, O. Ersen, D.D. Hibbitts, Y.J. Chabal, R. Schlogl, J.P. Tessonnier, Interfacial charge distributions in carbon-supported palladium catalysts, Nature Communications, 8 (2017) 340.

[33]    H. Liu, J. Diao, Q. Wang, S. Gu, T. Chen, C. Miao, W. Yang, D. Su, A nanodiamond/CNT-SiC monolith as a novel metal free catalyst for ethylbenzene direct dehydrogenation to styrene, Chemical Communications, 50 (2014) 7810-7812.

[34]    G. Tuci, M. Pilaski, H. Ba, A. Rossin, L. Luconi, S. Caporali, C. Pham-Huu, R. Palkovits, G. Giambastiani, Unraveling surface basicity and bulk morphology relationship on covalent triazine frameworks with unique catalytic and gas adsorption properties, Advanced Functional Materials, 27 (2017) 1605672.

[35]    L. Liu, Y.-P. Zhu, M. Su, Z.-Y. Yuan, Metal-free carbonaceous materials as promising heterogeneous catalysts, ChemCatChem, 7 (2015) 2765-2787.

[36]    W. Qi, D. Su, Metal-free carbon catalysts for oxidative dehydrogenation reactions, ACS Catalysis, 4 (2014) 3212-3218.

[37]    W. Qi, W. Liu, B. Zhang, X. Gu, X. Guo, D.S. Su, Oxidative dehydrogenation on nanocarbon: Identification and quantification of active sites by chemical titration, Angewandte Chemie International Edition, 52 (2013) 14224-14228.

[38]    W. Qi, W. Liu, X. Guo, R. Schlogl, D.S. Su, Oxidative dehydrogenation on nanocarbon: Intrinsic catalytic activity and structure-function relationships, Angewandte Chemie International Edition, 54 (2015) 13682-13685.

[39]    J.J. Delgado, D.S. Su, G. Rebmann, N. Keller, A. Gajovic, R. Schlogl, Immobilized carbon nanofibers as industrial catalyst for ODH reactions, Journal of Catalysis, 244

(2006) 126-129.

[40]    M.F.R. Pereira, J.J.M. Órfão, J.L. Figueiredo, Oxidative dehydrogenation of ethylbenzene on activated carbon catalysts. I. Influence of surface chemical groups, Applied Catalysis A: General, 184 (1999) 153-160.

[41]    B. Frank, J. Zhang, R. Blume, R. Schlogl, D.S. Su, Heteroatoms increase the selectivity in oxidative dehydrogenation reactions on nanocarbons, Angewandte Chemie International Edition, 48 (2009) 6913-6917.

[42]    R. Huang, J. Xu, J. Wang, X. Sun, W. Qi, C. Liang, D.S. Su, Oxygen breaks into carbon nanotubes and abstracts hydrogen from propane, Carbon, 96 (2016) 631-640.

[43]    Z.-j. Sui, J.-h. Zhou, Y.-c. Dai, W.-k. Yuan, Oxidative dehydrogenation of propane over catalysts based on carbon nanofibers, Catalysis Today, 106 (2005) 90-94.

[44]    V. Schwartz, H. Xie, H.M. Meyer, S.H. Overbury, C. Liang, Oxidative dehydrogenation of isobutane on phosphorous-modified graphitic mesoporous carbon, Carbon, 49 (2011) 659-668.

[45]    H. Ba, L. Truong-Phuoc, Y. Liu, C. Duong-Viet, J.-M. Nhut, L. Nguyen-Dinh, P. Granger, C. Pham-Huu, Hierarchical carbon nanofibers/graphene composite containing nanodiamonds for direct dehydrogenation of ethylbenzene, Carbon, 96 (2016) 1060-1069.

[46]    H. Ba, Y. Liu, X. Mu, W.-H. Doh, J.-M. Nhut, P. Granger, C. Pham-Huu, Macroscopic nanodiamonds/β-SiC composite as metal-free catalysts for steam-free dehydrogenation of ethylbenzene to styrene, Applied Catalysis A: General, 499 (2015) 217-226.

[47]    H. Ba, Y. Liu, L. Truong-Phuoc, C. Duong-Viet, J.-M. Nhut, D.L. Nguyen, O. Ersen, G. Tuci, G. Giambastiani, C. Pham-Huu, N-doped food-grade-derived 3D mesoporous foams as metal-free systems for catalysis, ACS Catalysis, 6 (2016) 1408-1419.

[48]    J. Zhang, D.S. Su, R. Blume, R. Schlogl, R. Wang, X. Yang, A. Gajovic, Surface chemistry and catalytic reactivity of a nanodiamond in the steam-free dehydrogenation of ethylbenzene, Angewandte Chemie International Edition, 49 (2010) 8640-8644.

[49]    L. Liu, Q.-F. Deng, Y.-P. Liu, T.-Z. Ren, Z.-Y. Yuan, $HNO_3$-activated mesoporous carbon catalyst for direct dehydrogenation of propane to propylene, Catalysis

Communications, 16 (2011) 81-85.

[50]   J. Wang, R. Huang, Z. Feng, H. Liu, D.S. Su, Multi-walled carbon nanotubes as a catalyst for gas-phase oxidation of ethanol to acetaldehyde, ChemSusChem, 9 (2016) 1820-1826.

[51]   J.P.S. Sousa, M.F.R. Pereira, J.L. Figueiredo, Catalytic oxidation of NO to $NO_2$ on N-doped activated carbons, Catalysis Today, 176 (2011) 383-387.

[52]   J.P.S. Sousa, M.F.R. Pereira, J.L. Figueiredo, NO oxidation over nitrogen doped carbon xerogels, Applied Catalysis B: Environmental, 125 (2012) 398-408.

[53]   I. Mochida, Y. Korai, M. Shirahama, S. Kawano, T. Hada, Y. Seo, M. Yoshikawa, A. Yasutake, Removal of $SO_x$ and $NO_x$ over activated carbon fibers, Carbon, 38 (2000) 227-239.

[54]   K. Chizari, A. Deneuve, O. Ersen, I. Florea, Y. Liu, D. Edouard, I. Janowska, D. Begin, C. Pham-Huu, Nitrogen-doped carbon nanotubes as a highly active metal-free catalyst for selective oxidation, ChemSusChem, 5 (2012) 102-108.

[55]   C. Duong-Viet, Y. Liu, H. Ba, L. Truong-Phuoc, W. Baaziz, L. Nguyen-Dinh, J.-M. Nhut, C. Pham-Huu, Carbon nanotubes containing oxygenated decorating defects as metal-free catalyst for selective oxidation of $H_2S$, Applied Catalysis B: Environmental, 191 (2016) 29-41.

[56]   Y. Liu, C. Duong-Viet, J. Luo, A. Hébraud, G. Schlatter, O. Ersen, J.-M. Nhut, C. Pham-Huu, One-pot synthesis of a nitrogen-doped carbon composite by electrospinning as a metal-free catalyst for oxidation of $H_2S$ to sulfur, ChemCatChem, 7 (2015) 2957-2964.

[57]   Z. Xu, C. Duong-Viet, H. Ba, B. Li, T. Truong-Huu, L. Nguyen-Dinh, C. Pham-Huu, Gaseous nitric acid activated graphite felts as hierarchical metal-free catalyst for selective oxidation of $H_2S$, Catalysts, 8 (2018) 145-162.

[58]   H. Teng, Y.-T. Tu, Y.-C. Lai, C.-C. Lin, Reduction of NO with $NH_3$ over carbon catalysts the effects of treating carbon with $H_2SO_4$ and $HNO_3$, Carbon, 39 (2001) 575-582.

[59]   G.S. Szymański, T. Grzybek, H. Papp, Influence of nitrogen surface functionalities on the catalytic activity of activated carbon in low temperature SCR of $NO_x$ with $NH_3$,

Catalysis Today, 90 (2004) 51-59.

[60]     I. Matos, P.D. Neves, J.E. Castanheiro, E. Perez-Mayoral, R. Martin-Aranda, C. Duran-Valle, J. Vital, A.M. Botelho do Rego, I.M. Fonseca, Mesoporous carbon as an efficient catalyst for alcoholysis and aminolysis of epoxides, Applied Catalysis A: General, 439-440 (2012) 24-30.

[61]     V.L. Budarin, J.H. Clark, R. Luque, D.J. Macquarrie, A. Koutinas, C. Webb, Tunable mesoporous materials optimised for aqueous phase esterifications, Green Chemistry, 9 (2007) 992.

[62]     V.L. Budarin, J.H. Clark, R. Luque, D.J. Macquarrie, Versatile mesoporous carbonaceous materials for acid catalysis, Chemical Communications, (2007) 634-636.

[63]     R. Luque, V. Budarin, J.H. Clark, P. Shuttleworth, R.J. White, Starbon® acids in alkylation and acetylation reactions: Effect of the Brönsted-Lewis acidity, Catalysis Communications, 12 (2011) 1471-1476.

[64]     X. Liang, C. Li, C. Qi, Novel carbon-based strong acid catalyst from starch and its catalytic activities for acetalization, Journal of Materials Science, 46 (2011) 5345-5349.

[65]     Z. Ma, S. Dou, A. Shen, L. Tao, L. Dai, S. Wang, Sulfur-doped graphene derived from cycled lithium-sulfur batteries as a metal-free electrocatalyst for the oxygen reduction reaction, Angewandte Chemie International Edition, 54 (2015) 1888-1892.

[66]     Y. Ito, W. Cong, T. Fujita, Z. Tang, M. Chen, High catalytic activity of nitrogen and sulfur co-doped nanoporous graphene in the hydrogen evolution reaction, Angewandte Chemie International Edition, 54 (2015) 2131-2136.

[67]     C. Tang, H.F. Wang, X. Chen, B.Q. Li, T.Z. Hou, B. Zhang, Q. Zhang, M.M. Titirici, F. Wei, Topological defects in metal-free nanocarbon for oxygen electrocatalysis, Advanced Materials, 28 (2016) 6845-6851.

[68]     G. Tuci, C. Zafferoni, P. D'Ambrosio, S. Caporali, M. Ceppatelli, A. Rossin, T. Tsoufis, M. Innocenti, G. Giambastiani, Tailoring carbon nanotube N-dopants while designing metal-free electrocatalysts for the oxygen reduction reaction in alkaline medium, ACS Catalysis, 3 (2013) 2108-2111.

[69]     K. Zhou, B. Li, Q. Zhang, J.Q. Huang, G.L. Tian, J.C. Jia, M.Q. Zhao, G.H. Luo, D.S. Su, F. Wei, The catalytic pathways of hydrohalogenation over metal-free nitrogen-doped carbon nanotubes, ChemSusChem, 7 (2014) 723-728.

[70]     L. Feng, Y. Yan, Y. Chen, L. Wang, Nitrogen-doped carbon nanotubes as efficient and durable metal-free cathodic catalysts for oxygen reduction in microbial fuel cells, Energy & Environmental Science, 4 (2011) 1892.

[71]     L. Truong-Phuoc, T. Truong-Huu, L. Nguyen-Dinh, W. Baaziz, T. Romero, D. Edouard, D. Begin, I. Janowska, C. Pham-Huu, Silicon carbide foam decorated with carbon nanofibers as catalytic stirrer in liquid-phase hydrogenation reactions, Applied Catalysis A: General, 469 (2014) 81-88.

[72]     Y. Liu, H. Ba, D.-L. Nguyen, O. Ersen, T. Romero, S. Zafeiratos, D. Begin, I. Janowska, C. Pham-Huu, Synthesis of porous carbon nanotubes foam composites with a high accessible surface area and tunable porosity, Journal of Materials Chemistry A, 1 (2013) 9508.

[73]     Y. Shen, L. Li, K. Xiao, J. Xi, Constructing three-dimensional hierarchical architectures by integrating carbon nanofibers into graphite felts for water purification, ACS Sustainable Chemistry & Engineering, 4 (2016) 2351-2358.

[74]     D.-V. Cuong, L. Truong-Phuoc, T. Tran-Thanh, J.-M. Nhut, L. Nguyen-Dinh, I. Janowska, D. Begin, C. Pham-Huu, Nitrogen-doped carbon nanotubes decorated silicon carbide as a metal-free catalyst for partial oxidation of $H_2S$, Applied Catalysis A: General, 482 (2014) 397-406.

[75]     R. Vieira, M.J. Ledoux, C. Pham-Huu, Synthesis and characterisation of carbon nanofibres with macroscopic shaping formed by catalytic decomposition of $C_2H_6/H_2$ over nickel catalyst, Applied Catalysis A: General, 274 (2004) 1-8.

[76]     C. Pham-Huu, M.-J. Ledoux, Carbon nanomaterials with controlled macroscopic shapes as new catalytic materials, Topics in Catalysis, 40 (2006) 49-63.

[77]     C. Mu, K. Huang, T. Cheng, H. Wang, H. Yu, F. Peng, Ni foams decorated with carbon nanotubes as catalytic stirrers for aerobic oxidation of cumene, Chemical Engineering Journal, 306 (2016) 806-815.

[78]     S. Zhao, H. Yin, L. Du, G. Yin, Z. Tang, S. Liu, Three dimensional N-doped

graphene/PtRu nanoparticle hybrids as high performance anode for direct methanol fuel cells, Journal of Materials Chemistry A, 2 (2014) 3719.

[79]   Y. Yang, Z. Tong, T. Ngai, C. Wang, Nitrogen-rich and fire-resistant carbon aerogels for the removal of oil contaminants from water, ACS Applied Material & Interfaces, 6 (2014) 6351-6360.

[80]   E. Frank, L.M. Steudle, D. Ingildeev, J.M. Spörl, M.R. Buchmeiser, Carbon fibers: Precursor systems, processing, structure, and properties, Angewandte Chemie International Edition, 53 (2014) 5262-5298.

[81]   R.E.G. Smith, T.J. Davies, N.d.B. Baynes, R.J. Nichols, The electrochemical characterisation of graphite felts, Journal of Electroanalytical Chemistry, 747 (2015) 29-38.

[82]   T.X. Huong Le, M. Bechelany, M. Cretin, Carbon felt based-electrodes for energy and environmental applications: A review, Carbon, 122 (2017) 564-591.

[83]   T.X.H. Le, M. Bechelany, S. Lacour, N. Oturan, M.A. Oturan, M. Cretin, High removal efficiency of dye pollutants by electron-fenton process using a graphene based cathode, Carbon, 94 (2015) 1003-1011.

[84]   http://www.ceramaterials.com/graphitecarbonfelt.html.

[85]   J.J. Park, J.H. Park, O.O. Park, J.H. Yang, Highly porous graphenated graphite felt electrodes with catalytic defects for high-performance vanadium redox flow batteries produced via NiO/Ni redox reactions, Carbon, 110 (2016) 17-26.

[86]   T.X.H. Le, C. Charmette, M. Bechelany, M. Cretin, Facile preparation of porous carbon cathode to eliminate paracetamol in aqueous medium using electro-fenton system, Electrochimica Acta, 188 (2016) 378-384.

[87]   Z. Zhang, J. Xi, H. Zhou, X. Qiu, KOH etched graphite felt with improved wettability and activity for vanadium flow batteries, Electrochimica Acta, 218 (2016) 15-23.

[88]   Z. He, Y. Jiang, W. Meng, F. Jiang, H. Zhou, Y. Li, J. Zhu, L. Wang, L. Dai, HF/$H_2O_2$ treated graphite felt as the positive electrode for vanadium redox flow battery, Applied Surface Science, 423 (2017) 111-118.

[89]   T. Wu, K. Huang, S. Liu, S. Zhuang, D. Fang, S. Li, D. Lu, A. Su, Hydrothermal ammoniated treatment of PAN-graphite felt for vanadium redox flow battery, Journal

of Solid State Electrochemistry, 16 (2011) 579-585.

[90]    L. Zhang, B. Wang, Y. Ding, G. Wen, S.B.A. Hamid, D. Su, Disintegrative activation of Pd nanoparticles on carbon nanotubes for catalytic phenol hydrogenation, Catalysis Science & Technology, 6 (2016) 1003-1006.

[91]    D.-Q. Yang, B. Hennequin, E. Sacher, XPS demonstration of π-π interaction between benzyl mercaptan and multiwalled carbon nanotubes and their use in the adhesion of Pt nanoparticles, Chemistry of Materials, 18 (2006) 5033-5038.

[92]    C. Costentin, S. Drouet, M. Robert, J.-M. Savéant, A local proton source enhances $CO_2$ electroreduction to CO by a molecular Fe catalyst, Science, 338 (2012) 90-94.

[93]    T.T. Thanh, H. Ba, L. Truong-Phuoc, J.-M. Nhut, O. Ersen, D. Begin, I. Janowska, D.L. Nguyen, P. Granger, C. Pham-Huu, A few-layer graphene-graphene oxide composite containing nanodiamonds as metal-free catalysts, Journal of Materials Chemistry A, 2 (2014) 11349-11357.

[94]    D.S. Su, J. Zhang, B. Frank, A. Thomas, X. Wang, J. Paraknowitsch, R. Schlogl, Metal-free heterogeneous catalysis for sustainable chemistry, ChemSusChem, 3 (2010) 169-180.

[95]    Z. Zhao, G. Ge, W. Li, X. Guo, G. Wang, Modulating the microstructure and surface chemistry of carbocatalysts for oxidative and direct dehydrogenation: A review, Chinese Journal of Catalysis, 37 (2016) 644-670.

[96]    C. Tang, M.-M. Titirici, Q. Zhang, A review of nanocarbons in energy electrocatalysis: Multifunctional substrates and highly active sites, Journal of Energy Chemistry, 26 (2017) 1077-1093.

[97]    Z. Sun, B. Sun, M. Qiao, J. Wei, Q. Yue, C. Wang, Y. Deng, S. Kaliaguine, D. Zhao, A general chelate-assisted Co-assembly to metallic nanoparticles-incorporated ordered mesoporous carbon catalysts for Fischer-Tropsch synthesis, Journal of the American Chemical Society, 134 (2012) 17653-17660.

[98]    D.D. Nguyen, N.-H. Tai, S.-B. Lee, W.-S. Kuo, Superhydrophobic and superoleophilic properties of graphene-based sponges fabricated using a facile DIP coating method, Energy & Environmental Science, 5 (2012) 7908.

[99]    Z. Li, J. Liu, Z. Huang, Y. Yang, C. Xia, F. Li, One-pot synthesis of Pd nanoparticle

catalysts supported on N-doped carbon and application in the domino carbonylation, ACS Catalysis, 3 (2013) 839-845.

[100] J.L. Stevens, A.Y. Huang, H. Peng, I.W. Chiang, V.N. Khabashesku, J.L. Margrave, Sidewall amino-functionalization of single-walled carbon nanotubes through fluorination and subsequent reactions with terminal diamines, Nano Letters, 3 (2003) 331-336.

[101] A. Chakravarty, K. Bhowmik, G. De, A. Mukherjee, Synthesis of amine functionalized graphite nanosheets and their water-soluble derivative for drug loading and controlled release, New Journal of Chemistry, 39 (2015) 2451-2458.

[102] H. Jing, S. Ren, Y. Shi, X. Song, Y. Yang, Y. Guo, Y. An, C. Hao, Ozonization, amination and photoreduction of graphene oxide for triiodide reduction reaction: An experimental and theoretical study, Electrochimica Acta, 226 (2017) 10-17.

[103] D. Tang, X. Sun, D. Zhao, J. Zhu, W. Zhang, X. Xu, Z. Zhao, Nitrogen-doped carbon xerogels supporting palladium nanoparticles for selective hydrogenation reactions: The role of pyridine nitrogen species, ChemCatChem, 10 (2018) 1291-1299.

[104] W. Kiciński, M. Szala, M. Bystrzejewski, Sulfur-doped porous carbons: Synthesis and applications, Carbon, 68 (2014) 1-32.

[105] H. Wang, X. Bo, Y. Zhang, L. Guo, Sulfur-doped ordered mesoporous carbon with high electrocatalytic activity for oxygen reduction, Electrochimica Acta, 108 (2013) 404– 411.

[106] J.L. Figueiredo, M.F.R. Pereira, M.M.A. Freitas, J.J.M. Orfao, Characterization of active sites on carbon catalysts, Industrial & Engineering Chemistry Research, 46 (2007) 4110-4115.

[107] K.A. Worsley, I. Kalinina, E. Bekyarova, R.C. Haddon, Functionalization and dissolution of nitric acid treated single-walled carbon nanotubes, Journal of the American Chemical Society, 131 (2009) 18153–18158.

[108] M. Fan, C. Zhu, Z.Q. Feng, J. Yang, L. Liu, D. Sun, Preparation of N-doped graphene by reduction of graphene oxide with mixed microbial system and its haemocompatibility, Nanoscale, 6 (2014) 4882-4888.

[109] B.K. Pradhan, N.K. Sandle, Effect of different oxidizing agent treatments on the

surface properties of activated carbons, Carbon, 37 (1999) 1323–1332.

[110] J. Luo, Y. Liu, H. Wei, B. Wang, K.-H. Wu, B. Zhang, D.S. Su, A green and economical vapor-assisted ozone treatment process for surface functionalization of carbon nanotubes, Green Chemistry, 19 (2017) 1052-1062.

[111] W. Xia, C. Jin, S. Kundu, M. Muhler, A highly efficient gas-phase route for the oxygen functionalization of carbon nanotubes based on nitric acid vapor, Carbon, 47 (2009) 919-922.

[112] H. Aguilar-Bolados, D. Vargas-Astudillo, M. Yazdani-Pedram, G. Acosta-Villavicencio, P. Fuentealba, A. Contreras-Cid, R. Verdejo, M.A. López-Manchado, Facile and scalable one-step method for amination of graphene using Leuckart reaction, Chemistry of Materials, 29 (2017) 6698-6705.

[113] L. Lai, L. Chen, D. Zhan, L. Sun, J. Liu, S.H. Lim, C.K. Poh, Z. Shen, J. Lin, One-step synthesis of $NH_2$-graphene from in situ graphene-oxide reduction and its improved electrochemical properties, Carbon, 49 (2011) 3250-3257.

[114] Y.-T. Kim, K. Ohshima, K. Higashimine, T. Uruga, M. Takata, H. Suematsu, T. Mitani, Fine size control of platinum on carbon nanotubes: From single atoms to clusters, Angewandte Chemie International Edition, 118 (2006) 421-425.

[115] M.-H. Hsu, H. Chuang, F.-Y. Cheng, Y.-P. Huang, C.-C. Han, K.-C. Pao, S.-C. Chou, F.-K. Shieh, F.-Y. Tsai, C.-C. Lin, D.-S. Wu, C.-C. Chang, Simple and highly efficient direct thiolation of the surface of carbon nanotubes, RSC Advances, 4 (2014) 14777-14780.

[116] D. Deng, X. Pan, L. Yu, Y. Cui, Y. Jiang, J. Qi, W.-X. Li, Q. Fu, X. Ma, Q. Xue, G. Sun, X. Bao, Toward N-doped graphene via solvothermal synthesis, Chemistry of Materials, 23 (2011) 1188-1193.

[117] H. Jin, H. Zhang, H. Zhong, J. Zhang, Nitrogen-doped carbon xerogel: A novel carbon-based electrocatalyst for oxygen reduction reaction in proton exchange membrane (PEM) fuel cells, Energy & Environmental Science, 4 (2011) 3389–3394.

[118] C. Tang, Q. Zhang, M.Q. Zhao, J.Q. Huang, X.B. Cheng, G.L. Tian, H.J. Peng, F. Wei, Nitrogen-doped aligned carbon nanotube/graphene sandwiches: Facile catalytic growth on bifunctional natural catalysts and their applications as scaffolds for

high-rate lithium-sulfur batteries, Advanced Materials, 26 (2014) 6100-6105.

[119] S. Zhang, S. Tsuzuki, K. Ueno, K. Dokko, M. Watanabe, Upper limit of nitrogen content in carbon materials, Angewandte Chemie International Edition, 54 (2015) 1302-1306.

[120] Y. Chen, X. Li, K. Park, J. Song, J. Hong, L. Zhou, Y.W. Mai, H. Huang, J.B. Goodenough, Hollow carbon-nanotube/carbon-nanofiber hybrid anodes for Li-ion batteries, Journal of the American Chemical Society, 135 (2013) 16280-16283.

[121] T.P. Fellinger, F. Hasche, P. Strasser, M. Antonietti, Mesoporous nitrogen-doped carbon for the electrocatalytic synthesis of hydrogen peroxide, Journal of the American Chemical Society, 134 (2012) 4072-4075.

[122] Y. Deng, Y. Xie, K. Zou, X. Ji, Review on recent advances in nitrogen-doped carbons: Preparations and applications in supercapacitors, Journal of Materials Chemistry A, 4 (2016) 1144-1173.

[123] H. Wang, T. Maiyalagan, X. Wang, Review on recent progress in nitrogen-doped graphene: Synthesis, characterization, and its potential applications, ACS Catalysis, 2 (2012) 781-794.

[124] Z. Shi, Y. Lian, F.H. Liao, X. Zhou, Z. Gua, Y. Zhang, S. Iijima, H. Li, K.T. Yue, S.-L. Zhang, Large scale synthesis of single-wall carbon nanotubes by arc-discharge method, Journal of Physics and Chemistry of Solids, 61 (2000) 1031–1036.

[125] K. Chizari, I. Janowska, M. Houllé, I. Florea, O. Ersen, T. Romero, P. Bernhardt, M.J. Ledoux, C. Pham-Huu, Tuning of nitrogen-doped carbon nanotubes as catalyst support for liquid-phase reaction, Applied Catalysis A: General, 380 (2010) 72-80.

[126] J.-P. Tessonnier, D.S. Su, Recent progress on the growth mechanism of carbon nanotubes: A review, ChemSusChem, 4 (2011) 824 – 847.

[127] E.-G. Wang, A new development in covalently bonded carbon nitride and related materials, Advanced Materials, 11 (1999) 1129-1133.

[128] Y.T. Lee, N.S. Kim, S.Y. Bae, J. Park, S.-C. Yu, H. Ryu, H.J. Lee, Growth of vertically aligned nitrogen-doped carbon nanotubes: Control of the nitrogen content over the temperature range 900- 1100 $^o$C, The Journal of Physical Chemistry B, 107 (2003) 12958-12963.

[129]  J. Liu, S. Webster, D.L. Carroll, Temperature and flow rate of NH$_3$ effects on nitrogen content and doping environments of carbon nanotubes grown by injection CVD method, The Journal of Physical Chemistry B, 109 (2005) 15769-15774.

[130]  K. Chizari, A. Vena, L. Laurentius, U. Sundararaj, The effect of temperature on the morphology and chemical surface properties of nitrogen-doped carbon nanotubes, Carbon, 68 (2014) 369-379.

[131]  R. Sen, B.C. Satishkumar, A. Govindaraj, K.R. Harikumar, M.K. Renganathan, C.N.R. Rao, Nitrogen-containing carbon nanotubes, Journal of Materials Chemistry, 7 (1997) 2335-2337.

[132]  M. Terrones, P. Redlich, N. Grobert, S. Trasobares, W.-K. Hsu, H. Terrones, Y.-Q. Zhu, J.P. Hare, C.L. Reeves, A.K. Cheetham, M. Rühle, H.W. Kroto, D.R.M. Walton, Carbon nitride nanocomposites: Formation of aligned C$_x$N$_y$ nanofibers, Advanced Materials, 11 (1999) 655-658.

[133]  M. José-Yacamán, M. Miki-Yoshida, L. Rendón, J.G. Santiesteban, Catalytic growth of carbon microtubules with fullerene structure, Applied Physics Letters, 62 (1993) 202-204.

[134]  W. Shi, B. Zhang, Y. Lin, Q. Wang, Q. Zhang, D.S. Su, Enhanced chemoselective hydrogenation through tuning the interaction between Pt nanoparticles and carbon supports: Insights from identical location transmission electron microscopy and X-ray photoelectron spectroscopy, ACS Catalysis, 6 (2016) 7844-7854.

[135]  S. Yang, L. Zhi, K. Tang, X. Feng, J. Maier, K. Müllen, Efficient synthesis of heteroatom (N or S)-doped graphene based on ultrathin graphene oxide-porous silica sheets for oxygen reduction reactions, Advanced Functional Materials, 22 (2012) 3634-3640.

[136]  J. Guo, Y. Luo, A.C. Lua, R.-a. Chi, Y.-l. Chen, X.-t. Bao, S.-x. Xiang, Adsorption of hydrogen sulphide (H$_2$S) by activated carbons derived from oil-palm shell, Carbon, 45 (2007) 330-336.

[137]  W. Feng, S. Kwon, X. Feng, E. Borguet, M.A. Radisav D. Vidic, Sulfur impregnation on activated carbon fibers through H$_2$S oxidation for vapor phase mercury removal, Journal of Environmental Engineering, 132 (2006) 292-300.

[138] W. Feng, E. Borguet, R.D. Vidic, Sulfurization of carbon surface for vapor phase mercury removal - i: Effect of temperature and sulfurization protocol, Carbon, 44 (2006) 2990-2997.

[139] J. Wang, B. Deng, X. Wang, J. Zheng, Adsorption of aqueous Hg(ii) by sulfur-impregnated activated carbon, Environmental Engineering Science, 26 (2009) 1693-1699.

[140] H.-C. Hsi, M.A. Mark J. Rood, M. Rostam-Abadi, S. Chen, R. Chang, Mercury adsorption properties of sulfur-impregnated adsorbents, Journal of Environmental Engineering, 128 (2002) 1080-1089.

[141] Y. Otani, C. Kanaoka, H. Emi, I. Uchijima, H. Nishino, Removal of mercury vapor from air with sulfur-impregnated adsorbents, Environmental Science & Technology, 22 (1988) 708-711.

[142] N. Asasian, T. Kaghazchi, Comparison of dimethyl disulfide and carbon disulfide in sulfurization of activated carbons for producing mercury adsorbents, Industrial & Engineering Chemistry Research, 51 (2012) 12046-12057.

[143] A.Macías-García, C.Valenzuela-Calahorro, V.Gómez-Serrano, A.Espínosa-Mansilla, Adsorption of $Pb^{2+}$ by heat-treated and sulfurized activated carbon, Carbon, 31 (1993) 1249-1255.

[144] E.A. Morris, D.W. Kirk, C.Q. Jia, K. Morita, Correction to roles of sulfuric acid in elemental mercury removal by activated carbon and sulfur-impregnated activated carbon, Environmental Science & Technology, 46 (2012) 10857-10857.

[145] N. Mahata, M.F. Pereira, F. Suarez-Garcia, A. Martinez-Alonso, J.M. Tascon, J.L. Figueiredo, Tuning of texture and surface chemistry of carbon xerogels, Journal of Colloid and Interface Science, 324 (2008) 150-155.

[146] X. Zhang, Y. Tang, S. Qu, J. Da, Z. Hao, $H_2S$-selective catalytic oxidation: Catalysts and processes, ACS Catalysis, 5 (2015) 1053-1067.

[147] N. Keller, C. Pham-Huu, C. Crouzet, M.J. Ledoux, S. Savin-Poncet, J.-B. Nougayrede, J. Bousquet, Direct oxidation of $H_2S$ into S. New catalysts and processes based on SiC support, Catalysis Today, 53 (1999) 535–542.

[148] A. Piéplu, O. Saur, J.-C. Lavalley, O. Legendre, C. Nédez, Claus catalysis and $H_2S$

selective oxidation, Catalysis Reviews - Science and Engineering, 40 (1998) 409-450.

[149] N. Keller, C. Pham-Huu, C. Estournes, M.J. Ledoux, Low-temperature selective oxidation of hydrogen sulfide into elemental sulfur on a NiS$_2$/SiC catalyst, Catalysis letters, 61 (1999) 151–155.

[150] H. Ba, Y. Liu, L. Truong-Phuoc, C. Duong-Viet, X. Mu, W.H. Doh, T. Tran-Thanh, W. Baaziz, L. Nguyen-Dinh, J.-M. Nhut, I. Janowska, D. Begin, S. Zafeiratos, P. Granger, G. Tuci, G. Giambastiani, F. Banhart, M.J. Ledoux, C. Pham-Huu, A highly N-doped carbon phase "dressing" of macroscopic supports for catalytic applications, Chemical Communications, 51 (2015) 14393-14396.

[151] M. Zhao, K. Yuan, Y. Wang, G. Li, J. Guo, L. Gu, W. Hu, H. Zhao, Z. Tang, Metal-organic frameworks as selectivity regulators for hydrogenation reactions, Nature, 539 (2016) 76-80.

[152] D. Wang, Y. Zhu, C. Tian, L. Wang, W. Zhou, Y. Dong, H. Yan, H. Fu, Synergistic effect of tungsten nitride and palladium for the selective hydrogenation of cinnamaldehyde at the C=C bond, ChemCatChem, 8 (2016) 1718-1726.

[153] D. Wang, Y. Zhu, C. Tian, L. Wang, W. Zhou, Y. Dong, Q. Han, Y. Liu, F. Yuan, H. Fu, Synergistic effect of Mo$_2$N and Pt for promoted selective hydrogenation of cinnamaldehyde over Pt-Mo$_2$N/SBA-15, Catalysis Science & Technology, 6 (2016) 2403-2412.

[154] P. Gallezot, D. Richard, Selective hydrogenation of α, β-unsaturated aldehydes, Catalysis Reviews - Science and Engineering, 40 (1998) 81-126.

[155] F. Delbecq, P. Sautet, Competitive C=C and C=O adsorption of α-β unsaturated aldehydes on Pt and Pd surfaces in relation with the selectivity of hydrogenation reactions: A theoretical approach, Journal of Catalysis, 152 (1995) 217-236.

[156] S. Galvagno, G. Capannelli, A.D. G. Neri, R. Pietropaolo, Hydrogenation of cinnamaldehyde over Ru/C catalysts: Effect of Ru particle size, Journal of Molecular Catalysis, 64 (1991) 237-246.

[157] A. Giroir-Fendler, D. Richard, P. Gallezot, Chemioselectivity in the catalytic hydrogenation of cinnamaldehyde. Effect of metal particle morphology, Catalysis letters, 5 (1990) 175-182.

[158] C. Minot, P. Gallezot, Competitive hydrogenation of benzene and toluene: Theoretical study of their adsorption on ruthenium, rhodium, and palladium, Journal of Catalysis, 123 (1990) 341-348.

[159] M.L. Toebes, F.F. Prinsloo, A. Jos van Dillen, J.H. Bitter, K.P. de Jong, Influence of oxygen-containing surface groups on the activity and selectivity of carbon nanofiber-supported ruthenium catalysts in the hydrogenation of cinnamaldehyde, Journal of Catalysis, 214 (2003) 78-87.

[160] M.L. Toebes, A. Jos van Dillen, Y. Zhang, J. Hájek, D.Y. Murzin, T.A. Nijhuis, D.C. Koningsberger, J.H. Bitter, K.P. de Jong, Support effects in the hydrogenation of cinnamaldehyde over carbon nanofiber-supported platinum catalysts: Characterization and catalysis, Journal of Catalysis, 226 (2004) 215-225.

[161] M.L. Toebes, T. Alexander Nijhuis, J. Hájek, J.H. Bitter, A. Jos van Dillen, D.Y. Murzin, K.P. de Jong, Support effects in hydrogenation of cinnamaldehyde over carbon nanofiber-supported platinum catalysts: Kinetic modeling, Chemical Engineering Science, 60 (2005) 5682-5695.

[162] A.J. Plomp, H. Vuori, A.O.I. Krause, K.P. de Jong, J.H. Bitter, Particle size effects for carbon nanofiber supported platinum and ruthenium catalysts for the selective hydrogenation of cinnamaldehyde, Applied Catalysis A: General, 351 (2008) 9-15.

[163] H. Vu, F. Goncalves, R. Philippe, E. Lamouroux, M. Corrias, Y. Kihn, D. Plee, P. Kalck, P. Serp, Bimetallic catalysis on carbon nanotubes for the selective hydrogenation of cinnamaldehyde, Journal of Catalysis, 240 (2006) 18-22.

[164] B.F. Machado, H.T. Gomes, P. Serp, P. Kalck, J.L. Faria, Liquid-phase hydrogenation of unsaturated aldehydes: Enhancing selectivity of multiwalled carbon nanotube-supported catalysts by thermal activation, ChemCatChem, 2 (2010) 190-197.

[165] S.C. Tsang, N. Cailuo, W. Oduro, A.T.S. Kong, L. Clifton, K.M.K. Yu, B. Thiebaut, J. Cookson, P. Bishop, Engineering preformed cobalt-doped platinum nanocatalysts for ultraselective hydrogenation, ACS Nano, 2 (2008) 2547-2553.

# Chapter 2

**Catalysts preparation, characterization**

**and catalytic applications**

# Catalysts preparation, characterization and catalytic applications

## 1. Catalyst preparation

## 1.1 Graphite felt (GF) and gaseous HNO$_3$ treatment of GF (Chapter 3)

### 1.1.1 Graphite felt

The commercial filamentous GF, ex-polyacrinonitrile (PAN), with a dimension of 1 x 3 m$^2$ (thickness of 6 mm) was supplied by Carbone Lorraine. The as-received GF was shaped in the form of pellets ($\varnothing$ x thickness of 4 x 6 mm) for the experiment. The GF displays a relatively low specific surface area, 10 $\pm$ 2 m$^2$/g measured by means of N$_2$ adsorption, which is mostly linked with the geometric surface area and is in good agreement with the extremely low porosity of the material. It is worthy to note that the GF can also be shaped in various dimensions including pellets, disks or complexes structures, depending to the downstream applications, i.e. gas- or liquid-phase reactions, which represent a net advantage compared to other metal-free catalysts where low-dimensional shape is a main concern for further industrial development.

### 1.1.2 Gaseous HNO$_3$ treatment of GF

For the gaseous acid treatment, as shown in Figure 1, the GF was first oxidized at moderate temperature (500 $^o$C) in air for 1 h in order to remove as much as possible residue from it surface. The as-treated and pre-shaped GF was loaded inside a tubular reactor and heated to the desired temperature of 250 $^o$C by an external electrical furnace. The treatment temperature was fixed at 250 $^o$C according to the previous investigation results reported by Duong-Viet et al. [1]. The treatment temperature was controlled by a thermocouple inserted inside the furnace. The reactor containing GF in the form of pellet ($\varnothing$ x thickness of 4 x 6 mm) was connected to a round bottom flask filled with 150 mL of HNO$_3$ with a concentration of 65%. The temperature of the round bottom flask was fixed at 125 $^o$C and the HNO$_3$ solution was keep under magnetic stirring. The gaseous acid was passed upward through the GF pellet keep at 250 $^o$C. The gaseous acid passed through the GF bed was further condensed in another

flask which can be re-used for the process and thus, reducing in a significant manner the problem linked with liquid waste recycling and recovery. The sample was treated with different durations in order to rule out the influence of these treatments on its final microstructure and chemical properties and to correlate these physical properties with the catalytic activity. The sample was washed one time with deionized water after the acid treatment and oven dried at $130\,^{o}C$ for overnight. In this work, the GF after acid treated are noted as follows: OGF-X, X stands for the treatment duration in hour, for example: OGF-24 indicates that the raw GF was treated for 24 h under gaseous $HNO_3$. It is noted that the treatment is not only limited to small amount of catalyst as higher amount of GF can be also prepared by changing the reactor size.
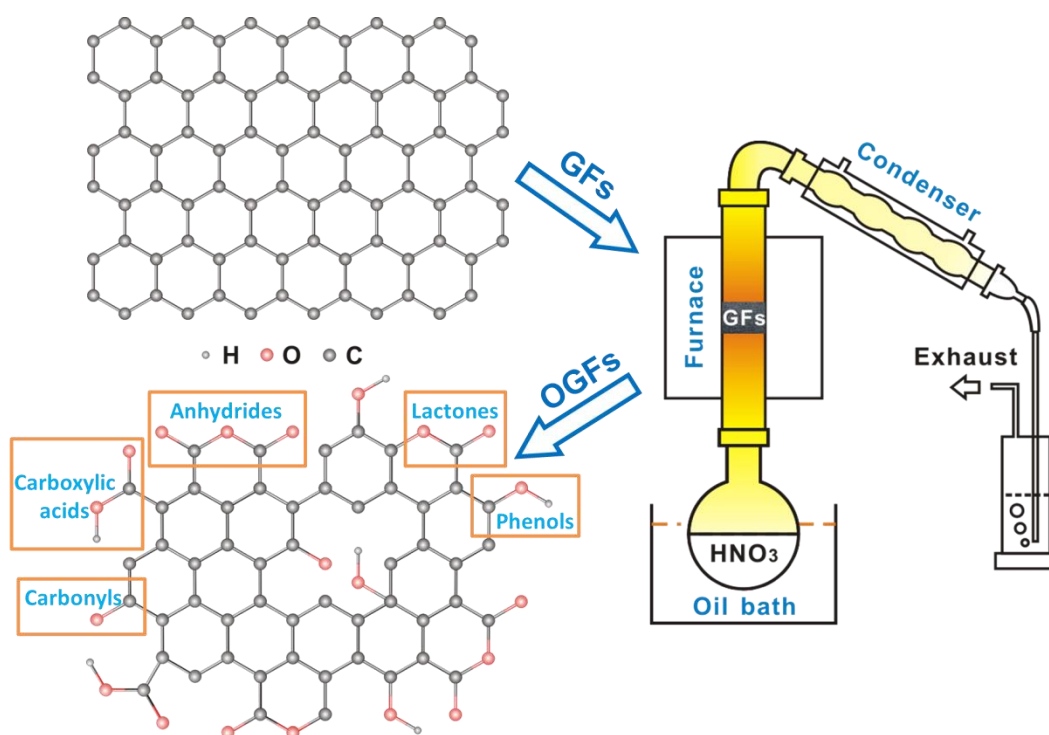


**Figure 1.** Schematic illustration of the OGF prepared by the gaseous $HNO_3$ treatment and the different oxygenated functional groups generated on the graphite surface after the acid treatment.

## 1.2 Materials and catalysts (Chapter 4)

### 1.2.1 Materials

The commercial GF constituted by carbon microfilamentous (Carbone Lorraine Ltd) were firstly treated by gaseous $HNO_3$ as reported previous (Figure 2) [1, 2]. In a typical procedure, the GF in the form of disk ($\varnothing$ x thickness of 24 x 6 mm, 0.24 g) was loaded in a tubular reactor which was connected to a round bottom flask filled with 10 mL of $HNO_3$ (65%). The round bottom flask with $HNO_3$ solution was heated at 125 $^o$C and keep under magnetic stirring. Meanwhile the 10 mL/min of Ar was introduced into the flask to drive the gaseous acid upwards through the GF. The GF sample was treated in the presence of gaseous acid at 250 $^o$C for 4 h. The reactant gas passed through the GF bed was further condensed in another flask. The pressure of the treatment system is 1 atm. The as-treated sample was then washed once with deionized water to remove trace amount of impurities followed by an oven drying at 130 $^o$C overnight. The as-treated GF were denoted as OGF.
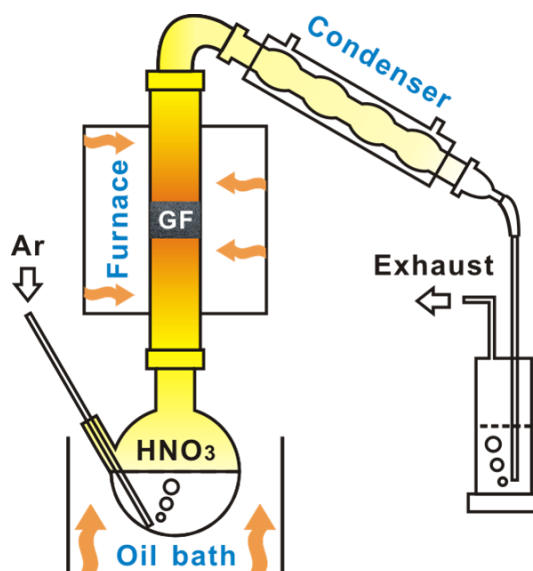


**Figure 2.** Schematic illustration of the gaseous $HNO_3$ thermal treatment of GF.

### 1.2.2 Catalysts

The palladium was deposited onto the carbon support via an incipient wetness impregnation method using a palladium nitrate ($Pd(NO_3)_2 \cdot 6H_2O$, Fluka) as salt precursor in aqueous solution. The theoretical concentration of metallic Pd was fixed at 5 wt. %. The impregnated solid was oven dried at $110\,^{o}C$ for 2 h and calcined in air at $350\,^{o}C$ for 2 h in order to decompose the palladium nitrate into its corresponding oxide. The catalyst was further reduced under hydrogen flow at $350\,^{o}C$ for 2 h. The catalyst was removed from the reactor at room temperature and stored in close vial before characterizations or catalytic experiments.

## 1.3 Support synthesis and catalyst preparation (Chapter 5)

### 1.3.1 Support synthesis

The commercial carbon felt (CF) constituted by carbon microfilamentous (Carbone Lorraine Ltd) were firstly treated by gaseous $HNO_3$ as Chapter 4 [3]. The as-received CF was shaped in the form of disk ($\varnothing$ x thickness of 24 x 14 mm, 0.56 g) for the experiment. The as-treated CF was denoted as OCF.

For the preparation of aminated samples, the pre-synthesized OCF were immersed in an aqueous solution (20 mL) of urea (6 mol/L) followed by sonication for 1 h. The above solution was then transferred into a 50 mL Teflon-lined autoclave and kept at 150 $^{o}C$ under autogenous pressure for 24 h. After urea-hydrothermal treatment, the product denoted as AOCF was washed and dried at 130 $^{o}C$ overnight. The synthesis procedure of ACF was the same as AOCF using pristine CF without pre-oxidation.

The nitrogen-doped NAOCF sample was then obtained by thermal annealing of the pre-synthesized AOCF at 900 $^{o}C$ for 2 h under the inert atmosphere of Ar flow.

### 1.3.2 Catalysts preparation

The palladium was deposited onto the carbon support as follows: the CF-based support (0.13 g) including CF, ACF, OCF, AOCF and NAOCF was firstly immersed in an aqueous solution (15 mL) with a controlled amount of palladium nitrate ($Pd(NO_3)_2 \cdot 6H_2O$, Fluka),

followed by stirring for 3 h. Subsequently, the Pd precursor was reduced and supported on the carbon support by adding $NaBH_4$ (Sigma-Aldrich) at room temperature. After stirring for 3 h, the sample was washed and dried at room temperature in vacuum overnight. The final composite was labeled as Pd/CF, Pd/ACF, Pd/OCF, Pd/AOCF and Pd/NAOCF, respectively. Before characterizations or catalytic experiments the catalyst was further reduced in the hydrogenation reaction condition (80 $^o$C) as described below without any reactant. The real amount of loading Pd was detected by inductively coupled plasma-atomic emission spectroscopy.

## 1.4 Carbon support synthesis and Pd catalyst preparation (Chapter 6)

### 1.4.1 Carbon support synthesis

The commercial carbon felt (CF) constituted by carbon microfilamentous (Carbone Lorraine Ltd) were firstly treated by gaseous $HNO_3$ as Chapter 4 and 5 [3]. The as-received CF was shaped in the form of disk ($\varnothing$ x thickness of 24 x 14 mm, 0.56 g) for the experiment. The as-treated CF was denoted as OCF.

For the preparation of thiolated samples, the reaction between the pre-synthesized OCF and $H_2S$ was carried out in an all glass microreactor working isothermally at atmospheric pressure. The temperature was controlled by a K-type thermocouple and a Minicor regulator. The gas mixture was passed downward through the reaction bed. Before the treatment, the reactor was flushed with helium at room temperature. The sample was slowly heated up to 230 $^o$C, and then the helium flow was replaced by the reactant mixture of 25 mL/min (0.25 mL/min $H_2S$, 2.5 mL/min $H_2O$ and 22.25 mL/min He). The gases ($H_2S$, $H_2O$ and He) flow rate was monitored by Brooks 5850TR mass flow controllers linked to a control unit. The composition of the reactant feed was $H_2S$ (1 or 4 vol. %), $H_2O$ (10 vol. % or not) and He (balance). The steam (10 vol. %) was fed to the gas mixture by bubbling a helium flow through a liquid tank containing water maintained at 52 $^o$C. After the reaction of 2 h, the products obtained using different reactant were denoted as T4OCF (4 vol.% $H_2S$), T1OCF (1 vol.% $H_2S$) and T1H1OCF (1 vol.% $H_2S$ and 10 vol.% $H_2O$). The T4OCF was also denoted as TOCF for the sake of discussion. The synthesis procedure of thiolated CF (TCF) was the same

as TOCF by replacing OCF with pristine CF without pre-oxidation.

The sulfur-doped TOCF (STOCF) was then obtained by the thermal annealing of pre-synthesized TOCF at 700 $^{o}$C for 2 h under the inert atmosphere of Ar flow.

### 1.4.2 Pd catalysts preparation

The palladium was deposited onto the carbon support as follows: the CF-based support (0.13 g) including OCF, TOCF and STOCF was firstly immersed in an aqueous solution (15 mL) with a controlled amount of palladium nitrate ($Pd(NO_3)_2 \cdot 6H_2O$, Fluka), followed by stirring for 3 h. Subsequently, the Pd precursor was reduced and directly supported on the carbon support by adding $NaBH_4$ (Sigma-Aldrich) at room temperature into the solution. After stirring for 3 h, the sample was washed and dried at room temperature under vacuum overnight. The final composite was labeled as $Pd_s$/OCF, $Pd_s$/TOCF, $Pd_{us}$/TOCF and $Pd_{us}$/STOCF, where the subscript "s" and "us" stand for the saturated and unsaturated loading palladium, respectively. The $Pd_{us}$/TOCF was further treated with 30 % of hydrogen peroxide (-$H_2O_2$) at room temperature and air (-Air) as well as hydrogen (-$H_2$) flow at 400 $^{o}$C for 2 h to remove the sulfur content. The samples were denoted $Pd_{us}$/TOCF-X where X stands for $H_2O_2$, air or $H_2$. Before characterizations or catalytic experiments the catalyst was further reduced in the hydrogenation reaction condition as described below without any reactant. The real amount of loading Pd was detected via inductively coupled plasma-atomic emission spectroscopy.

## 2. Catalysts characterization

The scanning electron microscopy (SEM) and elemental mapping were carried out on a ZEISS GeminiSEM 500 microscope with a resolution of 5 nm. The sample was deposited onto a double face graphite tape in order to avoid the problem of charging effect during the analysis.

The loading amount of Pd was determined by inductively coupled plasma-atomic emission spectroscopy (ICP-AES, Plasma-Spec-II spectrometer).

The microstructure of the carbon filamentous and the deposited metal active phase was

analyzed by transmission electron microscopy (TEM). The TEM analyze was carried out on a JEOL 2100F working at 200 kV accelerated voltage and a point-to-point resolution of 0.1 nm. The sample was dispersed by ultrasounds in an ethanol solution for 5 min and a drop of the solution was deposited on a copper grid covered with a holey carbon membrane for observation.

The Raman spectra were recorded using a LabRAM ARAMIS Horiba Raman spectrometer equipped with a Peltier cooled CCD detector. A laser line (532 nm/100 mW (YAG) with Laser Quantum MPC600 PSU) was used to excite sample.

BET surface areas were measured using a commercial BET unit (Tristar, Micromeritics) using $N_2$ adsorption at 77 K. Before the $N_2$ adsorption, samples were outgassed at 250 $^o$C for 14 h under dynamic vacuum to desorb surface impurities. $S_{BET}$ is the surface area of the sample calculated from the nitrogen isotherm using the BET method. The pore size distribution was determined from the results obtained on the desorption branch of the $N_2$ isotherm.

Fourier transform infrared (FTIR) measurements were carried out to check the surface composition of the pretreated samples using a Nicolet iS10 FTIR spectrometer (Thermo Scientific) equipped with a Smart Diamond ATR (attenuated total reflection) accessory in the spectral range of 400- 4000 cm$^{-1}$.

The oxygen functional groups of samples were determined by the temperature-programmed desorption conducted on a Micromeritics ASAP-2100 setup equipped with a multichannel mass spectrometer (TPD-MS). In a typical procedure, 50 mg of the samples was loaded in the reactor and then flushed with He (50 mL/min) at 50 $^o$C for 1 h. Afterward, the temperature was raised from 50 to 1000 $^o$C at a heating rate of 5 $^o$C/min. The evolved species were monitored with intensities of *m/e* 28 (CO) and 44 ($CO_2$), respectively.

Thermogravimetric analyses (TGA) were performed under air (25 mL/min) on a TGA-Q5000 Sorption Analyzer (TA Instrument), the temperature was raised to 1000 $^o$C at a heating rate of 10 $^o$C/min.

The temperature-programmed reduction of hydrogen ($H_2$-TPR) was conducted on a

Micromeritics ASAP-2100 setup equipped with a multichannel mass spectrometer. In a typical procedure, 50 mg of the sample was previously heated for 1 h at 130 $^{o}$C under an Ar stream, and then it was cooled to room temperature. After the stream was switched from Ar to 10% $H_2$/Ar mixture gas flow of 50 mL/min, the sample was heated by increasing the temperature linearly at a rate of 10 $^{o}$C/min. The evolved species were monitored with intensities of *m/e* 2 ($H_2$).

The X-ray photoelectron spectroscopy (XPS) measurements of the support and catalyst were performed by using a MULTILAB 2000 (THERMO) spectrometer equipped with an AlKα anode (hv = 1486.6 eV) with 10 min of acquisition to achieve a good signal to noise ratio. Peak deconvolution was performed with the "Avantage" program from the Thermoelectron Company. The C1s photoelectron binding energy was set at 284.6 eV relative to the Fermi level and used as reference to calibrate the other peak positions.

The temperature-programmed desorption of hydrogen ($H_2$-TPD) was conducted on a Micromeritics ASAP-2100 setup equipped with a multichannel mass spectrometer. In a typical procedure, 50 mg of the sample was reduced under 10% $H_2$/Ar mixture gas flow of 50 mL/min at 350 $^{o}$C for 1 h before experiment. And then the temperature of sample was kept at 50 $^{o}$C under 10% $H_2$/Ar mixture gas flow for 1 h. The He was switched in with a flow rate of 50 mL/min and the sample was flushed at 50 $^{o}$C for 1 h. Afterward, the temperature was raised from 50 to 800 $^{o}$C at a heating rate of 10 $^{o}$C/min. The evolved species were monitored with intensities of *m/e* 2 ($H_2$).

## 3. Catalytic applications

### 3.1 Gas-phase selective oxidation of $H_2S$

The catalytic selective oxidation of $H_2S$ by oxygen (Eq. 1) was carried out in an all glass microreactor working isothermally at atmospheric pressure. During the reaction other secondary reactions could also take place: consecutive oxidation of the formed sulphur with an excess of oxygen or direct oxidation of $H_2S$ to yield $SO_2$ (Eq. 2 and 3). The temperature was controlled by a K-type thermocouple and a Minicor regulator. The gas mixture was

passed downward through the catalyst bed. Before the test, the reactor was flushed with helium at room temperature until no trace of oxygen was detected at the outlet. The helium flow was replaced by the one containing steam. The catalyst was slowly heated up to the reaction temperature, and then the wet helium flow was replaced by the reactant mixture. The gases ($H_2S$, $O_2$, He) flow rate was monitored by Brooks 5850TR mass flow controllers linked to a control unit. The composition of the reactant feed was $H_2S$ (1 vol. %), $O_2$ (1.25 vol. % or 2.5 vol. %), $H_2O$ (10 vol. % or 30 vol. %) and He (balance). The use of a relatively high concentration of steam in the feed is motivated by the will to be as close as possible to the industrial working conditions as the steam formed during the former Claus units is not removed before the oxidation step and remains in the treated tail gas. The steam (10 vol. % or 30 vol. %) was fed to the gas mixture by bubbling a helium flow through a liquid tank containing water maintained at $56\,^{\circ}C$ or $81\,^{\circ}C$. The $O_2$-to-$H_2S$ molar ratio was varied from 1.25 to 2.5 with a Weight Hourly Space Velocity (WHSV) at $0.05\ h^{-1}$ or $0.1\ h^{-1}$. It is worth to note that the WHSV used in the present work is close to the usual WHSV used in the industrial process for this kind of reaction, i.e. $0.09\ h^{-1}$.

$$H_2S \ + \ 1/2\ O_2 \ \rightarrow \ 1/n\ S_n \ + \ H_2O \qquad \Delta H \ = \ -\ 222\ kJ.mol^{-1} \qquad (1)$$

$$1/n\ S_n + O_2 \rightarrow SO_2 \qquad \Delta H = -\ 297\ kJ.mol^{-1} \qquad (2)$$

$$H_2S \ + \ 3/2\ O_2 \ \rightarrow \ SO_2 \ + \ H_2O \qquad \Delta H \ = \ -\ 519\ kJ.mol^{-1} \qquad (3)$$
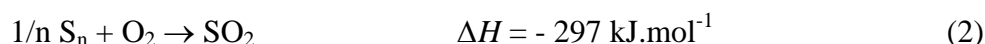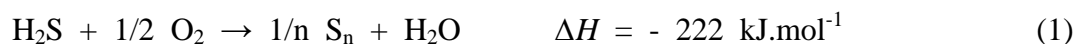
The reaction was conducted in a continuous mode and the sulfur formed during the reaction was vaporized, due to the relatively high partial pressure of sulfur at these reaction temperatures, and was further condensed at the exit of the reactor in a trap maintained at room temperature.

The analysis of the inlet and outlet gases was performed on-line using a Varian CP-3800 gas chromatography (GC) equipped with a Chrompack CP-SilicaPLOT capillary column coupled with a thermal conductivity detector (TCD), allowing the detection of $O_2$,

$H_2S$, $H_2O$ and $SO_2$. The limit detection of the $H_2S$ and $SO_2$ is about 10 ppm. The results are reported in terms of $H_2S$ conversion and sulfur selectivity in percent. The percent of sulfur and $SO_2$ selectivity is calculated on a basis of 100%. The sulfur balance is calculated on the basis of the sum of sulfur detected in the solid sulfur recovered in the cold trap and the selectivity towards $SO_2$ and the theoretical sulfur calculated from the $H_2S$ conversion on the catalyst. The sulfur balance is about 92% and the difference could be attributed to (i) some dissolution of $SO_2$ into the condensed water at the exit of the reactor, (ii) the incomplete recovery of the solid sulfur in the cold trap, and (iii) the incomplete recovery of the condensed sulfur in the cold trap leading to uncertainty during the weighting of the sample.

## 3.2 Liquid-phase selective hydrogenation of α, β-unsaturated cinnamaldehyde

The selective hydrogenation of cinnamaldehyde (CAD) led to the formation of three reaction products namely hydrocinnamaldehyde (HCAD), which was formed by the selective hydrogenation of the C=C bond, cinnamyl alcohol (CAL), which was formed by the selective hydrogenation of the C=O bond, and hydrocinnamylalcohol (HCAL) which was formed by a complete hydrogenation of both unsatured C=C and C=O bonds (Figure 3).

In Chapter 4, the selective hydrogenation of the CAD was carried out in a glass reactor (volume = 250 mL) at atmospheric pressure. The Pd/GF catalyst was mounted on a glass holder fixed to a mechanical stirrer and thus, acting both as a catalyst and as mechanical stirrer. Work is ongoing to evaluate the influence of the other stirrer-catalyst configuration such as those reported by Schouten and co-workers [4], i.e. T-shaped stirrer, on the hydrogenation performance. The reaction medium contained a known concentration (0.08 mol/L) of CAD (Sigma-Aldrich) in dioxane (Alfa Aesar) solvent (100 mL) and was heated up from room temperature to the reaction temperature (80 $^o$C) with an oil bath at a heating rate of 5 $^o$C/min. Dioxane was used instead of alcohol in order to avoid any homogeneous reactions which could lead to the formation of heavier by-products. At 80 $^o$C the catalyst was immersed into the reaction medium and rotated at different speeds (250-500 rpm).The hydrogen was continuously supplied into the reactor medium at a flow rate of 50 mL/min.

In Chapter 5 and 6, the selective hydrogenation of the CAD was carried out in an all glass reactor (volume = 25 mL) at atmospheric pressure. The reaction medium contained a known concentration (0.08 mol/L) of CAD (Sigma-Aldrich) in dioxane (Alfa Aesar) solvent (10 mL) and was heated up from room temperature to the reaction temperature (80 $^{\circ}$C) with an oil bath at a heating rate of 5 $^{\circ}$C/min. The reaction was stirred with a magnetic stirrer at a rate of 300 rpm. The hydrogen was continuously supplied into the reactor medium at a flow rate of 25 mL/min.

The hydrogen stream was regulated by Brooks 5850 TR mass flow controller. The liquid medium was withdrawn at a regular time and analyzed by a gas chromatography (GC) on a Varian 3800 CX equipped with a PONA column and a Flame Ionization Detector (FID). The products were calibrated by using pure components diluted in a dioxane solution. The conversion and product distribution were calculated from the GC results.
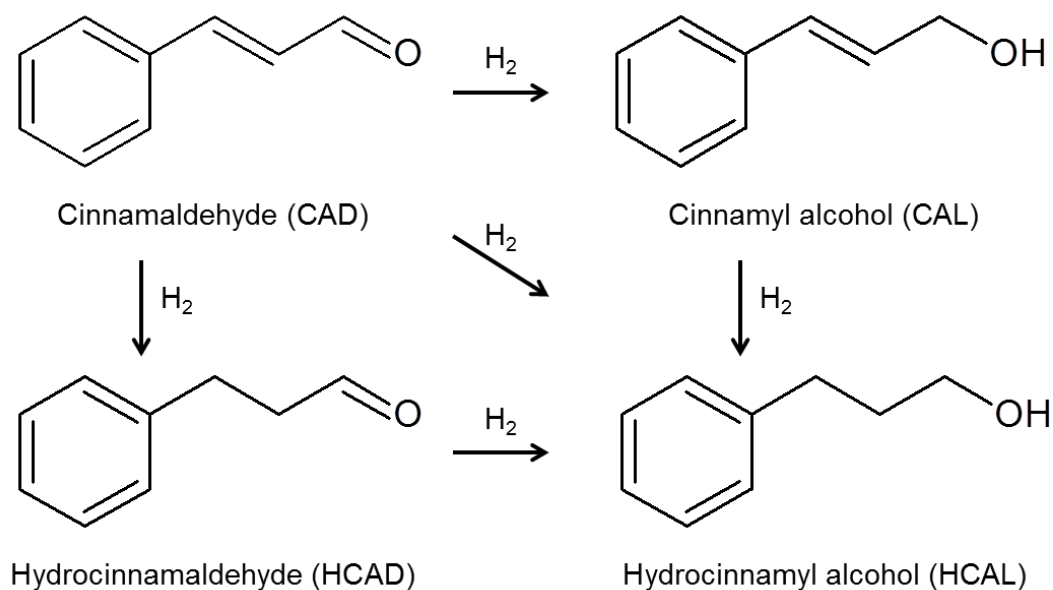


**Figure 3.** Reaction scheme for the hydrogenation of cinnamaldehyde.

# References

[1]    C. Duong-Viet, Y. Liu, H. Ba, L. Truong-Phuoc, W. Baaziz, L. Nguyen-Dinh, J.-M. Nhut, C. Pham-Huu, Carbon nanotubes containing oxygenated decorating defects as metal-free catalyst for selective oxidation of $H_2S$, Applied Catalysis B: Environmental, 191 (2016) 29-41.

[2]    Z. Xu, C. Duong-Viet, H. Ba, B. Li, T. Truong-Huu, L. Nguyen-Dinh, C. Pham-Huu, Gaseous nitric acid activated graphite felts as hierarchical metal-free catalyst for selective oxidation of $H_2S$, Catalysts, 8 (2018) 145-162.

[3]    Z. Xu, C. Duong-Viet, Y. Liu, W. Baaziz, B. Li, L. Nguyen-Dinh, O. Ersen, C. Pham-Huu, Macroscopic graphite felt containing palladium catalyst for liquid-phase hydrogenation of cinnamaldehyde, Applied Catalysis B: Environmental, 244 (2019) 128–139.

[4]    M.A. Leon, T.A. Nijhuis, J.v.d. Schaaf, J.C. Schouten, Mass transfer modeling of a consecutive reaction in rotating foam stirrer reactors: Selective hydrogenation of a functionalized alkyne, Chemical Engineering Science, 73 (2012) 412-420.

# Chapter 3

**Gaseous nitric acid activated graphite felts as hierarchical metal-free catalyst for selective oxidation of H$_2$S**

*Chapter 3*

# Gaseous nitric acid activated graphite felts as hierarchical metal-free catalyst for selective oxidation of H₂S

*Zhenxin Xu [a,\*], Cuong Duong-Viet [b,\*], Housseinou Ba [a], Bing Li [a],*

*Tri Truong-Huu [c], Lam Nguyen-Dinh [c] and Cuong Pham-Huu [a,\*]*

*(a) Institut de Chimie et Procédés pour l'Energie, l'Environnement et la Santé (ICPEES), ECPM, UMR 7515 du CNRS-Université de Strasbourg, 25 rue Becquerel, 67087 Strasbourg Cedex 02, France*

*(b) Ha Noi University of Mining and Geology, 18 Pho Vien, Duc Thang – Bac Tu Liem – Ha Noi, Viet-Nam*

*(c) The University of Da-Nang, University of Science and Technology, 54 Nguyen Luong Bang, Da-Nang, Viet-Nam*

**\****Corresponding authors:*

*zhenxin.xu@etu.unistra.fr (Zhenxin Xu)*

*duongviet@unistra.fr (Cuong Duong-Viet)*

*cuong.pham-huu@unistra.fr (Cuong Pham-Huu)*

**Abstract**

In this study, we reported on the influence of gaseous $HNO_3$ treatment on the formation of defects decorated with oxygenated functional groups on commercial graphite felts (GFs). The gaseous acid treatment also leads to a remarkable increase of the specific as well as effective surface area through the formation of a highly porous graphite structure from dense graphite filamentous. The as-synthesized catalyst was further used as a metal-free catalyst in the selective oxidation of $H_2S$ in industrial waste effluents. According to the results the defects decorated with oxygenated groups were highly active for performing selective oxidation of $H_2S$ into elemental sulfur. The desulfurization activity was relatively high and extremely stable as a function of time on stream which indicated the high efficiency of these oxidized un-doped GFs as metal-free catalysts for the selective oxidation process. The high catalytic performance was attributed to both the presence of structural defects on the filamentous carbon wall which acting as a dissociative adsorption center for the oxygen and the oxygenated functional groups which could play the role of active sites for the selective oxidation process.

# 1. Introduction

Nanocarbon-based metal-free catalysts consisted by nitrogen-doped carbon matrix have received an ever increasing scientific and industrial interest in the field of heterogeneous catalysis since the last decade for several potential processes [1-6]. The introduction of hetero-element atoms, i.e. N, S or P, inside the carbon matrix leads to the formation of metal-free catalysts which can activate oxygen bond to generate reactive intermediates in different catalytic reactions according to the first report from Dai and co-workers [7]. The most studied form of these metal-free catalysts is consisted by carbon nanotubes doped with nitrogen atoms, which has been extensively used in several catalytic processes [8-13]. Recently, work reported by Pham-Huu and Gambastiani [14, 15] has shown that nitrogen-doped mesoporous carbon film, synthesized from food stuff raw materials, displays a high performance for different catalytic processes such as oxygen reduction reaction (ORR), direct dehydrogenation of ethylbenzene and selective oxidation of $H_2S$. Such nitrogen-doped metal-free catalysts display an extremely high stability as a function of time on stream or cycling tests which could be directly attributed to the complete lack of sintering consecutively to the direct incorporation of the nitrogen atoms inside the carbon matrix.

Nitrogen sites could also be efficiently replaced by carbon nanotubes containing surface defects decorated with oxygenated functional groups for the selective oxidation of $H_2S$ into elemental sulfur [16]. Such all carbon metal-free catalyst displays a high stability as a function of the test duration and under severe reaction conditions, i.e. high space velocity, low $O_2$-to-$H_2S$ ratio. In the literature, the incorporation of these oxygenated functional groups has generally been carried out through oxidation treatments of the pristine carbon materials with different oxidants such as liquid $HNO_3$ [17, 18], $H_2SO_4$ [19], $KMnO_4$ [20], $H_2O_2$ [21] or through gaseous reactants like oxygen plasma [22], ozone [23] or $CO_2$ [24]. The main drawbacks of the liquid-phase treatments are the generation of a large amount of acid waste and the need for subsequence washing step to remove the residual acid adsorbed on the sample surface. The gas-phase treatments seem to be the most appropriate ones for generating oxygenated functional groups on the carbon-based surface. Recent work by Su and co-workers [25] has shown that catalyst consisted by carbon nanotubes treated under ozone displays a high catalytic performance for different catalytic processes. The main drawback of such nano-catalyst is its nanoscopic dimension which renders difficult handling and transport and induce high pressure drop in an industrial fixed-bed configuration. The catalyst recovery also

represents a problem of health concern due to its high ability to be breathed. In addition, the carbon nanotubes synthesis also requires the use of explosive and toxic organic compounds and hydrogen which induce a high cost operation due to the post-synthesis treatment of the by-products [26, 27]. The purification process to remove the growth catalyst also leads to the generation of a large amount of wastewater, consecutive to the acid and basic treatment of the as-synthesized samples, which represents an environmental concern as well. It is thus of high interest to develop new metal-free carbon-based catalysts with high porosity, low cost, environmental benign, controlled macroscopic shape and easy for scale up to replace the metal-free based carbon nanomaterials.

In the present article we report on the use of gaseous oxidative $HNO_3$ to create surface defects, with exposed prismatic planes and decorated with oxygen functionalized groups, on the commercially available macroscopic carbon filamentous surface. The oxidized graphite felts (OGFs) will be directly tested as metal-free catalyst for the selective oxidation of $H_2S$ issued from the refinery stream effluents to prevent the problem of air pollution [28-33]. Indeed, sulfur recovery from $H_2S$ containing in industrial effluents, mostly generated from oil refineries and natural gas plants, has become an increasingly important topic as $H_2S$ is a highly toxic compound and represents a major air pollutant, which enters the atmosphere and causes acid rain [34, 35]. The general process is to selectively transform $H_2S$ into elemental sulfur by the equilibrated Claus process: $2 H_2S + SO_2 \rightarrow (3/n) S_n + 2 H_2O$ [36]. However, because of the thermodynamic limitations of the Claus equilibrium reaction, a residual concentration of $H_2S$ of up to 3 vol% is still present in the off-gas. To remove this residual $H_2S$ in the effluent gas before releasing into atmosphere, a new process called super-Claus has been developed, which is a single-step catalytic selective oxidation of $H_2S$ to elemental sulfur by using oxygen gas: $H_2S + 1/2 O_2 \rightarrow (1/n) S_n + H_2O$. The super-Claus process is a direct oxidation process and thus is not limited by thermodynamic equilibrium. In the present work the as-treated metal-free catalyst exhibits an extremely high catalytic performance as well as stability compared to the untreated. The catalytic sites could be attributed to the presence of oxygen species such as carbonyl, anhydride and carboxyl groups decorating the structural defects present on the GFs surface defects upon treating under gaseous $HNO_3$. It is worthy to note that as far as the literature results are concerned, no such catalytic study using oxidized commercial filamentous GFs directly as metal-free catalyst with controlled macroscopic shape has been reported so far. The GFs also avoids the use of nanoscopic carbon with uncertainty about health concerns along

with a validated industrial production and competitive production cost compared to the carbon nanotubes or carbon nanofibers.

## 2. Results and discussion

### 2.1. Characteristics of the acid treated graphite felts

The macroscopic shape of the filamentous GFs was completely retained after the gaseous $HNO_3$ treatment according to SEM micrographs with difference magnifications presented in Figure 1A to D. The $HNO_3$ treated filamentous GFs was decorated with an evenly carbon nodules as evidenced by the SEM analysis (Figure 1D and E). High magnification SEM micrographs (Figure 1E and F) also evidence the formation of cracks and holes on the cross section of the OGFs sample (indicated by arrows). Such cracks could be attributed to the degradation of the graphite structure during the acid treatment. It is worthy to note that the acid treatment also leads to the formation of a rougher graphite surface (Figure 1F) compared to the smooth one for the pristine graphite material. Such roughness could be attributed to the formation of defects on the surface of the treated sample.
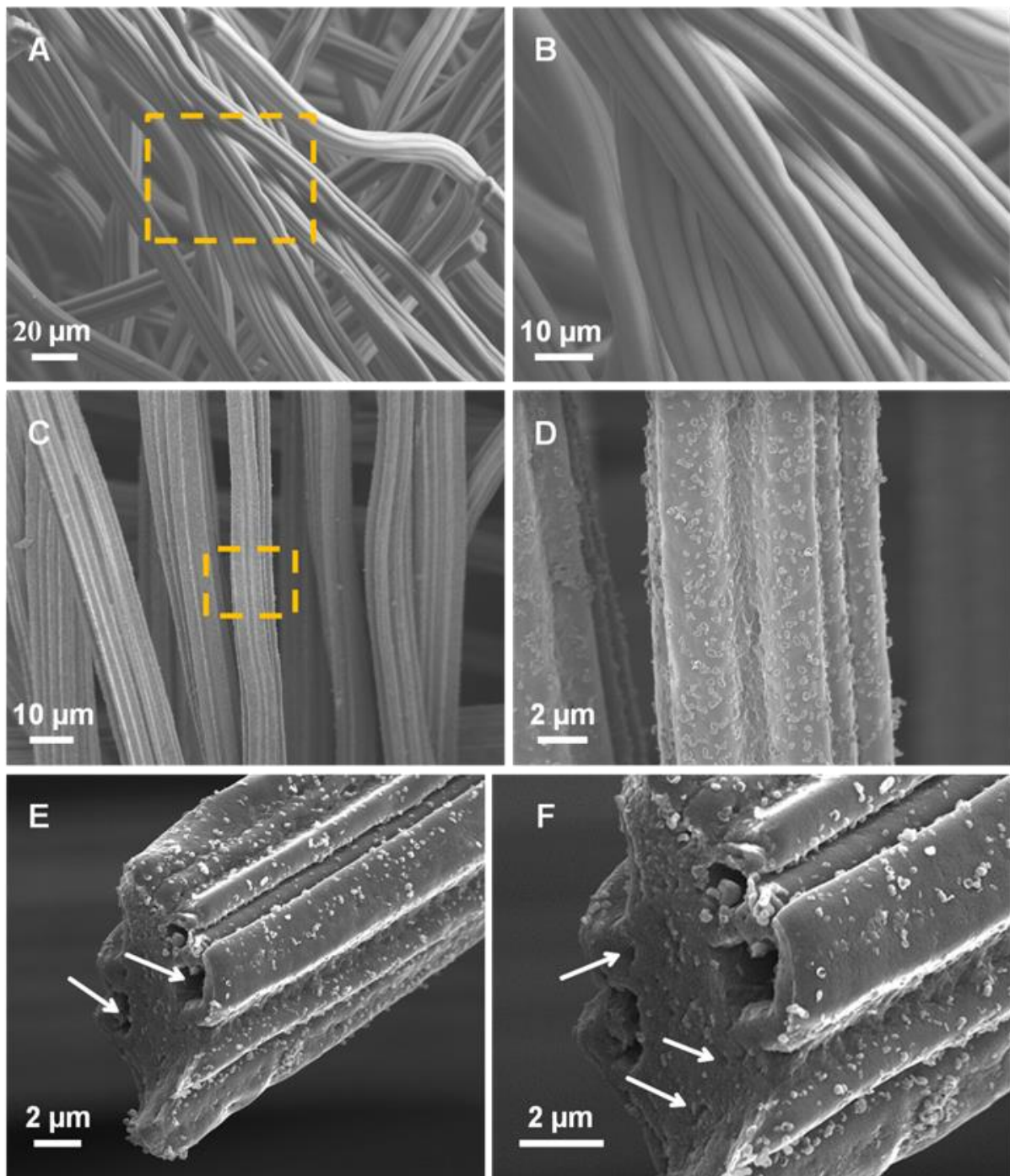
**Figure 1.** SEM micrographs of the (A, B) pristine commercial GFs, and (C, D) the same after treatment under gaseous HNO$_3$ at 250 $^o$C for 24 h, noted OGFs-24 showing the formation of nanoscopic nodules on its surface. SEM micrographs with medium and high resolution (E, F) reveal the formation of cracks on the cross section of the OGFs-24 (indicated by arrows) as well as a rougher surface after acid treatment.

High-resolution SEM image (Figure 2A) evidences the formation of defects on the whole surface of the carbon filamentous and some carbon extrusion in the form of discrete nodules. The Energy Dispersive X-ray analysis (EDX) carried out on the sample evidences the presence of oxygen intimately linked with carbon on the surface of the acid treated sample surface (Figure 2B to D) which confirms the high concentration of oxygenated functional groups decorating the surface defects.
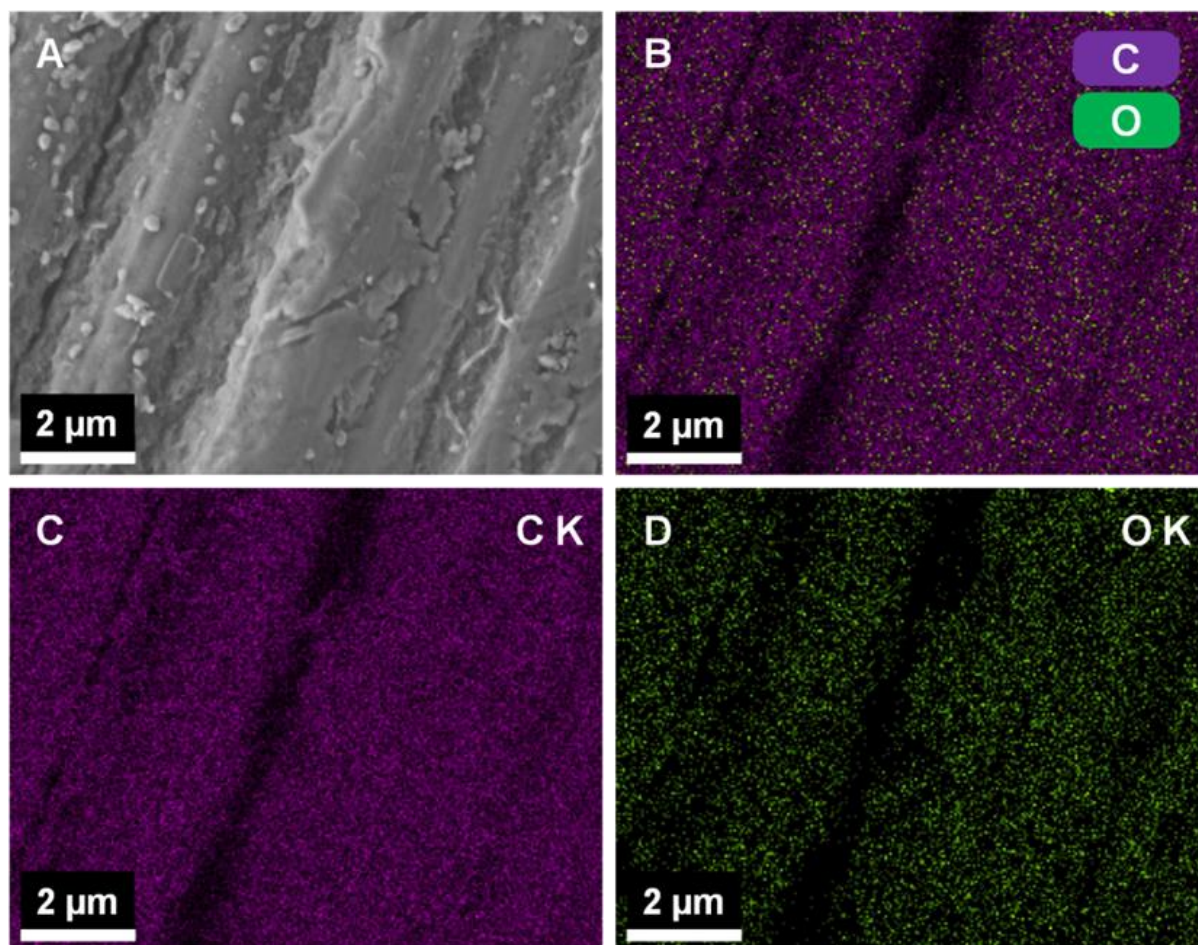


**Figure 2.** (A) SEM micrograph of the acid treated graphite felts, OGFs-24, (B) Elemental mapping showing the presence of C and O on the sample surface. (C, D) Elemental maps of carbon and oxygen elements on the OGFs-24 surface.

For industrial applications the catalyst should be prepared in a controlled macroscopic shape in order to avoid problems of handling and transport and also to prevent excessive pressure drop within the catalyst bed. In the present synthesis method, the GFs can be prepared

with different macroscopic shapes, i.e. pellets, disk with different holes, depending to the downstream applications as shown in Figure 3. The as-synthesized GFs could be directly used as metal-free catalyst, see catalytic application below, or also as catalyst support where the defective surface could lead to a high metal dispersion and stability. The macroscopic shape allows easy catalyst/products separation for liquid-phase catalytic processes which represents a costly process in the case of powdered catalysts.



**Figure 3.** Graphite felts with different macroscopic shapes for various catalytic applications both in gas- and liquid-phase processes.

According to our previous work on carbon nanotubes, the acid treatment lead to the formation of defects on the surface of the carbon material which was decorated by oxygenated functional groups. Such defects are expected to be formed through oxidative reaction between the gaseous nitric acid vapors and the graphite sample. The functionalization of the formed defects is expected to take place by the partial decomposition of the oxygen in the gas-phase medium. The formation of defects along the graphite microfilamentous surface during the acid treatment step also significantly increases the overall specific surface area (SSA) of the as-treated materials. The specific surface area of the acid treated filamentous GFs steadily increased as a function of the acid treatment duration as evidenced in Figure 4A and B. According to the results the SSA of the filamentous GFs was stepwise raised from 10 $m^2$/g to more than 300 $m^2$/g after the gaseous $HNO_3$ treatment for 30 h. It should be noted that such high SSA has never been accounted for chemical treated commercial microfilamentous carbon fibers. The increase of the SSA was attributed to the formation of a more porous graphite structure with higher effective surface area consecutive to the removal of carbon during the treatment from the sample (see TEM analysis below). It is expected that such porosity was formed in or close to the surface of the carbon filaments and thus, allows the complete maintain

of the macroscopic shape of the material. One cannot exclude some porosity network which could be generated inside the pristine graphite microfilamentous.

The gaseous acid treatment also induces an overall oxidation of carbon matrix leading to a weight loss of the treated material compared to that of the pristine one. Such phenomenon has already been reported by Xia and co-workers with a similar treatment [37] and also by several groups in the literature [18]. The weight loss during the acid treatment process is accounted for the corrosion of the filaments where part of the carbon with low degree of graphitization was removed leaving behind the carbon nodules or porosity as observed by SEM. The weight loss calculated on the basis of the initial weight and the one after acid treatment as a function of the treatment duration is presented in Figure 4 B.

It is expected that the corrosion phenomenon which occurring during the treatment was responsible for the increase of the SSA of the treated samples similarly to that reported for the carbon nanotubes treated with gaseous $HNO_3$ or $O_3$-$H_2O$ mixture [16, 25]. The treatment induces the formation of surface pores along the carbon fiber axis, i.e. corrosion, which significantly contribute to the improvement of the overall SSA of the treated samples. These defects are also the place for oxygen insertion to generate oxygenated functional groups on the surface of the OGFs samples as evidenced by XPS presented below.
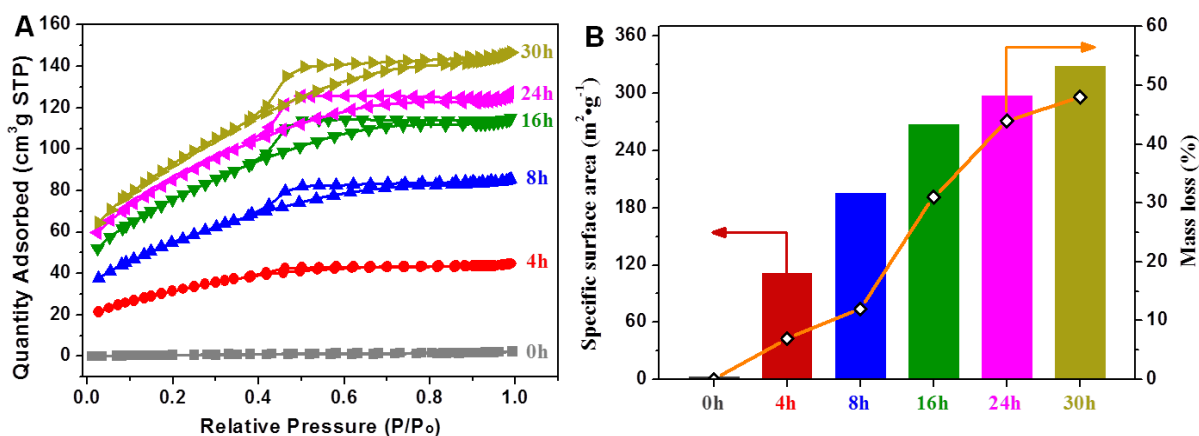


**Figure 4.** $N_2$ adsorption-desorption isotherms (A) and weight loss (open circles) and specific surface area (columns) modification of the acid treated carbon-based materials as a function of the treatment duration (B).

The weight loss increases with the treatment duration, especially for duration longer than 8 h. It is expected that the low temperature weight loss could be assigned to the removal of pore amorphous carbon, since they are considered to be more reactive than the graphitic carbon filamentous while at high temperature, weight loss is linked with the removal of carbon in the graphitic structure consecutive to the formation of structural defects and nodules on the remained filament wall. Indeed, under a more severe treatment, i.e. longer duration, the weight loss becomes significantly, i.e. the weight loss recorded for the sample after being treated at 250 $^o$C for 8 h and 24 h are 12% and 44%, respectively. According to the results the graphite displayed three distinct weight loss regions: (i) at treatment duration < 8 h, the oxidation process is relatively slow which could be attributed to the low reactivity of the graphite felt surface, (ii) at treatment ranged between 8 to 24 h, the oxidation rate is significantly increased and could be due to the depth oxidation of graphite matter through the surface defects generated previously, and (iii) at duration > 24 h, the oxidation process becomes almost flat which could be attributed to the fact that depth oxidation process could be hinder due to some diffusion problem.

The oxygen incorporation into the acid treated samples can be clearly observed through XPS survey spectra recorded on the fresh and $HNO_3$ treated samples (Figure 5A). It is worthy to note that XPS analysis allows one to map out elements concentration at a depth of ca. 6 nm from the surface and thus part of the oxygenated functional groups localized at a distance > 6 nm cannot be accurately detected. The deconvoluted O1s spectrum in Figure 5B shows the presence of three peaks which can be assigned to the C=O (ketone, aldehyde, quinone…), -C-OH, -C-O-C- (alcohol, ether) and –O-C=O (carboxylic, ester) oxygen species [25].

Raman spectroscopy was performed to investigate the change in the graphitic structure of the GFs after treatment with gaseous nitric acid at different duration. As shown in Figure 5C, every sample displayed three bands corresponding to the different carbonaceous structures: the G band attributed to an ideal graphitic lattice at around 1580 cm$^{-1}$ [38], the D band (~1350 cm$^{-1}$) associated with the structural defects [39] and D' corresponding to the disordered graphitic fragments at ~1620 cm$^{-1}$ [40], respectively. The $I_D/I_G$ ratio increases as increasing the acid treatment duration (Figure 5D). After the treatment of 24 h, the $I_D/I_G$ increased from 0.77 for GFs to 1.86. Meanwhile $I_D/I_G$ increased more than 3 times from 0.26 to 0.80, which indicated the strong acidic oxidant etched the graphene lattice of GFs and created more defects and disordered graphitic fragments. Furthermore, the more duration of the treatment on samples, the more structural defects and disordered fragments is obtained. Consistent with the

morphology from SEM, the etching effect of the treatment made the GFs with an extremely rough surface and much more macroscopic carbon fragments. Moreover, the G band shifted to the higher wavenumber by about 8 cm$^{-1}$, which may be attributed to the oxygen-containing functional groups generated on the surface of treated samples and confirmed by the results of XPS and TPD, such as the O-H bending and C=O stretching [41].
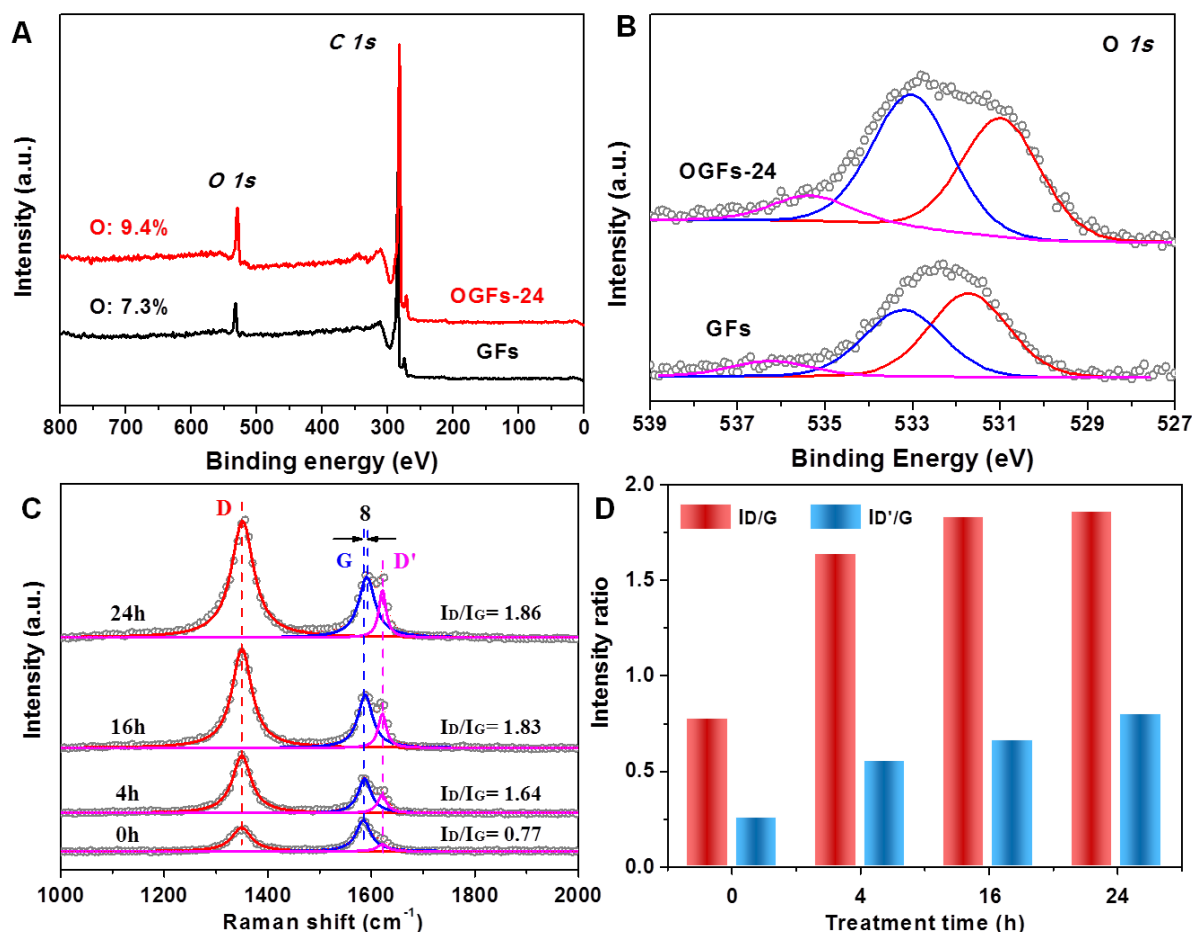


**Figure 5.** (A) Survey XPS of OGFs-24 in comparison with pristine GFs, (B) Deconvolution O1s present the oxygen species on the surface of the samples, (C) Raman spectra and (D) $I_D/I_G$ and $I_{D'}/I_G$ ratios of the pristine GFs and the OGFs after acid treatment with various durations.

The physical characteristics of the samples after acid treatment with different durations are summarized in Table 1.

**Table 1.** The physical chemistry properties of samples as a function of the acid treatment duration.

| Treatment duration | SSA$^a$ m$^2$/g | Mass loss$^b$ % | $I_D/I_G$$^c$ | $I_{D'}/I_G$$^c$ | O at%$^d$ | $T_{WL}$$^e$ ºC |
|---|---|---|---|---|---|---|
| 0 h | 10 | 0 | 0.77 | 0.26 | 7.3 | 802 |
| 4 h | 112 | 7 | 1.64 | 0.55 | - | - |
| 8 h | 196 | 12 | - | - | - | - |
| 16 h | 268 | 31 | 1.83 | 0.66 | - | 685 |
| 24 h | 298 | 44 | 1.86 | 0.80 | 9.4 | 612 |
| 30 h | 329 | 48 | - | - | - | - |

$^a$ BET specific areas. $^b$ The mass loss of samples after acid treatment. $^c$ The $I_D/I_G$ and $I_{D'}/I_G$ ratio calculated from Raman spectra. $^d$ The atom percent of surface Oxygen elemental from XPS analysis. $^e$ The temperature of weight loss peak determined by TG/DTG profiles. – Not detected.

TEM analysis is also used to investigate the influences of the $HNO_3$ treatment on the microstructure of the GFs (Figure 6). Compared with parallel graphitic layers on pristine GFs (Figure 6A and B), there are porous structures with disordered graphitic fragments formed on the outer region of the filamentous carbon of the acid treated GFs (pointed out by arrows in Figure 6C and D), which are consistent with the analysis of SSA and by Raman. TEM analysis reveals the formation of a less dense graphite structure in the OGFs sample (Figure 6C) compared to that observed for the pristine GFs (Figure 6B). High resolution TEM micrographs (Figure 6D) clearly evidence the porous structure of the treated sample. Such phenomenon can be attributed to the oxidation of a weakly graphitized carbon by the gaseous $HNO_3$ during the treatment, which forms entangled carbon sidewalls with high defect density.
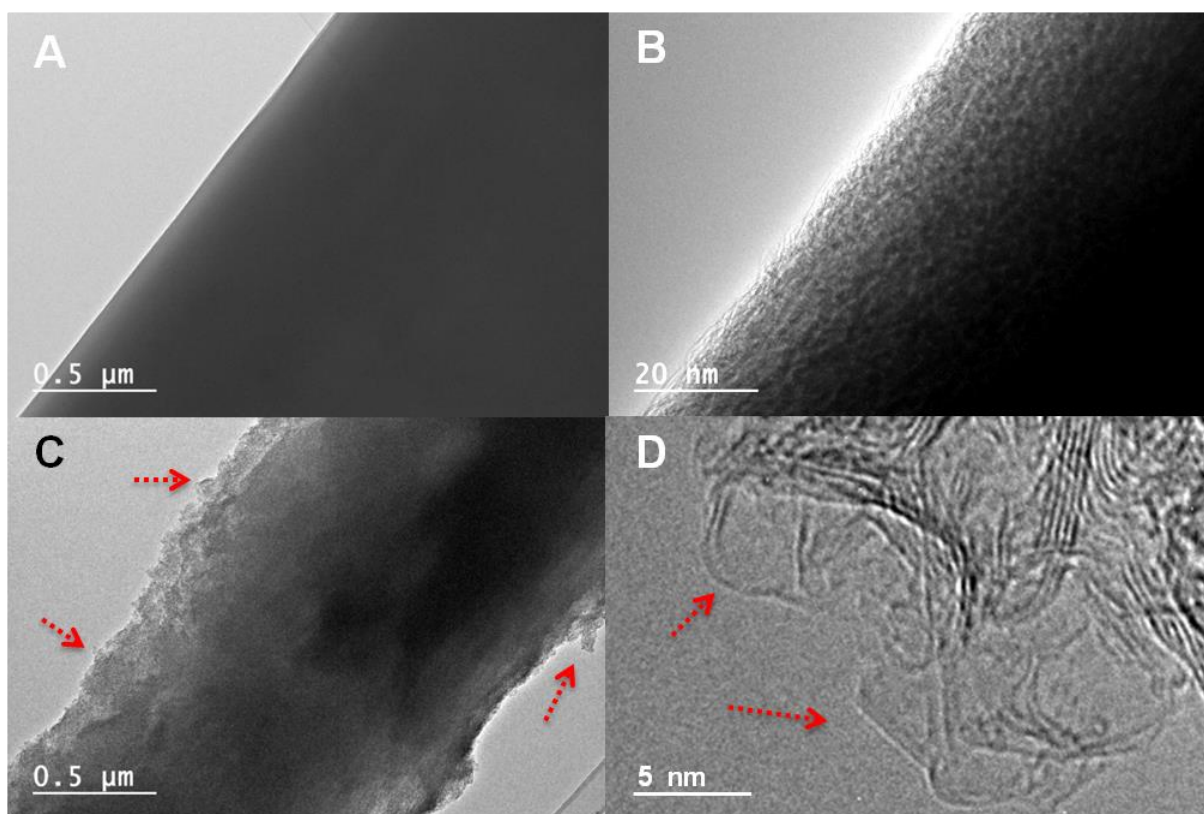
**Figure 6.** TEM images of GFs (A, B) and OGFs-24 (C, D). Surface defects generated on the OGFs are indicated by arrows.

According to the TEM results one could expected that during the acid treatment process part of the graphitic structure is slowly attacked, leading to a weight loss as a function of time of treatment, leaving behind porous structure with defects which contributes to an increase of the material SSA with time. Such corrosion process explains the formation of cracks and holes within the pristine graphite filamentous as observed by SEM. The as generated porosity with a highly defective surface decorated with oxygenated functional groups is expected to be of great interest for being used either as metal-free catalyst but also as catalyst support with high density of anchorage sites for hosting metal or oxide nanoparticles. Recent work has pointed out the high efficiency of defects decorated carbon nanotubes after treatment in the presence of ozone and water for anchoring gold nanoparticles[42]. The porous structure of the OGFs will be investigated in detail by mean of transmission electron microscopy tomography (TEM-3D) technique [43] to map out the porosity of the OGFs material and its influence on the metal nanoparticles dispersion.

The characterization of the different oxygenated groups present on the graphite surface was investigated by TPD-MS. The surface oxygen groups can be assessed by the type of released molecules with their relevant peak areas and decomposition temperatures [44]. The amount of CO (m/e = 28) and $CO_2$ (m/e = 44) generated during the TPD process is presented in Figure 7 as a function of the desorption temperature. The evolution of $CO_2$ was ascribed to the decomposition of carboxylic acids, anhydrides and lactones (Figure 7A), whereas the CO evolution was resulted from the decomposition of anhydrides, phenols and carbonyls (Figure 7B). The amounts of corresponding groups determined by TPD with the deconvolution of evolved $CO_2$ and CO peaks are summarized in Table 2. The CO and $CO_2$ concentration increases as increasing the treatment duration, confirming that the formation of oxygenated functional groups is directly depending to the acid treatment, which is in accordance with the XPS analysis (Figure 5A and B).
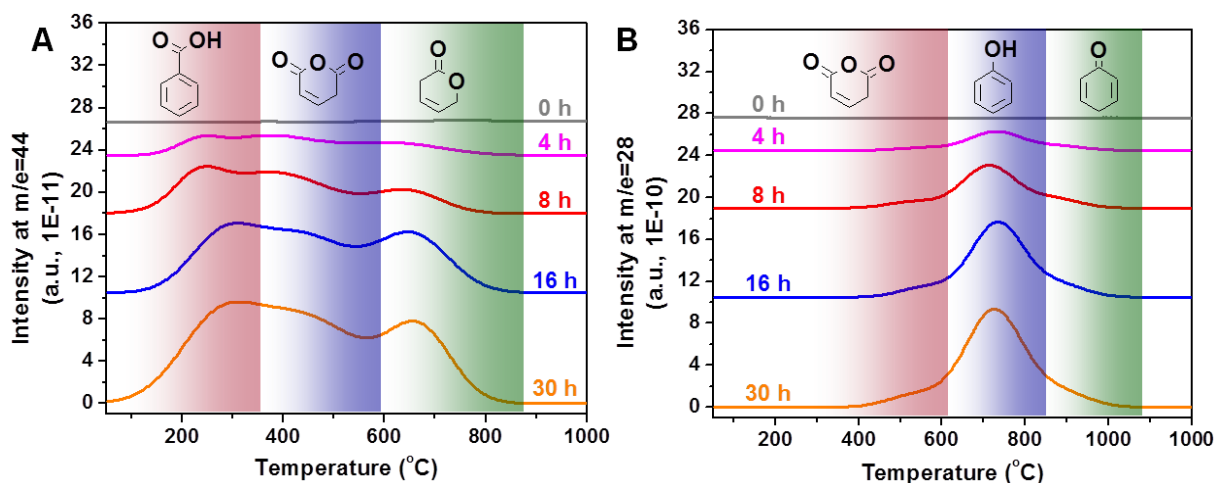


**Figure 7.** TPD profiles showing the evolvement of $CO_2$ (A) and CO (B) as a function of the desorption temperature on the different oxidized samples at 250 ℃ and with different treatment duration.

It is expected that the acid treatment duration increases the defect density which in turn increase the amount of oxygenated functional groups directly linked to such defects. Furthermore, the total amount of oxygen on the sample increased from 165 μmol/g, on the pristine GFs, to 9116 μmol/g, on the OGFs-30, after 30 h of gas-phase oxidation treatment. Such results have already been reported by other research groups in the literature during acid activation process for the synthesis of highly reactive carbon-based catalyst supports [45].

However, data deals with the use of such defective macroscopic OGFs materials with high effective surface area as metal-free catalyst has never been reported so far.

**Table 2.** The content of oxygen functional groups as a function of the acid treatment duration at 250 $^o$C on the samples determined from TPD profiles.

| Treatment duration | $CO_2$ desorption μmol/g | | | CO desorption μmol/g | | | Total O μmol/g |
|---|---|---|---|---|---|---|---|
| | Carboxylic acids | Anhydrides | Lactones | Anhydrides | Phenols | Carbonyls | |
| 0 h | - | - | - | - | - | - | 165 |
| 4 h | 53 | 187 | 128 | 141 | 951 | 230 | 1691 |
| 8 h | 134 | 486 | 148 | 332 | 2199 | 498 | 3797 |
| 16 h | 304 | 626 | 412 | 527 | 3865 | 660 | 6393 |
| 30 h | 422 | 1186 | 424 | 735 | 5462 | 887 | 9116 |

Thermogravimetry analysis (TG/DTG) has been generally used to study the oxidative stability of carbon materials [46-48]. As shown in Figure 8, all the samples exhibited a weight loss step during heat-treatment process, resulted from the combustion of carbon at high temperature. Obviously, the temperature of weight loss peak for OGFs-16 on the DTG curve (685 $^o$C) was lower than that of the pristine GFs (802 $^o$C), indicating the formation of highly reactive graphite species on the sample after the oxidation process. Meanwhile, a further decline of the oxidation temperature was observed for the OGF-24 (612 $^o$C) with the longer treatment duration, i.e. 24 h instead of 16 h. On one hand, these reactive carbon species may be linked with the presence of structural defects or from the disordered graphitic structure, according to the Raman and TEM results (Figure 5C and 6), which display lower thermal stability than the pristine graphite material [49]. On the other hand, higher SSA (Figure 4) of OGFs provides higher surface contact between the sample and reactant gas which could favor the oxidation process. Moreover, the abundant oxygen functional groups derived from acid treatment (Table 1) could be active sites for the dissociative adsorption of $O_2$ [40]. It is expected

that all those parameters will actively contribute to the lower oxidative resistance of the acid treated graphite felt.
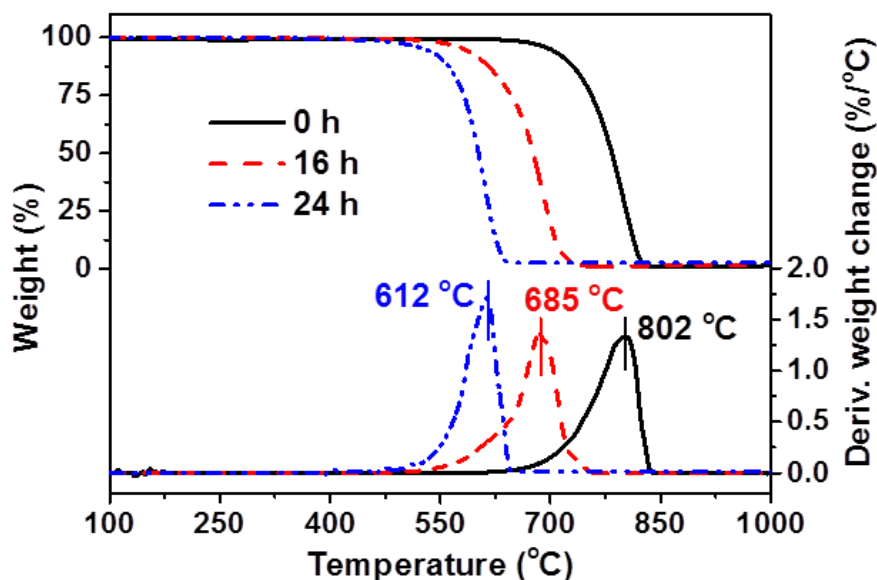


**Figure 8.** TG/DTG profiles of pristine GFs, OGFs-16 and OGFs-24.

## 2.2 OGFs as metal-free catalyst for selective oxidation of $H_2S$

The GFs and OGFs-16 catalysts were tested in the gas-phase selective oxidation of $H_2S$ into elemental sulfur under realistic reaction conditions. The OGFs-16 catalyst has been chosen among the other treated samples according to the following facts: (i) the OGFs-16 displays a relatively high SSA along with a lower weight loss during the acid treatment, and (ii) the OGFs-16 also displays higher oxidative resistance compared to the samples treated with longer duration. The pristine GFs catalyst shows no noticeable desulfurization activity under the operated reaction conditions (not reported) and confirms its inactivity for the reaction considered. The desulfurization performance obtained on the OGFs-16 catalyst at reaction temperature of 230 $^o$C and 250 $^o$C is presented in Figure 9A as a function of time on stream. The OGFs-16 catalyst displays a relative high $H_2S$ conversion at a WHSV of 0.05h$^{-1}$ with a total $H_2S$ conversion of 87% and a sulfur selectivity of 83%. In addition, it is worthy to note that the desulfurization activity remains stable as a function of time-on-stream for more than several dozen hours on stream, which indicates that no deactivation was occurred on the catalyst. Such relatively high desulfurization activity could be attributed to the high stability of the defect

decorated with oxygenated functional groups on the OGFs-16 catalyst which are generated at relatively high treatment temperature, i.e. 250$^{o}$C. Similar results have also been reported by the HNO$_3$ treated CNTs which is expected to bear the same active center [16]. Jiang et al. [50] have reported that pure carbon nanocages, which possess abundant holes, edges, and positive topological disclinations display a relatively good oxygen reductive performance which is even better than those reported for undoped CNTs. In the present work, the control of the macroscopic shape of the OGFs catalyst represents also a net advantage as the catalyst shape can be modified in a large range depending to the downstream applications.
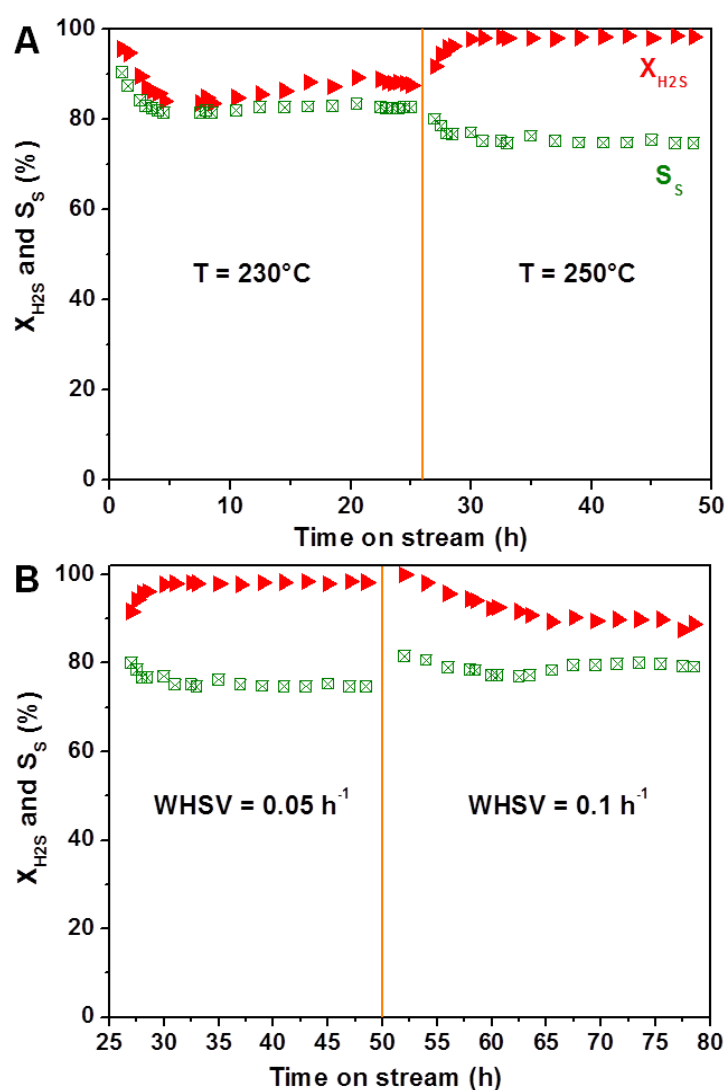


**Figure 9.** Desulfurization performance as a function of time on stream on the OGFs-16 catalyst. (A) Reaction conditions: [H$_2$S] = 1vol. %, [O$_2$] = 2.5 vol. %, [H$_2$O] = 30 vol. %, WHSV= 0.05 h$^{-1}$. (B) Reaction conditions: [H$_2$S] = 1vol. %, [O$_2$] = 2.5 vol. %, [H$_2$O] = 30 vol. %, reaction temperature = 250 $^{o}$C.

Increasing the reaction temperature from 230 $^{o}$C to 250 $^{o}$C leads to an improvement on the H$_2$S conversion, i.e. 99% instead of 87%, along with a slight decrease of the sulfur selectivity from 83% to 77% due to the fact that high reaction temperature favors the complete oxidation of S to SO$_2$ in the presence of excess oxygen in the feed [51]. However, after a period of induction where both H$_2$S conversion and sulfur selectivity are modified the catalyst reached a steady-state for the rest of the test which again confirm its high stability.

Increasing the WHSV from 0.05 h$^{-1}$ to 0.1 h$^{-1}$ keeping the reaction temperature at 250 $^{o}$C leads to a slight decrease of the H$_2$S conversion from 100% to 90% followed by a steady-state (Figure 9B). The sulfur selectivity slightly increases from 75% to 82% at high space velocity and remains stable for the test. Such results are in good agreement with literature results as increasing the WHSV leads to a shorter sojourn time of the reactant and thus, reduce the rate of reactant dissociation for the reaction. The specific activity calculated is 0.56 mol$_{H2S}$/g$_{catalyst}$/h which is relatively close to those reported for other metal-free catalysts [52]. Further improvement of the catalytic performance could be done by using compressed OGFs with higher specific weight in order to reduce the empty space inside the catalyst bed.

The results obtained indicate that the OGFs metal-free catalyst displays relatively high sulfur selectivity, i.e. > 70%, even at relatively high reaction temperature, i.e. 250 $^{o}$C, and in the presence of a high H$_2$S concentration. It is expected that such sulfur selectivity is linked with the high thermal conductivity of the graphite felt support which could efficiently disperse the reaction heat through the catalyst matrix to avoid local hot spots formation which is detrimental for the sulfur selectivity. Similar results have also been reported on the medium thermal conductive silicon carbide carrier where the lack of local hot spots leads to a significant improvement of the reaction selectivity for selective oxidation of H$_2$S [10] and also in other exothermal reactions such as Fisher-Tropsch synthesis [53, 54], dimethyl ether [55, 56] and propylene synthesis [57, 58]. The relatively high sulfur selectivity observed in the present work could also be attributed to the presence of large voids inside the sample which could favor the rapid evacuation of the sulfur intermediate species before complete oxidation.
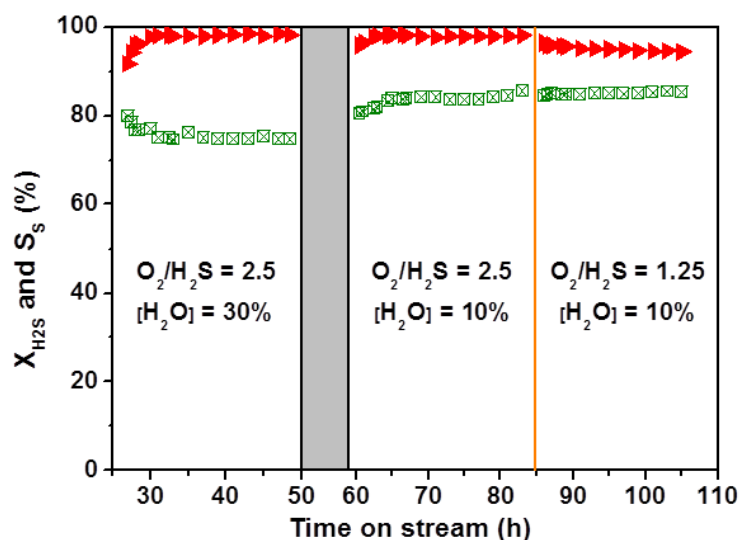
**Figure 10.** Influence of the steam concentration and $O_2$-to-$H_2S$ ratio on the desulfurization performance on the pristine GFs and the one after treatment under gaseous $HNO_3$ at $250^oC$ for 16 h (OGFs-16) catalysts. Reaction conditions: $[H_2S] = 1$ vol. %, reaction temperature $= 250\,^oC$ and WHSV$= 0.05$ h$^{-1}$.

The effluents containing $H_2S$ could be originated from different sources with various steam concentrations ranged from few to several percents, i.e. effluent from biogas plant or from the Claus reactor. It is expected that the steam concentration could have a significant influence on the desulfurization performance, i.e. $H_2S$ conversion and sulfur selectivity, due to the problem of competitive adsorption. The influence of steam concentration was investigated and the results are presented in Figure 10. Decreasing the steam concentration in the reactant feed from 30% to 10% leads to a similar $H_2S$ conversion, i.e. 99%, but to a significant increase of the sulfur selectivity from 75% to 85% keeping other reaction conditions similar. Such result indicates that steam could condense to yield water film inside the catalyst porosity, even at a relatively high reaction temperature, which favors oxygen dissociation leading to a higher complete oxidation to yield $SO_2$. Decreasing the steam concentration leads to a lower oxygen atoms available on the catalyst surface which in turn, reduces the selectivity towards $SO_2$. Such hypothesis can be confirmed by decreasing the $O_2$-to-$H_2S$ ratio keeping the other reaction conditions similar. Decreasing the $O_2$-to-$H_2S$ ratio seems to have hardly effect on the sulfur selectivity while a slight decrease of the $H_2S$ conversion is observed. Such result could be attributed to the fact that the dissociated oxygen on the catalyst surface reacts with $H_2S$ to yield both S and $SO_2$ in a parallel reaction pathway but with a different reaction rate. Decreasing the $O_2$-to-$H_2S$ ratio leads to a decrease of the available oxygen for the reaction and, as a

consequence lowers the $H_2S$ conversion. Finally, regarding the influence of steam on the $H_2S$ conversion it should be noted that under the reaction conditions used the $H_2S$ conversion is almost complete which could render the investigation of small effect, i.e. steam concentration, difficult as at such high conversion level one cannot rules out the fact that some active sites remain unemployed.

It is worthy to note that reaction temperature of 250 $^oC$ is slightly higher than that usually used for the selective oxidation of $H_2S$ into elemental sulfur on other metal-free carbon-based catalysts. However, on the OGFs-16 metal-free catalyst the sulfur selectivity remains relatively high, i.e. > 70% and even ≥ 85% at low steam concentration (Fig. 10), at almost complete conversion of $H_2S$. Such results could be attributed to the large open porosity of the catalyst, i.e. 90% of empty space, which allow the formed sulfur to rapidly escape the catalyst before secondary reaction with excess oxygen to yield $SO_2$.

It is also noted that the catalyst displays also a relatively high stability, both in terms of $H_2S$ conversion and sulfur selectivity under severe reaction conditions, i.e. 0.1 $h^{-1}$ of WHSV and high reaction temperature where the $H_2S$ conversion is not complete indicating that all the active sites were involved in the reaction, which confirm again the advantage of the oxygenated functional groups on the defect sites. Such results are of high interest as usually on oxides or metals containing catalysts sintering is the main cause of deactivation with time on stream under severe reaction conditions.

**Table 3.** Selective oxidation of $H_2S$ to sulfur over different metal-free catalysts.

| Catalysts | T $^oC$ | [$H_2S$] vol. % | [$O_2$] vol. % | [$H_2O$] vol. % | WHSV $h^{-1}$ | $X_{H2S}{}^a$ % | $S_S{}^b$ % | $Y_S{}^c$ % | Ref. |
|---|---|---|---|---|---|---|---|---|---|
| OGFs-16 | 250 | 1 | 2.5 | 10 | 0.1 | 98 | 86 | 84 | This work |
| O-CNT-250-24 | 230 | 1 | 2.5 | 30 | 0.6 | 95 | 76 | 72 | 16 |
| N-CNT/SiC-750 | 190 | 1 | 2.5 | 30 | 0.6 | 97 | 75 | 73 | 52 |

[a] Maximum $H_2S$ conversion. [b] The corresponding sulfur selectivity. [c] The corresponding yield of sulfur. ($Y_S = X_{H2S} \times S_S$).

The results obtained indicate that acid treated graphite felts could be efficiently used as metal-free catalyst for the selective oxidation of $H_2S$ into elemental sulfur. The different catalytic results are summarized in Table 3 and compared with those reported on other metal-free catalysts. The OGFs-16 catalyst displays a relatively high sulfur selectivity compared to the other metal-free catalysts operated at higher space velocity and temperature. Such results pointed out the high efficiency of the OGFs-16 catalyst to perform selective oxidation of $H_2S$ which could be attributed to the large open porosity of the catalyst providing high rate of intermediate sulfur escaping.

## 3. Conclusions

In summary, we have shown that oxidation with gaseous $HNO_3$ can be an efficient and elegant pre-activation step to generate active metal-free carbon-based catalysts decorated with surface defects containing oxygenated functional groups from available and low cost commercial filamentous graphite felts. The gaseous acid treatment leads to the formation of a high surface area carbon-based material which can find use in several catalytic processes as either metal-free catalyst or as catalyst support. It is worthy to note that it is the first time that such results are reported as literature only reports metal-free catalysts based on nanocarbons, whose synthesis requires harsh reaction conditions along with the problem linked with waste treatment. According to the obtained results the defects created on the filamentous carbon wall and the formation of oxygenated functional groups during the gaseous acid treatment provide active sites for $H_2S$ and oxygen adsorption which contribute to the selective oxidation of $H_2S$ into elemental sulfur under similar reaction conditions with those operated in the industrial plants. The catalyst displays a relatively high sulfur selectivity as well as relatively high stability as a function of time-on-stream, under severe reaction conditions, indicating that deactivation by surface fouling or oxygen groups removing is unlikely to occur. The high specific surface area as well as surface porous structure could be extremely helpful for developing new catalytic systems. Such hierarchical metal-free catalyst can be prepared with different macroscopic shapes for subsequence downstream applications. Work is ongoing to evaluate such carbon-based materials as hierarchical macroscopic support for metal nanoparticles which could find use in other catalytic processes where high dispersion and strong anchorage of the active phase are required in order to prevent long term deactivation through catalyst sintering (gas-phase reaction) or leaching (liquid-phase reaction) and also in terms of recovery.

**Acknowledgments:**

Zhenxin Xu and Bing Li would like to thank the Chinese Scholarship Council (CSC) for the PhD grant for their stay at the ICPEES. The project is partly supported by the National Foundation for Science and Technology Development of Vietnam (Nafosted) program of research. The SEM experiments were carried out at the facilities of the ICPEES-IPCMS platform. Dr. Vasiliki Papaefthimiou, Thierry Romero and Sécou Sall (ICPEES, UMR 7515) are gratefully acknowledged for performing XPS, TPD-MS and SEM experiments. Dr. Jean-Mario Nhut (ICPEES) is gratefully acknowledged for technical and scientific help during the project. Mr. Loïc Vidal (IS2M, UMR 7361) is gratefully acknowledged for TEM experiments.

# References

[1]     D.S. Su, S. Perathoner, G. Centi, Nanocarbons for the development of advanced catalysts, Chemical Reviews, 113 (2013) 5782-5816.

[2]     J.P. Tessonnier, D.S. Su, Recent progress on the growth mechanism of carbon nanotubes: A review, ChemSusChem, 4 (2011) 824-847.

[3]     C. Duong-Viet, H. Ba, L. Truong-Phuoc, Y. Liu, J.P. Tessonnier, J.M. Nhut, P. Granger, C. Pham-Huu, Nitrogen-doped carbon composites as metal-free catalysts, Elsevier Series Book, 2016.

[4]     J. Liang, X. Du, C. Gibson, X.W. Du, S.Z. Qiao, N-doped graphene natively grown on hierarchical ordered porous carbon for enhanced oxygen reduction, Advanced Materials, 25 (2013) 6226-6231.

[5]     W. Wei, H. Liang, K. Parvez, X. Zhuang, X. Feng, K. Mullen, Nitrogen-doped carbon nanosheets with size-defined mesopores as highly efficient metal-free catalyst for the oxygen reduction reaction, Angewandte Chemie International Edition, 53 (2014) 1570-1574.

[6]     Y. Tang, B.L. Allen, D.R. Kauffman, A. Star, Electrocatalytic activity of nitrogen-doped carbon nanotube cups, Journal of the American Chemical Society, 131 (2009) 13200-13201.

[7]     K. Gong, F. Du, Z. Xia, M. Durstock, L. Dai, Nitrogen-doped carbon nanotube arrays with high electrocatalytic activity for oxygen reduction, Science, 323 (2009) 760-764.

[8]     Y. Liu, Z. Jin, J. Wang, R. Cui, H. Sun, F. Peng, L. Wei, Z. Wang, X. Liang, L. Peng, Y. Li, Nitrogen-doped single-walled carbon nanotubes grown on substrates: Evidence for framework doping and their enhanced properties, Advanced Functional Materials, 21 (2011) 986-992.

[9]     G. Tuci, M. Pilaski, H. Ba, A. Rossin, L. Luconi, S. Caporali, C. Pham-Huu, R. Palkovits, G. Giambastiani, Unraveling surface basicity and bulk morphology relationship on covalent triazine frameworks with unique catalytic and gas adsorption properties, Advanced Functional Materials, 27 (2017) 1605672.

[10]    T. Truong-Huu, K. Chizari, I. Janowska, M.S. Moldovan, O. Ersen, L.D. Nguyen, M.J. Ledoux, C. Pham-Huu, D. Begin, Few-layer graphene supporting palladium nanoparticles with a fully accessible effective surface for liquid-phase hydrogenation reaction, Catalysis Today, 189 (2012) 77-82.

[11]    J. Zhang, L. Qu, G. Shi, J. Liu, J. Chen, L. Dai, N, P-codoped carbon networks as efficient metal-free bifunctional catalysts for oxygen reduction and hydrogen evolution reactions, Angewandte Chemie International Edition, 55 (2016) 2230-2234.

[12]    G. Tuci, C. Zafferoni, A. Rossin, L. Luconi, A. Milella, M. Ceppatelli, M. Innocenti, Y. Liu, C. Pham-Huu, G. Giambastiani, Chemical functionalization of N-doped carbon nanotubes: A powerful approach to cast light on the electrochemical role of specific N-functionalities in the oxygen reduction reaction, Catalysis Science & Technology, 6 (2016) 6226-6236.

[13]    R. Lv, T. Cui, M.-S. Jun, Q. Zhang, A. Cao, D.S. Su, Z. Zhang, S.-H. Yoon, J. Miyawaki, I. Mochida, F. Kang, Open-ended, N-doped carbon nanotube-graphene hybrid nanostructures as high-performance catalyst support, Advanced Functional Materials, 21 (2011) 999-1006.

[14]    H. Ba, Y. Liu, L. Truong-Phuoc, C. Duong-Viet, J.-M. Nhut, D.L. Nguyen, O. Ersen, G. Tuci, G. Giambastiani, C. Pham-Huu, N-doped food-grade-derived 3D mesoporous foams as metal-free systems for catalysis, ACS Catalysis, 6 (2016) 1408-1419.

[15]    G. Tuci, L. Luconi, A. Rossin, E. Berretti, H. Ba, M. Innocenti, D. Yakhvarov, S. Caporali, C. Pham-Huu, G. Giambastiani, Aziridine-functionalized multiwalled carbon nanotubes: Robust and versatile catalysts for the oxygen reduction reaction and knoevenagel condensation, ACS Applied Materials & Interfaces, 8 (2016) 30099-30106.

[16]    C. Duong-Viet, Y. Liu, H. Ba, L. Truong-Phuoc, W. Baaziz, L. Nguyen-Dinh, J.-M. Nhut, C. Pham-Huu, Carbon nanotubes containing oxygenated decorating defects as metal-free catalyst for selective oxidation of $H_2S$, Applied Catalysis B: Environmental, 191 (2016) 29-41.

[17]    W. Qi, W. Liu, X. Guo, R. Schlogl, D. Su, Oxidative dehydrogenation on nanocarbon: Intrinsic catalytic activity and structure-function relationships, Angewandte Chemie

International Edition, 54 (2015) 13682-13685.

[18]   M.F.R. Pereira, J.J.M. Órfão, J.L. Figueiredo, Oxidative dehydrogenation of ethylbenzene on activated carbon catalysts. I. Influence of surface chemical groups, Applied Catalysis A: General, 184 (1999) 153-160.

[19]   F. Avilés, J.V. Cauich-Rodríguez, L. Moo-Tah, A. May-Pat, R. Vargas-Coronado, Evaluation of mild acid oxidation treatments for MWCNT functionalization, Carbon, 47 (2009) 2970-2975.

[20]   H. Hiura, T.W. Ebbesen, K. Tanigaki, Opening and purification of carbon nanotubes in high yields, Advanced Materials, 7 (1995) 275-276.

[21]   N.V. Qui, P. Scholz, T. Krech, T.F. Keller, K. Pollok, B. Ondruschka, Multiwalled carbon nanotubes oxidized by $UV/H_2O_2$ as catalyst for oxidative dehydrogenation of ethylbenzene, Catalysis Communications, 12 (2011) 464-469.

[22]   N. Mahata, M.F. Pereira, F. Suarez-Garcia, A. Martinez-Alonso, J.M. Tascon, J.L. Figueiredo, Tuning of texture and surface chemistry of carbon xerogels, Journal of Colloid and Interface Science, 324 (2008) 150-155.

[23]   J.M. Simmons, B.M. Nichols, S.E. Baker, M.S. Marcus, O.M. Castellini, C.-S. Lee, R.J. Hamers, M.A. Eriksson, Effect of ozone oxidation on single-walled carbon nanotubes, Journal of Physical Chemistry B, 110 (2006) 7113-7118.

[24]   R. Huang, J. Xu, J. Wang, X. Sun, W. Qi, C. Liang, D.S. Su, Oxygen breaks into carbon nanotubes and abstracts hydrogen from propane, Carbon, 96 (2016) 631-640.

[25]   J. Luo, Y. Liu, H. Wei, B. Wang, K.-H. Wu, B. Zhang, D.S. Su, A green and economical vapor-assisted ozone treatment process for surface functionalization of carbon nanotubes, Green Chemistry, 19 (2017) 1052-1062.

[26]   J. Hu, Z. Guo, W. Chu, L. Li, T. Lin, Carbon dioxide catalytic conversion to nano carbon material on the iron-nickel catalysts using CVD-IP method, Journal of Energy Chemistry, 24 (2015) 620-625.

[27]   Y. Liu, T. Dintzer, O. Ersen, C. Pham-Huu, Carbon nanotubes decorated α-$Al_2O_3$ containing cobalt nanoparticles for Fischer-Tropsch reaction, Journal of Energy Chemistry, 22 (2013) 279-289.

[28]   J. Więckowska, Catalytic and adsorptive desulphurization of gases, Catalysis Today,

24 (1995) 405-465.

[29] X. Zhang, Y. Tang, S. Qu, J. Da, Z. Hao, $H_2S$-selective catalytic oxidation: Catalysts and processes, ACS Catalysis, 5 (2015) 1053-1067.

[30] S. Bashkova, F.S. Baker, X. Wu, T.R. Armstrong, V. Schwartz, Activated carbon catalyst for selective oxidation of hydrogen sulphide: On the influence of pore structure, surface characteristics, and catalytically-active nitrogen, Carbon, 45 (2007) 1354-1363.

[31] V.V. Shinkarev, A.M. Glushenkov, D.G. Kuvshinov, G.G. Kuvshinov, Nanofibrous carbon with herringbone structure as an effective catalyst of the $H_2S$ selective oxidation, Carbon, 48 (2010) 2004-2012.

[32] A. Piéplu, O. Saur, J.-C. Lavalley, O. Legendre, C. Nédez, Claus catalysis and $H_2S$ selective oxidation, Catalysis Reviews - Science and Engineering, 40 (1998) 409-450.

[33] Y. Liu, C. Duong-Viet, J. Luo, A. Hébraud, G. Schlatter, O. Ersen, J.-M. Nhut, C. Pham-Huu, One-pot synthesis of a nitrogen-doped carbon composite by electrospinning as a metal-free catalyst for oxidation of $H_2S$ to sulfur, ChemCatChem, 7 (2015) 2957-2964.

[34] N. Keller, C. Pham-Huu, M.J. Ledoux, Continuous process for selective oxidation of $H_2S$ over SiC-supported iron catalysts into elemental sulfur above its dewpoint, Applied Catalysis A: General, 217 (2001) 205-217.

[35] E.-K. Lee, K.-D. Jung, O.-S. Joo, Y.-G. Shul, Catalytic wet oxidation of $H_2S$ to sulfur on V/MgO catalyst, Catalysis Letters, 98 (2004) 259-263.

[36] C.F. Claus, British patent, In, 1883, 5958.

[37] W. Xia, C. Jin, S. Kundu, M. Muhler, A highly efficient gas-phase route for the oxygen functionalization of carbon nanotubes based on nitric acid vapor, Carbon, 47 (2009) 919-922.

[38] L.G. Cancado, A. Jorio, E.H. Ferreira, F. Stavale, C.A. Achete, R.B. Capaz, M.V. Moutinho, A. Lombardo, T.S. Kulmala, A.C. Ferrari, Quantifying defects in graphene via raman spectroscopy at different excitation energies, Nano Letters, 11 (2011) 3190-3196.

[39] A. Sadezky, H. Muckenhuber, H. Grothe, R. Niessner, U. Pöschl, Raman

microspectroscopy of soot and related carbonaceous materials: Spectral analysis and structural information, Carbon, 43 (2005) 1731-1742.

[40]    V. Datsyuk, M. Kalyva, K. Papagelis, J. Parthenios, D. Tasis, A. Siokou, I. Kallitsis, C. Galiotis, Chemical oxidation of multiwalled carbon nanotubes, Carbon, 46 (2008) 833-840.

[41]    T.T. Thanh, H. Ba, L. Truong-Phuoc, J.-M. Nhut, O. Ersen, D. Begin, I. Janowska, D.L. Nguyen, P. Granger, C. Pham-Huu, A few-layer graphene-graphene oxide composite containing nanodiamonds as metal-free catalysts, Journal of Materials Chemistry A, 2 (2014) 11349-11357.

[42]    J. Luo, H. Wei, Y. Liu, D. Zhang, B. Zhang, W. Chu, C. Pham-Huu, D.S. Su, Oxygenated group and structural defect enriched carbon nanotubes for immobilizing gold nanoparticles, Chemical Communications, 53 (2017) 12750-12753.

[43]    O. Ersen, C. Hirlimann, M. Drillon, J. Werckmann, F. Tihay, C. Pham-Huu, C. Crucifix, P. Schultz, 3D-TEM characterization of nanometric objects, Solid State Sciences, 9 (2007) 1088-1098.

[44]    J.L. Figueiredo, Functionalization of porous carbons for catalytic applications, Journal of Materials Chemistry A, 1 (2013) 9351-9364.

[45]    W. Shi, B. Zhang, Y. Lin, Q. Wang, Q. Zhang, D.S. Su, Enhanced chemoselective hydrogenation through tuning the interaction between Pt nanoparticles and carbon supports: Insights from identical location transmission electron microscopy and X-ray photoelectron spectroscopy, ACS Catalysis, 6 (2016) 7844-7854.

[46]    B. Scheibe, E. Borowiak-Palen, R.J. Kalenczuk, Oxidation and reduction of multiwalled carbon nanotubes - preparation and characterization, Materials Characterization, 61 (2010) 185-191.

[47]    W. Chu, M. Ran, X. Zhang, N. Wang, Y. Wang, H. Xie, X. Zhao, Remarkable carbon dioxide catalytic capture (CDCC) leading to solid-form carbon material via a new CVD integrated process (CVD-IP): An alternative route for $CO_2$ sequestration, Journal of Energy Chemistry, 22 (2013) 136-144.

[48]    D. Bom, R. Andrews, D. Jacques, J. Anthony, B. Chen, M.S. Meier, J.P. Selegue, Thermogravimetric analysis of the oxidation of multiwalled carbon nanotubes:

Evidence for the role of defect sites in carbon nanotube chemistry, Nano Letters, 2 (2002) 615-619.

[49] M. Ran, W. Sun, Y. Liu, W. Chu, C. Jiang, Functionalization of multi-walled carbon nanotubes using water-assisted chemical vapor deposition, Journal of Solid State Chemistry, 197 (2013) 517-522.

[50] Y. Jiang, L. Yang, T. Sun, J. Zhao, Z. Lyu, O. Zhuo, X. Wang, Q. Wu, J. Ma, Z. Hu, Significant contribution of intrinsic carbon defects to oxygen reduction activity, ACS Catalysis, 5 (2015) 6707-6712.

[51] V.V. Shinkarev, A.M. Glushenkov, D.G. Kuvshinov, G.G. Kuvshinov, New effective catalysts based on mesoporous nanofibrous carbon for selective oxidation of hydrogen sulfide, Applied Catalysis B: Environmental, 85 (2009) 180-191.

[52] C. Duong-Viet, L. Truong-Phuoc, T. Tran-Thanh, J.-M. Nhut, L. Nguyen-Dinh, I. Janowska, D. Begin, C. Pham-Huu, Nitrogen-doped carbon nanotubes decorated silicon carbide as a metal-free catalyst for partial oxidation of $H_2S$, Applied Catalysis A: General, 482 (2014) 397-406.

[53] Y. Liu, O. Ersen, C. Meny, F. Luck, C. Pham-Huu, Fischer-Tropsch reaction on a thermally conductive and reusable silicon carbide support, ChemSusChem, 7 (2014) 1218-1239.

[54] M. Lacroix, L. Dreibine, B. de Tymowski, F. Vigneron, D. Edouard, D. Bégin, P. Nguyen, C. Pham, S. Savin-Poncet, F. Luck, M.-J. Ledoux, C. Pham-Huu, Silicon carbide foam composite containing cobalt as a highly selective and re-usable Fischer–Tropsch synthesis catalyst, Applied Catalysis A: General, 397 (2011) 62-72.

[55] M.M. Elamin, O. Muraza, Z. Malaibari, H. Ba, J.-M. Nhut, C. Pham-Huu, Microwave assisted growth of SAPO-34 on β-SiC foams for methanol dehydration to dimethyl ether, Chemical Engineering Journal, 274 (2015) 113-122.

[56] Y. Liu, S. Podila, D.L. Nguyen, D. Edouard, P. Nguyen, C. Pham, M.J. Ledoux, C. Pham-Huu, Methanol dehydration to dimethyl ether in a platelet milli-reactor filled with H-ZSM5/SiC foam catalyst, Applied Catalysis A: General, 409-410 (2011) 113-121.

[57] Y. Jiao, X. Yang, C. Jiang, C. Tian, Z. Yang, J. Zhang, Hierarchical ZSM-5/SiC

nano-whisker/SiC foam composites: Preparation and application in MTP reactions, Journal of Catalysis, 332 (2015) 70-76.

[58]  C. Duong-Viet, H. Ba, Z. El-Berrichi, J.-M. Nhut, M.J. Ledoux, Y. Liu, C. Pham-Huu, Silicon carbide foam as a porous support platform for catalytic applications, New Journal of Chemistry, 40 (2016) 4285-4299.

# Chapter 4

**Macroscopic graphite felt containing palladium catalyst for liquid-phase hydrogenation of cinnamaldehyde**

*Chapter 4*

# Macroscopic graphite felt containing palladium catalyst for liquid-phase hydrogenation of cinnamaldehyde

*Zhenxin Xu,[a,]\* Cuong Duong-Viet,[a,b] Yuefeng Liu,[c] Walid Baaziz,[d]*

*Bing Li,[a] Lam Nguyen-Dinh,[e] Ovidiu Ersen[d] and Cuong Pham-Huu[a,]\**

*(a) Institut de Chimie et Procédés pour l'Energie, l'Environnement et la Santé (ICPEES), ECPM, UMR 7515 du CNRS-Université de Strasbourg, 25 rue Becquerel, 67087 Strasbourg Cedex 02, France*

*(b) Ha-Noi University of Mining and Geology, 18 Pho Vien, Duc Thang, Bac Tu Liem, Ha-Noi, Vietnam*

*(c) Dalian National Laboratory for Clean Energy (DNL), Dalian Institute of Chemical Physics, Chinese Academy of Science, 457 Zhongshan Road, 116023 Dalian, China*

*(d) Institut de Physique et Chimie des Matériaux de Strasbourg (IPCMS), UMR 7504 du CNRS-Université de Strasbourg, 23 rue du Loess, 67037 Strasbourg Cedex 08, France*

*(e) The University of Da-Nang, University of Science and Technology, 54, Nguyen Luong Bang, Da-Nang, Vietnam*

\**Corresponding authors:*

*zhenxin.xu@etu.unistra.fr (Zhenxin Xu)*

*cuong.pham-huu@unistra.fr (Cuong Pham-Huu)*

**Abstract**

Developing of both effective and stable noble metal nanoparticle (NPs) catalysts with easy catalyst-product recovery is still challenging in the liquid-phase catalytic processes. Here, we report on the synthesis of a hierarchical structured catalyst that consisted of oxygen functionalized graphite felt (OGF) support for liquid-phase processes. The monolith palladium-based catalyst was used as catalytic stirrer and displays excellent stability as well as complete recyclability for liquid-phase hydrogenation of α, β-unsaturated cinnamaldehyde. The surface defects decorated with abundant oxygenated groups as well as highly accessible porous structure generated from the acid treatment of carbon support, construct a bridge between Pd and support providing the charge transfer to alter the metal-support interactions. The electron-deficient high-valent $Pd^{\delta+}$ species, formed on the metal NPs, and defects on the support help to enhance the Pd dispersion and resistance to sintering and/or aggregation during both catalyst preparation and cycling tests, leading to the high and stable hydrogen dissociative adsorption for hydrogenation process.

**Keywords:**

# 1. Introduction

Catalytic processes represent an important part in the production of goods and chemical compounds for the everyday life in our society [1, 2]. Numerous catalytic processes are conducted in liquid-phase medium where diffusion of gaseous/liquid reactants to the active site, localized on the solid catalyst surface, is several orders of magnitude higher than that occurs in the gas-phase processes. Such diffusion could significantly decrease the intrinsic activity of the catalyst and also modifies the overall selectivity of the process through secondary reaction. In addition, most of the liquid-phase catalysts are in powder form which calls for an efficient catalyst-product recovery step. Indeed, the powdered catalyst-product recovery represents an incentive process and catalyst loss is frequently encountered during the recovery process. Several attempts have been developed in order to facilitate the catalyst-products separation, i.e. magnetic support [3, 4], basket containing catalyst and structured catalysts with nanoscopic carbon support coated on monolith or foam host matrix [5-8]. However, most of the structured systems, based on the use of monolith and foam, are constituted by relatively thick host matrix structure exceeding hundred micrometers or even more, which could hinder the diffusion of the reactant to the active phase localized inside the pores of the support. The tortuosity of the porous network also induces long apparent sojourn time which favors secondary reactions. Despite the advantages regarding the recovery step such structured catalysts still suffer from low catalytic performance due to the diffusion limitations. The development of new catalyst support with better performance represents another aspect for the improvement of the catalytic performance by providing adequate structure with high effective surface area, reduced diffusion limitations and low pressure drop. It significantly contributes to the selectivity of the process as well as to the long-term stability of the catalyst by reducing deactivation through poisoning by secondary products. For liquid-phase reactions the use of the structured catalysts instead of slurry ones allows the avoidance of the costly and time consuming filtration process to separate the catalyst from the final product [9]. Structured catalysts also prevent the problem of fine formation as encountered with slurry reactor due to the attrition of small particles, consecutive to the repeated impacts between the catalyst particles and the stirrer, under vigorous stirring that

leads to the plugging of filtration device. Finally, microturbulences generated inside the structured catalyst also contribute to a higher degree of reactant mixing leading to a better catalytic performance [10].

The development of carbon materials (CMs), especially carbon nanotubes/nanofibers and graphene, has drawn increasing attention from both scientific and industrial researchers operated in the heterogeneous catalysis processes [11-13]. Because of their high porous structure, excellent resistance to acid or basic media, remarkable electrical and thermal conductivity, especially facile recovery for loading metal by combustion, CMs used as heterogeneous catalyst supports play an essential role in the noble metal catalyzed liquid-phase reaction. However, for the noble metal catalyst deposited on the pristine CMs, the rapid deactivation with extremely weak cycling stability and the low selectivity of catalysts restrict their potential application, which are caused from the leaching out or the aggregation of metal nanoparticles (NPs) during the catalyst evaluation due to the low metal-support interaction [14, 15]. It is demonstrated that these problems can be overcome by the modification of surface chemistry on the CMs with the introduction of oxygen-containing functional groups or heteroatoms (e.g., nitrogen, sulfur, phosphorus), which could reinforce the interaction between the carbon support and metal NPs or anchor the metal NPs on the carbon [16-20].

Commercial graphite felt (GF) constituted by entangled graphite filamentous with few micrometers in diameter displays high effective surface along with large voids (connected porosity), which could be of high interest for acting as catalyst support [21]. In addition, GF is widely produced for application in numerous fields such as filter for fume hood, insulation structure for high temperature ovens, sounds absorber, etc. However, commercial GF when used as catalyst support display several drawbacks: low specific surface area for dispersing of the active phase, hydrophobic character which prevents the anchoring of the active phase and low metal (oxide)/support interaction for preventing excessive sintering of metal NPs during the catalytic process. GF composites decorated with a layer of carbon nanofibers, growth through the Chemical Vapor deposition (CVD) method using nickel as growth catalyst, have been developed for being used as catalyst support with high dispersion properties along with

strong interaction to prevent excessive metal sintering [22]. However, such composites require the use of metal catalyst for the growth of carbon nanofibers as well as relatively high temperature synthesis process in the presence of explosive gaseous reactants, i.e. hydrocarbons and hydrogen, and a tedious purification process to remove the growth catalyst [23, 24]. It is of high interest to develop new synthesis method to functionalize the readiness commercial GF surface in order to improve the metal nanoparticles dispersion as well as the reduction of active phase sintering during the catalytic and regeneration processes if any. The method should be simple and easy for scaling up in order to facilitate the industrial development while the support should be robust enough for facing harsh reaction conditions to reduce the frequent replacement of the catalyst. The catalyst should also display controlled macroscopic shape, i.e. hierarchical structured catalysts, which could facilitate the catalyst-products recovery after the test [9].

The present work reports on the use of gaseous acid treated commercial GF as support for anchoring palladium NPs and it use as catalyst in the liquid-phase hydrogenation of α, β-unsaturated compounds. The GF is constituted by micrometers graphite filamentous with open structure (90% of voidage), which will significantly reduce the diffusion path of the reactant towards the active phase. The acid treatment was carried out under gaseous nitric acid at medium temperature leading to the formation of a micro- and mesoporous carbon structure, especially localized on or near the graphite surface, with a high specific surface area, accessible porosity along with oxygenated functional groups decorating defects on the surface. The oxygenated groups and the defects provide strong anchorage sites for dispersing palladium particles while the lack of ink-bottled pores significantly improve the diffusion rate allowing the maintenance of a high hydrogenation activity along with high selectivity. The as-synthesized GF-based catalyst is subsequently used as catalyst stirrer for liquid-phase hydrogenation process which allows one to phase out the costly filtration step to recover the catalyst from the reactant mixture.

## 2. Results and Discussion

### 2.1 GF and OGF Materials

The monolithic GF can be prepared with different macroscopic shapes depending to the downstream catalytic processes as presented in Figure 1A. The SEM micrographs (Figure 2) of the pristine carbon GF and the same after oxygen functionalization (OGF), through gaseous $HNO_3$ treatment at 250 $^o$C for 4 h, indicated that the gross morphology of the structured carbon was retained after the oxidation treatment despite some mass loss due to oxidation (see discussion below).

The gaseous acid treatment induces a significant increase of the OGF specific surface area (SSA) compared to that of the pristine GF. As shown in Figure 1B, the $N_2$ adsorption-desorption isotherm of GF and Pd/GF displayed the negligible adsorption of $N_2$, indicating the very little surface area without any porous structure. On the other hand, the isotherm of OGF and Pd/OGF exhibited the type IV isotherm curves with $H_4$-type hysteresis loops according to the IUPAC classification, which signified the presence of capillary condensation in the mesoporous structure and the narrow slit-shaped pores [25]. Indeed, the $HNO_3$ treated sample (OGF) displayed a SSA of 168 $m^2$/g compared to 4 $m^2$/g for the pristine GF. Such large SSA increases could be directly attributed to the formation of pores or defects within the pristine GF during the oxidation process according to the TEM analysis presented below. The pore size distribution (inset of Figure 1B) clearly evidences the formation of micro- and mesopores inside the oxidized GF which is expected to be at the origin of the SSA increase. It is worthy to note that the porosity formation did not alter the macroscopic shape of the material according to the SEM analysis presented above as a whole part of the pristine carbon microfilamentous was retained after the oxidation treatment despite some mass loss inherent to the oxidation process. Indeed, the defects and oxygen functionalization were carried out through oxidation of the pristine GF during the process which resulted to an increase of the SSA and also a mass loss accounted for about 13 wt. % [26, 27].
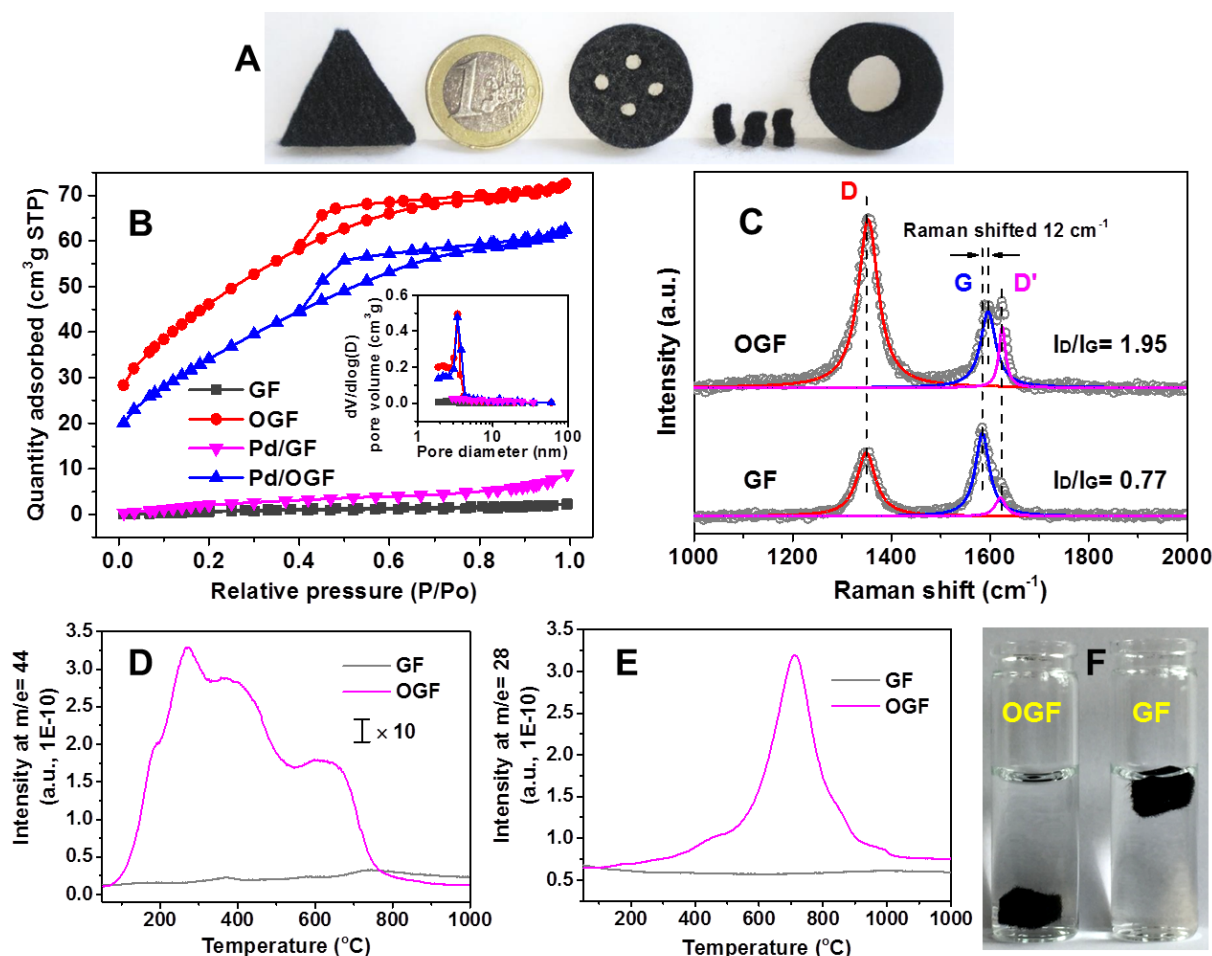
**Figure 1.** (A) Digital photo of the GF with different macroscopic shaping. The macroscopic shapes were completely retained after the acid treatment while a mass loss of ca. 13 wt.% was observed. (B) $N_2$ adsorption/desorption isotherms and pore size distributions (inset) of the pristine GF, OGF, Pd/GF and Pd/OGF. (C) Raman spectra, (D) $CO_2$ (m/z = 44) and (E) CO (m/z = 28) generated during the TPD analysis of the GF and OGF. (F) Digital photo of samples in water showing the surface character change before (GF) and after acid (OGF) treatment.

Raman spectroscopy was performed to investigate the change in the graphitic structure of GF after the oxidation process. As shown in Figure 1C, both GF and OGF fitted three bands corresponding to the different carbonaceous structures: the G band attributed to an ideal graphitic lattice at around 1580 cm$^{-1}$, the D band (~1350 cm$^{-1}$) associated with the structural defects and D' band corresponding to the disordered graphitic fragments at ~1620 cm$^{-1}$,

respectively [28, 29]. After the oxidation process, the $I_D/I_G$ increased from 0.77 for GF to 1.95 for OGF while the $I_{D'}/I_G$ increased more than 3 times from 0.26 to 0.84. Such results indicated that the gaseous oxidant treatment significantly modified the graphitic lattice of GF by creating more defects and disordered graphitic fragments inside the sample. Moreover, the G band of treated OGF shifted to the higher wavenumber by about 12 cm$^{-1}$ compared to that of GF, which may be attributed to the presence of oxygen-containing functional groups generated on the surface [30].



**Figure 2.** SEM images of GF (A), OGF (B, C) and EDX of OGF (D).

The surface oxygen groups present on GF and OGF were characterized by TPD-MS and the results are presented in Figure 1D and E. The oxygen functional groups are decomposed according to the evolution of $CO_2$ (originated from carboxylic acids, anhydrides
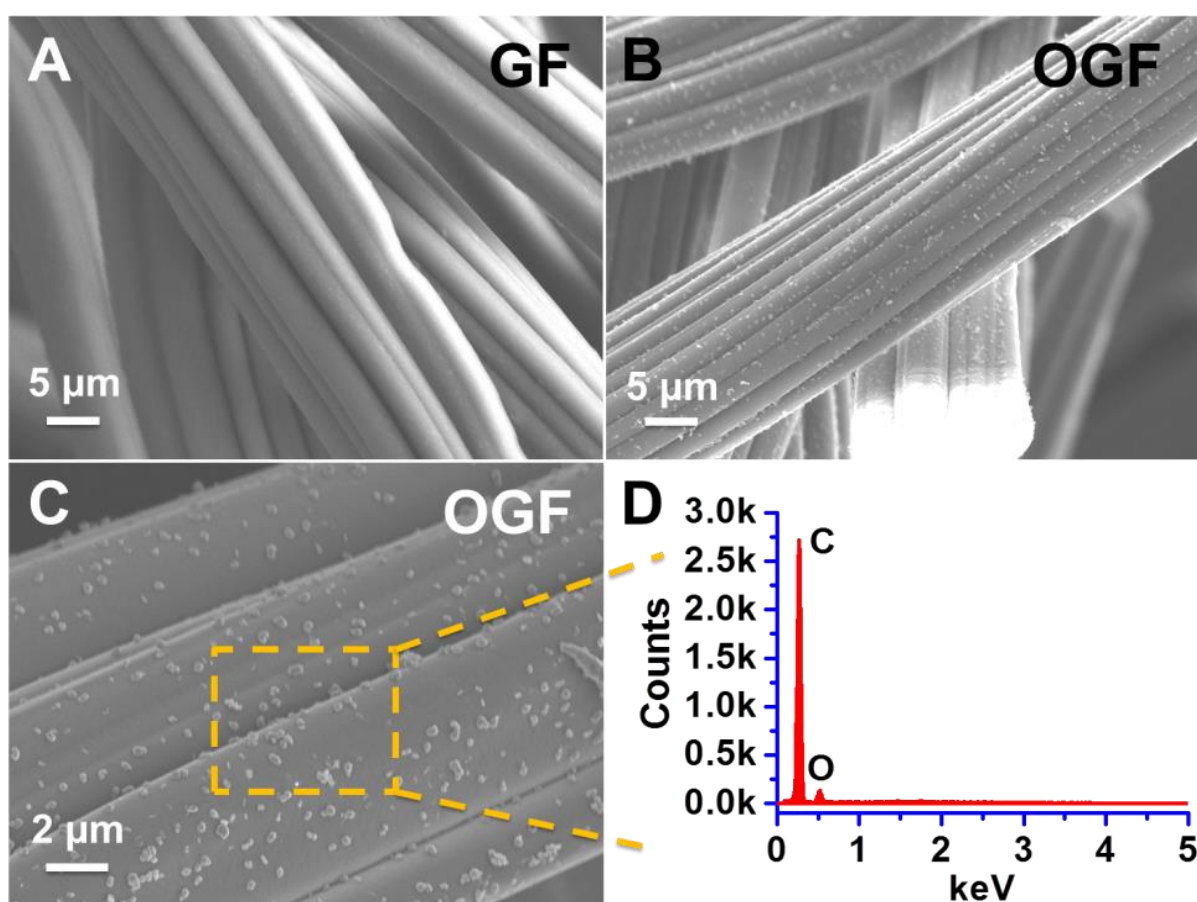
and lactones) or/and CO (originated from anhydrides, phenols and carbonyls) at different temperatures [31, 32]. The total amounts of $CO_2$ and CO released and surface oxygen contents were calculated from the corresponding TPD spectra (Table 1). The TPD results indicated that there were extremely few oxygen groups on the surface of the pristine GF which is in good agreement with the hydrophobic character of the material. After the oxidation treatment in the presence of gaseous $HNO_3$ at 250 °C for 4 h, the amount of surface oxygen functional groups increased more than 18 times for OGF according to the TPD experiments. Furthermore, the oxidation treatment also introduces hydrophilicity to the composite as shown in Figure 1F where untreated GF remains on top of the water medium while the treated, OGF, steadily sinks to the bottom, which is due to the incorporation of oxygenated functional groups on the defects or surface of the treated sample [33].

**Table 1.** Surface oxygen determined by TPD-MS (in the form of CO and $CO_2$)

| Sample | CO | $CO_2$ | Surface oxygen contents | |
|--------|------|--------|-------------------------|--------|
|        | (µmol/g) | (µmol/g) | (µmol/g) | (wt %) |
| **GF** | 107 | 29 | 165 | 0.26 |
| **OGF** | 2423 | 280 | 2983 | 4.77 |

TEM analysis is used to investigate the influence of oxidation treatment on the microstructure of GF. As displayed in Figure 3, the pristine GF is composed of ordered graphitic layers with very little pore on the surface which is in good agreement with it low SSA. After the gaseous acid treatment, TEM analysis evidences the formation of a highly porous carbon structure on the outer region of the fiber of OGF (pointed out by arrows in Figure 3C and D).
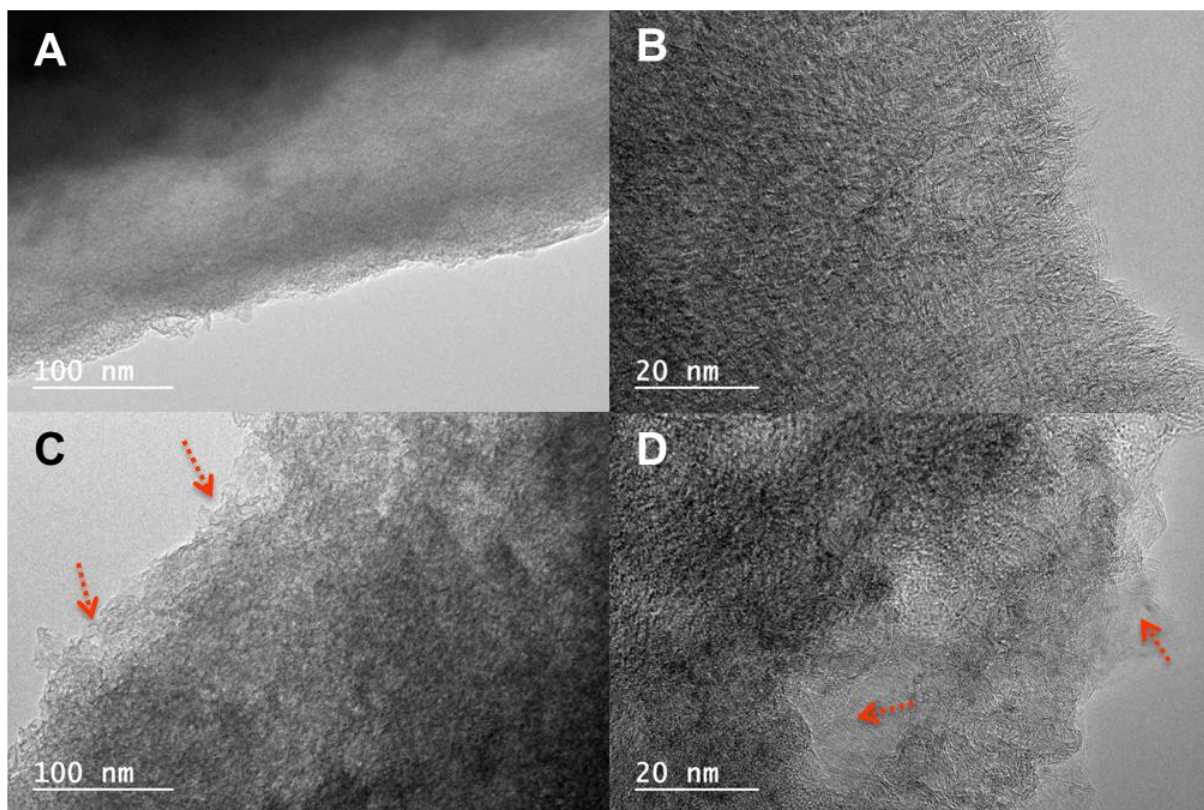
**Figure 3.** TEM images of the pristine GF (A, B) and OGF (C, D). The porous microstructure generated after the oxidation treatment inside the OGF is highlighted by arrows.

According to the TEM analysis the dense carbon structure of the GF was converted into a highly porous carbon structure with a large number of pores. It is expected that during the treatment to generate such highly porous carbon a large number of surface defects was also formed. This is in good agreement with the previous analysis of $N_2$ adsorption-desorption isotherm which clearly suggests the significant increased SSA on OGF. Such structure is expected to be formed through oxidation of a weakly graphitized carbon by the gaseous $HNO_3$ during the treatment, which leaving behind entangled carbon structure with high oxygenated decorating defects according to the Raman and TPD results presented above. Additional investigation will be made using TEM in tomography mode (TEM-3D) [34] which will allow one to get access to the porosity distribution of the sample and the localization of the metal nanoparticles with respect to such porosity. The results reported above confirmed that the gaseous $HNO_3$ thermal oxidation process is an efficient method for the synthesis of

high SSA carbon materials containing structural defects decorated with oxygenated functional groups as well as porous architecture.

## 2.2 Pd/OGF Characteristics

The profiles of $H_2$-TPR equipped with mass spectrometer for the supported Pd catalysts are shown in Figure 4. The sharp positive peak that appears in both of samples can be attributed to the $H_2$ release due to the decomposition of Pd hydride [35]. The absence of any $H_2$ consumption (negative peak) preceding hydride decomposition suggests the formation of zero-valent Pd at room temperature. The hydride decomposition temperature of Pd/OGF (88 $^o$C) is lower than that recorded of Pd/GF (96 $^o$C), indicating the smaller Pd particle size in Pd/OGF [36]. Moreover, there is no any $H_2$ consumption in Pd/GF, suggesting the complete reduction of sample at room temperature. Notably, the evolution of $H_2$ in Pd/OGF is accompanied by appreciable negative $H_2$ consumption peak around 122 $^o$C, which can be attributed to the reduction of palladium species that interact with the support more strongly [37].
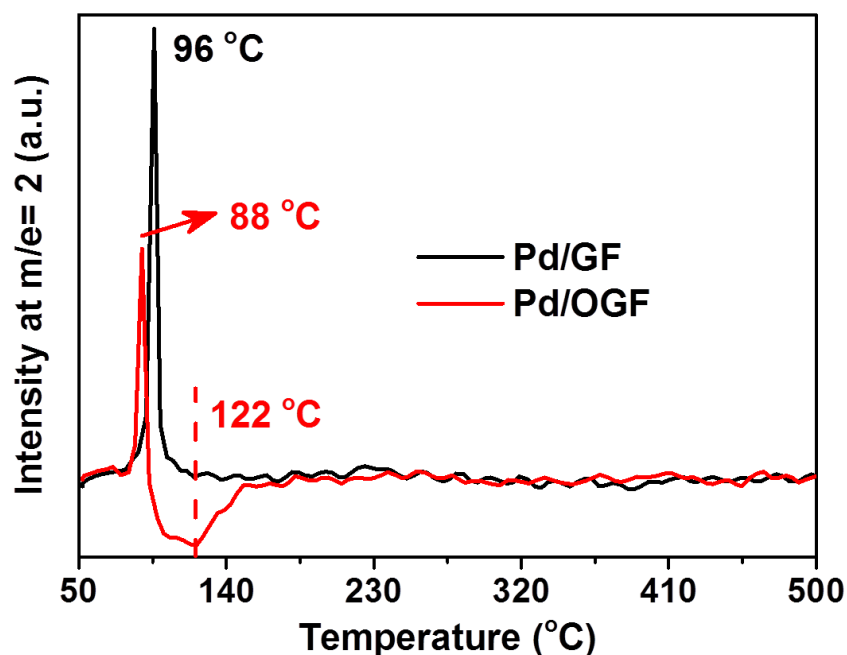


**Figure 4.** $H_2$ (m/z = 2) generated during the $H_2$-TPR analysis of the Pd/GF and Pd/OGF.

XPS was conducted to perform surface elemental analysis of the catalyst, including the metal dispersion and the impact of support on the electronic structure of Pd phase via metal-support interactions. The Pd 3d XPS spectra of catalysts (Figure 5A) present two main peaks at about 335.2 and 340.5 eV, corresponding to the doublet of Pd $3d_{5/2}$ and $3d_{3/2}$, respectively. In agreement with the literature, the deconvolution of core level Pd $3d_{5/2}$ reveals the presence of predominant metallic phase ($Pd^0$, 335.0 eV), oxide state metal ($Pd^{2+}$, 337.2 eV) and a satellite peak (338.4 eV) [38, 39]. There is an additional prominent signal (336.0 eV) between $Pd^0$ and $Pd^{2+}$, which is ~1.0 eV higher than bulk Pd, suggesting electron transfer from Pd to the carbon support, resulting in electron-deficient metal atoms ($Pd^{\delta+}$). The percentage of each peak as well as the atom percent of surface Pd on the catalyst, determined from the XPS survey spectra, are shown in Table 2. The oxide state $Pd^{2+}$, which was ascribed to the formation of Pd oxides upon sample storage in air, accounted for very little part in all Pd species. Interestingly, in this work, the proportion of $Pd^{\delta+}$ in GF supported Pd increased after the oxidization of the carbon carrier, indicating a direct correlation between support properties and electronic characters of the Pd phase. These metal-support interactions are crucial to catalytic performance because they further improve the metal dispersion and thermal stability. Moreover, under the similarity of Pd loading amounts in two samples, the higher atom percent for surface Pd on Pd/OGF demonstrated that the oxidation process enriches the dispersion of Pd species on the surface of GF support (Table 2).

Some other groups have also reported the presence of $Pd^{\delta+}$ phase in the carbon supported palladium catalysts, and linked these findings to the existence of metal-support interactions or electronic transfer associated with residual surface Cl [40-42]. Besides the experimental results [43, 44], the theoretical calculations have also indicated that the electron transfer may occur between the carbon and the supported metal, including Pd, Pt, Ru and Ni [45-48]. The bonds between metal and carbon atoms can be formed at metal-carbon interface, thus providing an efficient link for charge transfer [49]. The transfer orientation could be considered by using the simple descriptors, such as electronegativity, which is commonly used in solid-state physics/chemistry [50-52]. The difference in electronegativity between palladium (2.20) and carbon (2.55) leads to the electron transfer from Pd NPs to carbon

support at Pd-C interface. Furthermore, due to the much bigger electronegativity of oxygen (3.44), the oxidized carbon support, which is decorated with abundant oxygen functional groups at or near to the defects, would have a stronger tendency to attract more electrons from Pd NPs than untreated support. By density functional theory calculations, the charge transfer from Pd to graphene at graphene-Pd interface was confirmed in the system of monolayer graphene on Pd (111) [45]. Moreover, the interaction energies for Pd clusters on oxidized graphene are higher than those on a pure graphene support, indicating a significantly stronger interaction between the metal and the functionalized carbon support [38]. These results corroborate the Pd 3d XPS data (Figure 5A and Table 2) and suggest the high proportion of $Pd^{\delta+}$ along with the strong metal-support interaction in Pd/OGF catalyst.
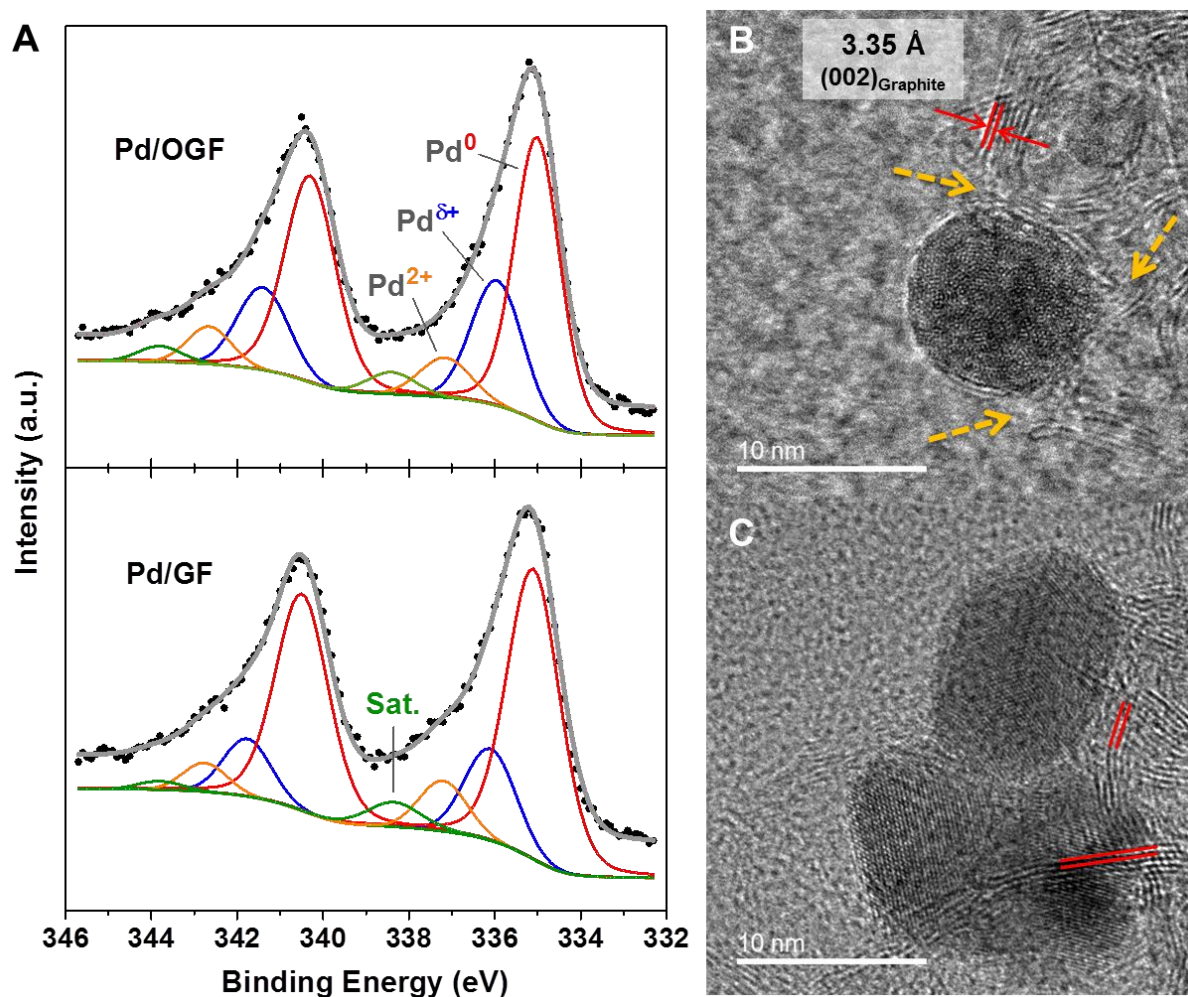


**Figure 5.** (A) XPS Pd 3d spectra of reduced catalysts and high resolution TEM micrographs for (B) Pd/OGF and (C) Pd/GF.

In order to understand the origin of the additional $Pd^{\delta+}$ contribution in the XPS analysis from the morphology, high-resolution TEM of Pd/OGF and Pd/GF are displayed in Figure 3B and C. In contrast to the majority of straight and ordered graphitic layers at the Pd-C interface in Pd/GF (Figure 5C), the Pd NPs in Pd/OGF interface (Figure 5B) follows more broken and curved carbon layers, suggesting that most of them bind to the structural defects decorated with oxygenated functional groups (pointed out by arrows in Figure 5B), as well as the charge transfer at Pd-C interface can be induced by the oxygen functionalization of carbon support.

**Table 2.** Pd elemental analysis and metal particle sizes of the samples

| Sample | Pd loading (wt%) | Percentage of peak area (%) | | | | Pd at%$^a$ | Pd particle sizes$^b$ (nm) | |
|--------|------------------|-----------------|-----------------|-----------------|-----------------|------------|--------------|--------------|
| | | $Pd^0$ | $Pd^{\delta+}$ | $Pd^{2+}$ | Sat. | | Reduced | Spent |
| **Pd/GF** | 4.3 | 73.1 | 15.1 | 7.5 | 4.3 | 2.7 | > 13.5 | > 42.5 |
| **Pd/OGF** | 4.6 | 61.6 | 25.4 | 8.8 | 4.2 | 3.6 | 3.8 ±0.8 | 3.8 ±1.1 |

$^a$ The atom percent of surface Pd elemental on the catalysts determined from the XPS survey spectra. $^b$ Pd particle sizes of reduced and spent samples determined by TEM analysis.

The Pd particle size distribution on both GF and OGF was investigated by means of TEM and the corresponding results are presented in Figure 6. According to the low magnification TEM analysis the Pd particles are smaller and homogeneous in size in the Pd/OGF catalyst compared to that deposited on the untreated Pd/GF (Figure 6A-B and D-E). High resolution TEM micrographs (Figure 6C and F) confirm the high dispersion of the palladium nanoparticles with extremely homogeneous in size on the Pd/OGF sample compared to that of the Pd/GF, which could be directly attributed to the strong interaction between the metal NPs with the defective carbon support surface. On the other hand, TEM analysis reveals much lower palladium particles dispersion on the untreated support which is in good agreement with the preceding XPS analysis. It is also worthy to note that the Pd NPs

are well separate from each other in the Pd/OGF sample with an almost absence of aggregate (Figure 6F) while they are presence in the form of large aggregates on the Pd/GF (Figure 6C) which pointed out the existence of a strong metal-support interactions with the defective carbon support. The particle size distribution of the Pd NPs, determined from more than 200 particles, is relatively narrow and centered at around 4 nm (Inset of Figure 6F).
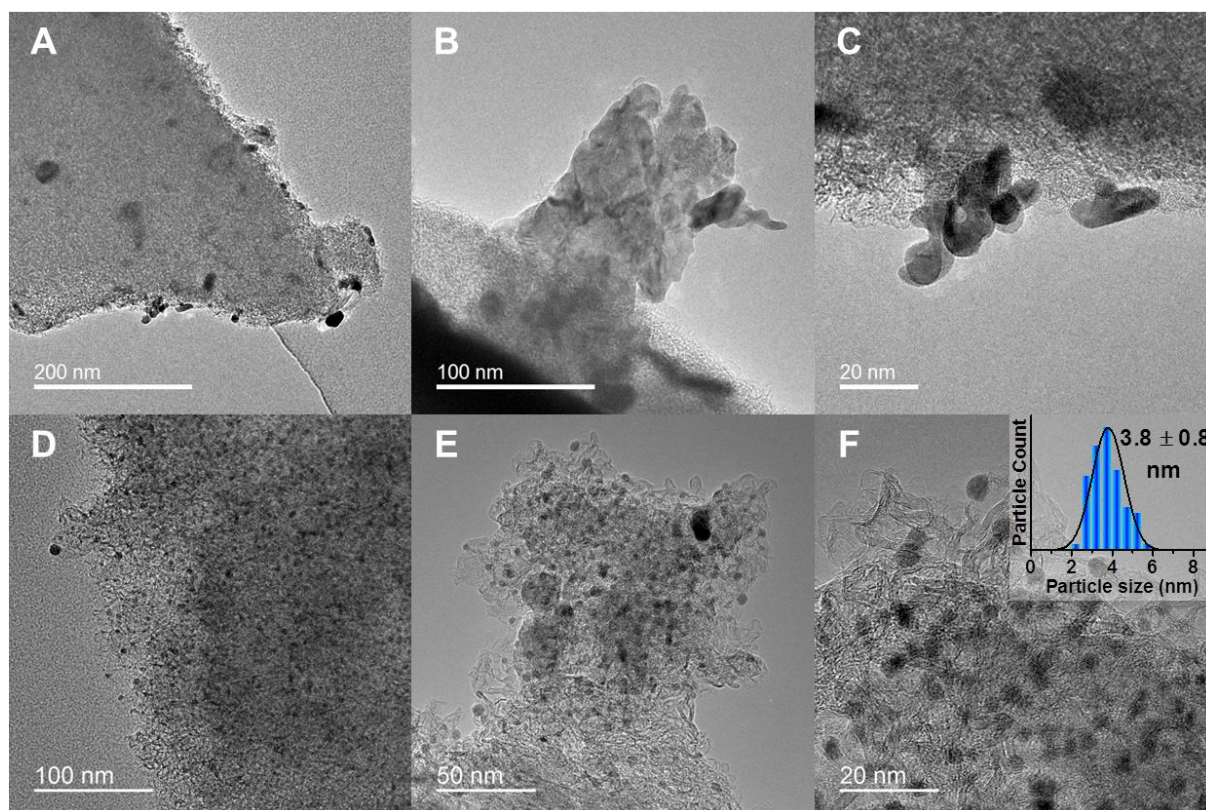


**Figure 6.** TEM micrographs of the Pd/GF (A, B and C) and Pd/OGF (E, E and F) catalysts after reduction and before reaction. Inset of (F): Pd particle size distribution determined from > 200 particles.

$H_2$-TPD was also conducted for the analysis of metal dispersion (Figure 7), the peak area of desorbed $H_2$ on Pd/OGF is much larger than that on Pd/GF, indicating that not only the higher dispersion of the Pd NPs, but also the stronger hydrogen uptake capacity of Pd/OGF, which is an important consideration in $H_2$-mediated liquid-phase catalysis where the $H_2$ dissociation on the catalyst surface is a rate limiting step (see discussion below on the

influence of $H_2$ concentration on the hydrogenation performance). Such results pointed out the importance of structural and functionalization properties of carbon support for obtaining high and stable metal NPs dispersion under elevated temperature reduction during catalyst preparation.
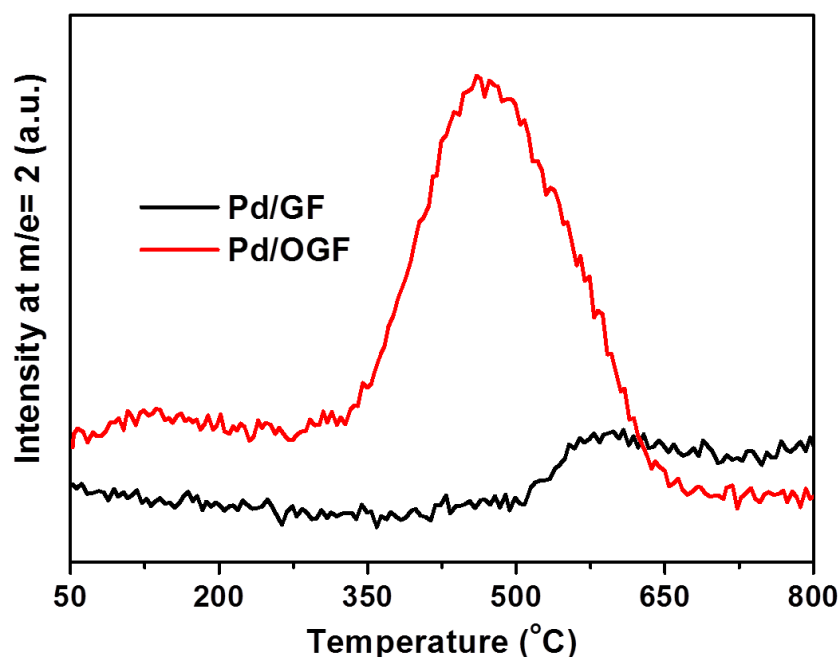


**Figure 7.** $H_2$ (m/z = 2) generated during the $H_2$-TPD analysis of the Pd/GF and Pd/OGF.

Based on the result and discussion above, the oxygen functionalization of GF by gaseous $HNO_3$ thermal treatment generates a unique architecture consist of abundant oxygenated groups decorated structural defects as well as porous structure with high exposure surface area. The high specific surface area of OGF provides a large Pd-support interface which significantly improve the metal dispersion [53]. Meanwhile the oxygen-rich functional groups have great potential as electron acceptors which could provide anchorage sites for the metal NPs [54, 55]. Combined with the modification of support electronic property from the structural defects, the oxygen functionalization in OGF induces the charge transfer from Pd atom to carbon support at metal-C interface, giving rise to a Strong Metal-Support Interaction (SMSI) in Pd/OGF associated with the high performance of high dispersed Pd NPs with good thermal stability.

## 2.3 Catalytic Performance

The liquid-phase hydrogenation of cinnamaldehyde using such structured catalyst as catalytic stirrer was conducted under different reaction conditions, i.e. stirring speed, initial CAD concentration, reaction temperature and hydrogen flow rate, to evaluate the catalytic performance between monolithic pristine GF and oxidative OGF supported Pd catalysts.

*Influence of Stirring Speed.* The hydrogenation reaction was carried out at 80 ℃ with different stirring speed ranged between 250 and 500 rpm. The catalytic results, expressed in terms of CAD concentration, mol/L, as a function of time-on-stream (TOS) are presented in Figure 8A. The hydrogenation activity increases and reaches a maximum rate at 375 rpm while it slightly decreases at higher stirring rate, i.e. 500 rpm (Figure 8A). The deviation of the cinnamaldehyde conversion at the end of the test could be attributed to the depletion of CAD in the medium and thus, inducing a CAD gradient concentration in the liquid medium which slower the adsorption rate of CAD on the catalyst surface. The influence of the stirring rate on the activity has already been reported by Tschentscher et al. for the oxygen/water system with rotating foam catalyst and could be explained by the contacting mode between liquid and stirrer during mixing process [56]. As shown in Figure 8C-F, the liquid would rotate following the rotated stirrer, and then the strong centrifugal force from high stirring speed could make the liquid reactant accumulate close to the wall of the reactor with descending liquid interface and then far away from the center of stirrer [57]. Under this situation, the reactant could not effectively contact the middle of the catalyst. On the other hand, high rate of agitation might cause the swirling flow, which further destroyed the micro-mixing. Therefore, the high rotating speed brought the loss of catalytic activity. For the subsequence tests, a stirring speed of 375 rpm will be used unless specified.

The selectivity of the C=C bond hydrogenation product slightly increases as a function of the stirring speed and remains almost unchanged between 375 and 500 rpm. The increase of the C=C bond hydrogenation selectivity from 250 to 375 rpm could be attributed to the rapid refreshment of the liquid layer on the catalyst surface which contributes to a higher desorption rate of the intermediate product before secondary hydrogenation occurs. Similar results have already been reported previously [58]. The refreshment seems to attaining a limit

at higher stirring speed, due to the problem of liquid/catalyst contact as discussed above, and only a marginally improvement of the C=C bond hydrogenation was observed.
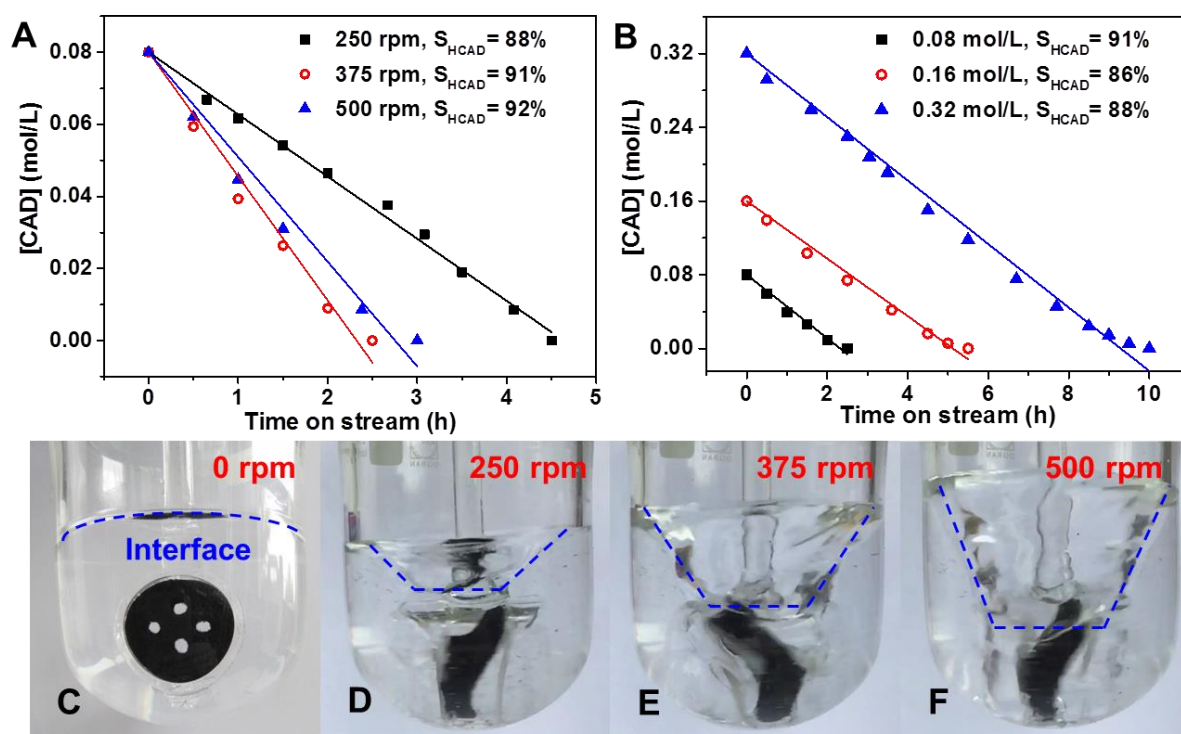


**Figure 8.** Influence of the reaction parameters on the C=C bond hydrogenation on the Pd/OGFs catalyst: (A) stirring rate and (B) cinnamaldehyde concentration. (C-F) Digital photo of the reactor using catalytic stirrer with different stirring rate. Reference conditions: 50 mL/min $H_2$, 80 °C, 1 atm, 375 rpm and 0.08 mol/L of CAD.

*Influence of Initial CAD Concentration.* The catalytic results, expressed in terms of CAD concentration, mol/L, obtained at 80 °C with different initial CAD concentrations are presented in Figure 8B as a function of time-on-stream (TOS). According to the results the C=C bond hydrogenation performance is almost proportional to the CAD concentration which confirm that the diffusion is not the limiting steps for the reaction at atmospheric pressure. Such results could be explained by the highly porous and micrometric dimension of the carbon filamentous and also to the lack of inner porosity of the support which significantly increase the reactant diffusion towards the active sites. The fact of using the catalyst as stirrer

also provides faster reactant refreshment on the catalyst surface which could contribute to such results.    The CAD initial concentration does not modify in a significant manner the C=C bond hydrogenation selectivity which remains between 86 and 91% taken into account experimental errors consecutive to the GC analysis.

*Influence of the Reaction Temperature.* The influence of the reaction temperature was evaluated between 40 and 80 ℃ and under atmospheric pressure. The stirring rate was keep at the most efficient value of 375 rpm. The CAD conversion was almost double when increasing the reaction temperature from 40 ℃ to 80 ℃ along with the increased C=C bond hydrogenation selectivity (Figure 9A). Such results indicate that secondary reaction, i.e. complete hydrogenation, is not favored by medium reaction temperature on the Pd/OGF catalyst. It seems that the intermediate hydrogenated product is steadily desorbed from the catalyst surface before complete hydrogenation occurs while re-adsorption is unlikely to occur regardless the reaction temperature. Again, the C=C bond hydrogenation selectivity remains between 88 and 91% which indicates that at such reaction temperature almost no additional secondary reaction was expected.

*Influence of the Hydrogen Flow Rate.* In the hydrogenation process the ability of the catalyst to dissociate hydrogen is primordial and the high dissociative adsorption of hydrogen allows the reduction of hydrogen in both inlet and exit stream which could be of high interest for recycling step. For comparison, the reaction is carried out on both Pd/OGF and Pd/GF catalysts, with different palladium dispersions according to the TEM analysis reported above, under similar reaction conditions, i.e. [CAD] = 0.08 mol/L and $H_2$ flow rate of 50 mL/min. According to the results presented in Figure 9B the two catalysts display a similar activity. In light of the results one can conclude that, at low CAD concentration and relatively high $H_2$ flow rate, dissociative adsorbed hydrogen on the catalyst surface on both high and low metal dispersion catalysts is largely sufficient for performing the hydrogenation of the CAD on the catalysts surface.

The catalytic hydrogenation performance of the Pd/OGF catalyst was evaluated under a more severe reaction conditions, i.e. CAD concentration of 0.32 mol/L and atmospheric pressure with various $H_2$ flow rate (Figure 9C). According to the results the time for complete

conversion of CAD slightly increased about 10% when the $H_2$ flow rate was decreased from 50 mL/min to 12.5 mL/min which confirms that on the Pd/OGF catalyst, with high palladium dispersion, the hydrogen dissociative adsorption on the Pd NPs under lower $H_2$ flow rate hardly influences the hydrogenation activity, despite in the presence of a higher CAD on the catalyst surface due to the increase of CAD concentration in the reaction medium. It seems that the rate of hydrogen dissociative adsorption on the small palladium particles of the Pd/OGF is high and provides enough adsorbed hydrogen to convert the adsorbed CAD on the catalyst surface.
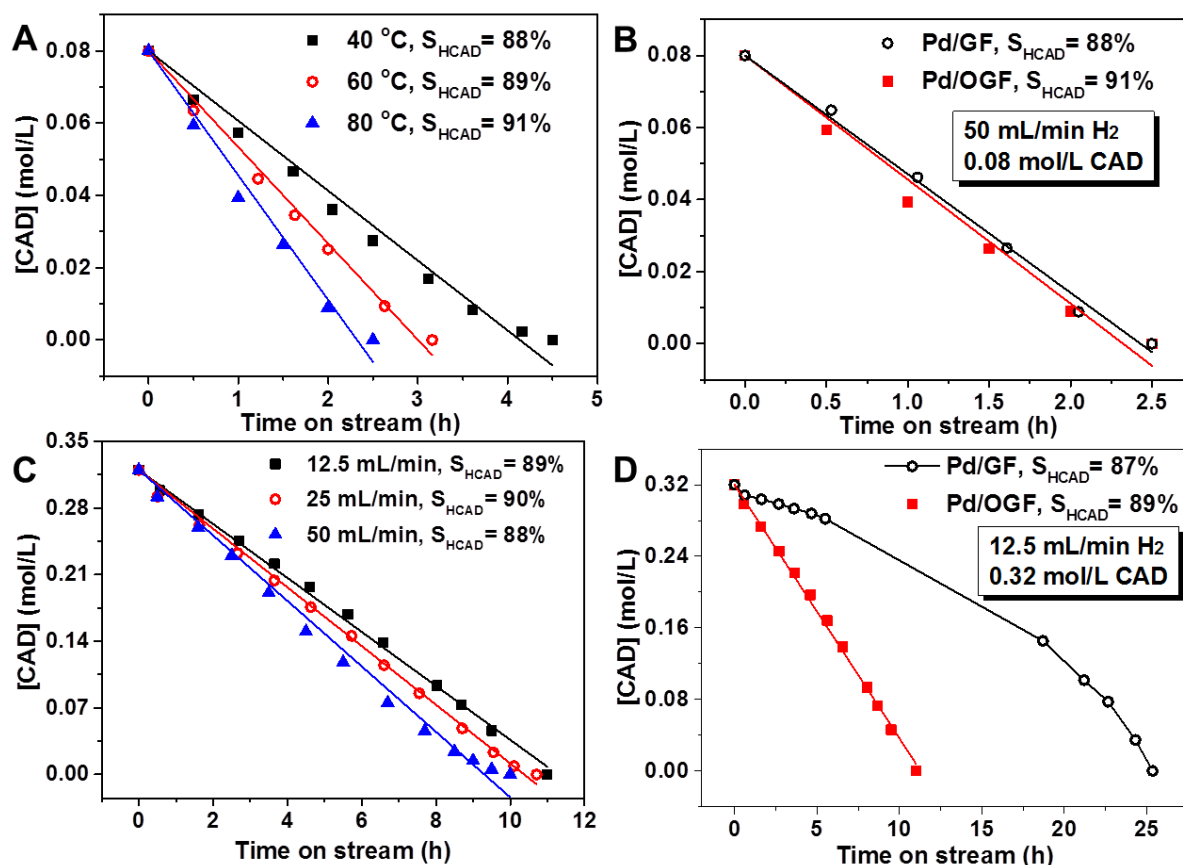


**Figure 9**. (A) Influence of the reaction temperature, (B) Cinnamaldehyde conversion as a function of the hydrogen flow rate on the Pd/OGF catalyst, (C and D) Cinnamaldehyde conversion as a function of the adverse cinnamaldehyde concentration to hydrogen flow rate on Pd/OGF and Pd/GF catalysts. Reference conditions: 50 mL/min $H_2$, 80 ℃, 1 atm, 375 rpm, and 0.08 mol/L of CAD.

In order to verify such assumption the same reaction was carried out on both catalysts under severe reaction conditions: [CAD] = 0.32 mol/L and $H_2$ flow rate = 12.5 mL/min. Under these reaction conditions the hydrogenation rate obtained on the Pd/OGF is much higher, i.e. more than twice, than the one obtained on the Pd/GF catalyst according to the results presented in Figure 9D whereas the hydrogenation rate is similar between the two catalysts at high hydrogen flow rate and at low CAD concentration as shown in Figure 9B. It is expected that on the Pd/GF with lower palladium dispersion, and as a consequence of larger palladium particle size, the rate of hydrogen dissociation seems to be much slower at low hydrogen flow rate leading to an insufficient adsorbed hydrogen for the complete hydrogenation of the adsorbed CAD on the catalyst surface, and resulting thus to a lower hydrogenation performance. Such results indicate that acid treatment allows one to produce OGF support with high dispersion properties for metal which, in turn, leads to a highly active catalyst for operating under severe reaction conditions.

The selectivity towards the C=C bond hydrogenation remains almost unchanged which indicates that consecutive reaction leading to complete hydrogenated product is not depending on the amount of adsorbed hydrogen at the catalyst surface but only on the desorption rate of the intermediate product.

*Catalyst Stability as a Function of Cycling Tests.* Catalyst deactivation as a function of cycling tests is the most common observed trend in heterogeneous liquid-phase processes due to several factors such as active phase loss consecutive to leaching or fine formation, catalyst loss during the recovery step and also to sintering. In this section the stability behavior of the Pd/OGF, Pd/GF and commercial Pd/AC (Pd/activated charcoal provided by Sigma-Aldrich) catalysts was evaluated. The weight amount of the catalyst was adjusted in order to have the same metal active phase weight for the comparison tests. The cycling tests were carried out as follow: for the catalytic stirrers (Pd/GF and Pd/OGF), after reaction the liquid was removed and the reactor was filled with 100 mL of dioxane, the catalyst was stirred at 375 rpm for 30 minutes in order to desorb the adsorbed products on its surface or inside the porosity; for the commercial Pd/AC catalyst the powdered catalyst was allowed to settle down before removal of the supernatant liquid followed by two consecutive washing steps. The efficiency of the

washing step was controlled by analyzing the solution by GC to determine if any reactant or product remains in the washing solution. The catalytic performance under the reference conditions (50 mL/min H$_2$, 80 °C, 1 atm, 375 rpm, and 0.08 mol/L of CAD), expressed in terms of the conversion of CAD and selectivity of HCAD, as a function of cycling tests is presented in Figure 10A and B, respectively.
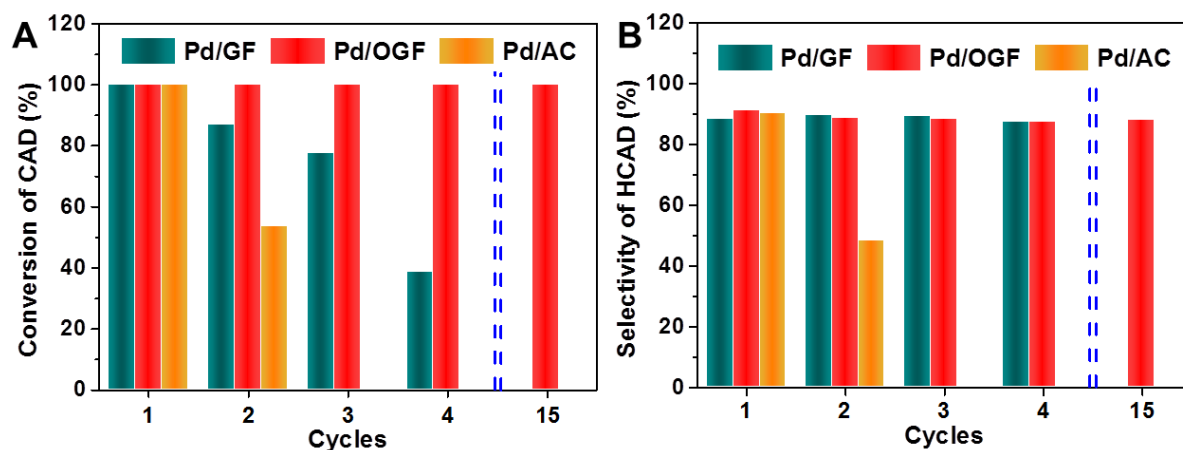


**Figure 10.** (A) Cinnamaldehyde conversion and (B) C=C bond hydrogenation selectivity as a function of the cycling tests on Pd/OGF, Pd/GF and commercial Pd/AC catalysts. Conditions: 80 °C, 50 mL/min H$_2$, 1 atm, 375 rpm and 0.08 mol/L of CAD.

The Pd/OGF catalyst displays an extremely high stability as no deactivation is observed even after up to 15 cycling tests (Figure 10A). On the contrary, the commercial Pd/AC catalyst shows a drastic hydrogenation activity loss as only 50% of conversion is retained after the second test. The untreated Pd/GF catalyst displays a high hydrogenation activity at the beginning followed by a gradual but slower deactivation, compared to that observed for the commercial powdered Pd/AC catalyst, as a function of cycling tests. However, after fourth cycles only 40% of the initial hydrogenation activity was retained on the Pd/GF catalyst which indicates that severe deactivation has occurred. The catalyst stability of Pd/OGF was further demonstrated under low conversion, as shown in Figure 11, the conversion of CAD over Pd/OGF still remain at 22% along with the HCAD selectivity of 90% during the fifteen cycling tests. It is worthy to note that a significant selectivity loss on

the commercial powder catalyst was observed after only two cycles, but on the contrary, the selectivity towards HCAD on both structured catalysts remains unchanged as a function of cycling tests (Figure 10B).
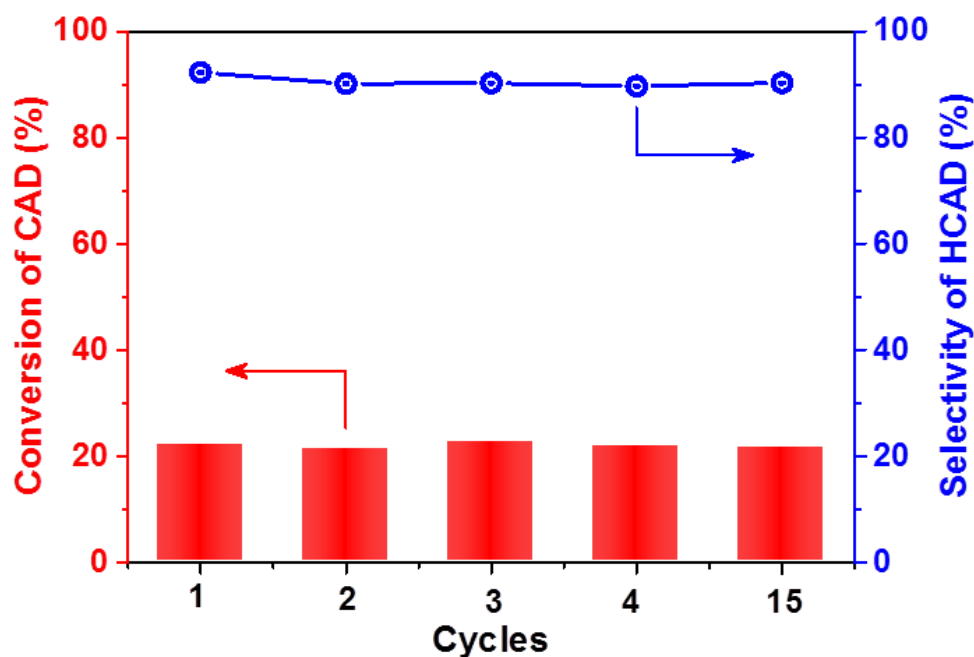


**Figure 11.** Recycling tests of Pd/OGF catalyst for liquid-phase hydrogenation of CAD at low conversion. Conditions: 80 $^{o}$C, 50 mL/min H$_2$, 1 atm, 375 rpm and 0.08 mol/L of CAD.

TEM analysis was carried out on the spent Pd/GF and Pd/OGF and the results are displayed in Figure 12 and Table 2. The palladium particles on the Pd/OGF, after fifteen cycling tests, remain high dispersion with a similar particle size as that observed for the freshly reduced catalyst (Figure 12A-C). The Pd particle size distribution (Figure 12C inset) determined from more than 200 particles remains at around 3.8 nm which is similar to that of the freshly reduced catalyst. On the other hand, there was a dramatic change for the Pd particle size on the Pd/GF after only 4 cycling tests where Pd particles assembled in large aggregates were observed (Figure 12D-F and Table 2). These data suggest that the aggregation or sintering of metal particles was the key factor contributing to the deactivation of Pd/GF catalyst during the cycling tests. Indeed, on such structured catalyst the catalyst loss

during the recovery step is unlikely occurs. The sintering phenomenon observed could be attributed to the low metal-support interactions, i.e. lack of defects and oxygenated functional groups, compared to that of the OGF support. It is expected that the sintering of Pd NPs on the Pd/GF catalyst is at the origin of the lower hydrogen dissociative adsorption on the catalyst as mentioned before, which results in the hydrogenation activity loss with cycling tests while maintaining the C=C hydrogenation bond selectivity. Such phenomenon could also happen to the deactivated Pd/AC powdered catalyst. On the other hand, the striking selectivity loss of this powdered catalyst pointed out the important variation on the catalyst nature, i.e. microstructural change. Indeed, the slurry suspension of powder catalysts suffers from the inevitable attrition of solid particles under vigorous stirring during the test, and then the finer powders formed could led to a troublesome mass transfer of the hydrogenated intermediate product in the porosity, which could induce longer sojourn time leading to over-hydrogenation before escaping [58]. Besides, as shown in Figure 13, compared with powdery samples, the structured catalysts also exhibit easier catalyst-product recovery which represents an important parameter for operating liquid-phase reactions.
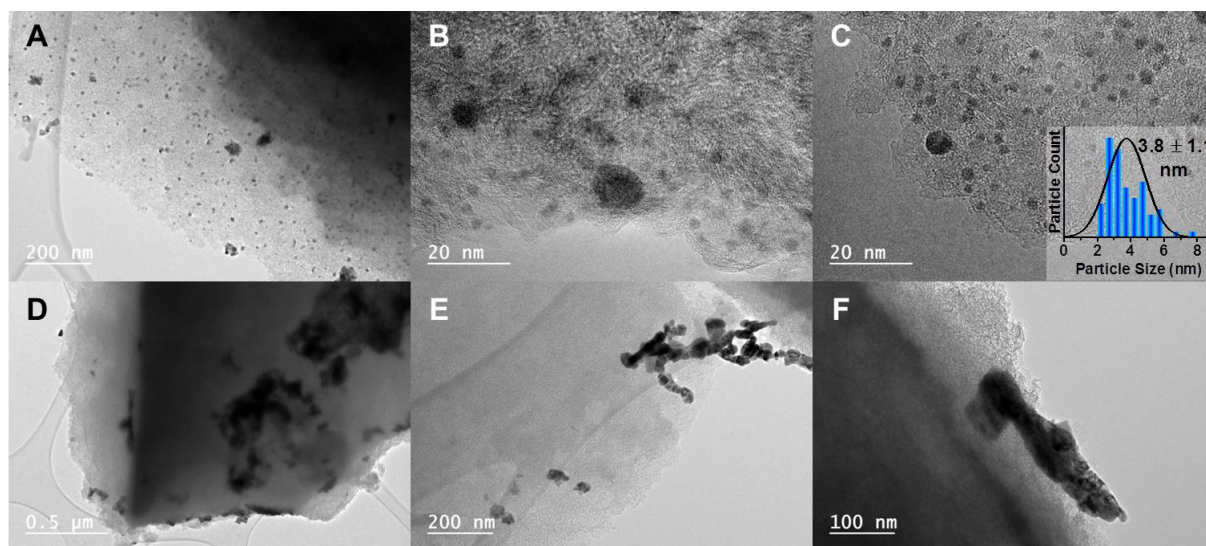


**Figure 12.** TEM images of the spent Pd/OGF (A, B, C) after 15 cycling tests and Pd/GF (D, E, F) after 4 cycling tests.
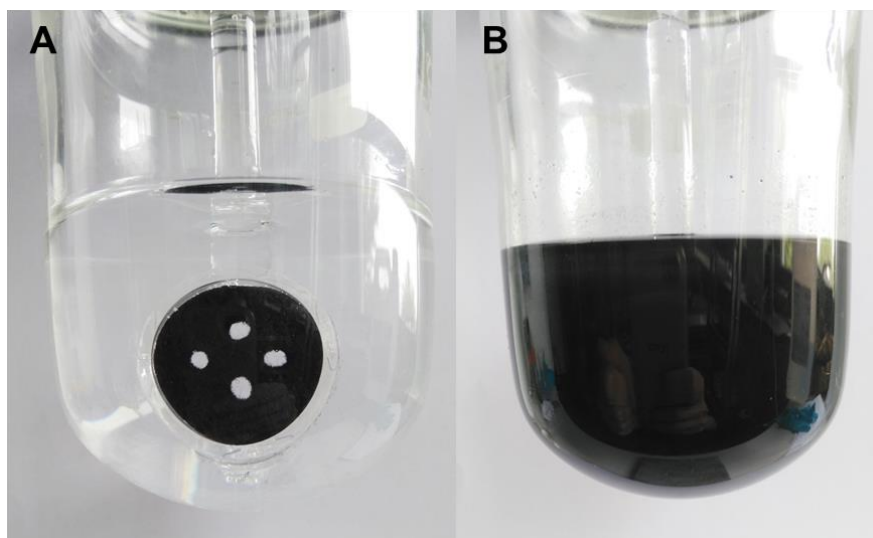
**Figure 13.** Optical photographs of the structured catalyst as catalytic stirrer (A) and commercial Pd/AC powder (B) after the liquid-phase reaction.

The leaching test was carried out to exclude active species loss of Pd/OGF, as follows: after the first hydrogenation run the structured catalyst was separated from the reaction solution, and then the identical amount of cinnamaldehyde was added to the recovered solution for a second hydrogenation without the catalyst. The test was done in the same reaction condition as before. Moreover, in order to verify the recyclability of the catalyst and to confirm the leaching tests, the recovered catalyst was further employed in other successive catalytic cycles, up to 15 times. In addition, to evaluate the metal loss throughout the cycling tests, the leaching test was repeated three times after the first, seventh and fifteenth cycle, respectively. In all leaching tests, there was no additional CAD conversion observed, which indicates there was the almost negligible leaching of active metal on Pd/OGF catalyst during the 15 cycling tests inside the solution medium, thus confirming the strong metal-support interaction, which helps not only the Pd dispersion and stability against sintering but also its anchorage. The catalyst was compared with other reported Pd-based catalysts in hydrogenation of cinnamaldehyde and the different catalytic results are summarized in Table 3. The Pd/OGF catalyst shows a relatively high catalytic activity and stability as well as recyclability compared to the other monolith or powder catalysts operated at lower cycling tests, which could be attributed to the strong metal-support interaction to prevent active phase

sintering or leaching. Combined with the easier catalyst-product recovery of structured catalyst in the liquid-phase process, these results pointed out the high efficiency of the monolith Pd/OGF catalyst to perform liquid-phase hydrogenation of cinnamaldehyde.

## 3. Conclusion

In summary, using a simple gaseous acid treatment we succeeded in the synthesis of a novel structured catalyst support with high anchorage sites through defects and oxygenated functional groups from commercial graphite felt raw material. Such support displays strong interaction with the deposited metal NPs which showed excellent catalytic activity and stability as well as recyclability through an easy recovery in liquid-phase hydrogenation of cinnamaldehyde. It is demonstrated that the charge transfer at Pd-support interface can be induced by the oxygen functionalization of GF. The partial positively charged metal phase $Pd^{\delta+}$, because of the electron transfer from Pd atoms to the OGF through oxygenated functional groups decorating defects, are responsible for both anchoring and stabilization of Pd NPs, which ultimately account for the enhanced resistance of Pd/OGF to sintering and/or aggregation during both catalyst preparation and cycling tests. The as-synthesized Pd/OGF catalyst displays high hydrogenation activity even at low hydrogen rate supply and high reactant concentration along with high stability with cycling tests. In addition, it is expected that the stabilization of metal NPs on oxygen functionalized carbon supports via the charge-transfer mechanism is not limited to the Pd/OGF system, but can be extended further and made applicable to other carbon supported metal systems. Work is ongoing to evaluate such metal/oxidized carbon catalyst, in other gas-phase reactions, i.e. $CO_2$ methanation, where highly dispersed metal NPs with good thermal stability play a vital role for catalytic performance.

**Table 3.** Hydrogenation of cinnamaldehyde over different Pd catalysts

| Catalyst | Shape | Pd wt% | [CAD] mol/L | Solvent | Condition | $X^a$ % | $S^b$ % | Cycling test | | Ref. |
|---|---|---|---|---|---|---|---|---|---|---|
| | | | | | | | | Runs | $X^c$ % | |
| Pd/OGF | Monolith | 5 | 0.08 | Dioxane, 100 mL | 80 $^o$C, 1 atm, 50 mL/min H$_2$, 375rpm and 2.5 h | 100 | 91 | 15 | 100 | This work |
| Pd/CNF/SiC | Monolith | 5 | 0.72 | Dioxane | 80 $^o$C, 1 atm, 60 mL/min H$_2$, 400 rpm and 6 h | 100 | 90 | 10 | 91 | [8] |
| Pd/N-CNTs | Powder | 10 | 0.38 | Dioxane, 100 mL | 80 $^o$C, 1 atm, 60 mL/min H$_2$, 400 rpm and 11 h | 100 | 92 | 2 | 88 | [59] |
| Pd/NRGO$_{300}$ | Powder | 4.6 | 4 | H$_2$O, 2.5 mL | 70 $^o$C, 2 MPa, 1000 rpm and 1.75 h | 100 | 96 | 5 | 90 | [15] |
| Pd/ZIF-8 | Powder | 1 | 0.2 | Isopropanol, 10 mL | 40 $^o$C, 2 MPa, 600 rpm and 6 h | 100 | 90 | 4 | 85 | [60] |
| Pd-MWCNT/AC | Powder | 1.5 | 0.76 | Dioxane, 10 mL | 70 $^o$C, 1 MPa and 2 h | 100 | 74 | 5 | 100 | [61] |
| Pd-NMC | Powder | 2 | 0.3 | 2-propanol, 25 mL | 30 $^o$C, 5 bar, 800 rpm and 3h | 100 | 93 | 7 | 100 | [62] |

[a] The conversion of CAD in the initial hydrogenation reaction.

[b] The selectivity of HCAD in the initial hydrogenation reaction.

[c] The conversion of CAD in the last cycling test.

**Acknowledgements**

# References

[1] P. Lanzafame, S. Perathoner, G. Centi, S. Gross, E.J.M. Hensen, Grand challenges for catalysis in the science and technology roadmap on catalysis for europe: Moving ahead for a sustainable future, Catalysis Science & Technology, 7 (2017) 5182-5194.

[2] M. Beller, G. Centi, L. Sun, Chemistry future: Priorities and opportunities from the sustainability perspective, ChemSusChem, 10 (2017) 6-13.

[3] S.C. Tsang, V. Caps, I. Paraskevas, D. Chadwick, D. Thompsett, Magnetically separable, carbon-supported nanocatalysts for the manufacture of fine chemicals, Angewandte Chemie International Edition, 116 (2001) 5763-5767.

[4] W. Baaziz, L. Truong-Phuoc, C. Duong-Viet, G. Melinte, I. Janowska, V. Papaefthimiou, O. Ersen, S. Zafeiratos, D. Begin, S. Begin-Colin, C. Pham-Huu, Few layer graphene decorated with homogeneous magnetic $Fe_3O_4$ nanoparticles with tunable covering densities, Journal of Materials Chemistry A, 2 (2014) 2690-2700.

[5] E. García-Bordejé, I. Kvande, D. Chen, M. Rønning, Carbon nanofibers uniformly grown on γ-alumina washcoated cordierite monoliths, Advanced Materials, 18 (2006) 1589-1592.

[6] S.R.A.d. Loos, J.v.d. Schaaf, M.H.J.M.d. Croon, T.A. Nijhuis, J.C. Schouten, Heterogeneous catalysis in a microchannel using a layer of carbon nanofibers on the channel wall, Chemical Engineering Journal, 179 (2012) 242-252.

[7] K. Chizari, A. Deneuve, O. Ersen, I. Florea, Y. Liu, D. Edouard, I. Janowska, D. Begin, C. Pham-huu, Nitrogen-doped carbon nanotubes as a highly active metal-free catalyst for selective oxidation, ChemSusChem, 5 (2012) 102-108.

[8] L. Truong-Phuoc, T. Truong-Huu, L. Nguyen-Dinh, W. Baaziz, T. Romero, D. Edouard, D. Begin, I. Janowska, C. Pham-Huu, Silicon carbide foam decorated with carbon nanofibers as catalytic stirrer in liquid-phase hydrogenation reactions, Applied Catalysis A: General, 469 (2014) 81-88.

[9] E. Garcia-Bordejé, Y. Liu, D.S. Su, C. Pham-Huu, Hierarchically structured reactors containing nanocarbons for intensification of chemical reactions, Journal of Materials

Chemistry A, 5 (2017) 22408-22441.

[10] Y. Peng, J.T. Richardson, Properties of ceramic foam catalyst supports one-dimensional and two-dimensional heat transfer correlations, Applied Catalysis A: General, 266 (2004) 235-244.

[11] D.S. Su, S. Perathoner, G. Centi, Nanocarbons for the development of advanced catalysts, Chemical Reviews, 113 (2013) 5782-5816.

[12] J.-P. Tessonnier, M. Becker, W. Xia, F. Girgsdies, R. Blume, L. Yao, D.S. Su, M. Muhler, R. Schlögl, Spinel-type cobalt-manganese-based mixed oxide as sacrificial catalyst for the high-yield production of homogeneous carbon nanotubes, ChemCatChem, 2 (2010) 1559-1561.

[13] P. Serp, M. Corrias, P. Kalck, Carbon nanotubes and nanofibers in catalysis, Applied Catalysis A: General, 253 (2003) 337-358.

[14] Z. Li, J. Liu, C. Xia, F. Li, Nitrogen-functionalized ordered mesoporous carbons as multifunctional supports of ultrasmall Pd nanoparticles for hydrogenation of phenol, ACS Catalysis, 3 (2013) 2440-2448.

[15] R. Nie, M. Miao, W. Du, J. Shi, Y. Liu, Z. Hou, Selective hydrogenation of C=C double bond over N-doped reduced graphene oxides supported Pd catalyst, Applied Catalysis B: Environmental, 180 (2016) 607-613.

[16] W. Shi, B. Zhang, Y. Lin, Q. Wang, Q. Zhang, D.S. Su, Enhanced chemoselective hydrogenation through tuning the interaction between Pt nanoparticles and carbon supports: Insights from identical location transmission electron microscopy and X-ray photoelectron spectroscopy, ACS Catalysis, 6 (2016) 7844-7854.

[17] J. Luo, H. Wei, Yuefeng Liu, D. Zhang, B. Zhang, W. Chu, C. Pham-Huu, D.S. Su, Oxygenated group and structural defect enriched carbon nanotubes for immobilizing gold nanoparticles, Chemical Communications, 53 (2017) 12750-12753.

[18] J. Amadou, K. Chizari, M. Houllé, I. Janowska, O. Ersen, D. Bégin, C. Pham-Huu, N-doped carbon nanotubes for liquid-phase C=C bond hydrogenation, Catalysis Today, 138 (2008) 62-68.

[19] D. Higgins, M.A. Hoque, M.H. Seo, R. Wang, F. Hassan, J.-Y. Choi, M. Pritzker, A. Yu, J. Zhang, Z. Chen, Development and simulation of sulfur-doped graphene

supported platinum with exemplary stability and activity towards oxygen reduction, Advanced Functional Materials, 24 (2014) 4325-4336.

[20] C. Chen, X. Li, L. Wang, T. Liang, L. Wang, Y. Zhang, J. Zhang, Highly porous nitrogen- and phosphorus-codoped graphene an outstanding support for Pd catalysts to oxidize 5-hydroxymethylfurfural into 2,5-furandicarboxylic acid, ACS Sustainable Chemistry & Engineering, 5 (2017) 11300-11306.

[21] M. Sun, X.-R. Ru, L.-F. Zhai, In-situ fabrication of supported iron oxides from synthetic acid mine drainage: High catalytic activities and good stabilities towards electro-fenton reaction, Applied Catalysis B: Environmental, 165 (2015) 103-110.

[22] R. Vieria, C. Pham-Huu, N. Keller, M.J. Ledoux, New carbon nanofiber/graphite felt composite for use as a catalyst support for hydrazine catalytic decomposition, Chemical Communications, (2002) 954-955.

[23] J. Luo, Y. Liu, H. Wei, B. Wang, K.-H. Wu, B. Zhanga, D.S. Su, A green and economical vapor-assisted ozone treatment process for surface functionalization of carbon nanotubes, Green Chemistry, 19 (2017) 1052-1062.

[24] C. Duong-Viet, L. Truong-Phuoc, T. Tran-Thanh, J.-M. Nhut, L. Nguyen-Dinh, I. Janowska, D. Begin, C. Pham-Huu, Nitrogen-doped carbon nanotubes decorated silicon carbide as a metal-free catalyst for partial oxidation of $H_2S$, Applied Catalysis A: General, 482 (2014) 397-406.

[25] H. Yu, Q. Zhang, M. Dahl, J.B. Joo, X. Wang, L. Wang, Y. Yin, Dual-pore carbon shells for efficient removal of humic acid from, Chemistry - A European Journal, 23 (2017) 16249-16256.

[26] C. Duong-Viet, Y. Liu, H. Ba, L. Truong-Phuoc, W. Baaziz, L. Nguyen-Dinh, J.-M. Nhut, C. Pham-Huu, Carbon nanotubes containing oxygenated decorating defects as metal-free catalyst for selective oxidation of $H_2S$, Applied Catalysis B: Environmental, 191 (2016) 29-41.

[27] Z. Xu, C. Duong-Viet, H. Ba, B. Li, T. Truong-Huu, L. Nguyen-Dinh, C. Pham-Huu, Gaseous nitric acid activated graphite felts as hierarchical metal-free catalyst for selective oxidation of $H_2S$, Catalysts, 8 (2018) 145.

[28] L.G. Cancado, A. Jorio, E.H.M. Ferreira, F. Stavale, C.A. Achete, R.B. Capaz, M.V.O.

Moutinho, A. Lombardo, T.S. Kulmala, A.C. Ferrari, Quantifying defects in graphene via raman spectroscopy at different excitation energies, Nano Letters, 11 (2011) 3190-3196.

[29]   A. Sadezky, H. Muckenhuber, H. Grothe, R. Niessner, U. Pöschl, Raman microspectroscopy of soot and related carbonaceous materials spectral analysis and structural information, Carbon, 43 (2005) 1731-1742.

[30]   T.T. Thanh, H. Ba, L. Truong-Phuoc, J.-M. Nhut, O. Ersen, D. Begin, I. Janowska, D.L. Nguyen, P. Granger, C. Pham-Huu, A few-layer graphene-graphene oxide composite containing nanodiamonds as metal-free catalysts, Journal of Materials Chemistry A, 2 (2014) 11349-11357.

[31]   R. Huang, J. Xu, J. Wang, X. Sun, W. Qi, C. Liang, D.S. Su, Oxygen breaks into carbon nanotubes and abstracts hydrogen from propane, Carbon, 96 (2016) 631-640.

[32]   J.L. Figueiredo, Funtionalization of porous carbons for catalytic applications, Journal of Materials Chemistry A, 1 (2013) 9351-9364.

[33]   Z. Zhang, J. Xi, H. Zhou, X. Qiu, KOH etched graphite felt with improved wettability and activity for vanadium flow batteries, Electrochimica Acta, 218 (2016) 15-23.

[34]   O. Ersen, C. Hirlimann, M. Drillon, J. Werckmann, F. Tihay, C. Pham-Huu, C. Crucifix, P. Schultz, 3D-TEM characterization of nanometric objects, Solid State Sciences, 9 (2007) 1088-1098.

[35]   W.-J. Shen, M. Okumura, Y. Matsumura, M. Haruta, The influence of the support on the activity and selectivity of Pd in CO hydrogenation, Applied Catalysis A: General, 213 (2001) 225-232.

[36]   C. Amorim, M.A. Keane, Palladium supported on structured and nonstructured carbon: A consideration of Pd particle size and the nature of reactive hydrogen, Journal of Colloid and Interface Science, 322 (2008) 196-208.

[37]   S. Jujjuri, M.A. Keane, Catalytic hydrodechlorination at low hydrogen partial pressures: Activity and selectivity response, Chemical Engineering Journal, 157 (2010) 121-130.

[38]   R.G. Rao, R. Blume, T.W. Hansen, E. Fuentes, K. Dreyer, S. Moldovan, O. Ersen, D.D. Hibbitts, Y.J. Chabal, R. Schlögl, J.-P. Tessonnier, Interfacial charge

distributions in carbon-supported palladium catalysts, Nature Communications, 8 (2017) 340.

[39] T. Pillo, R. Zimmermann, P. Steiner, S. Hüfner, The electronic structure of PdO found by photoemission (UPS and XPS) and inverse photoemission (BIS), Journal of Physics: Condensed Matter, 9 (1997) 3987-3999.

[40] F. Cárdenas-Lizana, Y. Hao, M. Crespo-Quesada, I. Yuranov, X. Wang, M.A. Keane, L. Kiwi-Minsker, Selective gas phase hydrogenation of p-chloronitrobenzene over Pd catalysts: Role of the support, ACS Catalysis, 3 (2013) 1386-1396.

[41] L. Jiang, H. Gu, X. Xu, X. Yan, Selective hydrogenation of o-chloronitrobenzene (o-CNB) over supported Pt and Pd catalysts obtained by laser vaporization deposition of bulk metals, Journal of Molecular Catalysis A: Chemical, 310 (2009) 144-149.

[42] A.L. Dantas Ramos, P.d.S. Alves, D.A.G. Aranda, M. Schmal, Characterization of carbon supported palladium catalysts: Inference of electronic and particle size effects using reaction probes, Applied Catalysis A: General, 277 (2004) 71-81.

[43] Y. Wang, Z. Rong, Y. Wang, J. Qu, Ruthenium nanoparticles loaded on functionalized graphene for liquid-phase hydrogenation of fine chemicals: Comparison with carbon nanotube, Journal of Catalysis, 333 (2016) 8-16.

[44] S. He, Z.J. Shao, Y. Shu, Z. Shi, X.M. Cao, Q. Gao, P. Hu, Y. Tang, Enhancing metal-support interactions by molybdenum carbide: An efficient strategy toward the chemoselective hydrogenation of α, β-unsaturated aldehydes, Chemistry - A European Journal, 22 (2016) 5698-5704.

[45] Y. Murata, E. Starodub, B.B. Kappes, C.V. Ciobanu, N.C. Bartelt, K.F. McCarty, S. Kodambaka, Orientation-dependent work function of graphene on Pd(111), Applied Physics Letters, 97 (2010) 143114.

[46] G. Ramos-Sanchez, P.B. Balbuena, Interactions of platinum clusters with a graphite substrate, Physical Chemistry Chemical Physics, 15 (2013) 11950-11959.

[47] K.X. Yao, X. Liu, Z. Li, C.C. Li, H.C. Zeng, Y. Han, Preparation of a Ru-nanoparticles/defective-graphene composite as a highly efficient arene-hydrogenation catalyst, ChemCatChem, 4 (2012) 1938-1942.

[48] X. Zhou, W. Chu, W. Sun, Y. Zhou, Y. Xue, Enhanced interaction of nickel clusters

with pyridinic-N (B) doped graphene using DFT simulation, Computational and Theoretical Chemistry, 1120 (2017) 8-16.

[49]  F. Su, L. Lv, Fang Yin Lee, T. Liu, A.I. Cooper, X.S. Zhao, Thermally reduced ruthenium nanoparticles as a highly active heterogeneous catalyst for hydrogenation of monoaromatics, Journal of American Chemical Society, 129 (2007) 14213-14223.

[50]  K. Tedsree, T. Li, S. Jones, C.W. Chan, K.M. Yu, P.A. Bagot, E.A. Marquis, G.D. Smith, S.C. Tsang, Hydrogen production from formic acid decomposition at room temperature using a Ag-Pd core-shell nanocatalyst, Nature Nanotechnology, 6 (2011) 302-307.

[51]  Q. Lu, X. Chen, D. Liu, C. Wu, M. Liu, H. Li, Y. Zhang, S. Yao, Synergistic electron transfer effect-based signal amplification strategy for the ultrasensitive detection of dopamine, Talanta, 182 (2018) 428-432.

[52]  L. Yang, D. Liu, S. Hao, F. Qu, R. Ge, Y. Ma, G. Du, A.M. Asiri, L. Chen, X. Sun, Topotactic conversion of $\alpha$-$Fe_2O_3$ nanowires into FeP as a superior fluorosensor for nucleic acid detection: Insights from experiment and theory, Analytical Chemistry, 89 (2017) 2191-2195.

[53]  Y. Li, Y. Hu, Y. Zhao, G. Shi, L. Deng, Y. Hou, L. Qu, An electrochemical avenue to green-luminescent graphene quantum dots as potential electron-acceptors for photovoltaics, Advanced Materials, 23 (2011) 776-780.

[54]  G. Liao, S. Chen, X. Quan, H. Yu, H. Zhao, Graphene oxide modified g-$C_3N_4$ hybrid with enhanced photocatalytic capability under visible light irradiation, Journal of Materials Chemistry, 22 (2012) 2721-2726.

[55]  K.P. Loh, Q. Bao, P.K. Ang, J. Yang, The chemistry of graphene, Journal of Materials Chemistry, 20 (2010) 2277-2289.

[56]  R. Tschentscher, T.A. Nijhuis, J.v.d. Schaaf, B.F.M. Kuster, J.C. Schouten, Gas-liquid mass transfer in rotating solid foam reactors, Chemical Engineering Science, 65 (2010) 472-479.

[57]  C. Mu, K. Huang, T. Cheng, H. Wang, H. Yu, F. Peng, Ni foams decorated with carbon nanotubes as catalytic stirrers for aerobic oxidation of cumene, Chemical Engineering Journal, 306 (2016) 806-815.

[58]    C. Pham-Huu, N. Keller, M.J. Ledoux, L.J. Charbonniere, R. Ziessel, Carbon nanofiber supported palladium catalyst for liquid-phase reactions. An active and selective catalyst for hydrogenation of C=C bonds, Chemical Communications, (2000) 1871-1872.

[59]    K. Chizari, I. Janowska, M. Houllé, I. Florea, O. Ersen, T. Romero, P. Bernhardt, M.J. Ledoux, C. Pham-Huu, Tuning of nitrogen-doped carbon nanotubes as catalyst support for liquid-phase reaction, Applied Catalysis A: General, 380 (2010) 72-80.

[60]    Y. Zhao, M. Liu, B. Fan, Y. Chen, W. Lv, N. Lu, R. Li, Pd nanoparticles supported on ZIF-8 as an efficient heterogeneous catalyst for the selective hydrogenation of cinnamaldehyde, Catalysis Communications, 57 (2014) 119-123.

[61]    P.H.Z. Ribeiro, E.Y. Matsubara, J.M. Rosolen, P.M. Donate, R. Gunnella, Palladium decoration of hybrid carbon nanotubes/charcoal composite and its catalytic behavior in the hydrogenation of trans-cinnamaldehyde, Journal of Molecular Catalysis A: Chemical, 410 (2015) 34-40.

[62]    A.S. Nagpure, L. Gurrala, P. Gogoi, S.V. Chilukuri, Hydrogenation of cinnamaldehyde to hydrocinnamaldehyde over Pd nanoparticles deposited on nitrogen-doped mesoporous carbon, RSC Advances, 6 (2016) 44333-44340.

# Chapter 5

**Palladium decorated chemically functionalized macroscopic carbon for selective hydrogenation of cinnamaldehyde**

*Chapter 5*

# Palladium decorated chemically functionalized macroscopic carbon for selective hydrogenation of cinnamaldehyde

*Zhenxin Xu,[a],\* Bing Li,[a] Vasiliki Papaefthimiou,[a] Yuefeng Liu,[b]*

*Spiridon Zafeiratos[a] and Cuong Pham-Huu[a],\**

*(a) Institut de Chimie et Procédés pour l'Energie, l'Environnement et la Santé (ICPEES), ECPM, UMR 7515 du CNRS-Université de Strasbourg, 25 rue Becquerel, 67087 Strasbourg Cedex 02, France*

*(b) Dalian National Laboratory for Clean Energy (DNL), Dalian Institute of Chemical Physics, Chinese Academy of Science, 457 Zhongshan Road, 116023 Dalian, China*

*Corresponding authors:*

*zhenxin.xu@etu.unistra.fr (Zhenxin Xu)*

*cuong.pham-huu@unistra.fr (Cuong Pham-Huu)*

**Abstract**

Structured carbon supports with various surface oxygen and nitrogen functionalities were synthesized using commercial carbon felt and were further employed as supports for Pd nanoparticles (NPs) in liquid-phase hydrogenation of α, β-unsaturated cinnamaldehyde. The surface oxygenated groups, generated previously through vapor acid treatment, play the role of exchange site for the selective introduction of the nitrogen-containing functional groups on the carbon support during amination of the oxidized carbon support. The nitrogen-containing functional groups were converted into nitrogen-doping sites through a high temperature annealing step. The surface functionalized sites can play the roles for anchoring Pd NPs, further improving the hydrogenation activity and stability. Such doping also leads to the polarity change of the catalyst surface, which affect the catalytic activity through the adsorption of reactant. The trend of catalytic selectivity towards hydrocinnamaldehyde was also correlated with the electronic structure of the Pd NPs. Finally, the macroscopic shape of the carbon support enables an easy recovery of the catalyst from the liquid-phase media, hereby providing a strategy to rationally design monolith carbon supported catalysts.

**Keywords:**

# 1. Introduction

Structured carbon materials such as graphite/carbon felt (CF) have been extensively employed as macroscopic scaffolds for the growth of nanocarbons, i.e. carbon nanotubes/nanofibers, which will be further used as metal-free or as catalyst support in the different catalytic processes during the past decades [1, 2]. These hierarchical structured catalysts allow one to develop the extensive use of nanocarbons either as catalyst or catalyst support without their inherent drawbacks, i.e. large pressure drop along the catalyst-packed bed and the costly separation between the powdered catalyst and the product in liquid-solid or gas-liquid-solid catalytic processes. However, due to the low specific surface area (SSA) and inert surface properties pristine commercial CF cannot be efficiently used directly as support in catalysis [3] and is generally associated with nanocarbons, growth from the Chemical Vapor Deposition (CVD) on its surface which contribute to an increase of the SSA of the composite on one hand, and to modify its final surface properties on the other hand [4, 5] for the anchorage of metal active phase nanoparticles. According to the literature reports these hierarchical nanocarbon(s)/CF composites display relatively high catalytic performance compared to other macroscopic catalysts [6, 7]. Such improved catalytic performance could be attributed to the nanoscopic dimension of the outer nanocarbon(s) network, i.e. nanofibers or nanotubes, which provides efficient anchorage of the metal nanoparticles, high effective surface area for the reactant access and rapid desorption of intermediate product [8, 9]. Nonetheless, this composite architecture also displays drawbacks such as energy and time consuming for nanocarbons synthesis process, a large waste release (thermal by-products during the synthesis and post-synthesis purification steps) and last but not least, the final purification to remove the growth catalyst. It is still challenging to develop the structured commercial carbon felt with targeted functions for catalytic applications. Meanwhile, despite existing industrial mass production and low prices [10], CF-based materials are still scarcely developed in the field of catalysis [11-13].

Nowadays, carbon materials, including active carbon, carbon nanotubes/fibers and graphene, can be functionalized with oxygenated groups or doped by introducing heteroatoms (i.e. N, O, S, etc.) into the graphitic matrix [14-16]. Such modification allows the tailoring of

the physicochemical properties of the final materials, such as surface functional groups, defective sites as well as surface reactivity and chemical properties, i.e. electronic alteration or basic/acid strength modification, by introducing heteroatoms doping, which allow them to be efficiently used not only as metal-free catalysts [17-21], but also as catalyst carrier for metal nanoparticles (NPs) [22-24]. As far as the literature reports are concerned, only very scarcely results have been reported for the functionalization and catalytic use of commercial macroscopic carbon/graphite felt. It is expected that such materials which are commercially available could be of high interest for catalysis field application through adequate activation process and can be a potential candidate for replacing traditional nanocarbons/felt composites for the drawbacks mentioned above.

The selective liquid-phase hydrogenation of α, β-unsaturated aldehydes such as cinnamaldehyde (CAD) to α, β-unsaturated alcohols or saturated aldehydes is a practically significant process as it produces useful intermediates for fine chemical industries including pharmaceuticals, food additives and fragrances [25-27]. Recently, hydrocinnamaldehyde (HCAD) was found to be an important intermediate in the synthesis of pharmaceuticals used in the treatment of HIV [28]. The selectivity to the desired product, i.e. C=C or C=O bond hydrogenation, resulted from hydrogenation of cinnamaldehyde is mainly based on the microstructure of the active metal, by improving the dispersion or by adding promoter, as well as the surface chemistry of the support. In general, Pd-based catalysts are of the most used for the selective hydrogenation of the C=C bond to produce HCAD [29, 30]. Although the reduction of the C=C group is favored thermodynamically [31], it is still challenging to achieve exclusive selectivity of unsaturated C=C group to its hydrogenated corresponding over heterogeneous Pd catalyst with hydrogen and the total hydrogenated product is still presence at different concentration depending to the catalyst [32]. Carbonaceous materials are desirable supports for the noble metal catalysts due to their low cost, customized textural and physical properties, along with an easy recycling of the precious metal, which can be carried out simply by combustion of the spent catalyst [33-35]. However, carbon materials without any functionalization usually display weak anchorage properties for noble metal NPs, and thus, the active NPs are prone to sintering during the preparation and reaction, as well as

leaching in liquid-phase reactions, which contribute to the shortening of the catalyst lifetime [36]. In addition, micropores, i.e. activated charcoal, should also be avoided as much as possible as their induced long apparent sojourn time of the intermediate product leading to a degradation of the process selectivity.

In this work, the commercial carbon felt (CF) was stepwise chemically functionalized through the redox process. Firstly, the oxidation treatment with gaseous $HNO_3$ was used to produce oxidized CF (OCF), and then aminated OCF (AOCF) was synthesized by reductive amination of OCF using urea under hydrothermal conditions. After further high temperature annealing under inert atmosphere, the AOCF was transformed into nitrogen-doped CF (NAOCF). For bench-marking process the commercial carbon felt was also tested. The catalysts consisted by depositing palladium nanoparticles (Pd NPs) on the different supports are tested in the liquid-phase hydrogenation of cinnamaldehyde. The results provide evidences that the NAOCF with N-doping and defective surface is the most effective to anchor Pd NPs and keep them dispersed and thus, exhibits a significant improvement of the hydrogenation performance compared to the other catalysts. The Pd/NAOCF catalyst also displays significant improved selectivity for the selective hydrogenation of C=C bond with high stability as a function of cycling tests.

## 2 Results and discussion

### 2.1 Synthesis and characterization of the carbon supports

The specific surface area (SSA) of CF-based samples was raised from 29 $m^2$/g, for the pristine CF, to 300 to > 500 $m^2$/g, for the chemically functionalized ones depending to the pre-oxidation process conditions (Figure 1A). The AOCF sample displays a highest SSA, i.e. 550 $m^2$/g, which further decreases to about 350 $m^2$/g after annealing at high temperature for introducing the nitrogen-doped sites inside the carbon framework. The pore size distribution remains close for the OCF, AOCF and NAOCF samples with a higher pore volume for the AOCF sample which is in good agreement with the high SSA. The large SSA increase after amination process could be explained by the fact that water and $CO_2$ generated during the hydrothermal synthesis could further react with the carbon leading to the consumption of this

later along with the formation of additional pores which contributes to the increase of the sample SSA.

The treatment also induced a weight loss of OCF of about 16% compared with the untreated one (Figure 1C). The main weight loss occurs after the $HNO_3$ treatment according to our previous work [13, 18, 37]. Such weight loss can be attributed to the reaction between the carbon and the oxygen containing reactant which is at the origin of the formation of defects and oxygenated functional groups on the sample with a concomitant increase of the SSA. Additional chemical/thermal treatment of the OCF leads to a marginal weight loss which could be attributed to some oxidation during the hydrothermal or the high temperature annealing process. The introduction of defects and oxygenated functional groups on the OCF sample can be also evidenced according to the Raman results which show an increase of the $I_D/I_G$ ratio from 1.4 to 1.8 for the CF and OCF respectively (Figure 1D). Meanwhile the D' peak of the OCF which is assigned to the disordered graphitic fragments becomes more sharp than that of CF. In addition, the blue shift of G peak in the OCF may be attributed to the O–H bending and C=O stretching generated on the surface of treated sample. The oxidation treatment also increased the atomic percent of surface oxygen elemental on the OCF more than twofold to reach 10.6 at%, compared to 4.4 at% of that on the pristine commercial CF (Table 1) which is in good agreement with the presence of large oxygenated functional groups.
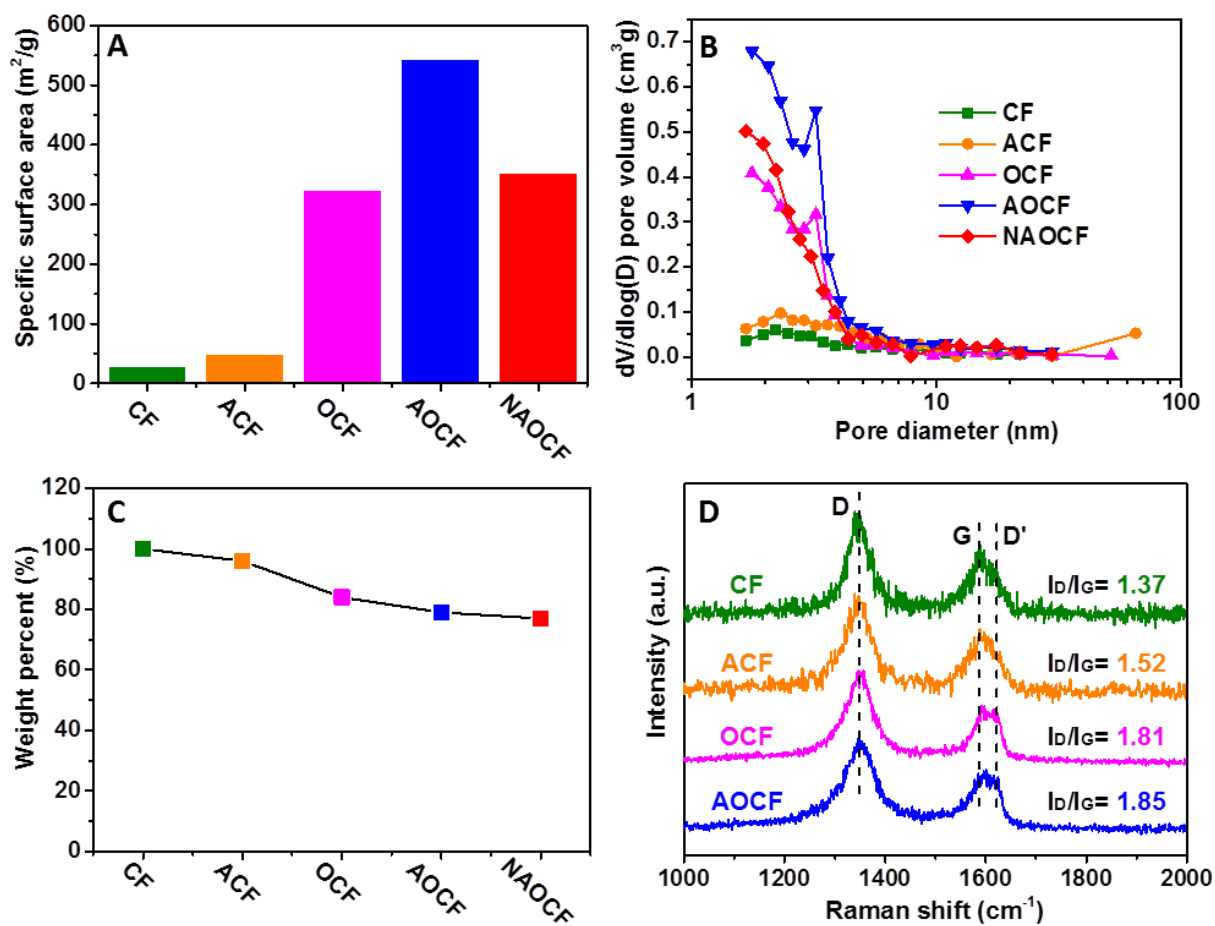
**Figure 1.** (A) Specific surface area, (B) pore size distribution, (C) weight percent loss, and (D) Raman spectra of different carbon-based samples.

The TPD-MS results based on the $CO_2$ (m/z = 44) and CO (m/z = 28) evolution as a function of the temperature on the different carbon samples, i.e. CF, OCF and AOCF, are presented in Figure 2A and B. According to the results a significant amount of oxygen was incorporated in the CF sample after the $HNO_3$ treatment. The TPD-MS spectra of the AOCF sample indicates that a large amount of the oxygenated compounds incorporated during the $HNO_3$ treatment was removed after the amine treatment. It was suggested that during the amination process under hydrothermal conditions, the ammonia derived from the urea hydrolysis was further reacting with the hydroxyl groups present on the OCF surface, such as carboxylic acids, anhydrides, and phenols, leading to the formation of amine groups (-$NH_2$ and -NH-) on the surface of the aminated carbon felt (AOCF) with a concomitant release of

water [38]. The significant exchange of oxygenated functional groups by nitrogen groups is also evidenced by the ATR-FTIR in Figure 2C. The XPS survey spectra in Figure 2D confirm the oxygen incorporation after the $HNO_3$ treatment followed by oxygen-nitrogen exchange during the hydrothermal amination, leading to a significant oxygen loss from the OCF sample.



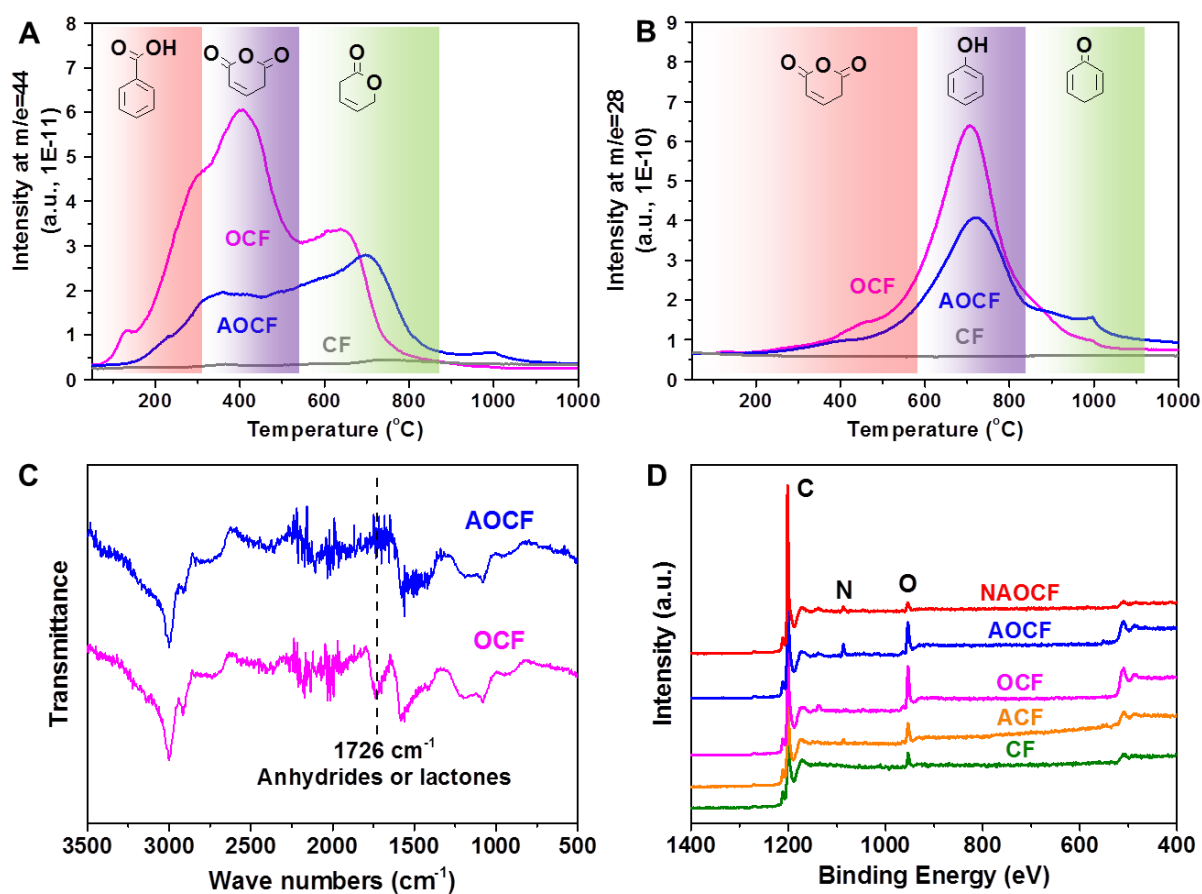**Figure 2.** (A) $CO_2$ (m/z = 44) and (B) CO (m/z = 28) generated during the TPD analysis of the CF, OCF and AOCF, (C) ATR-FTIR spectra of CF and OCF, and (D) XPS survey scan of samples, respectively.

The surface concentration of C, O and N species, determined by semi-quantitative analysis from the XPS survey spectra, is summarized in Table 1 and confirms the results obtained by TPD-MS and ATR-FTIR.

**Table 1.** Elemental analysis of different samples

| Samples | Atom percentage (at%)[a] | | | O/C (%) | N/C (%) |
|---------|:---:|:---:|:---:|:---:|:---:|
| | **C** | **O** | **N** | | |
| CF | 95.6 | 4.4 | - | 4.6 | 0 |
| ACF | 92.8 | 5.5 | 1.7 | 5.9 | 1.8 |
| OCF | 89.4 | 10.6 | - | 11.9 | 0 |
| AOCF | 87.4 | 8.4 | 4.2 | 9.6 | 4.8 |
| NAOCF | 94.8 | 2.1 | 3.1 | 2.2 | 3.3 |

[a] The atom percent of surface element on the samples determined by the XPS survey spectra.

The high resolution and deconvoluted O 1s and N 1s XPS spectra recorded on the different samples are presented in Figure 3 and 4. According to the results presented in Figure 3A to C, the O 1s concentration significantly increases after the different treatments, i.e. ACF and OCF, which could be attributed to the surface corrosion in the presence of oxidant reactants such as water, $CO_2$ and $HNO_3$. XPS analysis (Figure 3C) confirms the presence of a wide variety of oxygen functional groups including C=O, O-C=O and C-O groups formed on the treated sample [39], at a concentration of 36 %, 25 % and 33 %, respectively. Such results indicated that the strong oxidant derived from gaseous $HNO_3$ etched the graphene lattice of carbon felt during the treatment, which created a unique architecture made up of abundant oxygen-containing functional groups with porous structure decorated surface defects (Figure 1B and D) [40]. The samples after nitrogen incorporation through hydrothermal process and after high temperature annealing display a significant loss of the oxygenated groups which could be attributed to reactions with the nitrogen containing species (Figure 3D and E). These results can be clearly observed in the graph of Figure 3F and in Table 2.

**Figure 3.** O 1s high-resolution XPS spectra of (A) CF, (B) ACF, (C) OCF, (D) AOCF, (E) NAOCF, and (F) oxygen-containing functional groups and total oxygen content of the samples determined from the XPS results.

**Table 2.** Oxygen elemental analysis on the different samples

| Samples | $O_{total}/C^a$ (%) | Surface O species/C (%) | | | |
|---------|---------|------|-------|-----|----------------------------------------|
| | | C=O | O-C=O | C-O | Chemisorbed $O_2$ or adsorbed $H_2O$ |
| CF | 4.6 | 0.4 | 2.6 | 1.2 | 0.4 |
| ACF | 5.9 | 1.4 | 1.7 | 2.1 | 0.7 |
| OCF | 11.9 | 4.2 | 3.1 | 3.9 | 0.7 |
| AOCF | 9.6 | 3.2 | 1.8 | 3.5 | 1.1 |
| NAOCF | 2.2 | 1.1 | 0.5 | 0.5 | 0.1 |

[a] The content ratio of surface oxygen to carbon element on the samples determined by the XPS survey spectra.

The nitrogen species are detected on the different samples after amine groups incorporation through hydrothermal step and after annealing process as shown in Figure 4A to C. The AOCF sample displays a highest amine concentration up to 4.8 at. % (Table 1) and is constituted by 70 % primary amine ($-NH_2$) and 30% of secondary amine ($-NH-$) groups [41], respectively (Table 3). The nitrogen content and nitrogen species incorporated in the different samples are presented in Figure 4D and in Table 3.
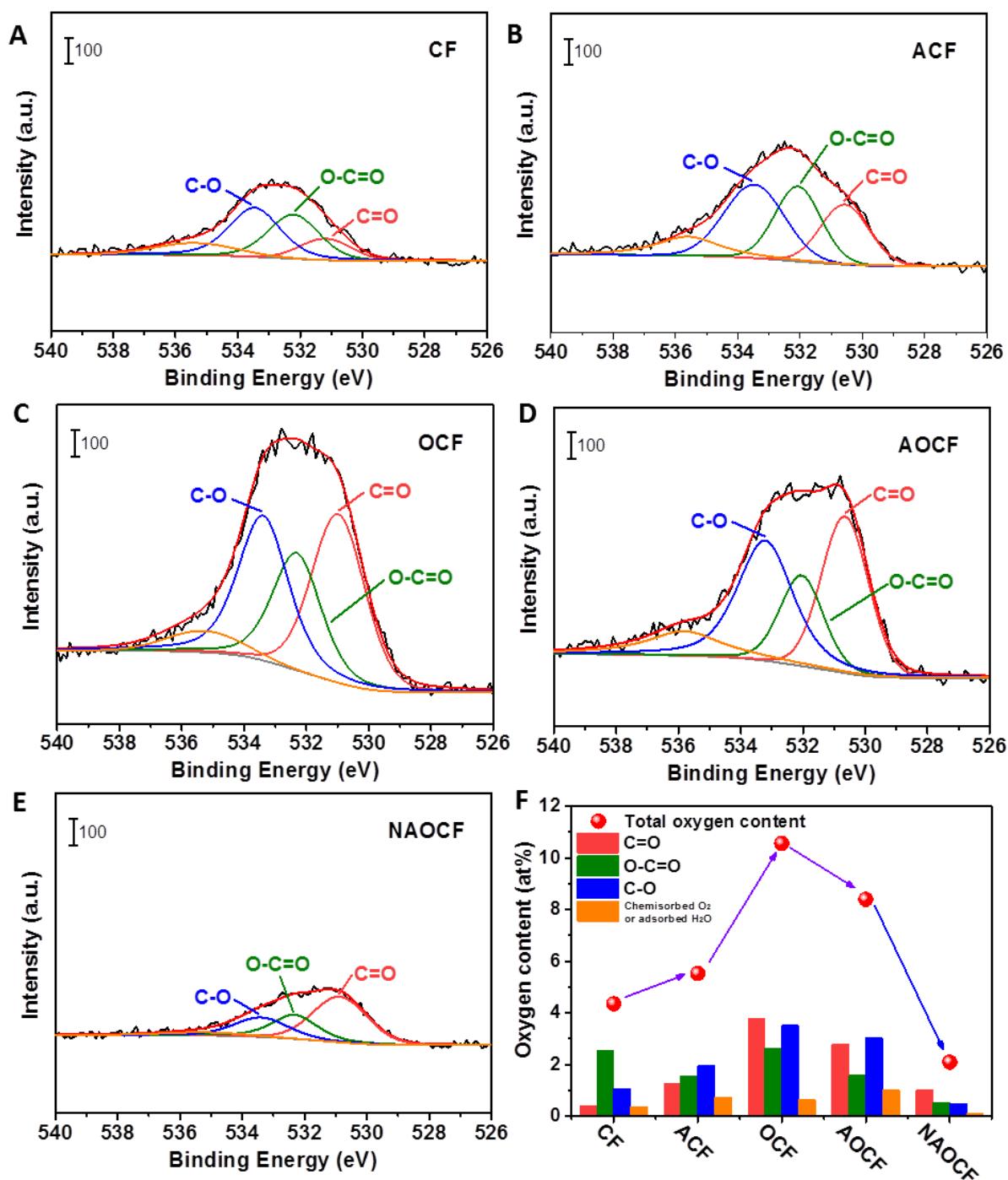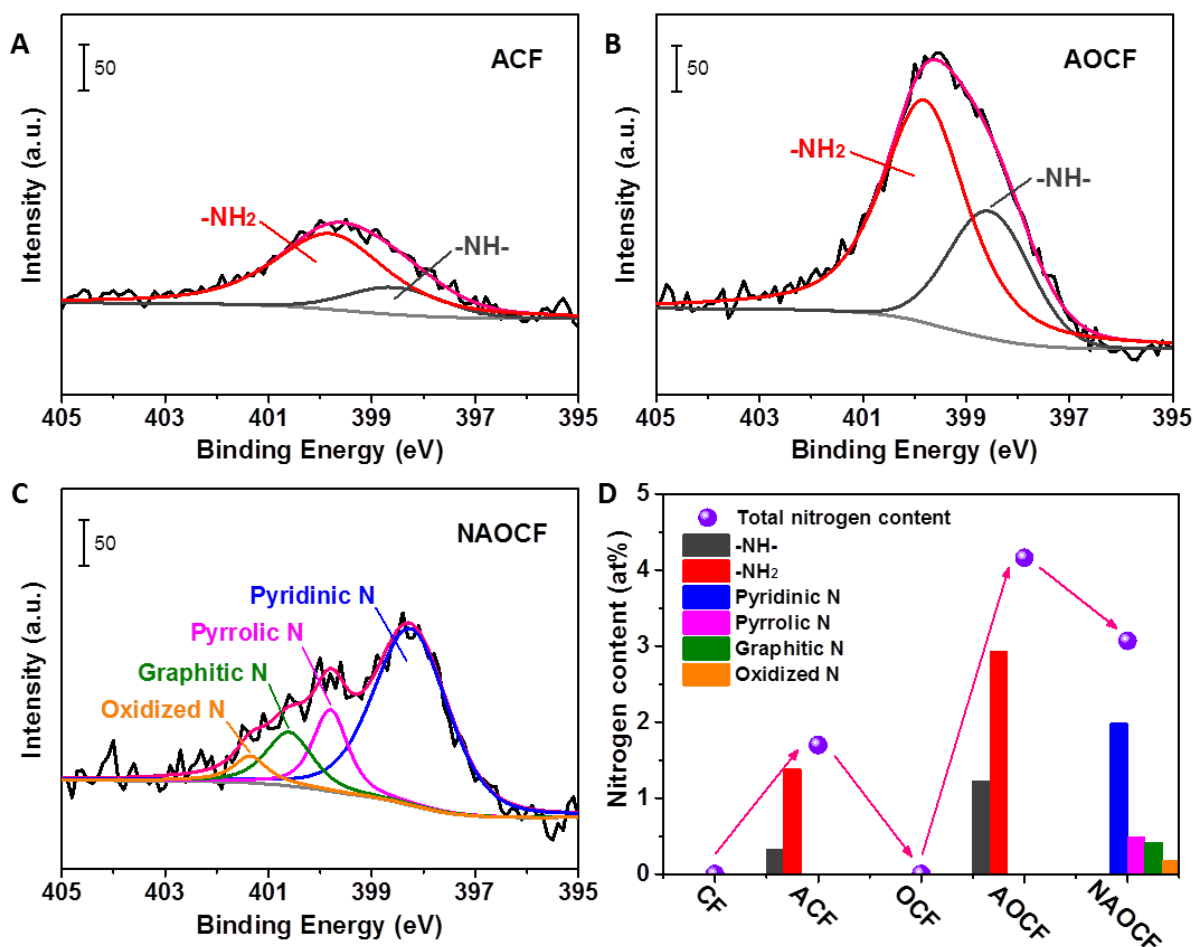
**Figure 4.** N 1s high-resolution XPS spectra of (A) ACF, (B) AOCF, (C) NAOCF, and (D) nitrogen-containing functional groups and total nitrogen content of the samples determined from the XPS results.

Additional thermal treatment under inert atmosphere allows one to convert the amine (-NH$_2$ and -NH-) groups on the AOCF sample into N-doped carbon composite, i.e. NAOCF [42], which contains majority of pyridinic N species, along with few pyrrolic and graphitic N as shown in Figure 4C and in Table 3. After the annealing process to convert the amine functional groups into nitrogen-doped carbon a significant loss of nitrogen was observed as shown in Figure 4D. Such nitrogen loss could be attributed to the decomposition or desorption of the amine groups during the annealing process. As a result of the thermal decomposition of functional groups, the oxygen atom percent of AOCF sample was dropped from 8.4 at% (O/C= 9.6 %) to 2.1 % (O/C = 2.2 %) for the N-doped AOCF (Table 1). The

high-temperature annealing also led to a reduction of the specific surface area of the NAOCF (Figure 1A), which may be resulted from the collapse of the porous channels (Figure 1B).

**Table 3.** Nitrogen elemental analysis on the different samples

| Samples | N at%[a] | Surface N species/$N_{total}$ (%) | | | | | |
|---|---|---|---|---|---|---|---|
| | | -NH$_2$ | -NH- | Pyridinic N | Pyrrolic N | Graphitic N | Oxidized N |
| ACFs | 1.7 | 81.2 | 18.8 | - | - | - | - |
| AOCFs | 4.2 | 70.5 | 29.5 | - | - | - | - |
| NAOCFs | 3.1 | - | - | 64.7 | 16.0 | 13.5 | 5.8 |

[a] The atom percent of surface nitrogen element on the samples determined by the XPS survey spectra.

The oxidative stability of the structured carbon without or with functionalization was studied by TGA (Figure 5). Compared with pristine blank CF, the carbon samples after functionalization display lower oxidative resistance values. On one hand, the evident increment on SSA of functionalized carbon materials provided higher surface contact between reactant gas and the samples [13], which could promote the oxidation process. On the other hand, the large number of different oxygen- or nitrogen-containing functional groups or nitrogen-doped species decorated structural defects, which could be involved as active sites for the dissociative adsorption of O$_2$ [43], would also participated in the combustion reaction of CF samples.
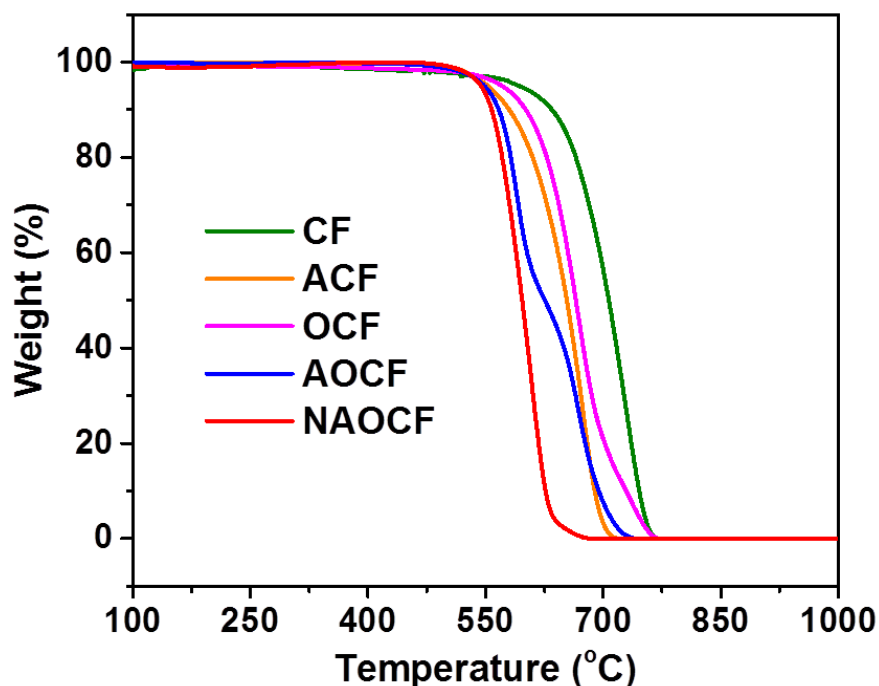
**Figure 5.** TGA profiles of different carbon materials without or with functionalization.

The morphologies of the samples were characterized by SEM and the representative SEM micrographs are presented in Figure 6. According to the SEM results the gross morphology of the functionalized samples remains similar to that of the pristine CF. Such results confirm the complete retention of the hierarchical structure of the CF upon treatment which represents a net advantage for the catalytic application. It is expected that changes, i.e. defects decorated with functional groups and porosity, induced by the different functionalization processes are not accurately evidenced by SEM technique. Combined with previous discussions of activated CF with the porous structures, i.e. mass loss and graphite structural defects, it is suggested that all the chemically functionalizations of carbon felt during the different treatments in this work, including the oxidation, amination and nitrogen-doping, give rise to the variation of carbonaceous framework, which is mainly controlled at the nanoscale.
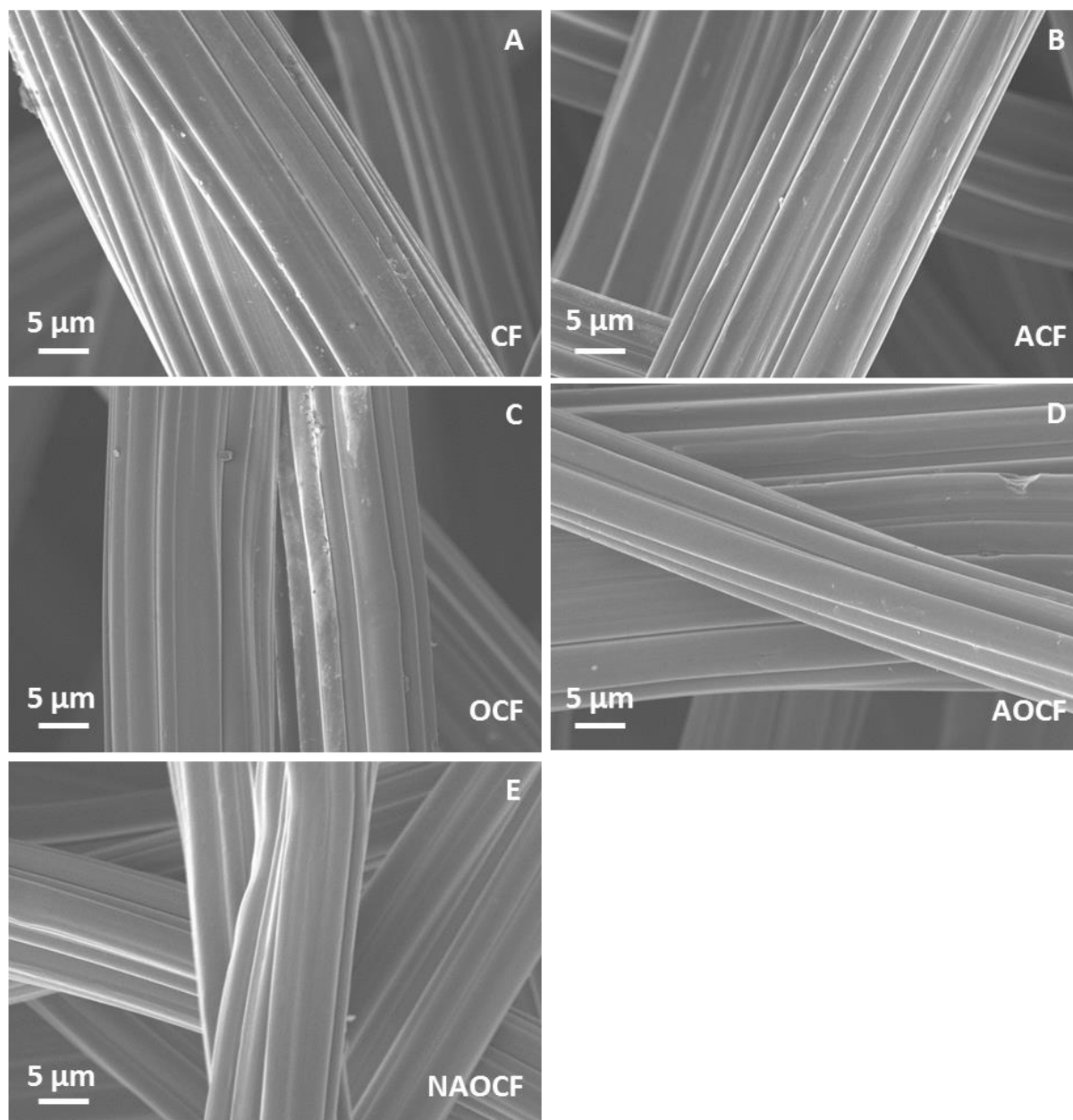
**Figure 6.** SEM micrographs of (A) CF, (B) ACF, (C) OCF, (D) AOCF and (E) NAOCF.

## 2.2 Synthesis and characterization of the catalysts

In the catalysts preparation, the palladium precursor (0.8 mmol/L) in the aqueous solution was reduced at room-temperature in the presence of $NaBH_4$ and directly deposited on the carbon supports. The reduction with subsequence anchorage of active metal onto the support will induce a color change in the supernatant solution. The Pd species seemed to be

easily reduced and anchored on the OCF, AOCF and NAOCF supports as witnessed by the change in color of the solution as shown in Figure 7. On the other hand, reduction seems to occur in the liquid phase despite no or very low Pd anchorage happens with the CF and ACF supports according to the fact that the solution still remains dark brown (Figure 7). The results observed indicate the complete reduction/anchorage of active metal on the OCF, AOCF and NAOCF. The oxygen- and nitrogen-containing as well as structural defects on the carbon supports are expected to play the role of active sites for anchoring metal species, at the same time the porous structure will provide the interface for the interaction between the active metal and carbon support [34]. By comparing the quantity of these anchorage sites and surface area as discussed above, OCF and AOCF as well as NAOCF display high adsorption and stronger metal immobilizing capacity than the pristine CF and ACF, thereby leading to the more Pd loading on the supports. A series of carbon supported Pd catalysts were examined by ICP-AES, the Pd contents of Pd/OCF, Pd/AOC and Pd/NAOCF were as 1.0, 1.1 and 1.1 wt %, respectively, which are far higher than 0.1 wt % Pd for both Pd/CF and Pd/ACF.



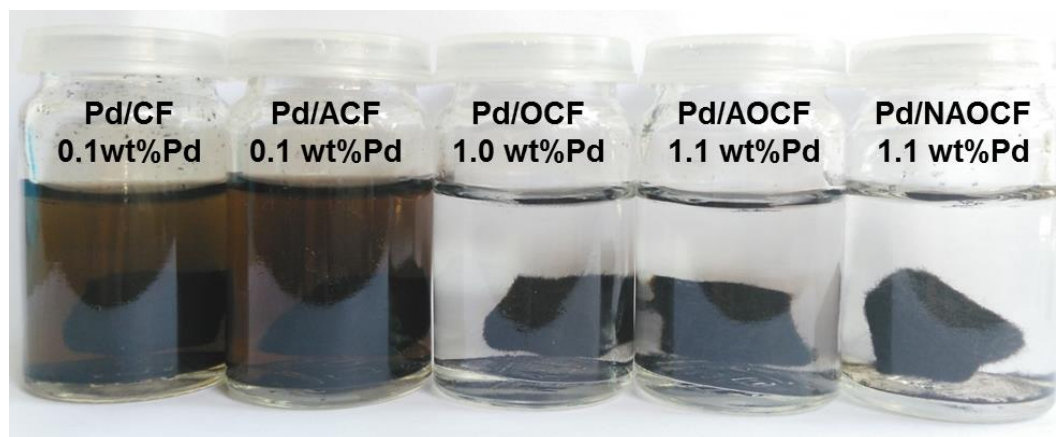**Figure 7.** Digital photos of aqueous palladium solutions with different carbon supports after in situ reduction with $NaBH_4$ at room-temperature, and the corresponding weight percent of the Pd supported on the catalyst (wt% Pd) measured by ICP-AES.

XPS analysis based on the intensity ratio and binding energy shift of Pd 3d (Figure 8 and Table 4) was used to investigate the dispersion of the active metal and the metal-support

interaction on the electronic structure of Pd nanoparticles. As listed in Table 4, although the Pd loading weight of Pd/OCF, Pd/AOCF and Pd/NAOCF is almost identical, there is a significant variation of surface Pd atom percent on these modified CF supports with the following sequence: Pd/NAOCF > Pd/AOCF > Pd/OCF, suggesting the higher dispersion of active metal as well as the smaller particle size on Pd/NAOCF catalyst.

The Pd 3d XPS spectra of the series catalysts (Figure 8A-C) present two main peaks at about 335.2 and 340.5 eV, corresponding to the spin-orbit split doublet of Pd $3d_{5/2}$ and $3d_{3/2}$, respectively. According to the result of the deconvolution of core level Pd $3d_{5/2}$, Pd is observed in the various contributions of electronic state, including the predominant metallic phase ($Pd^0$, 335.1 eV), ionic state metal ($Pd^{2+}$, 337.2 eV) and a satellite peak (338.4 eV) [44-46]. The presence of an additional prominent signal at 335.9 eV was required to fit the spectra in each sample, which is between $Pd^0$ and $Pd^{2+}$. This contribution here is attributed to the electron-deficient metal atoms ($Pd^{\delta+}$), resulting from the electronic interaction between Pd species and the carbon support via a charge transfer. The functional species on the surface of CF support are suggested to have a great influence on the Pd electronic structure with special distribution of metal states. Pd NPs supported on AOCF and NAOCF tends to have more $Pd^{\delta+}$ than that of Pd/OCF sample, indicating that the introduction of nitrogen on CF supports is in favor of forming $Pd^{\delta+}$ species during the reduction process, moreover, the Pd/NAOCF catalyst with nitrogen dopants possesses the highest percent of $Pd^{\delta+}$ phase among three samples.
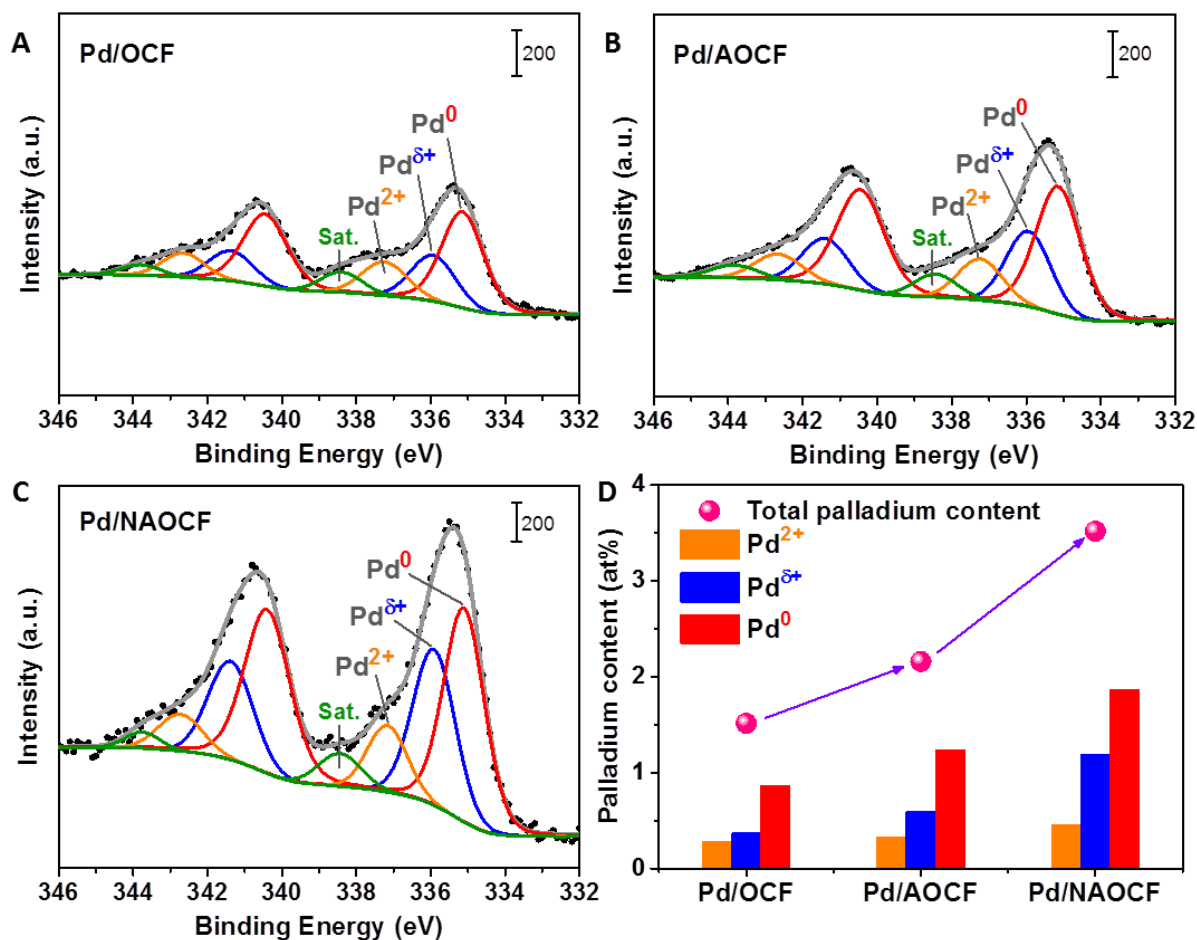
**Figure 8.** Pd 3d high-resolution XPS spectra of (A) Pd/OCF, (B) Pd/AOCF, (C) Pd/NAOCF and (D) Pd species and Pd total content determined from surface XPS analysis.

**Table 4.** Palladium elemental analysis of the samples from the XPS analysis

| Samples | Pd wt%[a] | Pd at%[b] | Surface Pd species/Pd$_{total}$ (%) | | | Pd$^0$/Pd$^{\delta+}$ |
|---|---|---|---|---|---|---|
| | | | Pd$^{2+}$ | Pd$^{\delta+}$ | Pd$^0$ | |
| Pd/OCF | 1.0 | 1.5 | 18.5 | 24.3 | 57.2 | 2.4 |
| Pd/AOCF | 1.1 | 2.2 | 15.3 | 27.3 | 57.4 | 2.1 |
| Pd/NAOCF | 1.1 | 3.5 | 13.0 | 33.9 | 53.1 | 1.6 |

[a] The palladium weight percent of the samples determined by the ICP-AES.

[b] The atom percent of surface palladium element on the samples determined by the XPS survey spectra.

These metal-support interactions are significant because they not only enhance the dispersion of Pd NPs, but also alter the Pd core (3d) electrons and oxidation states, and modify as a consequence the final catalytic performance of the catalysts.

TEM analysis was carried out on three catalysts, i.e. Pd/OCF, Pd/AOCF and Pd/NAOCF, and the results are displayed in Figure 9. According to the TEM results the metal dispersion is relatively high on the different catalysts and the most homogeneous dispersion was observed for the Pd/NAOCF catalyst.
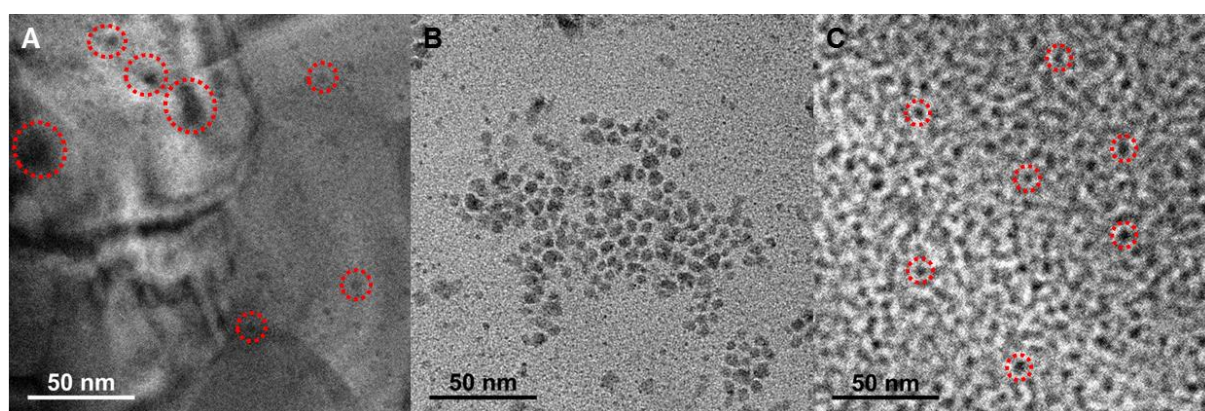


**Figure 9.** TEM micrographs of the Pd/OCF (A), Pd/AOCF (B) and Pd/NAOCF (C) catalysts after reduction and before reaction.

## 2.3 Catalytic performance on the selective hydrogenation of cinnamaldehyde

The liquid-phase hydrogenation of cinnamaldehyde was carried out on the different Pd-based catalysts. The catalytic performance, expressed in terms of CAD and HCAD concentration, mol/L, as a function of time-on-stream (TOS) are presented in Figure 10. The Pd/CF and Pd/ACF display poor hydrogenation activity which could be due to the low Pd loading and also to the poor dispersion. On the other hand, the Pd/NAOCF displays the highest catalytic performance for the hydrogenation of C=C bond in CAD among all the tested catalysts (Figure 10A). The high hydrogenation activity may be ascribed to the high dispersion of Pd NPs on NAOCF support, confirmed by XPS and TEM analysis (Table 4 and Figure 9), which provide more exposure of active sites for the reaction [37]. The Pd/OCF and

Pd/AOCF catalysts display intermediate hydrogenation activity compared to the Pd/NAOCF, Pd/CF and Pd/ACF catalysts. Although the surface atom percentages of Pd on both Pd/AOCF and Pd/NAOCF are higher, i.e. more metal exposure sites, than that of Pd/OCF, the Pd/AOCF displays a slightly lower hydrogenation activity than the Pd/OCF and much lower compared to the Pd/NAOCF. A possible explanation of these results could be attributed to the influence of support effect via the adsorption of CAD on the carbon surface [47]. In the case of Pd/OCF the introduction of abundant oxygenated groups on the CF defective surface after the oxidation treatment increases the polarity on the surface of carbon support which could play an effective role for the anchorage of the reactant [48]. However, as shown in Figure 11, the polar carbon surface is not effective for CAD adsorption via the phenyl ring directly on the catalyst support, and then the periphery of metal NPs that are in direct contact with the support cannot effectively participate in the reaction, thereby decreasing the hydrogenation activity [49, 50]. For the Pd/AOCF an increase of surface polarity is expected due to the presence of both oxygen and nitrogen functional groups on the surface after oxidation and amination process (Table 1). Such increase of the support surface polarity leads to the same problem of reactant adsorption as discussed above for the Pd/OCF catalyst.
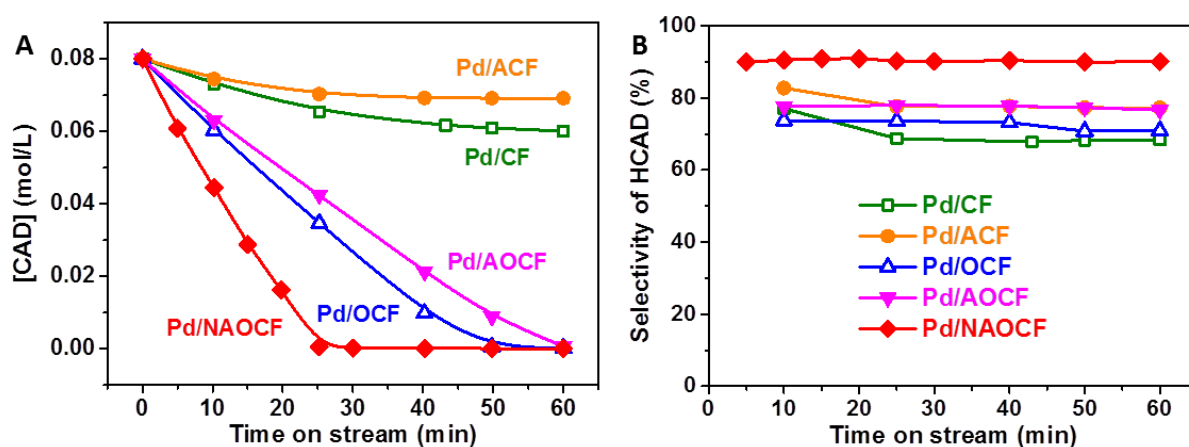


**Figure 10.** (A) Cinnamaldehyde conversion expressed in terms of CAD concentration and (B) C=C bond hydrogenation (HCAD) selectivity as a function of the time on stream on Pd/CF, Pd/ACF, Pd/OCF, Pd/AOCF and Pd/NAOCF catalysts, respectively. Conditions: 80 $^{\circ}$C, 25 mL/min H$_2$, 1 atm, 300 rpm and 0.08 mol/L of CAD.
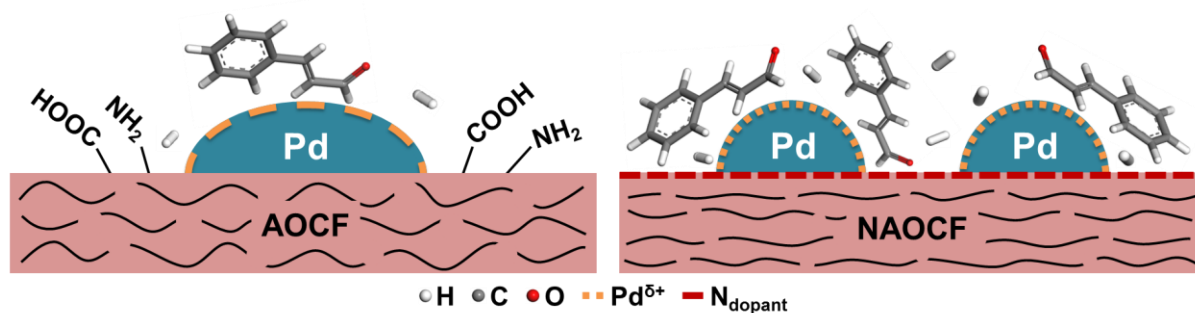
**Figure 11.** Schematic representation of CAD adsorption on the different Pd-based catalysts surface which could explain the enhanced activity of the Pd/NAOCF catalyst with nonpolar support surface.

On the Pd/ NAOCF catalyst a net change on the support polarity was expected after the annealing process at 900 $^{o}$C. During the annealing process the support surface is converted from polar to nonpolar one consecutively due to the removal of the surface oxygenated groups as well as the transformation of the surface nitrogen-containing functional groups into N-dopants within the graphite basal plane. This change in polarity of carbon support promotes the adsorption of the reactant, together with the high dispersion of active metal, resulting in the high hydrogenation performance of the Pd/NAOCF.

The Pd/NAOCF catalyst also displays a highest selectivity towards HCAD, i.e. C=C bond hydrogenation, compared to the other catalysts (Figure 10B). Such high C=C bond selectivity could be explained again by the combination of support surface polarity and metal active phase dispersion.

In batch reaction the intrinsic selectivity could be gradually decreased as increasing the total conversion due to the secondary reactions and thus, it is of interest to compare such selectivity at both low and high conversion. The selectivity to HCAD at 10% of CAD conversion on the different catalysts is shown in Figure 12. The Pd/NAOCF displays the highest selectivity towards HCAD at around 91 % among three samples while Pd/OCF displays the lowest one at 74 %. It was reported that the polarity of carbon support influences not only the reaction activity as discussed above, but also the hydrogenation selectivity on the

Pt/CNF [50]. The less polar catalyst surface enhanced the CAD adsorption via the phenyl ring on the carbon support, meanwhile the reactant might direct the C=O bond towards the periphery of Pt NPs leading to an increase in selectivity of CAL. It is clear that this explanation with Pt cannot directly be used in this work due to the difference in terms of active metal nature, i.e. Pd versus Pt. Indeed, Pd is more prone to catalyze the C=C bond hydrogenation and as expected there is no CAL, issued from the C=O bond hydrogenation, produced on all the tested catalysts in the present work. Furthermore, hydrogenation of CAD is suggested to be a structure-sensitive reaction in terms of selectivity. In previous studies, density functional theory (DFT) calculations confirmed that the smaller Pd NPs (represented by $Pd_4$ nanocluster) favor the C=C-centered adsorption on the metal surface, while the larger ones (represented by Pd(111) surface) were more conducive to the C=O-centered adsorption [51]. On the other hand, the aromatic rings could be repelled by the flat metal surface, on large metal particle, with a distance exceeding 0.3 nm owning to the energy barrier to the surface, in that way hampering the C=C bond to approach the metal surface [52]. Consistent with these explanations, the adsorption of C=C bond would be more beneficial on the smaller Pd particles of Pd/NAOCF thereby giving a higher selectivity to HCAD. However, real catalysts are seldom pure metallic surfaces but rather metal NPs dispersed on different supports. The structure of the active metal affected by the interaction with the support, especially electronic structure [53, 54], should be taken into account in the interpretation for the selectivity obtained in those cases. The correlations between electronic structure and selectivity to HCAD were established on different catalysts as shown in Figure 12. The carbon supported Pd catalyst with low $Pd^0/Pd^{\delta+}$ atomic ratio displays a high HCAD selectivity. It is demonstrated that the selective hydrogenation of CAD towards C=C or C=O bond is determined by the position of the *d* band center of the active metal. Metals with a *d* band center far from the Fermi level (e.g., Pt) are selective for C=O bond hydrogenation towards CAL, while Pd is more selective at C=C bond hydrogenation towards HCAD [55]. Furthermore, the high intensity of electron depleted $Pd^{\delta+}$ within the metal active phase from electronic metal-support interaction (EMSI), would bring about the up-shift of its *d* band center, thus increasing the hydrogenation selectivity of HCAD [56].
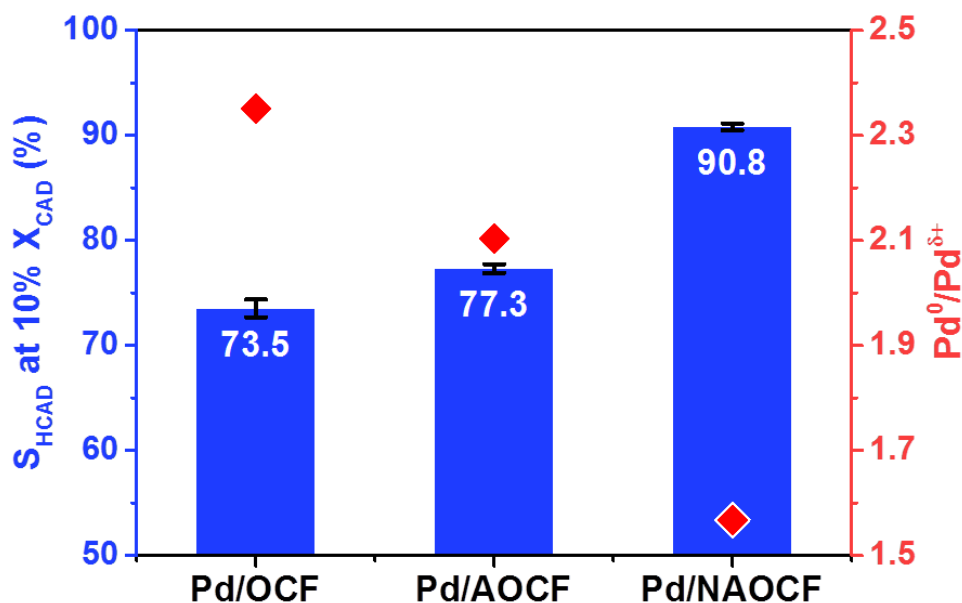
**Figure 12.** Effect of carbon supports on catalytic performance (the selectivity to HCAD at 10% CAD conversion, the values correspond to the average selectivity calculated for three independent experiments $\pm$ the corresponding standard deviation) and electronic structure of palladium (the peak ratio of $Pd^0$ to $Pd^{\delta+}$ determined by the Pd 3d XPS spectra,), respectively.

For liquid-phase process the major advantages of a heterogeneous catalyst are its stability under reaction conditions as well as easy recovery from reaction media compared to the homogeneous catalyst. The cycling tests of Pd/OCF, Pd/AOCF and Pd/NAOCF were conducted under the same conditions, and the catalytic stability of all three samples was investigated whether at low or high conversion as shown in Figure 13. During the four successive runs, the selectivity of HCAD on Pd/NAOCF still remains around 91% at both low and high conversion. While Pd/OCF and Pd/AOCF suffer from a decrease in HCAD selectivity at high conversion compared with low conversion, implying the distinctive structure of metal active phase against the occurrence of side reaction on Pd/NAOCF. The catalysts after the cycling tests were examined by ICP-AES in order to rule out any problem of metal leaching during the tests. The results indicated that the Pd content of the spent samples was between 1.0 and 1.1 wt % and remains close to the initial Pd content on the different catalysts (Table 4), indicating the existence of a strong anchoring effect derived from strong metal-support interaction (SMSI) provided by the different functionalized carbon

supports for the anchorage of the Pd NPs [57]. In addition, the macroscopic shape of these catalysts (Figure 7) allows one to easily perform the catalyst recovery from the liquid-phase medium without catalyst loss during the filtration and recovery process as encountered with the powdery catalysts.
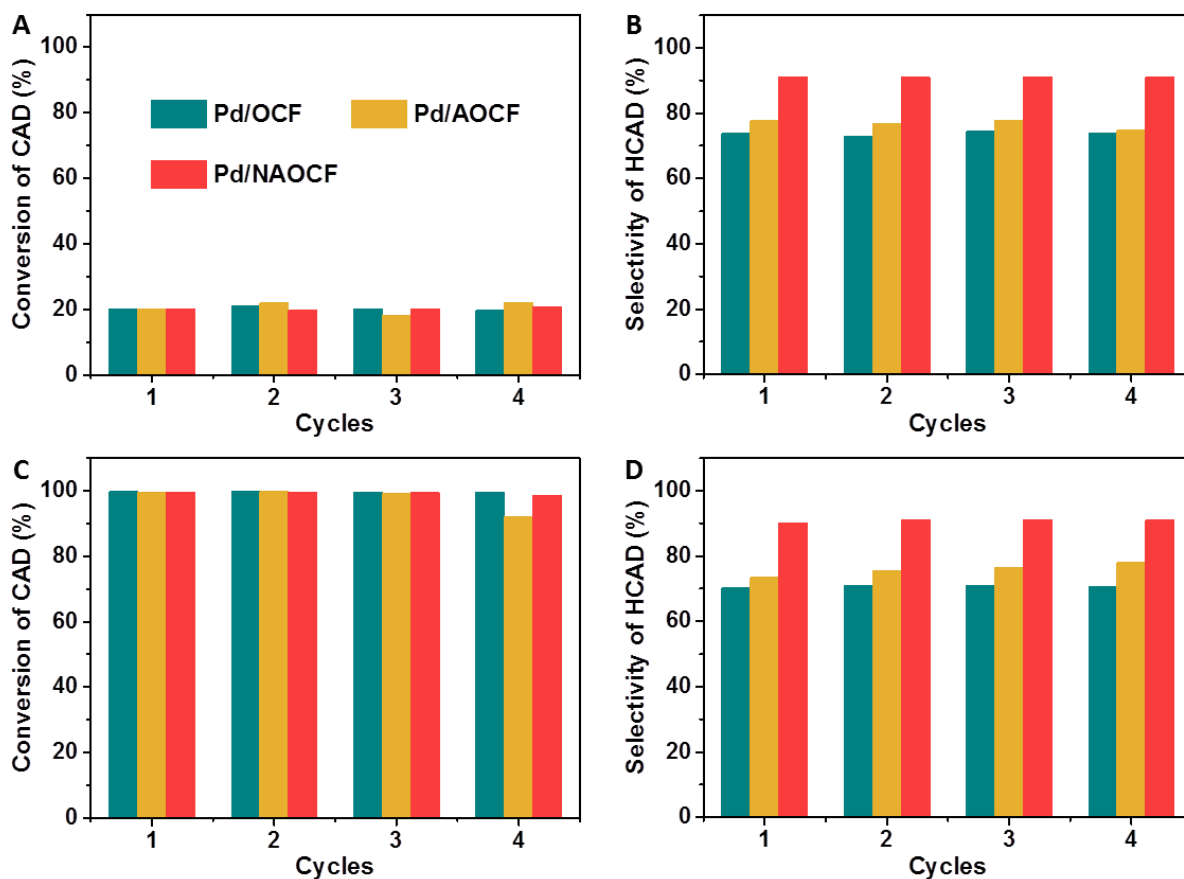


**Figure 13.** Cinnamaldehyde conversion and C=C bond hydrogenation selectivity as a function of the cycling tests at (A, B) low and (C, D) high conversion on Pd/OCF, Pd/AOCF and Pd/NAOCF catalysts, respectively. Conditions: 80 $^{\circ}$C, 25 mL/min H$_2$, 1 atm, 300 rpm and 0.08 mol/L of CAD.

## 3. Conclusions

In summary, a series of surface-modified commercial macroscopic shape carbon felt were developed by the interlocking treatments including the oxidation, amination and nitrogen-doping through thermal annealing process. The introduction of abundant oxygenated groups by gaseous $HNO_3$ treatment, i.e. OCF, facilitates the O↔N surface exchange during the amination using urea hydrothermal process and thus, leads to the formation of surface containing nitrogen species, i.e. AOCF. The surface amino groups on the AOCF were further converted into nitrogen-dopants directly in the graphite framework, i.e. NAOCF, after thermal annealing step. These supports present high interaction with the palladium salt leading to the formation of small and homogeneous palladium nanoparticles which display high catalytic performance for the liquid-phase hydrogenation of cinnamaldehyde. However, it is worthy to note that the less polar carbon support surface, i.e. NAOCF, further improved the catalytic activity of the supported Pd NPs. It was proven that the nitrogen functionalities could induce the higher dispersion of active metal phase with lower electron density than the oxygen functionalities, via the electronic interaction between metal and support. The Pd NPs with unique electronic structure with high $Pd^{\delta+}$ content in the Pd/NAOCF displayed a superior chemoselectivity hydrogenation toward hydrocinnamaldehyde. The macroscopic shaping of the catalysts provides an easy way for operating the catalysts recovery unlikely to the powdered ones where tedious filtration was necessary. The methodology presented in this work provides a new route for the rational design of structured catalysts through surface functionalization and thus enhancing the catalytic hydrogenation performance and improve the catalyst recovery. It is expected that such macroscopic and structured supports can also be effectively used for hosting other metal nanoparticles which can be used not only for liquid-phase but also for gas-phase catalytic processes, especially for exothermic reactions, where high accessibility and thermal conductive entangled support are of high interest.

**Acknowledgements**

# References

[1]     M.J. Ledoux, R. Vieira, C. Pham-Huu, N. Keller, New catalytic phenomena on nanostructured (fibers and tubes) catalysts, Journal of Catalysis, 216 (2003) 333-342.

[2]     D.S. Su, S. Perathoner, G. Centi, Nanocarbons for the development of advanced catalysts, Chemical Reviews, 113 (2013) 5782-5816.

[3]     T.X. Huong Le, M. Bechelany, M. Cretin, Carbon felt based-electrodes for energy and environmental applications: A review, Carbon, 122 (2017) 564-591.

[4]     R. Vieira, M.J. Ledoux, C. Pham-Huu, Synthesis and characterisation of carbon nanofibres with macroscopic shaping formed by catalytic decomposition of $C_2H_6/H_2$ over nickel catalyst, Applied Catalysis A: General, 274 (2004) 1-8.

[5]     Y. Shen, L. Li, K. Xiao, J. Xi, Constructing three-dimensional hierarchical architectures by integrating carbon nanofibers into graphite felts for water purification, ACS Sustainable Chemistry & Engineering, 4 (2016) 2351-2358.

[6]     R. Vieira, C. Pham-Huu, N. Keller, M.J. Ledoux, New carbon nanofiber/graphite felt composite for use as a catalyst support for hydrazine catalytic decomposition, Chemical Communications, (2002) 954-955.

[7]     J.J. Delgado, D.S. Su, G. Rebmann, N. Keller, A. Gajovic, R. Schlogl, Immobilized carbon nanofibers as industrial catalyst for ODH reactions, Journal of Catalysis, 244 (2006) 126-129.

[8]     L. Truong-Phuoc, T. Truong-Huu, L. Nguyen-Dinh, W. Baaziz, T. Romero, D. Edouard, D. Begin, I. Janowska, C. Pham-Huu, Silicon carbide foam decorated with carbon nanofibers as catalytic stirrer in liquid-phase hydrogenation reactions, Applied Catalysis A: General, 469 (2014) 81-88.

[9]     Y. Liu, J. Luo, M. Girleanu, O. Ersen, C. Pham-Huu, C. Meny, Efficient hierarchically structured composites containing cobalt catalyst for clean synthetic fuel production from Fischer-Tropsch synthesis, Journal of Catalysis, 318 (2014) 179-192.

[10]    E. Frank, L.M. Steudle, D. Ingildeev, J.M. Spörl, M.R. Buchmeiser, Carbon fibers: Precursor systems, processing, structure, and properties, Angewandte Chemie

International Edition, 53 (2014) 5262-5298.

[11]    Z. Zhang, J. Xi, H. Zhou, X. Qiu, KOH etched graphite felt with improved wettability and activity for vanadium flow batteries, Electrochimica Acta, 218 (2016) 15-23.

[12]    Z. He, Y. Jiang, W. Meng, F. Jiang, H. Zhou, Y. Li, J. Zhu, L. Wang, L. Dai, HF/$H_2O_2$ treated graphite felt as the positive electrode for vanadium redox flow battery, Applied Surface Science, 423 (2017) 111-118.

[13]    Z. Xu, C. Duong-Viet, H. Ba, B. Li, T. Truong-Huu, L. Nguyen-Dinh, C. Pham-Huu, Gaseous nitric acid activated graphite felts as hierarchical metal-free catalyst for selective oxidation of $H_2S$, Catalysts, 8 (2018) 145-162.

[14]    J.L. Figueiredo, M.F.R. Pereira, The role of surface chemistry in catalysis with carbons, Catalysis Today, 150 (2010) 2-7.

[15]    W. Qi, W. Liu, X. Guo, R. Schlogl, D.S. Su, Oxidative dehydrogenation on nanocarbon: Intrinsic catalytic activity and structure-function relationships, Angewandte Chemie International Edition, 54 (2015) 13682-13685.

[16]    S. Yang, L. Zhi, K. Tang, X. Feng, J. Maier, K. Müllen, Efficient synthesis of heteroatom (N or S)-doped graphene based on ultrathin graphene oxide-porous silica sheets for oxygen reduction reactions, Advanced Functional Materials, 22 (2012) 3634-3640.

[17]    R. Huang, J. Xu, J. Wang, X. Sun, W. Qi, C. Liang, D.S. Su, Oxygen breaks into carbon nanotubes and abstracts hydrogen from propane, Carbon, 96 (2016) 631-640.

[18]    C. Duong-Viet, Y. Liu, H. Ba, L. Truong-Phuoc, W. Baaziz, L. Nguyen-Dinh, J.-M. Nhut, C. Pham-Huu, Carbon nanotubes containing oxygenated decorating defects as metal-free catalyst for selective oxidation of $H_2S$, Applied Catalysis B: Environmental, 191 (2016) 29-41.

[19]    C. Tang, H.F. Wang, X. Chen, B.Q. Li, T.Z. Hou, B. Zhang, Q. Zhang, M.M. Titirici, F. Wei, Topological defects in metal-free nanocarbon for oxygen electrocatalysis, Advanced Materials, 28 (2016) 6845-6851.

[20]    G. Tuci, C. Zafferoni, P. D'Ambrosio, S. Caporali, M. Ceppatelli, A. Rossin, T. Tsoufis, M. Innocenti, G. Giambastiani, Tailoring carbon nanotube N-dopants while designing metal-free electrocatalysts for the oxygen reduction reaction in alkaline

medium, ACS Catalysis, 3 (2013) 2108-2111.

[21]     L. Dai, Y. Xue, L. Qu, H.J. Choi, J.B. Baek, Metal-free catalysts for oxygen reduction reaction, Chemical Reviews, 115 (2015) 4823-4892.

[22]     W. Shi, B. Zhang, Y. Lin, Q. Wang, Q. Zhang, D.S. Su, Enhanced chemoselective hydrogenation through tuning the interaction between Pt nanoparticles and carbon supports: Insights from identical location transmission electron microscopy and X-ray photoelectron spectroscopy, ACS Catalysis, 6 (2016) 7844-7854.

[23]     J. Luo, H. Wei, Y. Liu, D. Zhang, B. Zhang, W. Chu, C. Pham-Huu, D.S. Su, Oxygenated group and structural defect enriched carbon nanotubes for immobilizing gold nanoparticles, Chemical Communications, 53 (2017) 12750-12753.

[24]     D. Higgins, M.A. Hoque, M.H. Seo, R. Wang, F. Hassan, J.-Y. Choi, M. Pritzker, A. Yu, J. Zhang, Z. Chen, Development and simulation of sulfur-doped graphene supported platinum with exemplary stability and activity towards oxygen reduction, Advanced Functional Materials, 24 (2014) 4325-4336.

[25]     S. Cattaneo, S.J. Freakley, D.J. Morgan, M. Sankar, N. Dimitratos, G.J. Hutchings, Cinnamaldehyde hydrogenation using Au-Pd catalysts prepared by sol immobilisation, Catalysis Science & Technology, 8 (2018) 1677–1685.

[26]     D. Wang, Y. Zhu, C. Tian, L. Wang, W. Zhou, Y. Dong, Q. Han, Y. Liu, F. Yuan, H. Fu, Synergistic effect of $Mo_2N$ and Pt for promoted selective hydrogenation of cinnamaldehyde over Pt-$Mo_2$N/SBA-15, Catalysis Science & Technology, 6 (2016) 2403-2412.

[27]     Z. Tian, C. Liu, Q. Li, J. Hou, Y. Li, S. Ai, Nitrogen- and oxygen-functionalized carbon nanotubes supported Pt-based catalyst for the selective hydrogenation of cinnamaldehyde, Applied Catalysis A: General, 506 (2015) 134-142.

[28]     A.J. Muller, J.S. Bowers, Jr., J.R.I. Eubanks, C.C. Geiger, J.G. Santobianco, Processes for preparing hydrocinnamic acid, WO Patent Appl. No. WO 99/08989, (1999) First Chemical Corporation.

[29]     C. Pham-Huu, N. Keller, M.J. Ledoux, L.J. Charbonniere, R. Ziessel, Carbon nanofiber supported palladium catalyst for liquid-phase reactions. An active and selective catalyst for hydrogenation of C=C bonds, Chemical Communications, (2000)

1871-1872.

[30]  R. Li, W. Yao, Y. Jin, W. Jia, X. Chen, J. Chen, J. Zheng, Y. Hu, D. Han, J. Zhao, Selective hydrogenation of the C=C bond in cinnamaldehyde over an ultra-small Pd-Ag alloy catalyst, Chemical Engineering Journal, 351 (2018) 995–1005.

[31]  M. Zhao, K. Yuan, Y. Wang, G. Li, J. Guo, L. Gu, W. Hu, H. Zhao, Z. Tang, Metal-organic frameworks as selectivity regulators for hydrogenation reactions, Nature, 539 (2016) 76-80.

[32]  D. Wang, Y. Zhu, C. Tian, L. Wang, W. Zhou, Y. Dong, H. Yan, H. Fu, Synergistic effect of tungsten nitride and palladium for the selective hydrogenation of cinnamaldehyde at the C=C bond, ChemCatChem, 8 (2016) 1718-1726.

[33]  I. Janowska, G. Wine, M.J. Ledoux, C. Pham-Huu, Structured silica reactor with aligned carbon nanotubes as catalyst support for liquid-phase reaction, Journal of Molecular Catalysis A: Chemical, 267 (2007) 92–97.

[34]  J.L. Figueiredo, Functionalization of porous carbons for catalytic applications, Journal of Materials Chemistry A, 1 (2013) 9351-9364.

[35]  W. Shi, K.-H. Wu, J. Xu, Q. Zhang, B. Zhang, D.S. Su, Enhanced stability of immobilized platinum nanoparticles through nitrogen heteroatoms on doped carbon supports, Chemistry of Materials, 29 (2017) 8670-8678.

[36]  D. Tang, X. Sun, D. Zhao, J. Zhu, W. Zhang, X. Xu, Z. Zhao, Nitrogen-doped carbon xerogels supporting palladium nanoparticles for selective hydrogenation reactions: The role of pyridine nitrogen species, ChemCatChem, 10 (2018) 1291-1299.

[37]  Z. Xu, C. Duong-Viet, Y. Liu, W. Baaziz, B. Li, L. Nguyen-Dinh, O. Ersen, C. Pham-Huu, Macroscopic graphite felt containing palladium catalyst for liquid-phase hydrogenation of cinnamaldehyde, Applied Catalysis B: Environmental, 244 (2019) 128–139.

[38]  H. Aguilar-Bolados, D. Vargas-Astudillo, M. Yazdani-Pedram, G. Acosta-Villavicencio, P. Fuentealba, A. Contreras-Cid, R. Verdejo, M.A. López-Manchado, Facile and scalable one-step method for amination of graphene using Leuckart reaction, Chemistry of Materials, 29 (2017) 6698-6705.

[39]  W. Qi, W. Liu, B. Zhang, X. Gu, X. Guo, D.S. Su, Oxidative dehydrogenation on

nanocarbon: Identification and quantification of active sites by chemical titration, Angewandte Chemie International Edition, 52 (2013) 14224-14228.

[40] J. Luo, Y. Liu, H. Wei, B. Wang, K.-H. Wu, B. Zhang, D.S. Su, A green and economical vapor-assisted ozone treatment process for surface functionalization of carbon nanotubes, Green Chemistry, 19 (2017) 1052-1062.

[41] H. Jing, S. Ren, Y. Shi, X. Song, Y. Yang, Y. Guo, Y. An, C. Hao, Ozonization, amination and photoreduction of graphene oxide for triiodide reduction reaction: An experimental and theoretical study, Electrochimica Acta, 226 (2017) 10-17.

[42] Y. Liu, C. Duong-Viet, J. Luo, A. Hébraud, G. Schlatter, O. Ersen, J.-M. Nhut, C. Pham-Huu, One-pot synthesis of a nitrogen-doped carbon composite by electrospinning as a metal-free catalyst for oxidation of $H_2S$ to sulfur, ChemCatChem, 7 (2015) 2957-2964.

[43] K. Gong, F. Du, Z. Xia, M. Durstock, L. Dai, Nitrogen-doped carbon nanotube arrays with high electrocatalytic activity for oxygen reduction, Science, 323 (2009) 760-764.

[44] R. Arrigo, M.E. Schuster, S. Abate, G. Giorgianni, G. Centi, S. Perathoner, S. Wrabetz, V. Pfeifer, M. Antonietti, R. Schlögl, Pd supported on carbon nitride boosts the direct hydrogen peroxide synthesis, ACS Catalysis, 6 (2016) 6959-6966.

[45] T. Pilloy, R. Zimmermann, P. Steiner, S. Hufner, The electronic structure of PdO found by photoemission (UPS and XPS) and inverse photoemission (BIS), Journal of Physics: Condensed Matter, 9 (1997) 3987-3999.

[46] F. Cárdenas-Lizana, Y. Hao, M. Crespo-Quesada, I. Yuranov, X. Wang, M.A. Keane, L. Kiwi-Minsker, Selective gas phase hydrogenation of p-chloronitrobenzene over Pd catalysts: Role of the support, ACS Catalysis, 3 (2013) 1386-1396.

[47] M.L. Toebes, A. Jos van Dillen, Y. Zhang, J. Hájek, D.Y. Murzin, T.A. Nijhuis, D.C. Koningsberger, J.H. Bitter, K.P. de Jong, Support effects in the hydrogenation of cinnamaldehyde over carbon nanofiber-supported platinum catalysts: Characterization and catalysis, Journal of Catalysis, 226 (2004) 215-225.

[48] M.L. Toebes, F.F. Prinsloo, A. Jos van Dillen, J.H. Bitter, K.P. de Jong, Influence of oxygen-containing surface groups on the activity and selectivity of carbon nanofiber-supported ruthenium catalysts in the hydrogenation of cinnamaldehyde,

Journal of Catalysis, 214 (2003) 78-87.

[49] M.L. Toebes, T. Alexander Nijhuis, J. Hájek, J.H. Bitter, A. Jos van Dillen, D.Y. Murzin, K.P. de Jong, Support effects in hydrogenation of cinnamaldehyde over carbon nanofiber-supported platinum catalysts: Kinetic modeling, Chemical Engineering Science, 60 (2005) 5682-5695.

[50] A.J. Plomp, H. Vuori, A.O.I. Krause, K.P. de Jong, J.H. Bitter, Particle size effects for carbon nanofiber supported platinum and ruthenium catalysts for the selective hydrogenation of cinnamaldehyde, Applied Catalysis A: General, 351 (2008) 9-15.

[51] F. Jiang, J. Cai, B. Liu, Y. Xu, X. Liu, Particle size effects in the selective hydrogenation of cinnamaldehyde over supported palladium catalysts, RSC Advances, 6 (2016) 75541–75551.

[52] A. Giroir-Fendler, D. Richard, P. Gallezot, Chemioselectivity in the catalytic hydrogenation of cinnamaldehyde. Effect of metal particle morphology, Catalysis letters, 5 (1990) 175-182.

[53] S.C. Tsang, N. Cailuo, W. Oduro, A.T.S. Kong, L. Clifton, K.M.K. Yu, B. Thiebaut, J. Cookson, P. Bishop, Engineering preformed cobalt-doped platinum nanocatalysts for ultraselective hydrogenation, ACS Nano, 2 (2008) 2547-2553.

[54] H. Vu, F. Goncalves, R. Philippe, E. Lamouroux, M. Corrias, Y. Kihn, D. Plee, P. Kalck, P. Serp, Bimetallic catalysis on carbon nanotubes for the selective hydrogenation of cinnamaldehyde, Journal of Catalysis, 240 (2006) 18-22.

[55] P. Gallezot, D. Richard, Selective hydrogenation of α, β-unsaturated aldehydes, Catalysis Reviews - Science and Engineering, 40 (1998) 81-126.

[56] R.G. Rao, R. Blume, T.W. Hansen, E. Fuentes, K. Dreyer, S. Moldovan, O. Ersen, D.D. Hibbitts, Y.J. Chabal, R. Schlogl, J.P. Tessonnier, Interfacial charge distributions in carbon-supported palladium catalysts, Nature Communications, 8 (2017) 340.

[57] R. Nie, M. Miao, W. Du, J. Shi, Y. Liu, Z. Hou, Selective hydrogenation of C=C bond over N-doped reduced graphene oxides supported Pd catalyst, Applied Catalysis B: Environmental, 180 (2016) 607-613.

# Chapter 6

**Thiols decorated carbon felt containing Pd nanoparticles for selective hydrogenation of cinnamaldehyde**

# Thiols decorated carbon felt containing Pd nanoparticles for selective hydrogenation of cinnamaldehyde

*Zhenxin Xu,[a] Bing Li,[a] Vasiliki Papaefthimiou,[a] Yuefeng Liu,[b]*

*Cuong Duong-Viet,[a,c] Spiridon Zafeiratos[a] and Cuong Pham-Huu[a,\*]*

*(a) Institut de Chimie et Procédés pour l'Energie, l'Environnement et la Santé (ICPEES), ECPM, UMR 7515 du CNRS-Université de Strasbourg, 25 rue Becquerel, 67087 Strasbourg Cedex 02, France*

*(b) Dalian National Laboratory for Clean Energy (DNL), Dalian Institute of Chemical Physics, Chinese Academy of Science, 457 Zhongshan Road, 116023 Dalian, China*

*(c) Ha-Noi University of Mining and Geology, 18 Pho Vien, Duc Thang, Bac Tu Liem, Ha-Noi, Vietnam*

*Corresponding authors:*

*cuong.pham-huu@unistra.fr (Cuong Pham-Huu)*

**Abstract**

Thiol-containing modifiers with high affinity for active metal are considered to regulate the catalytic performance in heterogeneous catalysis but still with challenge due to their potential surface poisoning. Here, a novel structured carbon support decorated with thiol groups is successfully synthesized via thermal reaction between guest $H_2S$ gas and the oxidized carbon felts generated on the basis of gaseous acid treatment. By preparing such thiolated carbon monolith supported Pd NPs as a model catalyst, we demonstrate the electronic effect induced by the surface thiols to steer the catalytic performance in the liquid-phase hydrogenation of α, β-unsaturated cinnamaldehyde. Detailed studies reveal that during the catalyst preparation the thiol groups cannot only serve as anchoring sites for active metal at Pd-support interface, but also migrate from support to the surface of Pd NPs and thus exist as the capping "ligands" to hinder or moderate the catalytic activity. Furthermore, tuning the atomic ratio of sulfur to palladium in catalyst is able to prevent the poisoning effect on the reaction activity. The electronic metal-support interaction with charge transfer from Pd atom to thiol-S of carbon support through Pd-S bond helps to form the unique electronic configuration of Pd NPs with high intensity of electron depleted $Pd^{\delta+}$, leading to the excellent chemoselectivity towards C=C bond hydrogenation.

**Keywords:**

Thiols, carbon felts monolith, thiolation, Pd nanoparticles, electronic metal-support interaction, selective hydrogenation, surface poisoning effect

# 1. Introduction

The organosulfur compounds, especially aliphatic thiols, have been widely used to decorate the noble metal surface in the field of nanotechnology [1, 2]. The high affinity of sulfhydryl groups (-SH) for the noble metal surface provides self-assembled monolayers (SAMs) of long-chain alkanethiols to promote the reaction performance by controlling the surface environment of heterogeneous catalysts [3, 4]. These organic ligands on the metal substrates not only bring in the steric effects in catalysis [5], but also stabilize the metal surface atoms and modify the electronic states at metal-sulfur interfaces [6], which in turns, modify the catalytic performance of the system. The thiols can be further employed as direct linkages between precious metal nanoparticles (NPs) and support matrix to enhance the dispersion of active phase and then improve its activity in numerous catalytic processes [7, 8]. However, metal based catalysts are generally recognized to be susceptible to surface poisoning by strongly adsorbed sulfur-containing species [9, 10]. On the one hand, for the thiolated carbon supported catalysts the sulfur content should be removed by pretreatments before their catalytic uses [11-14]. On the other hand, the sulfur from thiol groups is reported to have no surface poisoning effect on the catalyst when the S-containing moiety is strongly adhered to the carbon support [15]. Hence, there still remains a room for the understanding of the effect of thiols on the reaction performance in the thiolated carbon supported catalytic systems. To date, the thiolated carbon materials are widely synthesized as powder-shaped samples by complex and continuous processes, including oxidation, halogenation and thiolation treatments [16]. Nevertheless, these procedures are mostly operated in the stirred liquid medium and then are linked with the troublesome washing and filtration steps, which are thus frequently accompanied by structural damages and quality loss of the treated material and are not suitable for mass production.

The hydrogenation of α,β-unsaturated aldehydes to the corresponding unsaturated alcohols or saturated aldehydes is a crucial step in the preparation of useful intermediates for fine chemical industries [17]. Recently, hydrocinnamaldehyde (HCAD), which is a hydrogenated product of α,β-unsaturated cinnamaldehyde (CAD), was found to be an important intermediate in the synthesis of pharmaceuticals used in the treatment of HIV

disease [18]. Several attempts on the CAD hydrogenation have been made to develop a suitable catalytic system for performing high catalytic activity along with high selectivity towards the desired product distributions [19-22]. The literature data reported that Pd catalysts are in favor of the hydrogenation of the C=C double bond to produce HCAD [17, 23], and the appropriate catalyst architecture along with the unique electronic structure of active metal will promote the reaction selectivity [24, 25]. As the most broadly studied catalytic systems for this process, although the reduction of the vinyl group is more readily achieved thermodynamically than that of carbonyl [26], it is still a difficult task for the selective hydrogenation of CAD into HCAD meanwhile refraining from the complete hydrogenation of both unsaturated C=C and C=O bonds into hydrocinnamylalcohol (HCAL) [27-29].

In this work, we report on the synthesis of thiols decorated carbon monolith felt by the combined functionalization of macroscopic commercial carbon felt (CF) with gaseous nitric acid and subsequent treatment in the presence of hydrogen sulfide. The facile and effective thiolation method is benefiting from the processing condition of gas phase and the employment of structured carbon material. The carbon pre-oxidation, the $H_2S$ concentration and the introduction of steam in the gas-phase thiolation process, as well as the post-treatment under high temperature were investigated for the development of thiol groups decorated carbon structure. The thiolated carbon felt was then used to support palladium nanoparticles (NPs) for the liquid-phase selective hydrogenation of α,β-unsaturated cinnamaldehyde. The catalytic performance, whether reaction activity or C=C bond hydrogenated selectivity, has been shown to be closely related to the interaction between thiols and Pd NPs. Furthermore, the Pd catalysts with reduced thiol content and S-dopant derived from thiol groups were tested in the hydrogenation reaction to help understand the effect of surface sulfur species on the catalyst.

## 2. Results and Discussion

### 2.1 Synthesis and characterization of the carbon supports

The structured commercial CF was firstly functionalized using the $HNO_3$ vapor at 250 $^o$C for 4 h leading to the formation of OCF. As shown in Figure 1, the $I_D/I_G$ ratios calculated

from Raman spectra of the different carbon samples increase from 1.37 for the pristine CF to 1.81 for the OCF. Meanwhile the D' peak of the OCF becomes more sharp than that of the CF, suggesting the change of the graphite structure with the generation of more defects and disordered graphitic fragments on the treated one after the gaseous oxidation [30]. The blue shift of G band on OCF may be attributed to the surface O–H bending and C=O stretching [31]. Furthermore, the increased $I_D/I_G$ ratios happen to the samples after the treatment with $H_2S$ (TCF, $H_2S$ reaction with pristine CF, and TOCF, $H_2S$ reaction with OCF), indicating the formation of structural defects on the graphite framework during the thiolation process. The STOCF sample denoted the one obtained after high temperature annealing of the TOCF one.
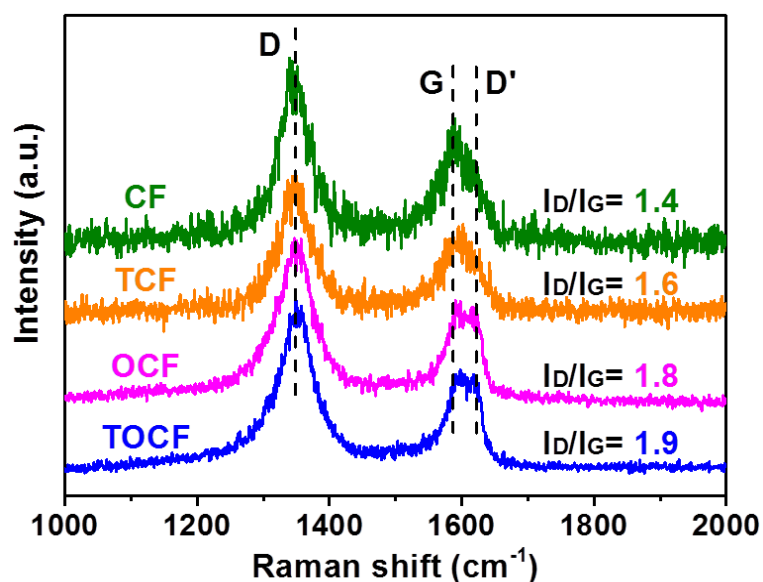


**Figure 1.** Raman spectra of CF, TCF, OCF and TOCF.

The analysis of O 1s XPS and TPD-MS indicate that abundant oxygen-containing functional groups (Figure 2, 3 and Table 1, 2), including C=O (531.0 eV), O-C=O (532.3 eV) and C-O (533.4 eV) groups, were incorporated into the OCF sample after the treatment [32]. According to the XPS results (Table 1) the total oxygen content decreases from OCF (10.6 at%, O/C = 11.9 %) to TOCF (9.1 at%, O/C = 10.1 %). As listed in Table 2, the atomic ratios of C=O and O-C=O groups to surface carbon element are reduced after the thiolation treatment, while that of C-O groups is increased on the contrary. The loss of oxygenated

groups, especially for carboxylic acids, anhydrides and phenols, is also confirmed by the TPD-MS results. As a result of the thermal decomposition of oxygen-containing functional groups, the oxygen atom percent decreases from the TOCF (9.1 at%, O/C= 10.1 %) to the STOCF (3.4 at%, O/C= 3.6 %), and the amount of each oxygenated groups is decreased after the calcination at 700 $^o$C.

**Table 1.** Elemental analysis of different samples

| Samples | Atom percentage (at%) | | | O/C (%) | S/C (%) |
|---|---|---|---|---|---|
| | C | O | S | | |
| CF | 95.6 | 4.4 | 0 | 4.6 | 0 |
| TCF | 95.6 | 4.3 | 0.1 | 4.5 | 0.2 |
| OCF | 89.4 | 10.6 | 0 | 11.9 | 0 |
| TOCF | 89.6 | 9.1 | 1.3 | 10.1 | 1.5 |
| STOCF | 95.9 | 3.4 | 0.7 | 3.6 | 0.7 |

**Table 2.** Oxygen elemental analysis of surface oxygen species taking carbon element as a reference on samples

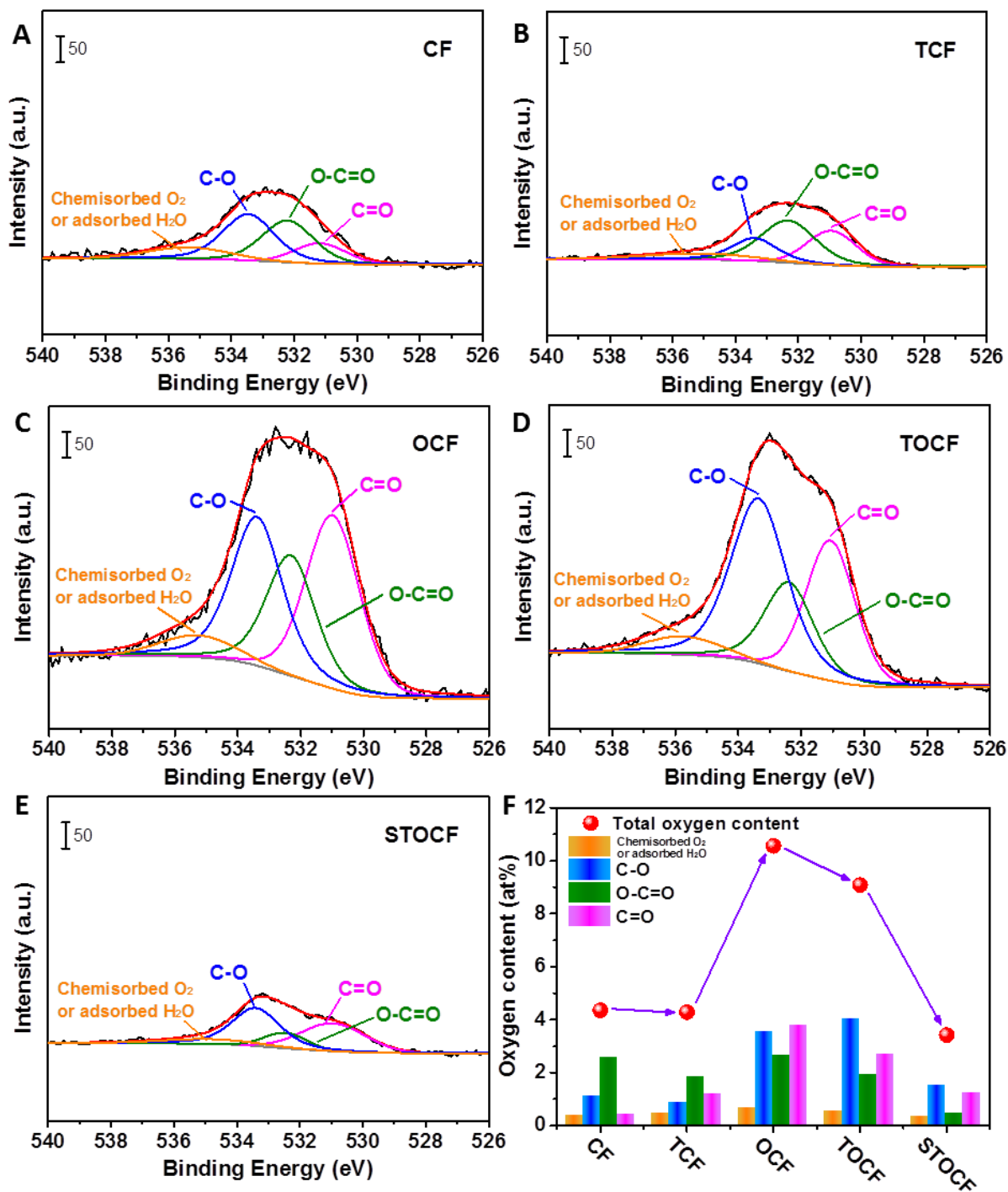| Samples | $O_{total}$/C (%) | Surface O species/C (%) | | | |
|---|---|---|---|---|---|
| | | C=O | O-C=O | C-O | Chemisorbed $O_2$ or adsorbed $H_2O$ |
| CF | 4.6 | 0.4 | 2.6 | 1.2 | 0.4 |
| TCF | 4.5 | 1.2 | 1.9 | 0.9 | 0.5 |
| OCF | 11.9 | 4.2 | 3.1 | 3.9 | 0.7 |
| TOCF | 10.1 | 3.0 | 2.1 | 4.5 | 0.5 |
| STOCF | 3.6 | 1.3 | 0.5 | 1.5 | 0.3 |

**Figure 2.** O 1s high-resolution XPS spectra of (A) CF, (B) TCF, (C) OCF, (D) TOCF and (E) STOCF, and (F) calculated contents of different oxygen-containing functional groups of the different samples, respectively.
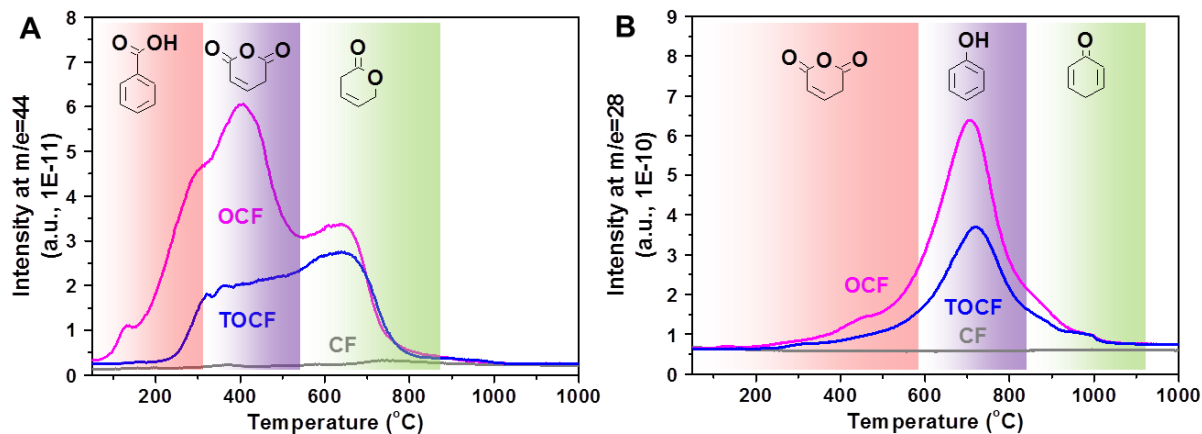
**Figure 3.** (A) $CO_2$ (m/z = 44) and (B) CO (m/z = 28) generated during the TPD analysis of the CF, OCF and TOCF, respectively.

The high resolution S 2p XPS spectrum of the T4OCF (Figure 4), which was prepared by the treatment of OCF with dry and diluted $H_2S$ (4 vol.%, He as balance) at 230 °C for 2 h, can be resolved into three different peaks located at the binding energies of around 163.5, 164.7 and 168.2 eV, respectively. The former two peaks with the expected 2:1 peak area ratio and a 1.2 eV peak separation are in agreement with the reported $2p_{3/2}$ and $2p_{1/2}$ positions of thiol-S (-C-SH) owing to their spin-orbit coupling [33]. The third peak should arise from some oxidized sulfur species (-C-$SO_X$-C-) [34]. Thereby, it can be inferred that the thiolated T4OCF is successfully synthesized through the functionalization of the OCF with $H_2S$ at low temperature. The overall content of sulfur in the T4OCF is about 1.3 at%, and approximately 83 % of the surface-bound sulfurs are in their reduced form of thiol groups (Table 3) [35]. By closely combining with the above analysis about the variation of surface oxygenated groups on the treated OCF (Figure 2 and 3), it is suggested that during the thiolation process, the $H_2S$ is capable of reacting with the hydroxyl groups present on the OCF surface, such as carboxylic acids, anhydrides and phenols, and the thiol groups are then implanted on the surface of carbon felt with the concomitant release of water. Meanwhile, C-O groups can be formed from the reaction of $H_2S$ and C=O groups. Therefore, according to the influence of the oxygen-containing groups which serve as baits for catching the thiol groups on carbon materials, as shown in Table 1, TCF with low surface oxygen only leads to an anchorage of a

very small amount 0.1 at% of sulfur.
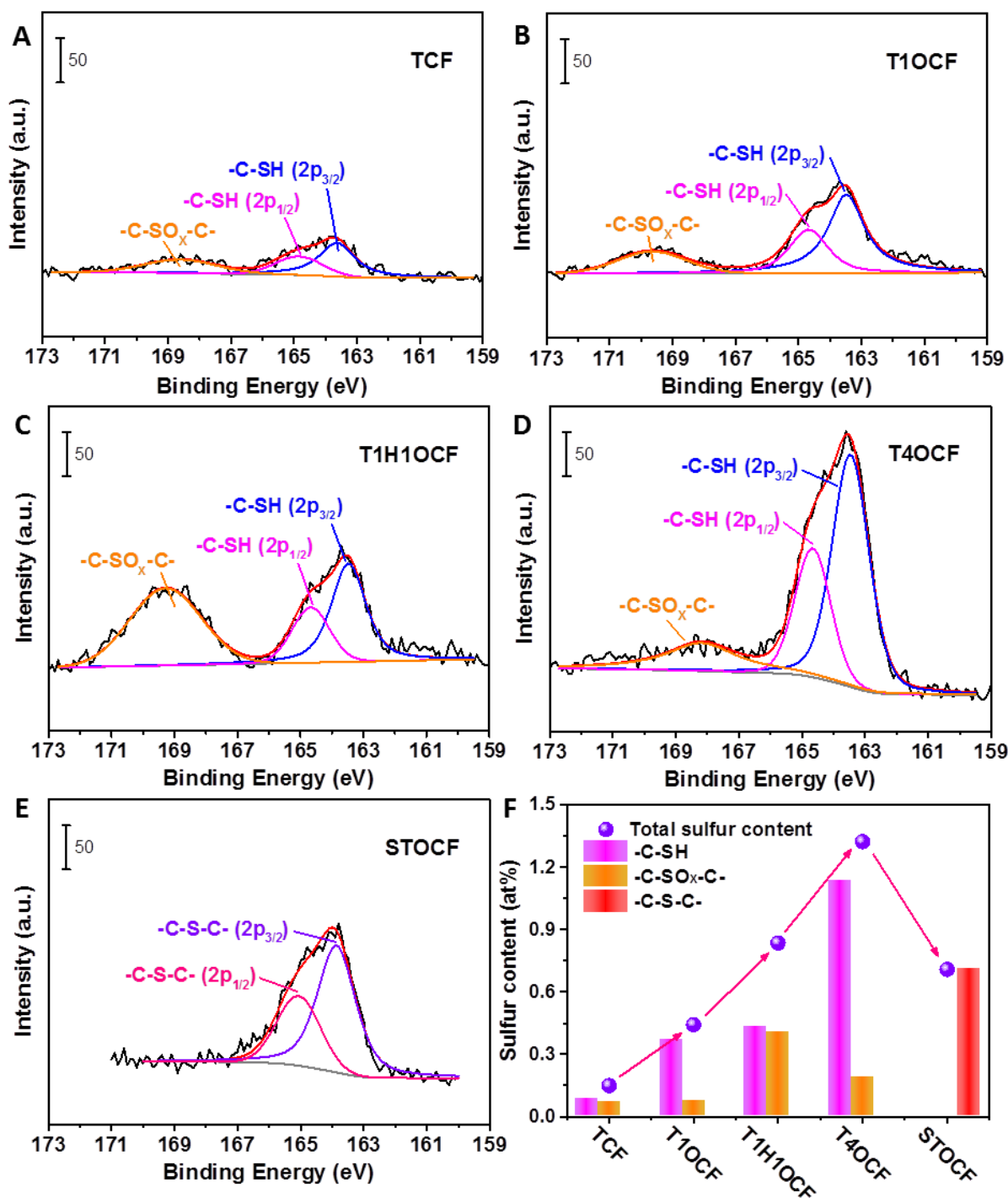


**Figure 4.** S 2p high-resolution XPS spectra of (A) TCF, (B) T1OCF and (C) T1H1OCF, (D) T4OCF, (E) STOCF and (F) calculated contents of different sulfur-containing functional groups and sulfur dopants of samples, respectively.

Moreover, the OCF was further functionalized by the low concentration of $H_2S$ (1 vol.%, He as balance) with or without steam (10 vol.%). The S 2p XPS analysis (Figure 4) confirms again that the thiol groups can be formed on the modified carbon samples using $H_2S$ as sulfur source in spite of the different concentration and in the presence of humidity. As summarized in Table 3, the surface sulfur content of thiolated sample under 1 vol.% of $H_2S$ with $H_2O$ (T1H1OCF, 0.8 at%) is twice as much as that of the one without $H_2O$ (T1OCF, 0.4 at%), however, both of them are lower than the sulfur content of T4OCF (1.3 at%), which is functionalized under 4 vol.% of $H_2S$. These results indicate that not only the $H_2S$ concentration, but also the presence of steam can promote the formation of sulfur-containing groups on the carbon surface. It can be explained that there may be a layer of $H_2O$ formed on the surface of the porosity of carbon samples in the humid environment, which could enhance the adsorption of $H_2S$ to participate in the thiolation as the same as the high concentration of reactive gas. Dissociative absorption of $H_2S$ in a water film has been reported by Sun et al. during the investigation of low temperature selective oxidation of $H_2S$ [36]. In addition, the percent of oxidized sulfur species on the T1H1OCF (46 %) is much higher than that of the T1OCF (19 %), suggesting that the water vapor is more conducive to generate oxidized sulfur groups than thiols.

**Table 3.** Sulfur elemental analysis of different surface S species on samples

| Samples | S at% | Surface S species/$S_{total}$ (%) | | |
|---------|-------|--------|----------|--------|
|         |       | -C-SH  | -C-SOX-C- | -C-S-C- |
| TCF     | 0.1   | 72.8   | 27.2     | -      |
| T1OCF   | 0.4   | 81.1   | 18.9     | -      |
| T1H1OCF | 0.8   | 53.9   | 46.1     | -      |
| T4OCF   | 1.3   | 82.9   | 17.1     | -      |
| STOCF   | 0.7   | -      | -        | 100    |

Interestingly, after the thermal treatment under inert atmosphere at 700 $^{\circ}$C for 2 h, the S $2p_{3/2}$ and $2p_{1/2}$ positions on the STOCF sample shift to the binding energies of 163.9 and 165.1 eV (Figure 4), respectively, corresponding to thiophene-S (-C-S-C-) [37]. It is demonstrated that the surface thiol groups can be transformed into S-dopant at the edges and defects of graphene in the form of thiophene-like structures at 700 $^{\circ}$C. The XPS intensity of the oxidized sulfur is significantly vanished at high annealing temperature, indicating the weak thermal stability of such species. The sulfur atom percent of STOCF is amounted to 0.7 at% (S/C= 0.7%) while it is about 1.3 at % (S/C= 1.5 %) on the initial TOCF (Table 1), which is due to the thermal decomposition of sulfur-containing functional groups.

## 2.2 Synthesis and characterization of the catalysts

Herein TOCF with high content of thiol groups and untreated OCF, with high oxygenated groups, were chosen as catalyst supports for palladium. The catalyst was prepared by the liquid-phase reduction of the Pd precursor $Pd(NO_3)_2$ with $NaBH_4$ in the presence of a support. Through varying the weight of $Pd(NO_3)_2$ in this preparation method, the metal loading is found to reach the maximum on the catalyst when an excess of palladium ($Pd_s$) was used for the synthesis step. This may be due to the limitation on the number of functional groups, such as thiols and oxygenated groups on the carbon support, which could act as anchoring sites for active metal [13, 38, 39]. Such anchorage mode is similar to that observed with nitrogen-doped carbon-based supports. The palladium elemental analysis by ICP-AES and XPS (Table 4) shows that the metal loading as well as surface Pd atom percent of $Pd_s$/TOCF catalyst (6.6 wt% and 7.4 at%) are higher than that of $Pd_s$/OCF (5.3 wt% and 5.8 at%), indicating the better metal adhesion with high dispersion on the TOCF which could be attributed to the presence of thiol groups. Meanwhile, the TOCF support with unsaturated Pd loading ($Pd_{us}$/TOCF, 1.5 wt% of Pd) was also synthesized by decreasing the amount of Pd precursor, thereby leading to the higher atomic ratio of sulfur to palladium in $Pd_{us}$/TOCF than $Pd_s$/TOCF.

The XPS measurements (Figure 5 and Table 4) reveal that the core level Pd $3d_{5/2}$ binding energies (BEs) of both TOCF and OCF supported Pd catalysts are higher than that of

bulk $Pd^0$ metal (335.1 eV) but lower than that of ionic state $Pd^{2+}$ metal (337.2 eV) [40, 41]. Furthermore, an additional prominent signal between $Pd^0$ phase and the other two of $Pd^{2+}$ and satellite peak (338.4 eV) [42], which can be attributed to the electron-deficient metal atoms ($Pd^{\delta+}$), is distinctly required to fit the Pd $3d_{5/2}$ spectrum deconvolution of each sample. The shifts of Pd 3d BEs and the presence of $Pd^{\delta+}$ provide the indication of electronic metal-support interaction (EMSI) accompanied by the charge transfer from active metal to functionalized carbon support with metal anchoring sites of thiol and oxygenated groups. The TOCF supported Pd catalysts exhibit a Pd $3d_{5/2}$ signal shifted to higher BE and more proportion of $Pd^{\delta+}$ than the OCF supported one, revealing the stronger electronic interaction between active metal and TOCF, which is attributable to the higher affinity for Pd of the surface thiol groups compared to that of the oxygenated groups. There is also a higher concentration of $Pd^{2+}$ species on the catalyst with thiols than on the thiol-free $Pd_s$/OCF, meaning the lower reducibility of the Pd precursor ions adsorbed on TOCF compared to that on OCF. Besides, the Pd $3d_{5/2}$ BE, the ratio of $Pd^{\delta+}$ to $Pd^0$ and the fraction of unreduced $Pd^{2+}$ species are all increased after reducing the metal loading by comparing $Pd_{us}$/TOCF and $Pd_s$/TOCF, asserting that the high ratio of sulfur to palladium further enhances the effect of EMSI on the electronic structure of Pd NPs and renders the difficult reduction of the sample.

**Table 4.** Palladium elemental analysis of $Pd_{us}$/TOCF, $Pd_s$/TOCF and $Pd_s$/OCF

| Samples | Pd wt%[a] | Pd at%[b] | Surface Pd species/Pd$_{total}$ (%) | | | $Pd^{\delta+}/Pd^0$ | Binding Energy (eV) Pd $3d_{5/2}$ |
|---|---|---|---|---|---|---|---|
| | | | $Pd^{2+}$ | $Pd^{\delta+}$ | $Pd^0$ | | |
| $Pd_{us}$/TOCF | 1.5 | 2.4 | 38.6 | 49.1 | 12.3 | 4.0 | 336.7 |
| $Pd_s$/TOCF | 6.6 | 7.4 | 27.1 | 49.0 | 23.9 | 2.1 | 335.6 |
| $Pd_s$/OCF | 5.3 | 5.8 | 24.5 | 37.8 | 37.7 | 1.0 | 335.4 |

[a] The palladium weight percent of the samples determined by the ICP-AES. [b] The atom percent of surface palladium element on the samples determined by the XPS survey spectra.
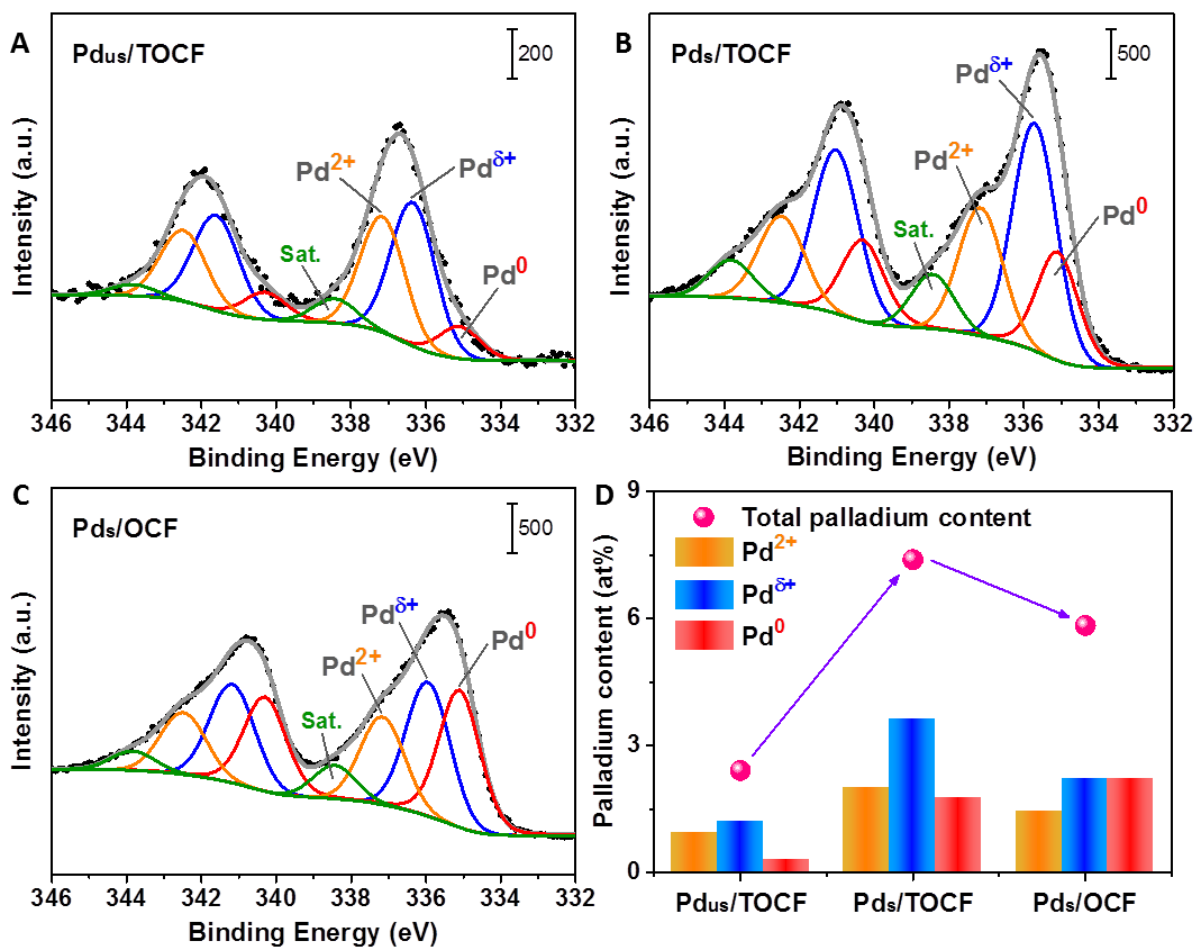
**Figure 5.** Pd 3d high-resolution XPS spectra of (A) Pd$_{us}$/TOCF, (B) Pd$_s$/TOCF and (C) Pd$_s$/OCF, and (D) calculated contents of different Pd species of samples, respectively.

Meanwhile, Figure 6A shows that the S 2p peak of TOCF supported Pd catalysts shifts toward the lower BE compared with that of TOCF, suggesting that the thiol groups participate in the EMSI as electron acceptor. Therefore, the positive and negative shifts of BEs for Pd 3d and S 2p, respectively, can be related to the charge transfer from Pd NPs to S atoms of thiols to form Pd$^{\delta+}$-S$^{\delta-}$ chemical bond [43, 44]. Compared with Pd$_s$/TOCF, Pd$_{us}$/TOCF displays lower BE of S 2p, illustrating that there are more Pd-S bonds formed after lessening the metal loading on TOCF and thus the remained sulfur species will receive more electrons from Pd atoms, leading to an existence of higher electron transfer between Pd and S although the S/Pd ratio is increased. This further demonstrates that there are more thiol groups binding to Pd NPs in Pd$_{us}$/TOCF than that in the Pd$_s$/TOCF, which may be due to the fact that the thiols are

not only served as anchoring sites in the interface between active metal and carbon support, but also existed as the ligands adsorbed on the surface of Pd NPs to form the thiol-based SAMs, which is enhanced in the case of unsaturated metal loading with high S/Pd ratio.
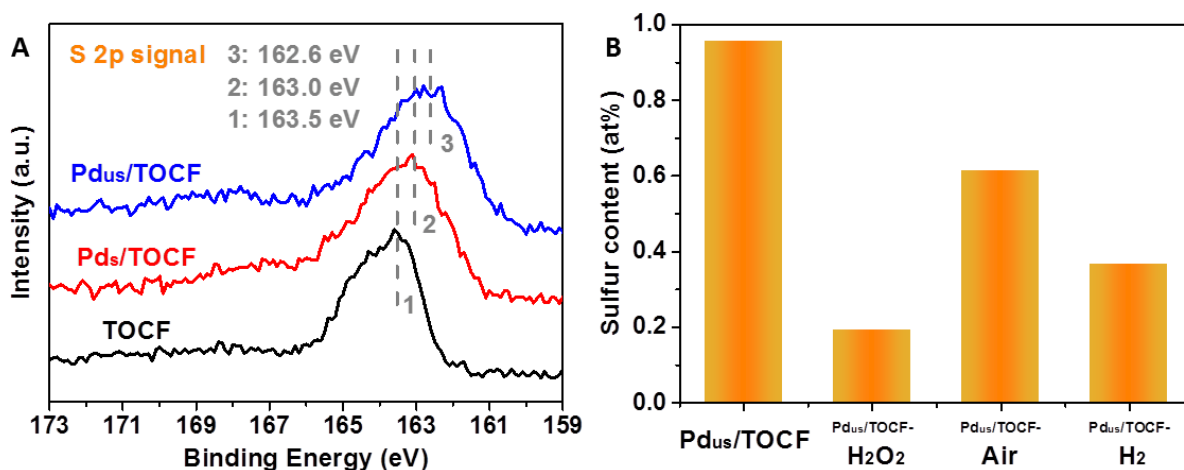


**Figure 6.** (A) S 2p high-resolution XPS spectra of TOCF, $Pd_s$/TOCF and $Pd_{us}$/TOCF, and (B) Surface sulfur content of $Pd_{us}$/TOCF, $Pd_{us}$/TOCF-$H_2O_2$, -Air and -$H_2$, respectively.

$Pd_{us}$/TOCF was further treated to remove sulfur species, i.e. 30 % of hydrogen peroxide ($H_2O_2$) at room temperature, air (Air) as well as hydrogen ($H_2$) flow at 400 °C for 2 h. The XPS analysis (Figure 6B) demonstrates that the sulfur content of $Pd_{us}$/TOCF is significantly decreased after these desulfurization processes. Meanwhile, as shown in Figure 7A-C and Table 5 , the Pd 3d peaks of $Pd_{us}$/TOCF shift toward the lower BEs after removing the sulfur content, which arises from the decrease in the number of thiols around Pd NPs and further supports the above notion about the effect of S/Pd ratio on EMSI.

Moreover, the $Pd_{us}$/STOCF catalyst with the same metal loading as $Pd_{us}$/TOCF was also prepared as a comparative sample. The positive shift of Pd 3d BE is observed on $Pd_{us}$/STOCF (Figure 7D and Table 5) compared with bulk $Pd^0$ metal, representing the EMSI with the influence on the electronic states of Pd NPs from the S-dopants in carbon support [45]. Whilst the Pd 3d BE of $Pd_{us}$/STOCF is lower than that of $Pd_{us}$/TOCF, which may be caused by the loss of sulfur content during the S-doping process at high temperature. All the

desulfurized $Pd_{us}$/TOCF-X and $Pd_{us}$/STOCF, albeit with the similar metal weight, show the reduction of surface Pd atom percent (Table 5), indicating the lower dispersion of active metal under the decreased content of sulfur species, which assist in anchoring Pd NPs.

**Table 5.** Palladium elemental analysis of the samples

| Samples | Pd at%[a] | Binding Energy (eV) Pd 3d$_{5/2}$ | Pd wt%[b] |
|---|---|---|---|
| $Pd_{us}$/TOCF-$H_2O_2$ | 1.2 | 335.7 | 0.9 |
| $Pd_{us}$/TOCF-Air | 1.1 | 335.8 | 0.8 |
| $Pd_{us}$/TOCF-$H_2$ | 1.2 | 335.5 | 1.0 |
| $Pd_{us}$/STOCF | 1.4 | 336.2 | 0.4 |

[a] The atom percent of surface palladium element on the samples determined by the XPS survey spectra.

[b] The palladium weight percent of spent samples determined by the ICP-AES.
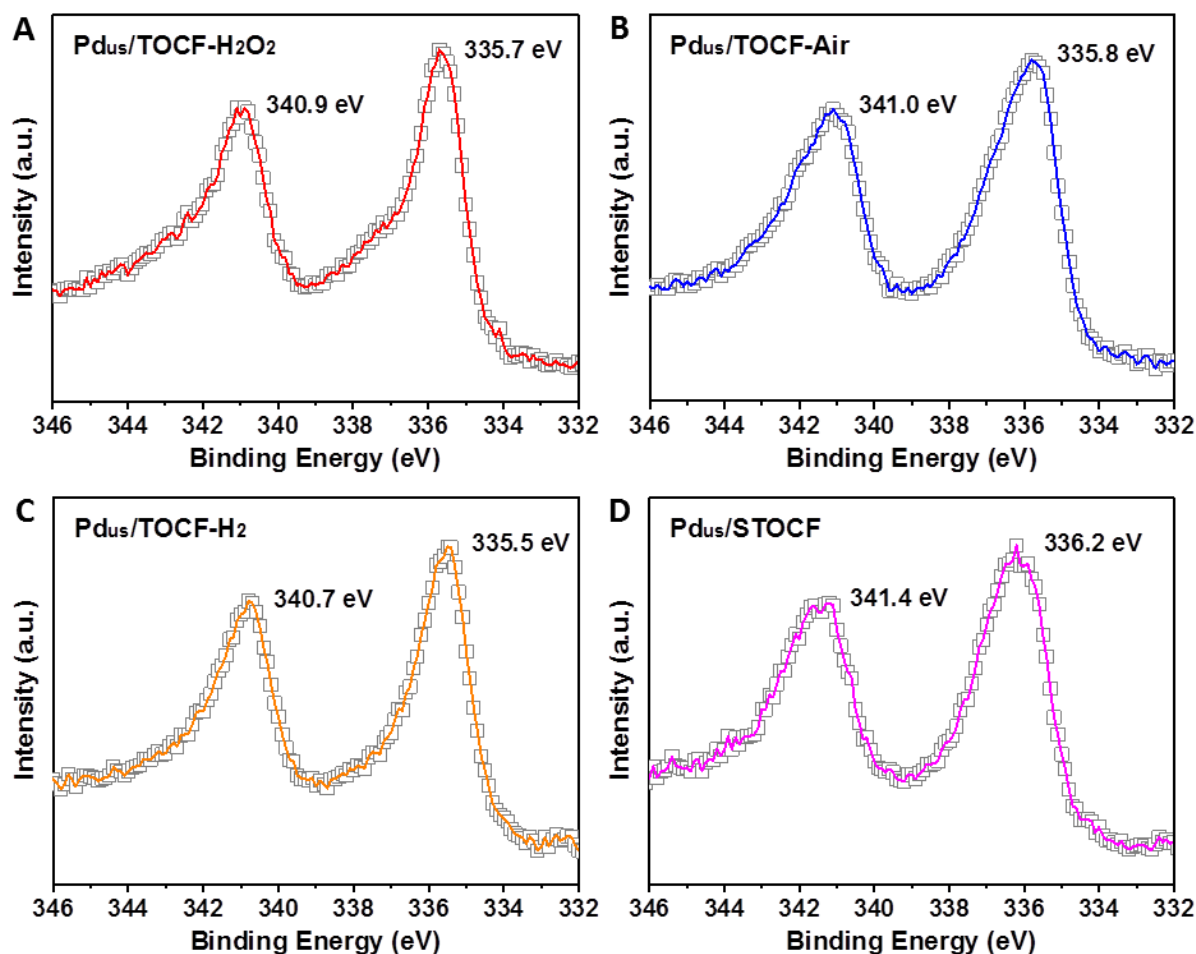
**Figure 7.** Pd 3d high-resolution XPS spectra of (A) Pd$_{us}$/TOCF-H$_2$O$_2$, (B) Pd$_{us}$/TOCF-Air (C) Pd$_{us}$/TOCF-H$_2$ and (D) Pd$_{us}$/STOCF, respectively.

## 2.3 Catalytic performance on the selective hydrogenation of cinnamaldehyde

The different Pd catalysts were tested in the liquid-phase hydrogenation of cinnamaldehyde under similar reaction conditions. The catalytic performance, expressed in terms of CAD and HCAD concentration, mol/L, as a function of time-on-stream (TOS) are presented in Figure 8. The Pd$_s$/TOCF, despite its high active metal loading, requires much longer time to complete the conversion of CAD compared to the Pd$_s$/OCF, indicating a lower reaction rate. It is also worthy to note that there is no observed hydrogenation activity on Pd$_{us}$/TOCF catalyst. The low hydrogenation activity of the TOCF-based catalysts appears to result primarily from the poisoning effect of thiol-S on their catalytic performance. According

to the XPS analysis, sulfur species present on the carbon surface not only play the role of anchorage sites for metal dispersion but they can also migrate from the support to the metal surface during the catalyst preparation due to their high affinity for Pd, thereby resulting in the formation of thiol-based SAMs on Pd NPs surface. These thiol ligands adsorbed on palladium surface contribute to the decreasing of the exposure of metal active surface atoms [46], giving rise to the loss of catalytic activity in the hydrogenation reaction. Especially for $Pd_{us}$/TOCF with low metal loading and thus, high thiol concentration with the high S to Pd ratio could completely inhibit the activity of Pd sites. On the other hand, the high Pd content on the $Pd_s$/TOCF catalyst allows it to still provide active sites for performing hydrogenation process with a lower reaction rate compared to the sulfur-free $Pd_s$/OCF catalyst.



**Figure 8.** (A) Cinnamaldehyde conversion and (B) C=C bond hydrogenation selectivity expressed in terms of CAD and HCAD concentration as a function of the time on stream on $Pd_{us}$/TOCF, $Pd_s$/TOCF and $Pd_s$/OCF catalysts, respectively. Conditions: 80 $^o$C, 25 mL/min H$_2$, 1 atm, 300 rpm, 10 mL dioxane and 0.08 mol/L of CAD.

On the other hand, the C=C bond hydrogenation selectivity displays a significant difference among the tested catalysts as shown in Figure 8B. The C=C bond hydrogenation selectivity on the $Pd_s$/OCF remains relatively low, at ca. 39 %, while the one on the $Pd_s$/TOCF is level up to more than 90 %. In addition, the C=C bond hydrogenation selectivity remains unchanged after complete conversion of CAD has been reached. Such results could be

explained by the fact that at high Pd loading and low CAD concentration, i.e. 0.08 mol/L of CAD inside the reactor, the C=O bond of reactant is most likely adsorbed on the active metal surface and then directly hydrogenated into saturated compound before desorption of the HCAD intermediate to the liquid phase. The desorbed HCAD is unlikely to be readsorbed which explain the 39 % of selectivity and the level-off value of selectivity after complete conversion of CAD in the reaction medium. On the $Pd_s$/TOCF the high C=C bond hydrogenation selectivity could be attributed to the presence of sulfur on the active metal sites which could inhibit the adsorption of C=O bond of the reactant contributing in such a way to the high selectivity. According to the results one can state that the presence of sulfur species on the Pd surface provides an interesting way to control the selectivity of the intermediate product, even at high conversion level.

In order to verify such assumption about the poisoning effect of thiols, CAD hydrogenation was further carried out on the desulfurized $Pd_{us}$/TOCF-X (X= -$H_2O_2$, -Air and -$H_2$) and $Pd_{us}$/STOCF (Table 5). The desulfurized catalysts display improved hydrogenation activity (Figure 9) compared to the undesulfurized one, i.e. $Pd_{us}$/TOCF, which confirms that sulfur crossover is at the origin of the low hydrogenation activity observed in Figure 8A. The treatment in the presence of different reagents, i.e. $H_2O_2$, air or hydrogen, leads to the removal of sulfur species along with a concomitant increase of the active Pd surface for the hydrogenation reaction. For $Pd_{us}$/STOCF, the S-dopants at the edges of the graphene layers and in basal plane defects [47], which are different from thiols on the surface of TOCF, cannot migrate from carbon support to the surface of Pd NPs, so there is no loss of exposed active sites for the reaction. However, the desulfurization of $Pd_{us}$/TOCF could also remove the thiols in the Pd-support interfaces, and the S-doping treatment for STOCF is capable of decreasing the content of sulfur- and oxygen-containing functionalities. Both of them can weaken the strength of the supports for the anchorage of the Pd NPs, therefore, as shown in Figure 9 and Table 5, the catalysts are easily deactivated and accompanied by the metal leaching during the liquid-phase reaction.
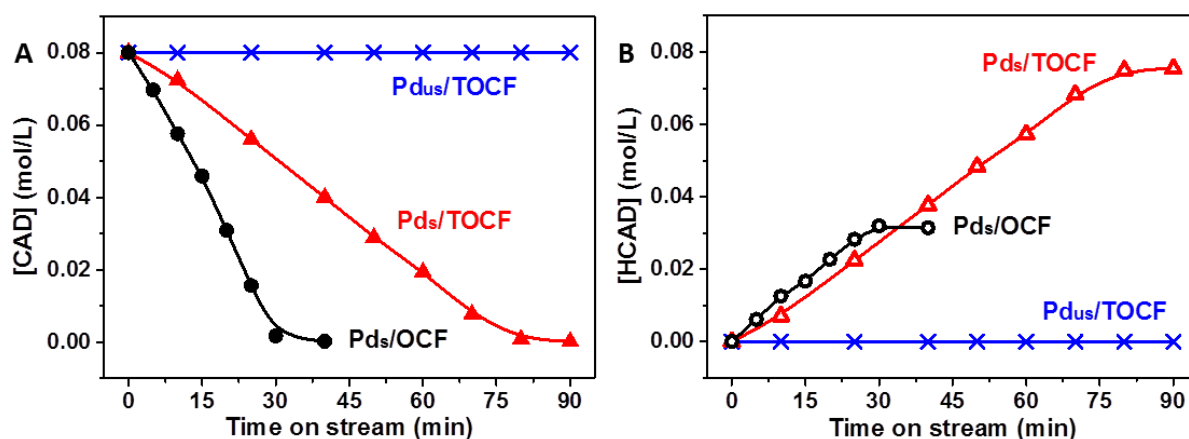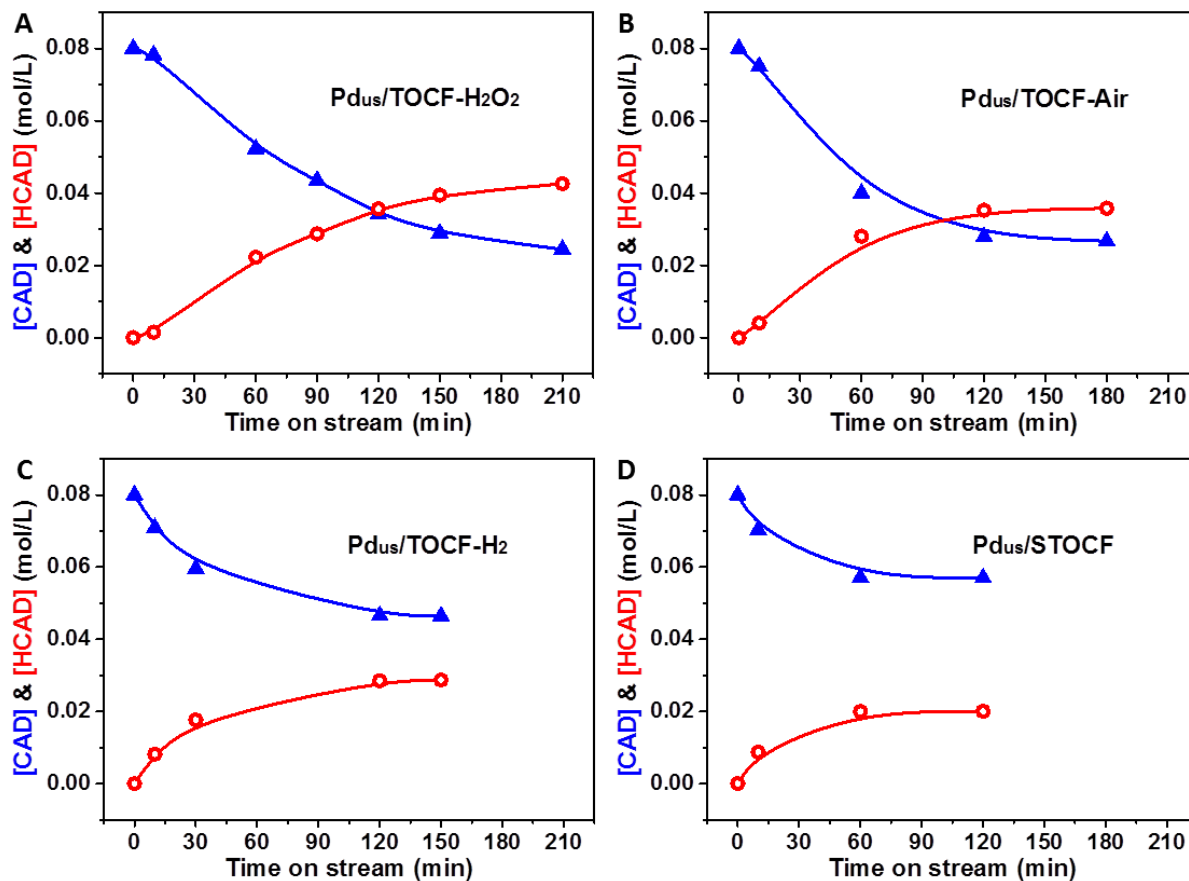
**Figure 9.** Cinnamaldehyde conversion and C=C bond hydrogenation selectivity expressed in terms of CAD and HCAD concentration as a function of the time on stream on (A) $Pd_{us}$/TOCF-$H_2O_2$, (B) $Pd_{us}$/TOCF-Air (C) $Pd_{us}$/TOCF-$H_2$ and (D) $Pd_{us}$/STOCF catalysts, respectively. Conditions: 80 $^{o}$C, 25 mL/min $H_2$, 1 atm, 300 rpm, 10 mL dioxane and 0.08 mol/L of CAD.

The capping ligands on the surface of metal NPs have been demonstrated to effectively steer the chemoselectivity of NPs-catalyzed liquid-phase reactions [22, 48]. For instance, the SAM coatings of 3-phenyl-1-propanethiol on Pt catalyst can enhance the hydrogenation of CAD at C=O bond into cinnamyl alcohol (CAL) as a result of their steric effect [49], which directing the adsorbed CAD in a standing-up orientation on platinum surface because of the interaction between its phenyl moiety and the phenyl ring of the SAM, and then only carbonyl group can interact with the active metal surface to produce CAL. However, the hydrogenation of C=O bond is not enhanced on $Pd_s$/TOCF compared to that of

the Pd$_s$/OCF, although the presence of thiol ligands on Pd NPs evidently decreases the reaction rate of the catalyst due to the surface poisoning of active metal, indicating that the steric effect of thiol groups here is not enough to promote the adsorption of carbonyl functionality on the Pd NPs. Furthermore, in terms of the steric effect, the presence of thiol ligands on Pd NPs is more likely to prevent the CAD lying flat on the metal surface and, therefore, avoids the direct contact of the C=C bond with the catalytic Pd surface. Nevertheless, as shown in Figure 8, Pd$_s$/TOCF catalyst performs much higher selectivity of HCAD (95%) than Pd$_s$/OCF (39%). This performance should profit from the unique electronic configuration of Pd NPs controlled by the electronic effect of thiol modifiers [50], which could destabilize the C=O adsorption of the intermediate product and thus, avoid the complete hydrogenation [21]. The high intensity of electron depleted Pd$^{\delta+}$ within the metal active phase on Pd$_s$/TOCF, which is generated from the EMSI with charge transfer through Pd-S bond, is also able to form the palladium with the up-shift of d band center, thereby increasing the selectivity towards C=C bond hydrogenation [51].

## 3. Conclusions

In summary, we have described a simple and efficient gas-phase functionalization approach for the production of a novel structured carbon support decorated with thiol groups via thermal reaction between oxidized carbon substrate and guest hydrogen sulfide gas. The existence of abundant surface oxygenated groups on the acid treated carbon material and the high H$_2$S concentration are proven to be conducive to the generation of the thiol groups on the carbon support. The introduction of steam in the H$_2$S reagent gas can increase the surface sulfur content of treated carbon due to the production of more oxidized sulfur species. After high temperature treatment, the sulfur from thiols can be directly incorporated into graphene framework in a major form of thiophene-like S. Moreover, such thiolated carbon support displays strong electronic interaction with the deposited Pd NPs which can perform excellent catalytic selectivity toward C=C bond in the liquid-phase hydrogenation of cinnamaldehyde. It is demonstrated that the EMSI with charge transfer at the interface between Pd NPs and carbon support is promoted through the formation of Pd-S bond where Pd and thiol-S play the role of electron donor and acceptor, respectively. Detailed studies reveal that during the

catalyst preparation, the thiol groups on the surface of TOCF are able not only to serve as anchoring sites for active metal at Pd-support interface, but also migrate to the surface of Pd NPs and then exist as the adsorbed ligands to form the thiol-based SAMs, which can be enhanced in the case of lessening metal loading with high atomic ratio of sulfur to palladium in the catalyst. The presence of thiol ligands on the surface of Pd NPs cannot result in the steric effect on the hydrogenation selectivity but leads to the poisoning effect on the catalytic activity, which can be weakened in the presence of high palladium concentration, i.e. $Pd_s$/TOCF, in the sample. The unique electronic configuration of Pd NPs with high electron depleted $Pd^{\delta+}$ in $Pd_s$/TOCF catalyst, which is derived from the electron transfer from Pd atom to thiol-S of carbon support, increases the hydrogenation selectivity of C=C bond even under drastic conditions such as low reactant concentration and high metal active sites. We believe that our synthetic approach can be further extended to produce a series of thiolated carbon materials. Meanwhile, this study provides an important insight into how surface thiol groups of carbon support control the catalytic performance of metal NPs.

## Acknowledgements

# References

[1]     F. Buckel, F. Effenberger, C. Yan, A. Gölzhäuser, M. Grunze, Influence of aromatic groups incorporated in long-chain alkanethiol self-assembled monolayers on gold, Advanced Materials, 12 (2000) 901-905.

[2]     Z. Li, S.-C. Chang, R.S. Williams, Self-assembly of alkanethiol molecules onto platinum and platinum oxide surfaces, Langmuir, 19 (2003) 6744-6749.

[3]     S.T. Marshall, M. O'Brien, B. Oetter, A. Corpuz, R.M. Richards, D.K. Schwartz, J.W. Medlin, Controlled selectivity for palladium catalysts using self-assembled monolayers, Nature Materials, 9 (2010) 853-858.

[4]     B. Wu, N. Zheng, Surface and interface control of noble metal nanocrystals for catalytic and electrocatalytic applications, Nano Today, 8 (2013) 168-197.

[5]     C.A. Schoenbaum, D.K. Schwartz, J.W. Medlin, Controlling the surface environment of heterogeneous catalysts using self-assembled monolayers, Accounts of Chemical Research, 47 (2014) 1438-1445.

[6]     J.C. Love, L.A. Estroff, J.K. Kriebel, R.G. Nuzzo, G.M. Whitesides, Self-assembled monolayers of thiolates on metals as a form of nanotechnology, Chemical Reviews, 105 (2005) 1103-1169.

[7]     S. Chen, Z. Wei, L. Guo, W. Ding, L. Dong, P. Shen, X. Qi, L. Li, Enhanced dispersion and durability of Pt nanoparticles on a thiolated CNT support, Chemical Communications, 47 (2011) 10984-10986.

[8]     R. Ahmadi, M.K. Amini, J.C. Bennett, Pt-Co alloy nanoparticles synthesized on sulfur-modified carbon nanotubes as electrocatalysts for methanol electrooxidation reaction, Journal of Catalysis, 292 (2012) 81-89.

[9]     G.A. Somorjai, On the mechanism of sulfur poisoning of platinum catalysts, Journal of Catalysis, 27 (1972) 453-456.

[10]    J. B. Miller, A. J. Gellman, Structural evolution of sulfur overlayers on Pd(111), Surface Science, 603 (2009) L82-L85.

[11]    D. Liang, J. Gao, H. Sun, P. Chen, Z. Hou, X. Zheng, Selective oxidation of glycerol

with oxygen in a base-free aqueous solution over MWNTs supported Pt catalysts, Applied Catalysis B: Environmental, 106 (2011) 423-432.

[12] J.D. Kim, T. Palani, M.R. Kumar, S. Lee, H.C. Choi, Preparation of reusable Ag-decorated graphene oxide catalysts for decarboxylative cycloaddition, Journal of Materials Chemistry, 22 (2012) 20665.

[13] G.-W. Yang, G.-Y. Gao, G.-Y. Zhao, H.-L. Li, Effective adhesion of Pt nanoparticles on thiolated multi-walled carbon nanotubes and their use for fabricating electrocatalysts, Carbon, 45 (2007) 3036-3041.

[14] M. Zhang, R. Nie, L. Wang, J. Shi, W. Du, Z. Hou, Selective oxidation of glycerol over carbon nanofibers supported Pt catalysts in a base-free aqueous solution, Catalysis Communications, 59 (2015) 5-9.

[15] Y. Kim, T. Mitani, Surface thiolation of carbon nanotubes as supports: A promising route for the high dispersion of Pt nanoparticles for electrocatalysts, Journal of Catalysis, 238 (2006) 394-401.

[16] Y.-T. Kim, K. Ohshima, K. Higashimine, T. Uruga, M. Takata, H. Suematsu, T. Mitani, Fine size control of platinum on carbon nanotubes: From single atoms to clusters, Angewandte Chemie International Edition, 118 (2006) 421-425.

[17] P. Gallezot, D. Richard, Selective hydrogenation of α, β-unsaturated aldehydes, Catalysis Reviews - Science and Engineering, 40 (1998) 81-126.

[18] A.J. Muller, J.S. Bowers, Jr., J.R.I. Eubanks, C.C. Geiger, J.G. Santobianco, Processes for preparing hydrocinnamic acid, WO Patent Appl. No. WO 99/08989, (1999) First Chemical Corporation.

[19] M.L. Toebes, A. Jos van Dillen, Y. Zhang, J. Hájek, D.Y. Murzin, T.A. Nijhuis, D.C. Koningsberger, J.H. Bitter, K.P. de Jong, Support effects in the hydrogenation of cinnamaldehyde over carbon nanofiber-supported platinum catalysts: Characterization and catalysis, Journal of Catalysis, 226 (2004) 215-225.

[20] S. Cattaneo, S.J. Freakley, D.J. Morgan, M. Sankar, N. Dimitratos, G.J. Hutchings, Cinnamaldehyde hydrogenation using Au-Pd catalysts prepared by sol immobilisation, Catalysis Science & Technology, 8 (2018) 1677–1685.

[21] F. Delbecq, P. Sautet, Competitive C=C and C=O adsorption of α-β unsaturated

aldehydes on Pt and Pd surfaces in relation with the selectivity of hydrogenation reactions: A theoretical approach, Journal of Catalysis, 152 (1995) 217-236.

[22]   B. Wu, H. Huang, J. Yang, N. Zheng, G. Fu, Selective hydrogenation of α,β-unsaturated aldehydes catalyzed by amine-capped platinum-cobalt nanocrystals, Angewandte Chemie International Edition, 51 (2012) 3440-3443.

[23]   C. Pham-Huu, N. Keller, M.J. Ledoux, L.J. Charbonniere, R. Ziessel, Carbon nanofiber supported palladium catalyst for liquid-phase reactions. An active and selective catalyst for hydrogenation of C=C bonds, Chemical Communications, (2000) 1871-1872.

[24]   S.C. Tsang, N. Cailuo, W. Oduro, A.T.S. Kong, L. Clifton, K.M.K. Yu, B. Thiebaut, J. Cookson, P. Bishop, Engineering preformed cobalt-doped platinum nanocatalysts for ultraselective hydrogenation, ACS Nano, 2 (2008) 2547-2553.

[25]   H. Vu, F. Goncalves, R. Philippe, E. Lamouroux, M. Corrias, Y. Kihn, D. Plee, P. Kalck, P. Serp, Bimetallic catalysis on carbon nanotubes for the selective hydrogenation of cinnamaldehyde, Journal of Catalysis, 240 (2006) 18-22.

[26]   M. Zhao, K. Yuan, Y. Wang, G. Li, J. Guo, L. Gu, W. Hu, H. Zhao, Z. Tang, Metal-organic frameworks as selectivity regulators for hydrogenation reactions, Nature, 539 (2016) 76-80.

[27]   D. Wang, Y. Zhu, C. Tian, L. Wang, W. Zhou, Y. Dong, H. Yan, H. Fu, Synergistic effect of tungsten nitride and palladium for the selective hydrogenation of cinnamaldehyde at the C=C bond, ChemCatChem, 8 (2016) 1718-1726.

[28]   R. Nie, M. Miao, W. Du, J. Shi, Y. Liu, Z. Hou, Selective hydrogenation of C=C bond over N-doped reduced graphene oxides supported Pd catalyst, Applied Catalysis B: Environmental, 180 (2016) 607-613.

[29]   A. Nagendiran, V. Pascanu, A. Bermejo Gómez, G. González Miera, C.-W. Tai, O. Verho, B. Martín-Matute, J.-E. Bäckvall, Mild and selective catalytic hydrogenation of the C=C bond in α,β-unsaturated carbonyl compounds using supported palladium nanoparticles, Chemistry - A European Journal, 22 (2016) 7184-7189.

[30]   C. Duong-Viet, Y. Liu, H. Ba, L. Truong-Phuoc, W. Baaziz, L. Nguyen-Dinh, J.-M. Nhut, C. Pham-Huu, Carbon nanotubes containing oxygenated decorating defects as

metal-free catalyst for selective oxidation of H₂S, Applied Catalysis B: Environmental, 191 (2016) 29-41.

[31]   Z. Xu, C. Duong-Viet, H. Ba, B. Li, T. Truong-Huu, L. Nguyen-Dinh, C. Pham-Huu, Gaseous nitric acid activated graphite felts as hierarchical metal-free catalyst for selective oxidation of H₂S, Catalysts, 8 (2018) 145-162.

[32]   J. Luo, Y. Liu, H. Wei, B. Wang, K.-H. Wu, B. Zhang, D.S. Su, A green and economical vapor-assisted ozone treatment process for surface functionalization of carbon nanotubes, Green Chemistry, 19 (2017) 1052-1062.

[33]   D.-Q. Yang, B. Hennequin, E. Sacher, XPS demonstration of π-π interaction between benzyl mercaptan and multiwalled carbon nanotubes and their use in the adhesion of Pt nanoparticles, Chemistry of Materials, 18 (2006) 5033-5038.

[34]   T. Jiang, Y. Wang, K. Wang, Y. Liang, D. Wu, P. Tsiakaras, S. Song, A novel sulfur-nitrogen dual doped ordered mesoporous carbon electrocatalyst for efficient oxygen reduction reaction, Applied Catalysis B: Environmental, 189 (2016) 1-11.

[35]   C.G. McKenas, J.M. Fehr, C.L. Donley, M.R. Lockett, Thiol-ene modified amorphous carbon substrates: Surface patterning and chemically modified electrode preparation, Langmuir, (2016).

[36]   F. Sun, J. Liu, H. Chen, Z. Zhang, W. Qiao, D. Long, L. Ling, Nitrogen-rich mesoporous carbons: Highly efficient, regenerable metal-free catalysts for low-temperature oxidation of H₂S, ACS Catalysis, 3 (2013) 862-870.

[37]   S. Yang, L. Zhi, K. Tang, X. Feng, J. Maier, K. Müllen, Efficient synthesis of heteroatom (N or S)-doped graphene based on ultrathin graphene oxide-porous silica sheets for oxygen reduction reactions, Advanced Functional Materials, 22 (2012) 3634-3640.

[38]   J. Luo, H. Wei, Y. Liu, D. Zhang, B. Zhang, W. Chu, C. Pham-Huu, D.S. Su, Oxygenated group and structural defect enriched carbon nanotubes for immobilizing gold nanoparticles, Chemical Communications, 53 (2017) 12750-12753.

[39]   Z. Xu, C. Duong-Viet, Y. Liu, W. Baaziz, B. Li, L. Nguyen-Dinh, O. Ersen, C. Pham-Huu, Macroscopic graphite felt containing palladium catalyst for liquid-phase hydrogenation of cinnamaldehyde, Applied Catalysis B: Environmental, 244 (2019)

128-139.

[40]   F. Cárdenas-Lizana, Y. Hao, M. Crespo-Quesada, I. Yuranov, X. Wang, M.A. Keane, L. Kiwi-Minsker, Selective gas phase hydrogenation of p-chloronitrobenzene over Pd catalysts: Role of the support, ACS Catalysis, 3 (2013) 1386-1396.

[41]   R. Arrigo, M.E. Schuster, S. Abate, G. Giorgianni, G. Centi, S. Perathoner, S. Wrabetz, V. Pfeifer, M. Antonietti, R. Schlögl, Pd supported on carbon nitride boosts the direct hydrogen peroxide synthesis, ACS Catalysis, 6 (2016) 6959-6966.

[42]   T. Pilloy, R. Zimmermann, P. Steiner, S. Hufner, The electronic structure of PdO found by photoemission (UPS and XPS) and inverse photoemission (BIS), Journal of Physics: Condensed Matter, 9 (1997) 3987-3999.

[43]   R. Ahmadi, M.K. Amini, Synthesis and characterization of Pt nanoparticles on sulfur-modified carbon nanotubes for methanol oxidation, International Journal of Hydrogen Energy, 36 (2011) 7275-7283.

[44]   S.-A. Park, D.-S. Kim, T.-J. Kim, Y.-T. Kim, Strong interaction between Pt and thiolated carbon for electrocatalytic durability enhancement, ACS Catalysis, 3 (2013) 3067-3074.

[45]   D. Higgins, M.A. Hoque, M.H. Seo, R. Wang, F. Hassan, J.-Y. Choi, M. Pritzker, A. Yu, J. Zhang, Z. Chen, Development and simulation of sulfur-doped graphene supported platinum with exemplary stability and activity towards oxygen reduction, Advanced Functional Materials, 24 (2014) 4325-4336.

[46]   J.T. Miller, D.C. Koningsberger, The origin of sulfur tolerance in supported platinum catalysts: The relationship between structural and catalytic properties in acidic and alkaline Pt/LTL, Journal of Catalysis, 162 (1996) 209-219.

[47]   W. Kiciński, M. Szala, M. Bystrzejewski, Sulfur-doped porous carbons: Synthesis and applications, Carbon, 68 (2014) 1-32.

[48]   S.H. Pang, C.A. Schoenbaum, D.K. Schwartz, J.W. Medlin, Directing reaction pathways by catalyst active-site selection using self-assembled monolayers, Nature Communications, 4 (2013) 2448.

[49]   K.R. Kahsar, D.K. Schwartz, J.W. Medlin, Control of metal catalyst selectivity through specific noncovalent molecular interactions, Journal of the American

Chemical Society, 136 (2014) 520-526.

[50] G. Chen, C. Xu, X. Huang, J. Ye, L. Gu, G. Li, Z. Tang, B. Wu, H. Yang, Z. Zhao, Z. Zhou, G. Fu, N. Zheng, Interfacial electronic effects control the reaction selectivity of platinum catalysts, Nature Materials, 15 (2016) 564-569.

[51] R.G. Rao, R. Blume, T.W. Hansen, E. Fuentes, K. Dreyer, S. Moldovan, O. Ersen, D.D. Hibbitts, Y.J. Chabal, R. Schlogl, J.P. Tessonnier, Interfacial charge distributions in carbon-supported palladium catalysts, Nature Communications, 8 (2017) 340.

# Chapter 7

## Conclusion and perspectives

# Conclusion and perspectives

## 1. Summary

In the quest for novel structured carbon materials for heterogeneous catalysis we explored the potential of commercial carbon/graphite felt (CF/GF) as hierarchical supports for catalytic applications. The hierarchical structure of the CF/GF is originated from the presence of entangled carbon microfilamentous forming a macroscopic shape with a large fraction of voids. Depending to the final graphitization treatment these carbon-based materials display different surface reactivity as well as porosity which can be finely tuned through chemical and/or thermal treatment. The surface modification/functionalization allows one to prepare carbon-based support with controlled surface reactivity acting as anchoring site for metal nanoparticles while keeping the macroscopic shape of the material unchanged for downstream applications. The macroscopic shaping allows an easy recovery of the catalyst, especially for liquid-phase reaction, and also to avoid problems linked with catalyst loss during the filtration process.

The aim of the work described in this thesis deals with the exploration of the potential of GF and CF monolith as metal-free catalyst for gas-phase oxidation reactions and as catalyst support material, notably for palladium, for liquid-phase hydrogenation reactions, and the influence of the surface functionalization on the final catalytic performance. Due to their chemical inertness with low wettability, a prerequisite for the use of these carbon-based materials consisted to activate the origin ones through different chemical processes. Therefore, the commercial GF and CF were functionalized by a series of chemical treatment processes. The physical and chemical properties of the supports and catalysts were investigated by different characterization techniques, including XPS, Raman, TPD-MS, TEM, $N_2$ adsorption and desorption, SEM, ICP-AES, TGA, $H_2$-TPR, $H_2$-TPD and ATR-FTIR.

The as-synthesized carbon-based catalysts were evaluated with two probe reaction: gas-phase partial oxidation of hydrogen sulfide into elemental sulfur and liquid-phase selective hydrogenation of α, β-unsaturated cinnamaldehyde. The relationship between the

catalysts properties and the catalytic performance has been established and discussed.

## 2. Concluding remarks

**Chapter 3** focused on the effective surface activation of commercial GF by using the gaseous $HNO_3$ treatment, and its influence on the formation of defects decorated with oxygenated functional groups was determined by Raman, TPD-MS and XPS, respectively. A highly porous graphite structure was also observed on the surface of the dense graphite filamentous after the gaseous acid treatment, exhibiting a remarkable increase of the specific as well as effective surface area. The abundant oxygenated groups and structural defects as well as high surface area decreased the thermal stability which was proven by TGA. The as-synthesized carbon material can be used as a metal-free catalyst in the selective oxidation of $H_2S$ present in industrial waste effluents. The experiment results revealed that the acid treated GF containing the defects decorated with oxygenated groups performed relatively high and extremely stable desulfurization activity as a function of time on stream compared with the un-activated one. The high desulfurization performance should be attributed to the presence of structural defects on the filamentous carbon wall which were decorated with oxygenated functional groups which could cooperatively play the role of active sites for the selective oxidation of $H_2S$ into elemental sulfur.

**Chapter 4** aimed at the effect of the acid oxidation treatment on the catalytic performance of GF as support for Pd catalysts. Here, we firstly optimized the process of gaseous $HNO_3$ treatment as reported in Chapter 3 by the introduction of argon flow to help the gas oxidizer to pass through GF efficiently and controllably. The oxygen functionalized GF samples were prepared using the gaseous $HNO_3$ treatment and then used as supports for anchoring Pd NPs. The monolith palladium-based catalyst was then used as catalytic stirrer in liquid-phase hydrogenation of cinnamaldehyde due to its macroscopic shape and displayed excellent stability as well as complete recyclability. The surface defects decorated with abundant oxygenated groups as well as highly accessible porous structure generated from the acid treatment of carbon support were demonstrated to bring in the electron-deficient

high-valent $Pd^{\delta+}$ species on the metal NPs, indicating the formation of strong metal-support interaction with charge transfer at Pd-support interface. All of these enhanced the Pd dispersion and resistance to sintering and/or aggregation during both catalyst preparation and cycling tests, thus leading to the high and stable $H_2$ dissociative adsorption in hydrogenation process.

**Chapter 5** is devoted to the synthesis of structured CF tailored with surface amino groups and nitrogen-doping for the preparation of Pd catalysts for selective hydrogenation of α, β-unsaturated cinnamaldehyde. The introduction of the nitrogen-containing functional groups on the carbon support during amination step using urea hydrothermal reaction was revealed to be related to the presence of surface oxygenated groups which were introduced during the gaseous acid treatment. The surface amino groups were further converted to N-doping sites of the graphitic framework using high temperature annealing process. The oxygenated groups, amino groups and N-dopants not only influenced the polarity of support surface, but also altered the anchorage of Pd NPs via the metal-support interaction. The effect of electronic structure of Pd NPs on the catalytic selectivity towards C=C bond was investigated in this work. According to the results the doping of the carbon framework with nitrogen atoms, which were generated during the annealing of the aminated support, provides anchoring sites for dispersing and stabilize Pd NPs on the catalyst surface leading to a high hydrogenation performance as well as long-term stability.

In **Chapter 6** we extended this work to the CF decorated with thiol groups, which was prepared by the thermal reaction between sulfur containing $H_2S$ gas and the acid treated CF synthesized according to the description reported in Chapter 5. The effect of the presence of oxygenated groups on the production of carbon-based support decorated with thiol groups was discussed. The supports decorated with different surface functional groups, i.e. thiols, containing Pd NPs were used as a model catalyst in the selective hydrogenation of α, β-unsaturated cinnamaldehyde. Detailed studies revealed that the thiol groups not only served as anchoring sites for active metal on the surface of support, but also participated as capping ligands on the surface of Pd NPs by the migration from support surface during the catalyst preparation. The thiol groups decorated the Pd NPs surface was at the origin of the poisoning

of the active metal sites leading to the low hydrogenation catalytic activity. However, it is worthy to note that this surface poisoning by sulfur species decorated the metal surface could be moderated by tuning the atomic ratio of sulfur to palladium through the modification of the Pd loading. The thiol-S could influence the electronic configuration of Pd NPs through the formation of Pd-S bond. Depending to the ratio between Pd and thiol one can modify the activity as well as the selectivity of the catalyst. In accordance with the discussion about the hydrogenation selectivity in Chapter 5, the presence of unique electronic structure of active metal phase helped to enhance the chemoselectivity towards C=C bond hydrogenation.

## 3. Perspectives

In summary, we have described in this thesis the potential of CF/GF monolith as metal-free catalyst and carbon support for gas- and liquid-phase reactions upon chemical functionalization process. The oxidized GF can be used as metal-free catalyst and displayed high activity in partial oxidation of $H_2S$ into elemental sulfur. The activated GF and CF, functionalized by different chemical methods, i.e. oxidation, functionalized or doped with other heteroelements such as N and S, were successfully used to support Pd NPs which displayed unique high catalytic performance in the selective hydrogenation of α, β-unsaturated cinnamaldehyde. Moreover, the macroscopic shape of these carbon-based materials provides low pressure drop along reactor bed for the gas-phase reaction and an easy recovery of the catalyst/product from the liquid-phase media, respectively. Therefore, this thesis can provide some strategies to rationally design monolith metal-free catalyst or carbon supported catalyst.

However, there still remain a lot of works to do for the further development of these macroscopic carbon-based materials in the catalysis field. Some perspectives, which can be derived from the results obtained in this thesis, are summarized below.

About the use of oxidized GF as metal-free catalyst for partial oxidation of $H_2S$, the catalytic performance is confirmed to be related to the structural defects decorated with oxygen-containing functional groups according to the characterization results. But the

definition of active sites is still unclear due to the presence of various kinds of oxygenated groups. Thereby the detailed study will be continued on the qualitative and quantitative analysis of the active sites by using chemical titration or thermal treatment to remove or inhibit selectively these different oxygenated groups, in order to build up a direct relationship between these active sites and the desulfurization activity. The defects present on the support can also be used to anchor other metal-free catalysts, i.e. mesoporous nitrogen-doped carbon layer, to produce hierarchical metal-free catalysts with high catalytic performance, improved accessibility and easy recovery.

The oxidized GF decorated with Pd catalyst displayed excellent stability in the liquid-phase hydrogenation of cinnamaldehyde at 80 $^{o}$C, indicating its enhanced resistance towards sintering and/or aggregation during both catalyst preparation (thermal treatment) and catalytic cycling tests. The future study will be conducted on such oxidized GF, with surface defective structure, decorated with other active metals for other gas-phase reaction, especially for those operated at high temperature (under reductive or inert media) where sintering frequently occur. The interconnected and thermal conductive structure of the carbon felt can be also an advantage for operating as catalyst support in some exothermic reactions where the rapid and homogeneous dissipation of heat is of high interest.

The anchorage of Pd NPs on the GF/CF surface has been demonstrated to be significantly improved by the introduction of heteroatoms-containing functional groups or heteroatoms-dopants, such as oxygen, nitrogen and sulfur. The optimization study will be continued with the aim to investigate the functionalization process step in order to increase the amount of anchoring sites on the carbon support. Moreover, the understand of interaction mechanism between active metal and anchoring sites will be further studied by the advanced characterization techniques, such as extended X-ray absorption fine structure (EXAFS).

The future study will be also dedicated to the noncontact heating (i.e. electromagnetic induction heating) of GF/CF-based metal-free catalyst or catalyst support due to their electrical conductivity, which could provide targeted heat into the catalyst as well as extremely high reaction temperature regulation thanks to high heating rate, i.e. several hundred degrees per minutes. The targeted heating mode will help to understand the catalytic

process of endothermic or exothermic reaction, which will be conducive to solving the hot spot problem of the catalyst bed in order to improve the catalytic performance.

# Annex

# Publications, oral presentations and poster

## 1. Publications

[1] Gaseous nitric acid activated graphite felts as hierarchical metal-free catalyst for selective oxidation of $H_2S$.

**Zhenxin Xu**, Cuong Duong-Viet, Housseinou Ba, Bing Li, Tri Truong-Huu, Lam Nguyen-Dinh and Cuong Pham-Huu.

*Catalysts*, 8 (2018) 145-162.

[2] Macroscopic graphite felt containing palladium catalyst for liquid-phase hydrogenation of cinnamaldehyde.

**Zhenxin Xu**, Cuong Duong-Viet, Yuefeng Liu, Walid Baaziz, Bing Li, Lam Nguyen-Dinh, Ovidiu Ersen, and Cuong Pham-Huu.

*Applied Catalysis B: Environmental*, 244 (2019) 128–139.

[3] Palladium decorated chemically functionalized macroscopic carbon for selective hydrogenation of cinnamaldehyde

**Zhenxin Xu**, Bing Li, Vasiliki Papaefthimiou, Yuefeng Liu, Spiridon Zafeiratos, and Cuong Pham-Huu.

In preparation.

[4] Thiols decorated carbon felt containing Pd nanoparticles for selective hydrogenation of cinnamaldehyde.

**Zhenxin Xu**, Bing Li, Vasiliki Papaefthimiou, Yuefeng Liu, Cuong Duong-Viet, Spiridon Zafeiratos, and Cuong Pham-Huu.

In preparation.

[5] CO$_2$ methanation under dynamic operational mode using nickel nanoparticles decorated carbon felt (Ni/OCF) combined with inductive heating.

Wei Wang, Cuong Duong-Viet, **Zhenxin Xu**, Housseinou Ba, Giulia Tuci, Giuliano Giambastiani, Yuefeng Liu, Tri Truong-Huu, Jean-Mario Nhut and Cuong Pham-Huu

*Catalysis Today*, https://doi.org/10.1016/j.cattod.2019.02.050

## 2. Oral presentations

[1] Macroscopic oxidized graphite felts containing palladium nanoparticles as an efficient liquid-phase hydrogenation catalyst with easy recovery.

**Zhenxin Xu**, Cuong Duong-Viet, Yuefeng Liu, Walid Baaziz, Bing Li, Lam Nguyen-Dinh, Ovidiu Ersen, Jean-Mario Nhut and Cuong Pham-Huu.

CARBOCAT-VIII, 28th June, 2018, Porto, Portugal.

[2] Macroscopic Graphite Felt Containing Palladium Catalyst for Liquid-Phase Processes.

**Zhenxin Xu**, Cuong Duong-Viet, Yuefeng Liu, Walid Baaziz, Bing Li, Lam Nguyen-Dinh, Ovidiu Ersen, Jean-Mario Nhut and Cuong Pham-Huu.

ICPEES - Department of Catalysis and Materials (C&M), 1st C&M Scientific Day, 6th November, 2018, Strasbourg, France.

## 3. Poster

[1] Gaseous nitric acid activated graphite felts as hierarchical metal-free catalyst for selective oxidation of H$_2$S.

Cuong Duong-Viet, **Zhenxin Xu**, Housseinou Ba, Bing Li, Tri Truong-Huu, Lam Nguyen-Dinh and Cuong Pham-Huu.

CARBOCAT-VIII, 28th June, 2018, Porto, Portugal.

**Zhenxin XU**

# Development of new macroscopic carbon materials for catalytic applications

## Résumé

De nos jours, les matériaux carbonés macroscopiques font face à un nombre croissant d'applications en catalyse, soit en tant que supports, soit directement en tant que catalyseurs sans métal. Cependant, il reste difficile de développer un support de catalyseur hiérarchisé à base de carbone ou un catalyseur utilisant un procédé de synthèse beaucoup plus simple. À la recherche de nouveaux matériaux carbonés structurés pour la catalyse hétérogène, nous avons exploré le potentiel du feutre de carbone / graphite du commerce (FC / FG).

Le but du travail décrit dans cette thèse a été le développement du monolithe FG et FC en tant que catalyseur sans métal pour les réactions d'oxydation en phase gazeuse et en tant que support de catalyseur, notamment pour le palladium, pour les réactions d'hydrogénation en phase liquide, et leur rôle dans la performances de réaction de ces catalyseurs. En raison de leur surface de chimie inerte avec une mouillabilité inappropriée, une telle étude avait pour condition d'activer celles d'origine. Par conséquent, des FG et des FC modifiés bien arrondis ont été synthétisés avec des propriétés physico-chimiques adaptées par une série de procédés de traitement chimique, tels que l'oxydation, l'amination, la thiolation, le dopage à l'azote et au soufre. L'oxydation partielle du sulfure d'hydrogène en soufre élémentaire et l'hydrogénation sélective du cinnamaldéhyde α, β-insaturé, en tant que réactions sensibles à l'effet des propriétés du catalyseur sur l'activité et la sélectivité, combinées à des techniques de caractérisation, ont été choisis pour étudier l'effet de la matériaux carbonés sur le comportement catalytique.

Mots-clés : Feutre de carbone / graphite macroscopique, oxydation, amination, thiolation, dopage azote / soufre, nanoparticules de palladium, interaction métal-support, oxydation / hydrogénation sélective, récupération du catalyseur.

## Résumé en anglais

Nowadays, macroscopic carbon materials are facing an increasing number of applications in catalysis, either as supports or directly as metal-free catalysts on their own. However, it is still challenging to develop hierarchical carbon-based catalyst support or catalyst using a much simple synthesis process. In the quest for novel structured carbon materials for heterogeneous catalysis we explored the potential of commercial carbon/graphite felt (CF/GF).

The aim of the work described in this thesis has been the development of GF and CF monolith as metal-free catalyst for gas-phase oxidation reactions and as catalyst support, notably for palladium, for liquid-phase hydrogenation reactions, and their roles in the reaction performance of these catalysts. Due to their inert chemistry surface with inappropriate wettability, a prerequisite for such a study was to activate the origin ones. Therefore, well-rounded modified GFs and CFs were synthesized with tailored physic-chemical properties by a series of chemical treatment processes, such as oxidation, amination, thiolation, nitrogen- and sulfur-doping. The partial oxidation of hydrogen sulfide into elemental sulfur and selective hydrogenation of α, β-unsaturated cinnamaldehyde, as the sensitive test reactions to the influence of the catalyst properties on activity and selectivity, combined with characterization techniques, were chosen to investigate the effect of functionalized carbon materials on the catalytic behavior.

Keywords : Macroscopic carbon/graphite felt, oxidation, amination, thiolation, nitrogen/sulfur doping, Pd nanoparticles, metal-support interaction, selective oxidation/hydrogenation, catalyst recovery.